

The University of Maine

DigitalCommons@UMaine

Electronic Theses and Dissertations

Fogler Library

Spring 5-25-2022

Primary Cilia of the Cardiac Neural Crest & Hedgehog-Mediated Mechanisms of Congenital Heart Disease

Lindsey A. Fitzsimons

University of Maine, lindsey.fitzsimons@maine.edu

Follow this and additional works at: <https://digitalcommons.library.umaine.edu/etd>



Part of the [Animal Structures Commons](#), [Cardiology Commons](#), [Cardiovascular Diseases Commons](#), [Cardiovascular System Commons](#), [Cell Anatomy Commons](#), [Cell Biology Commons](#), [Cells Commons](#), [Congenital, Hereditary, and Neonatal Diseases and Abnormalities Commons](#), [Developmental Biology Commons](#), [Disease Modeling Commons](#), [Embryonic Structures Commons](#), [Genetic Processes Commons](#), [Laboratory and Basic Science Research Commons](#), [Medical Cell Biology Commons](#), [Medical Genetics Commons](#), [Medical Molecular Biology Commons](#), [Pediatrics Commons](#), and the [Translational Medical Research Commons](#)

Recommended Citation

Fitzsimons, Lindsey A., "Primary Cilia of the Cardiac Neural Crest & Hedgehog-Mediated Mechanisms of Congenital Heart Disease" (2022). *Electronic Theses and Dissertations*. 3582.
<https://digitalcommons.library.umaine.edu/etd/3582>

This Open-Access Thesis is brought to you for free and open access by DigitalCommons@UMaine. It has been accepted for inclusion in Electronic Theses and Dissertations by an authorized administrator of DigitalCommons@UMaine. For more information, please contact um.library.technical.services@maine.edu.

**PRIMARY CILIA OF THE CARDIAC NEURAL CREST & HEDGEHOG-MEDIATED
MECHANISMS OF CONGENITAL HEART DISEASE**

By

Lindsey A. Fitzsimons

B.S. Skidmore College, 2010

M.S. East Stroudsburg University, 2012

A DISSERTATION

Submitted in Partial Fulfillment of the

Requirements for the Degree of

Doctor of Philosophy

(in Biomedical Science)

The Graduate School

The University of Maine

May 2022

Advisory Committee:

Kerry L. Tucker, PhD, Associate Professor, University of New England; Advisor

Thomas Gridley, PhD, Faculty Scientist III, Maine Medical Center Research Institute;

PhD Committee Chair

Lucy Liaw, PhD, Faculty Scientist III, Maine Medical Center Research Institute

James Schwob, MD/PhD, Professor, Tufts University

Kristy Townsend, PhD; Associate Professor, The Ohio State University

DISSERTATION ACCEPTANCE STATEMENT

On behalf of the Graduate Committee for Lindsey Avery Fitzsimons, I affirm that this manuscript is the final and accepted dissertation. Signatures of all committee members are on file with the Graduate School at the University of Maine, 42 Stodder Hall, Orono, Maine.

Dr. Kerry L. Tucker, Associate Professor

Date

Copyright 2022 Lindsey A. Fitzsimons

All Rights Reserved

LIBRARY RIGHTS STATEMENT

In presenting this dissertation in partial fulfillment of the requirements for an advanced degree at The University of Maine, I agree that the Library shall make it freely available for inspection. I further agree that permission for "fair use" copying of this dissertation for scholarly purposes may be granted by the Librarian. It is understood that any copying or publication of this dissertation for financial gain shall not be allowed without my written permission.

Signature:

Date:

PRIMARY CILIA OF THE CARDIAC NEURAL CREST & HEDGEHOG-MEDIATED MECHANISMS OF CONGENITAL HEART DISEASE

By Lindsey Avery Fitzsimons, M.S.
Dissertation Advisor: Dr. Kerry L. Tucker

An Abstract of the Dissertation Presented
in Partial Fulfillment of the Requirements for the
Degree of Doctor of Philosophy
(in Biomedical Science)
May 2022

Elimination of primary cilia in cardiac neural crest cell (CNCC) progenitors is hypothesized to cause a variety of congenital heart defects (CHDs), including atrioventricular septal defects, and malformations of the developing cardiac outflow tract. We present an *in vivo* model of CHD resulting from the conditional elimination of primary cilia from CNCC using multiple, *Wnt1:Cre-loxP*, neural crest-specific systems, targeting two distinctive, but critical, primary cilia structural genes: Intraflagellar transport protein 88 (*Ift88*) or kinesin family member 3A (*Kif3a*). CNCC loss of primary cilia leads to widespread CHD, where homozygous mutant embryos (MUT) display a variety of outflow tract malformations, septation defects and impaired maturation of the myocardium, resulting in early perinatal lethality. Noncompaction of the MUT ventricular myocardium coincides with widespread ventricular arrhythmias, measured using a method for noninvasive neonatal mutant pup electrocardiography developed by our lab. Near-global CNCC primary cilia loss was observed by E11.5, and by E12.5, the MUT displayed fewer cardiomyocytes, but increased cardiomyocyte proliferation when

compared to controls. Flow cytometry was used to explore ErbB signaling-mediated mechanisms of ventricular noncompaction and revealed a downregulation in ErbB2/4 expression in MUT hearts. Analysis of Hh signaling using qPCR and immunofluorescence revealed that loss of CNCC primary cilia led to a paradoxical upregulation of Sonic Hedgehog, Patched-1, Smoothed, and Gli1 in both the OFT and ventricular components of the MUT heart. Further analysis suggested that increased Hh signaling protein expression was likely originating from non-CNCC cells. Thus, CNCC loss of primary cilia and subsequent loss/reduction of CNCC Hh signaling in the developing outflow tract likely promotes increased cardiomyocyte proliferation, possibly enabled by disruptions to ErbB2/4 signaling in the ventricular myocardium. Taken together, these data support a causal role for primary cilia of CNCC in the pathogenesis of CHD, likely mediated by disruptions to both Hedgehog and ErbB signaling pathways.

DEDICATION

This Dissertation is dedicated to my boys, John and James, and to my mom, Rachel.

For John, the love of my life and greatest partner in every sense of the word:

I simply could not have done this without you. From the day we met, you have supported all of my passions, every pipedream and every aspiration, *every* step of the way. Even when I failed, over and over and OVER again, you continued to believe in me, even when I no longer believed in myself. For every late-night working session, every early morning workout, every meltdown, every additional year added onto what was supposed to be a 4-year timeline, thank you. Thank you for supporting me and the work I am most passionate about, and thank you for putting up with the nightmare of academic politics that has been my PhD journey. But most of all, thank you for loving me, and continuing to love me even more while I have struggled to finish what I, what we, started together, now almost a decade ago. I love you more than you'll ever know, forever and always.

For James, my littlest love bug and my GOAT developmental biology experiment:

Someday when you are older, I hope you will read this and be reminded of just how much I love you and just how very special you are to me. To become a mother in the thick of my PhD journey was a choice I made over four and a half years ago, and choice that I haven't questioned or regretted for even a microsecond. You bring the greatest joy, light and love to my life every single day; so much so, that I often wonder how in the

world I could have possibly been lucky enough that you chose ME, to be your mom. Being your mom, has made me a better scientist in so many ways I never imagined possible. Becoming a better scientist has (I hope), in turn, helped me to be the best mom I can be to you. One of the things I cherish most about my own mom, your Yaya, is her resiliency, passion and unwavering commitment to her children alongside her professional commitments to herself, and to the community. It is my hope that if you look back on and remember the stress and chaos that was this period of your life, that you do so with an understanding, a knowing that your mom, like your yaya, never compromised on pursuing her dreams, on living her professional passions alongside living and loving being your mom. I hope you will also know that this would never have been possible without your Dad to support me. Our little family has faced so much in these (your) early years, so much more than you deserve my little love bug. But it is also because of what we have been challenged by, that I believe, has allowed the depth, consistency and strength of our love for each other to grow exponentially. Always remember, my sweet boy, that anything is possible when you lean into your vulnerability. Embrace every failure as an window of new and greater possibility, and always, always, *always*, be true to yourself and all of the incredibly amazing person that you are and will continue to be as you grow. I love you with every ounce of my being and am so proud of who you are, just as you are, always.

For my Mom,

I would have never made it here without you. With all of my heart and soul, to the moon and back, forever and always, I love you, and thank you.

For my twins,

I see you, feel you and cherish you every day. How I wish things could have been different and that I could have been able to meet you, hold you and give you all the love you deserved. Your DNA is ingrained in my blood, and your souls will be carried with me in my heart for every day of this life, or until we meet again.

And finally, for all those who thought every failure would be my breaking point, May this one, BIG success, serve as the greatest of examples to remind you that there is absolutely no such thing as “the right background.” My career path will continue to be forged by grit, resiliency, creativity, integrity and authenticity. I am proud of my “non-traditional” background, and for all of the ways this has only empowered me to thrive in an environment where so many assumed I would never fit in, never survive. My wish for each of you is that you will someday reflect back and be reminded that these small interactions, though transient in nature, were critical opportunities to help shape the experience, integrity, and attrition within the next generation of scientists. Shaming your mentees solidifies their trauma and recapitulates a long-standing history of toxic workplace environments in science. I wish you a future of empowering your mentees, listening, affirming, encouraging and sharing in the many difficulties of this journey, the autonomy, necessary self-confidence and courage of conviction that can only improve the quality of both the mentoring process as well as the recipient and budding scientist nurtured therein.

ACKNOWLEDGEMENTS

I'd like to thank all of my mentors, past and present.

TABLE OF CONTENTS

DEDICATION	iii
ACKNOWLEDGEMENTS.....	vi
LIST OF TABLES	xv
LIST OF FIGURES	xvii
LIST OF ABBREVIATIONS	xxiii
Chapter	
1. INTRODUCTION & BACKGROUND.....	1
1.1 The Primary Cilium: Much More than a Vestigial organelle	2
1.1.1 The Primary Cilium: Structure Dictates Function	3
1.1.2 Ciliopathies: Increasingly Relevant to Our Understanding of CHD.....	7
1.2 The Developing Mammalian Heart	11
1.2.1 Overview of Embryonic, Mammalian Heart Development	11
1.2.2 Establishment of the cardiac crescent and the primitive heart tube	13
1.2.3 Linearization of the heart tube, cardiac looping and outflow tract formation	14
1.2.4 Cardiac septation and four-chamber remodeling, maturation of the ventricular myocardium	16
1.2.5 Ventricular Maturation and Compaction.....	17
1.2.6 Trabecular Emergence and Expansion	17

1.2.7 Thickening of the Compact Myocardium	19
1.2.8 Ventricular Compaction and the Formation of the Coronary Vasculature and Cardiac Conduction System	20
1.2.9 ErbB Signaling and the Developing Ventricular Myocardium	22
1.3 Primary Cilia of the Developing Heart.....	25
1.3.1 Primary Cilia and Hedgehog Signaling: A Long-Standing History.....	25
1.3.2 Primary Cilia of the Embryonic Node.....	26
1.3.3 Primary Cilia of the Migratory CNCC Population	28
1.3.4 Primary Cilia of the Endocardial Cushions	29
1.3.5 Primary Cilia of the Atrio-Ventricular Septa	31
1.3.5.1 Atrial Septation	31
1.3.5.2 Ventricular Septation	32
1.3.6 Primary Cilia of Cardiac Fibrocytes	33
1.3.7 Primary Cilia of the Endocardium	34
1.3.8 Primary Cilia of the Ventricular Myocardium	36
1.4 Hedgehog Signaling Pathway in Cardiac Development and Pathophysiology	39
1.4.1 Canonical vs. Noncanonical Hedgehog Signaling	40
1.4.2 Hedgehog Signaling and Progenitor Cells of Mammalian Heart Development	46
1.4.3 Hedgehog signaling in pre- and postnatal cardiomyocytes	49

2.	EXPERIMENTAL DESIGN & METHODS (PART I).....	52
2.1	Neural Crest-Specific Conditional Elimination of Primary Cilia (<i>In Vivo</i>).....	52
2.1.1	Experimental Animals and IACUC Statement of Compliance	52
2.1.2	Breeding, Timed Matings, Euthanasia and Collection of Embryonic Tissue	56
2.1.3	Genotyping	57
2.2	Histological Characterization and Analyses	59
2.2.1	Histology: Hematoxylin & Eosin (H&E) Staining	59
2.2.2	Ventricular Myocardial Assessments for Noncompaction Cardiomyopathy using Axial H&E Paraffin Sections	60
2.2.3	Histology: Immunohistochemistry and Immunofluorescence	62
2.2.4	Characterization of Primary Cilia: Integrity, Length, and Morphology	65
2.3	Micro-Magnetic Resonance Imaging and 3D Reconstructions	66
2.3.1	Preparation of Embryos for μ MRI	66
2.3.2	μ MRI Acquisition and Data Collection	67
2.3.3	Measurements and Analysis of Anatomical Parameters	67
2.4	Relative Gene Expression Using Quantitative, Real-Time PCR	68
2.5	Quantitative Flow Analysis	69
2.5.1	Tissue Extraction & Processing.....	69

2.5.2 Single-Cell Suspension Preparation for Quantitative Flow Analysis	71
2.6 Protein Expression & Quantification	71
2.6.1 Western Blot	71
2.6.2 Quantitative Immunofluorescence	73
2.7 Early Postnatal Cardiac Electrophysiology	74
2.7.1 Electromyography Technology Modified to Measure Cardiac ECG	74
2.7.2 Novel, Non-invasive ECG Developed for Neonatal Mice	74
2.8 Statistical Considerations and Analyses	75
3. METHODS (PART II): IN VIVO ANALYSIS OF POSTNATAL MAMMALIAN CARDIAC ELECTROPHYSIOLOGY	77
3.1 Utility and Translational Relevance of Perinatal ECG in mouse.....	78
3.2 Protocol	79
3.3 Representative Results	83
3.4 Discussion	89
3.5 Disclosures	94
3.5.1 Acknowledgements	94
3.5.2 References	94

4. LOSS OF CNCC PRIMARY CILIA CAUSES CONGENITAL HEART DEFECTS VIA UPREGULATION OF HEDGEHOG SIGNALING	95
4.1 Cardiac Neural Crest Cells Elaborate Primary Cilia Necessary for Cardiogenesis	95
4.1.1 Conditional Elimination of Primary Cilia from CNCC Leads to Global Congenital Heart Defects	96
4.1.2 <i>In Vivo</i> Loss of CNCC Primary Cilia Leads to Outflow Tract Defects and Multi-Component CHD.	100
4.1.3 Persistent, Embryonic and Perinatal Ventricular Myocardial Phenotype Resulting from the Loss of CNCC Primary Cilia <i>In Vivo</i>	106
4.1.4 Persistent Noncompaction Resulting from CNCC Loss of Cilia Occurs Concurrently with Disruption to the Cardiac Conduction System and Fatal Cardiac Arrhythmia.	107
4.1.5 Disappearance of CNCC primary cilia disrupts OFT Sonic Hedgehog Expression	110
4.2 Early Disruption to Ventricular Myocardial Organization Coincides with Loss of CNCC Primary Cilia	112
4.2.1 CNCC Loss of Primary Cilia Affects Development of Ventricular Myocardium Via Shh-Mediated Increases in Proliferation of Ventricular Cardiomyocytes	115
4.2.2 CNCC Loss of Primary Cilia Leads to Decreased Ventricular Cardiomyocyte Populations and Disrupts ErbB Signaling	116

4.3 Hedgehog <i>Gain-of-Function</i> in CNCC With and Without Intact Primary Cilia	122
4.3.1 Hedgehog <i>GoF</i> in CNCC With Intact Primary Cilia Exacerbates OFT Defects and Ventricular Hypertrabeculation	123
4.3.2 Hedgehog <i>GoF</i> in CNCC With Intact Primary Cilia Further Upregulates Hh Signaling and Cardiomyocyte Proliferation	126
4.4 Globally-upregulated cardiac Hh resulting from CNCC loss of primary cilia may be attributed to Non-CNCC primary cilia in a paracrine capacity... ..	130
5. LOSS OF CARDIOMYOCYTE PRIMARY CILIA IN THE DEVELOPING HEART	136
5.1 Cardiomyocyte-Specific Conditional Elimination of Primary Cilia in the Developing, Mammalian Heart.....	136
5.1.1 Conditional elimination of cardiomyocyte primary cilia mimics ventricular myocardial phenotypes observed with CNCC loss of primary cilia	137
5.2 Introduction of Hh <i>GoF</i> in Cardiomyocytes with and without Intact Primary Cilia Impacts Ventricular Maturation	141
5.2.1 Hh <i>GoF</i> in Cardiomyocytes with Some Intact Primary Cilia Preserves Trabecular Myocardial Thickness, but Persists in Limiting Adequate Expansion of the Compact Ventricular Myocardium	143

5.3 Characterizing Cardiomyocyte Primary Cilia in Human CHD	143
5.3.1 Characterizing breadth of cardiomyocytes phenotypes in human, pediatric CHD cases	143
5.3.2 Alterations in Primary Cilia Abundance and Morphology in Human CHD with and without Myocardial Disarray	146
6. DISCUSSION & CONCLUSIONS	149
6.1 Manipulation of CNCC Resulting in a Novel Ventricular Phenotype	149
6.1.1 CNCC (Tdt+/Cre+) Presence in the Ventricular Myocardium.....	151
6.2 CNCC Primary cilia are Associated with ErbB-Mediated Mechanisms of CM Proliferation, Cardiac Chamber Morphogenesis and Ventricular Compaction.....	154
6.3 Loss of CNCC Primary Cilia Increases Cardiac Proliferation and Impairs Ventricular Maturation	156
6.4 Conclusions	162
REFERENCES	164
APPENDICES	185
Appendix A. Supplementary Protocol: Cardiac cells staining for flow cytometry	185
Appendix B. Embedding whole embryos in agarose for micro-MRI	187

Appendix C. IHC/Immunofluorescence protocol for fixed, frozen, OCT- embedded tissue(s)	189
Appendix D. IHC/Immunofluorescence protocol for Formalin-fixed, paraffin- embedded tissue(s)	204
Appendix E. Supplementary Protocol: Trans-Cardiac Perfusion Protocol	218
Appendix F. Supplementary Protocol: Primary Antibody Validation for Immunofluorescence Analysis	240
BIOGRAPHY OF THE AUTHOR.....	244

LIST OF TABLES

Table 1.1	Summary Table of relevant primary cilia knockout models and incidence of CHD	10
Table 2.1	Mouse lines used to investigate and model congenital heart disease (<i>in vivo</i>) resulting from the loss of primary cilia in cardiac neural crest progenitor cells.	55
Table 2.2	Primers and primer pairs used for animal genotyping	58
Table 2.3.	Primary Antibodies used for IHC/Immunofluorescence.....	63
Table 2.4	Secondary Antibodies used for IHC/Immunofluorescence.....	64
Table 2.5	qRT-PCR targets & primer sequences	69
Table 2.6	Conjugated Antibodies used for Quantitative Flow Analyses	71
Table 3.1	Representative results of ECG measurements for the average perinatal mouse pup P1, P3, P5, and P7	88
Table 4.1	Summary of multiple Cre-drivers and primary cilia-specific conditional knockout mouse models and persistence of anatomical and cardiac electrophysiological phenotype	110
Table C.1.	Immunofluorescence Protocol for Fixed, Frozen, OCT-Embedded Tissue(s)	190
Table C.2.	Immunofluorescence Protocol for Formalin-Fixed, Paraffin-Embedded Tissue(s)	191

Table E1. Tissue fixation and Storage	239
---	-----

LIST OF FIGURES

Figure 1.1 Fundamentals of primary cilia in eukaryotic cells	4
Figure 1.2 Overview of embryonic heart development in the mouse.....	12
Figure 1.3 Primary cilia within the embryonic heart process Hedgehog signaling that in turn directs heart development.	13
Figure 1.4 The Cardiac Neural Crest	15
Figure 1.5 ErbB-mediated mechanisms of ventricular maturation and compaction	23
Figure 1.6 The primary cilium and its interaction with canonical and noncanonical Hedgehog (Hh) signal transduction is critical to many aspects of the developing mammal and maintenance of postnatal mammalian tissues	43
Figure 2.1 Illustrative overview of relevant genetic components for the <i>in vivo</i> elimination of primary cilia from CNCC in the developing mouse embryo.....	53
Figure 2.2 Experimental, genetic manipulation of conditional knockout.....	56
Figure 2.3 Genotyping mice and embryos for the <i>Ift88 floxed</i> allele	59
Figure 2.4 Diagnostic Evaluation of Ventricular Noncompaction (LV)	61
Figure 2.5 Overview of PyT Method for Measuring Primary Cilia Length.	66

Figure 3.1	Representative electrocardiographic reads from neonatal mice on the first (A, P1.0), third (B, P3.0), and seventh (C, P7.0) postnatal day	84
Figure 3.2	Illustration of traditional limb lead electrodes for noninvasive collection of early postnatal ECG	85
Figure 3.3	Representative ECG read with complications.....	86
Figure 3.4	Placement of the mouse pup and limb lead electrodes for collection of early postnatal ECG	87
Figure 3.5	Comparative electrocardiographic reads from littermate control pups and mutant pups with congenital heart disease on the first postnatal day (P1.0).	89
Figure 3.6	Representative ECG tracings of neonatal mice at multiple postnatal time points.....	93
Figure 4.1	Tracking and quantifying loss of primary cilia of CNCC during heart development using a td-tomato reporter.	98
Figure 4.2	CNCC loss of primary cilia impairs proper alignment of the developing outflow tract, leading to outflow tract defects	101
Figure 4.3	Phenotypic analysis of E14.5 CON and MUT embryos using micro-magnetic resonance imaging.....	104
Figure 4.4	Persistent, Embryonic and Perinatal ventricular myocardial phenotype resulting from the loss of CNCC primary cilia <i>in vivo</i>	106

Figure 4.5 CNCC loss of primary cilia impairs ventricular morphology and cardiac function	109
Figure 4.6 OFT Hedgehog signaling is upregulated following CNCC loss of primary cilia	111
Figure 4.7 Loss of primary cilia in CNCC disrupts ECC formation, OFT alignment and ventricular endocardial organization.	113
Figure 4.8 Hypertrabeculation aspect of ventricular noncompaction may be explained by increased proliferation of ventricular cardiomyocytes brought about by upregulation in Hedgehog signaling.	116
Figure 4.9 Flow analysis of mutant hearts reveals/shows a decreased cardiomyocyte cell population and disruption to ErbB signaling at E12.5.	120
Figure 4.10 CNCC loss of primary cilia does not affect expression of ventricular Neuregulin-1 (NRG-1).	121
Figure 4.11 Introduction of Hh <i>GoF</i> offers new insights into mechanisms for CNCC primary cilia-mediated ventricular maturation	124
Figure 4.12 Hh <i>GoF</i> (via SMOM2) further upregulates ventricular Hedgehog in the presence of partially intact (<i>Ift88</i> het) CNCC primary cilia population.....	126
Figure 4.13 CNCC loss of primary cilia and HH <i>GoF</i> is associated with changes in cardiomyocyte and overall ventricular myocardial proliferation	129

Figure 4.14 Expression of Hh components in Tdt+/CNCC and Tdt-/ Non-CNCC of the E12.5 Endocardial Cushions (OFT).	131
Figure 4.15 Pharyngeal Hh distribution supports paracrine mechanism of non-CNCC upregulation of HH in response to loss of CNCC primary cilia.	134
Figure 5.1 Generation of cardiomyocyte-specific, primary cilia conditional knockout mouse model with addition of Hh GoF perturbations.....	137
Figure 5.2 <i>In vivo</i> loss of CM primary cilia impairs myocardial maturation	138
Figure 5.3 Immunofluorescence analysis of the loss of primary cilia in embryonic, (ventricular) cardiomyocytes	140
Figure 5.4 Hh GoF in ventricular cardiomyocytes with and without intact primary cilia leads to a phenotype characterized by ventricular noncompaction	142
Figure 5.5 Characterizing breadth of cardiomyocytes phenotypes in human, pediatric CHD cases	145
Figure 5.6 Analysis of primary cilia prevalence of human tissue(s) using endomyocardial biopsies from pediatric CHD patients with and without myocardial disarray	146
Figure 5.7 Quantitative characterization of cardiomyocyte primary cilia from endomyocardial biopsies taken from human, pediatric CHD patients with and without myocardial disarray.	147

Figure 6.1 Summary of CNCC primary cilia mediated conditional knockout and resulting phenotype.	150
Figure E.1 Perfusion Apparatus Setup	219
Figure E.2 Baxter Interlink T-Connector Extension Set	220
Figure E.3 Connecting T-Connector to Perfusion Apparatus	220
Figure E.4 Overview of System Set-Up	221
Figure E.5 Complete set-up for trans-cardial perfusion (in mice).....	222
Figure E.6. Illustrative schema depicting desired mouse body positioning (supine) and approximate anatomical location for surgical incisions.....	223
Figure E7. Approximate location of jugular vein (right) in adult mouse.....	224
Figure E8. Cardiac Puncture for Fixative Point of Entry.....	225
Figure E9. Overview and Approximate Locations of Adipose Collection Sites in the Adult Mouse.....	228
Figure E10. Illustrative Approximation of mouse brain (including olfactory bulb) with the skull when the mouse is positioned in the prone position.....	229
Figure E11. Indication and approximate location of incision points for the excision and dissection of mouse brain tissue (olfactory intact).....	230

Figure E12. Approximate location for cardiac puncture to extract blood tissue collection.....	232
Figure E13. Anatomical approximation of location and incision orientation for the collection of perfused, skeletal muscle tissue extraction from the hindlimb of the adult mouse.....	234
Figure E14. Overview of post-excision mouse hindlimb skeletal muscle preparation and orientation for embedding in paraffin.....	236
Figure E15. Anatomy and approximate location of tissues of interest located within the peritoneal cavity of the adult mouse.....	237
Figure E16. Dissection Tools. (a) (b) (c).....	238
Figure F1. Validation of primary cilia and Hh signaling primary antibodies for immuno-fluorescence analysis	243

LIST OF ABBREVIATIONS

α	(alpha); primary antibody, antigen raised against (target)
Aa	aortic arch
Arl13b	ADP-ribosylation factor-like GTPase 13b
AVSD	Atrio-ventricular septal defect(s)
<i>cbbs</i>	<i>cobblestone</i> mutant mouse
CCS	cardiac conduction system
CHD	congenital heart defects/congenital heart disease
CFD	craniofacial defect(s)
CNCC	cardiac neural crest
CM	cardiomyocyte(s)
cMyoC	compact myocardium (Ventricular)
cko	conditional knockout
CON	control (genotype/condition unique and specified by section)
cTnT	Cardiac troponin-T
DAPI	4',6-diamidino-2-phenylindole
dECC	distal endocardial cushion(s)
De-I H ₂ O	Deionized water
dOFT	distal outflow tract (cardiac)
DORV	Double-outlet right ventricle
DPBS	Dulbecco's PBS
Dhh	Desert hedgehog
E	Embryonic gestational day (days post-coitus)
EC	Endocardium/endocardial cells
ECC	endocardial cushion(s)
ErbB	Epidermal growth factor receptor (HER/Human)
FFPE	Formalin-fixed, paraffin-embedded (tissue)
GAPDH	Glyceraldehyde-3-phosphate dehydrogenase (Housekeeper gene)
GLI/Gli	Glioma-associated oncogene (-1,2,3)
GoF	Gain of function

Hh	Hedgehog
Ihh	Indian hedgehog
IVS	Interventricular septum
L	Left
LA/La	left atrium
LV/Lv	left ventricle
MUT	mutant (genotype/condition unique and specified by section)
NC	neural crest
NCC	noncompaction cardiomyopathy
NDS	normal donkey serum
NGS	normal goat serum
NRG(-1)	Neuregulin(-1)
OCT	optimal cutting temperature (frozen tissue embedding medium)
OFT	outflow tract (cardiac)
PA	pulmonary artery
PBS	phosphate-buffered saline
pECC	proximal endocardial cushion(s)
PECAM-1	platelet endothelial cell adhesion molecule-1 (also known as CD-31)
PFA	paraformaldehyde (4% unless otherwise specified)
PFN	Purkinje fiber network
pOFT	proximal outflow tract (cardiac)
PTA	persistent truncus arteriosus
Ptch1	Patched-1
PVC	premature ventricular contraction
PVCS	peripheral ventricular conduction system
R	Right
RA/Ra	right atrium
RV/Rv	right ventricle
SAG	sagittal (anatomical plane)
SC	spinal cord
Smo	Smoothened

SMOM2	Smoothened mutant-M2
SMOM2+cilia	Smoothened mutant-M2 with intact cilia
SMOM2-cilia	Smoothened mutant-M2 without intact cilia
TdT	Td-tomato
tMyoC	trabecular myocardium (ventricular)
vMyoC	ventricular myocardium
VSD	ventricular-septal defect(s)
VECAM-1	Vascular cell adhesion molecule-1
Wnt1	Wingless-type integration site family member 1
YFP	yellow fluorescence protein

CHAPTER 1

INTRODUCTION & BACKGROUND

The heart is one of the first organs to form within the developing embryo, but it is also the organ most commonly plagued with congenital defects, affecting approximately 1% of live births in the United States each year (Hoffman, Kaplan, & Liberthson, 2004). Primary cilia are crucial for normal cardiac organogenesis via formation of cyto-architectural, anatomical, and physiological boundaries in the developing heart and outflow tract. These tiny, plasma membrane-bound organelles function in a sensory-integrative capacity, interpreting both the intra- and extra-cellular environments and directing changes in gene expression responses to promote, prevent, and modify cellular proliferation and differentiation. One distinct feature of this organelle is its involvement in the propagation of a variety of signaling cascades, most notably, the Hedgehog cascade. Three ligands, Sonic, Indian, and Desert hedgehog, function as growth factors reliant upon the presence of intact primary cilia. Hedgehog receptors Patched-1 and Smoothed localize directly within or at the base of the ciliary axoneme. Although closely linked in both physiological proximity as well as from a mechanistic perspective, Hh ligands and primary cilia-mediated Hh signaling is/are not exclusively dependent upon each other. In fact, codependence of primary cilia and Hedgehog signaling is highly context, tissue and cell-dependent. Hedgehog signaling functions to mediate many cell behaviors critical for normal embryonic tissue/organ development. However, inappropriate activation and/or upregulation of Hedgehog signaling in postnatal and adult tissue is known to initiate oncogenesis as well as

pathogenesis of other diseases. The focus of this first chapter is to provide an overview describing the role of Hedgehog signaling and its dependence upon the primary cilium in the cell types most essential for mammalian heart development. We outline the breadth of developmental defects and consequential pathologies resulting from inappropriate changes to Hedgehog signaling as it pertains to congenital heart disease and general cardiac pathophysiology.

1.1. The Primary Cilium: More than a Vestigial Organelle

Although primary cilia of living cells were first described well over 100 years ago (Zimmermann, 1898), it wasn't until much later on that scientists began to suspect that this organelle's function spanned far beyond a vestigial nature (Luck, 1984; Pazour et al., 2000). Not only was this nonmotile, plasma membrane extension inherently unique in its ultrastructure, but the primary cilium was also incredibly dynamic, functioning within and outside of eukaryotic cells in multiple, pathogenically, and clinically significant ways (Pazour et al., 2000). Aberrancies occurring to prevent, limit or later destroy these processes have been shown to impair overall sensory/ signaling function and have been associated with a number of pathological disease conditions, known as ciliopathies (Badano, Mitsuma, Beales, & Katsanis, 2006). Ciliopathies are commonly referred to as a spectrum of diseases, due to the fact that primary cilia have been implicated in various pathological processes ranging from congenital fibrocystic disease of the developing organs (M. Adams, Smith, Logan, & Johnson, 2008) to acquired and age-related diseases like obesity (Snell, Pan, & Wang, 2004), osteoporosis (Wann et al., 2012) and a growing number of cancers (Han et al., 2009; Jenks et al., 2018; Menzl et

al., 2014). Examples of ciliopathies include asphyxiating thoracic dysplasia, Leber congenital amaurosis, nephronophthisis, polycystic kidney disease and Alström, Bardet-Biedl, Ellis-van Creveld, Joubert, Kartagener, McKusick-Kafman, Meckel-Gruber, orofacioidigital, Senior-Løken, and Sensenbrenner syndromes (Reiter & Leroux, 2017).

In this chapter, we describe the morphological, functional and signaling mechanisms most relevant to furthering our understanding of primary cilia and their contributions to the pathogenesis of CHD. Specifically, we emphasize the importance of Hedgehog signaling throughout key developmental time points critical to embryonic heart development.

1.1.1. The Primary Cilium: Structure Dictates Function

Primary cilia are antenna-like structures that protrude from almost all eukaryotic cells types and range in size from 1-3 μm (Figure 1.1) in endothelial cells and up to 9 μm in neural cells(Goetz & Anderson, 2010).

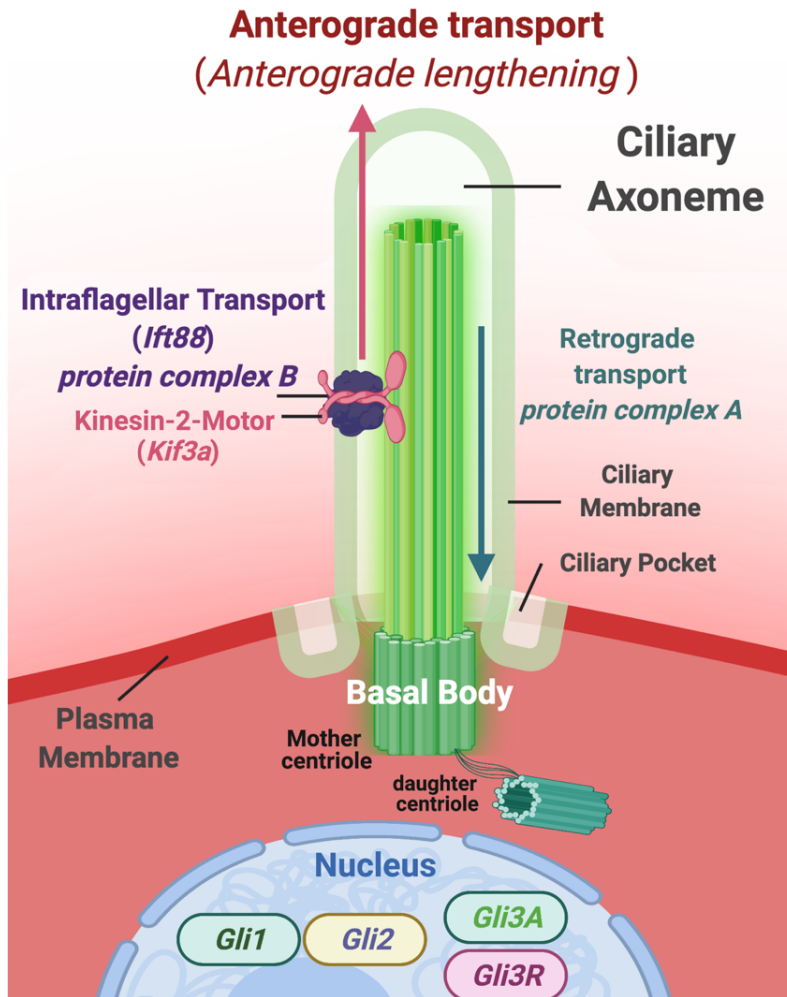


Figure 1.1 Fundamentals of the Primary Cilium in Eukaryotic Cells. Primary cilia are highly specialized cellular organelles that extend out from the plasma membrane of the cell into the extracellular environment, where they function as sensory mediators of transcriptional regulation and various cell behaviors. The cilium itself is composed of the axonemal projection (ciliary axoneme) which contains a microtubule scaffold arranged in a 9+0 circular core. The ciliary axoneme is anchored to the body of the cell via the ciliary membrane (extension of the plasma membrane) and the basal body, which is composed of the mother and daughter centrioles. The primary cilium operates efficiently as a sensory organelle due to its location at the apical portion of the cell as well as its proximity to the nucleus, where primary cilia-specific transcriptional regulators are responsible for carrying out various cellular processes critical for the development and maintenance of numerous pre- and postnatal eukaryotic tissues.

These microscopic organelles are known to function in the propagation and regulation of key sensory functions both inter- and intracellularly in both normal and pathogenic environments (Wheway, Nazlamova, & Hancock, 2018) [Wheway 2018]. The structure of the primary cilium is composed of a core axoneme of microtubule doublets arranged around a central core devoid of microtubules (Sun, Fisher, Bowser, Pentecost, & Sui, 2019). This extension initially forms when the cell enters a quiescent state, or growth arrest, when the mother centriole forms the basal body of the primary cilium and the lengthening process begins to extend towards the extracellular environment (Hoyer-Fender, 2013). The microtubule doublet core is essential for a process known as intraflagellar transport (IFT) that in turn maintains the axonemal structure and is responsible for bidirectional trafficking of proteins into and out of the cilium (Scholey, 2003). Key aspects of IFT transport in mammals is the use of Kif3a, a kinesin-II motor protein complex driving anterograde transport, which is required for ciliary assembly, and Ift88, an adaptor protein component of the IFT complex. In the retrograde direction, dynein-based motors are used. Interaction between the protein cargo and the two motor systems is mediated by the IFT scaffolding proteins, divided into classes A and B, for retro- and anterograde transport, respectively (Scholey, 2003). Knockout of Kif3a or Ift88 proteins has shown a necessity for the presence of primary cilia in developing mice (Haycraft et al., 2007; Koefoed et al., 2014). The deletion of the IFT complex or motor proteins results in the depletion of primary cilia in a cell. This ciliary depletion is detrimental to development and leads to ciliopathies in humans (Reiter & Leroux, 2017).

Starting in the mid 1960's, primary cilia were first reported in embryonic and adult hearts from various organisms, including rabbits, mice, and lizards, using transmission

electron microscopy (Manasek, 1968; Rash, Shay, & Biesele, 1969). This microscopic approach revealed the *sui generis* “9+0” transverse pattern of 9 microtubule doublets surrounding a central cavity devoid of microtubules, the characteristic of the primary cilium distinguishing them from motile cilia. To this day, transmission electron microscopy (TEM) remains the gold standard to unequivocally identify the organelle and distinguish it from other cilia-like plasma membrane protrusions such as motile cilia, stereocilia, and microvilli. Primary cilia have been shown to have a role as fluid shear stress sensors of kidney epithelial cells in culture (Nauli et al., 2013), although the exact nature and extent to which this mechanism functions is of ongoing debate (Delling et al., 2016; Hofherr & Köttgen, 2016). Employing scanning electron microscopy, Van der Heiden *et al.*, demonstrated that monocilia are present on endocardial cells in embryonic chicken, with a lower frequency on endothelial cells (Van Der Heiden et al., 2006). The primary cilia were oriented strikingly, projecting into the blood-filled chambers of both ventricles and atria. Subsequent immunofluorescence analysis revealed the presence of primary cilia in all three layers of the embryonic heart in mid-gestation mouse embryos: in the endocardium, the myocardium, and even the epicardium (Diguët, Le Garrec, Lucchesi, & Meilhac, 2015; Toomer et al., 2019). Importantly, primary cilia, organized in a random fashion, were found within the mesenchymal cells of the endocardial cushions (Slough, Cooney, & Brueckner, 2008; Toomer et al., 2019). These cilia bore the identifying “9+0” orientation and were positively identified with TEM in the embryonic atrioventricular and conotruncal cushions (Slough et al., 2008; Toomer et al., 2019; Marc August Willaredt, Gorgas, Gardner, & Tucker, 2012). Mesenchymal cells showed a random orientation, whereas endocardial

cells oriented their cilia to the lumen of the outflow and inflow tracts, but no cilia with the “9+2” orientation characteristic of motile cilia were observed (Slough et al., 2008; Toomer et al., 2019; Marc August Willaredt et al., 2012). Slough *et al.*, have demonstrated that cilia are found in the mouse embryo heart as early as E9.5 (Slough et al., 2008). Interestingly, *Kif3a*^{-/-} mouse embryos lacking cilia show defective development of the endocardial cushions and compact myocardium at E9.5. The authors have also investigated mouse embryos that, because of structurally normal but paralyzed cilia, have an abnormal left-right cardiac asymmetry (*Ird* and *Pkd2* mutants)(Slough et al., 2008). These embryos demonstrate abnormal development of endocardial cushions, although in a less severe form but possess a normal myocardium.

1.1.2 Ciliopathies: Increasingly Relevant to Our Understanding of CHD

Primary cilia have been shown to have a role as fluid shear stress sensors of kidney epithelial cells in culture(Praetorius & Spring, 2001) although the exact nature and extent to which this mechanism functions is of ongoing debate (Delling et al., 2016; Hofherr & Köttgen, 2016). A correlative study compared the distribution of primary cilia on endothelial and endocardial cells and the chicken embryonic expression pattern of the high shear stress marker *Krueppel-like factor-2* (Van Der Heiden et al., 2006). They revealed an inverse correspondence between the expression of this marker and the distribution of primary cilia. In areas where *Krueppel-like factor-2* is not detected, primary cilia are present, and the shear stress is expected to be low. Even though not all the endothelial and endocardial cells have a primary cilium, they all are shear stress-

responsive. The authors propose that the cytoskeleton can function as a transducer of the shear stress and that the primary cilia in the endothelial and endocardial cells sense changes in shear stress. The low shear forces are transmitted to the cytoskeleton and a shear stress response is generated; these shear stresses could in principle contribute to the morphological elaboration of the chambers in the heart (Van Der Heiden et al., 2006). Indeed, loss of primary cilia has been shown to change the propensity of endothelium-to-mesenchyme transition that is critical for the formation of the endocardial cushions (Egorova et al., 2011).

Defects in heart development in cilia mutants were actually recorded well before cilia were known to play a role in development. Mutations in the polycystin-2 gene (*Pkd2*) lead to autosomal dominant polycystic kidney disease. *Pkd2* encodes an integral membrane glycoprotein that shares similarities with calcium channel subunits and is localized to primary cilia. Wu *et al.*, generated a knock-out of *Pkd2* and mice homozygous for the mutation demonstrated a failure to form the interventricular septum and, to a lesser extent, the interatrial septum (Wu et al., 2000). Boulter *et al.*, described mice carrying a targeted mutation in *Pkd1*. Again, heart defects, including hemorrhagic pericardial effusion, atrio-ventricular septal defects, disorganization and thinning of the myocardial wall, and double-outlet right ventricles were observed (Boulter et al., 2001).

CHD resulting directly from damage to or loss of the primary cilia structure itself in the cardiac progenitor populations, is a topic that has raised ongoing scientific questions, and continues to be an important focus for many basic and clinical research labs (Y. Li et al., 2015). Thus, in refining our understanding of the mechanistic, causal aspects of primary cilia-mediated CHD, it is pertinent to consider the most relevant

investigations incorporating experimental manipulation of genes/proteins essential for both elongation as well as maintenance of the primary cilium structure itself, and specifically, Ift88 and Kif3a ciliary axonemal proteins (Table 1.1)

Table 1.1 Summary of known CHD phenotypes associated with *Ift88* and *Kif3a* primary cilia-specific genes:

Citation	Species	Primary Cilia Gene	Targeted location	Mutation	CHD Phenotype
Clemente <i>et al</i> , 2009*	* <i>In vitro</i> P19.CL6 cells; mouse embryonal carcinoma cells	1) <i>Ift88</i> +GFP knockdown 2) <i>Ift88</i> +GFP+ <i>Ift20</i> knockdown	siRNA targeting <i>Ift88</i> ±siRNA targeting <i>Ift20</i> i Nucleofected in P19.CL6 cells prior to CM differentiation	siRNA knock-down OR cyclopamine (Hh antagonist)	Decreased cardiogenesis (colocalization of <i>Ift88</i> +GFP± <i>Ift20</i> ; ±Nkx2.5 (CM lineage marker)
Willaredt <i>et al</i> , 2012	mouse	<i>Ift88</i> (via <i>cbbs</i>) hypomorph	Global; IFT Complex B/ Anterograde transport within ciliary axoneme	<i>Ift88</i> hypomorph resulting from SNP in <i>cbbs</i> allele*	OFT defects (PTA, Overriding Aorta) ASD VSD ECC defects
Toomer <i>et al</i> , 2017	mouse	<i>Ift88</i> floxed	Endothelial-specific conditional knockout	Targeted mutation via Cre-Lox	Bicuspid Aortic Valve
Toomer <i>et al</i> , 2019	mouse human	<i>Ift88</i> floxed	Endothelial-specific conditional knockout	Targeted mutation via Cre-Lox	Mitral Valve Prolapse
Burns <i>et al</i> , 2019	mouse	<i>Ift88</i> floxed	1) Col3.6:Cre (osteoblast lineage)	Targeted mutation via Cre-Lox	1) OFT defects (DORV, PTA); malalignment of pulmonary vein to ASD VSD
			2) Mef2C-AHF:Cre (SHF)		2) VSD
Slough <i>et al</i> , 2008	mouse	<i>Kif3a</i> floxed	Global primary and nodal cilia knockout; focus on all cardiac progenitors	<i>Kif3a</i> floxed, targeted mutation using Actin:Cre (Cre-Lox)	Loss of cardiac primary cilia; abnormal ECC formation; Impaired trabeculation by E9.5)
Takeda <i>et al</i> , 1999	mouse	<i>Kifa3a</i> -/-	Global primary and nodal cilia knockout; focus on whole-embryo, laterality, neural tube morphology, and cardiac development	<i>Kif3a</i> knockout/targeted mutation	Mid-gestation embryonic lethality (~E10.5) due to “cardiac insufficiency”; Neural tube defects; severe pericardial effusion; vascular insufficiency

Most relevant of these findings were those reported by Willaredt *et al.*, who examined a hypo-morphic allele of *Ift88* and made the first comprehensive overview of the consequences of global primary cilium loss for the middle third period of embryogenesis (Marc August Willaredt *et al.*, 2012). They reported many common CHD phenotypes, including persistent truncus arteriosus and atrial (ASD) and ventricular (VSD) septal defects. Examination of a complete, targeted deletion of *Ift88* revealed defects in the OFT and reduced ventricular trabeculation (Clement *et al.*, 2009).

1.2 The Developing Mammalian Heart

1.2.1 Overview of Embryonic, Mammalian Heart Development

Embryonic heart development in the vertebrate involves a highly complex, tightly-coordinated series of developmental signaling and gene expression patterning (Figure 1.2).

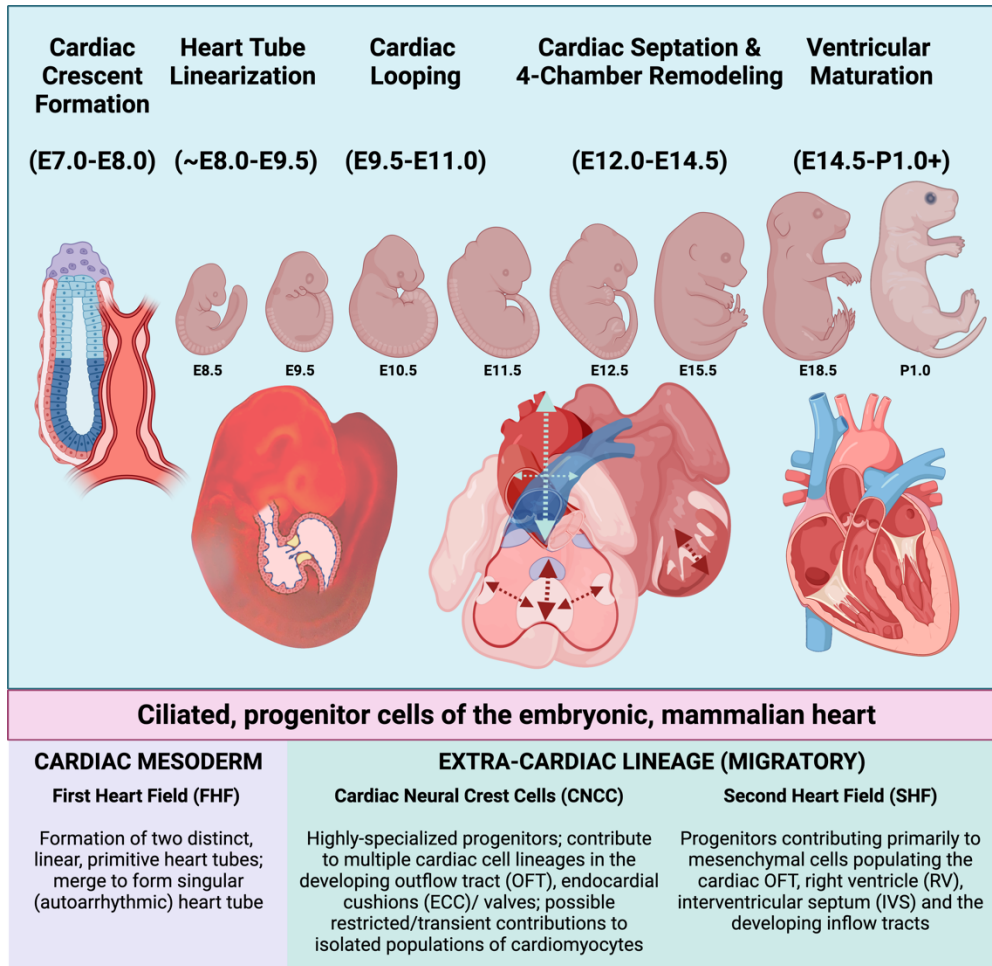


Figure 1.2. Schematic overview of embryonic heart development in the mouse. Embryonic days of gestation (E) are indicated beneath each stage. Progenitor cells of the embryonic, mammalian heart are explained in the following sections.

Here, we present one summary model of murine and human embryonic cardiac development broken down into distinct, transitional phases: Establishment of the cardiac crescent (mouse embryonic day (E) E7.0-E8.0), formation and linearization of the heart tube (E8.25-E9.5), cardiac looping (E9.5-E11.0), four-chamber remodeling (E.12.5-E14.5), and ventricular maturation (E14.5-Perinatal day 1.0). In addition to this overview of the important check points of mammalian heart development, we also summarize the pro-genitor and other differentiated cell/tissue types required to build the healthy heart. Finally, we provide a detailed report describing what is known about

primary cilia of the cell/tissue types contributing to the developing heart, (Figure 1.3) and how damage to these organelles along with aberrations in the Hedgehog signaling pathway are both correlatively and causatively linked to the pathogenesis of congenital heart diseases.

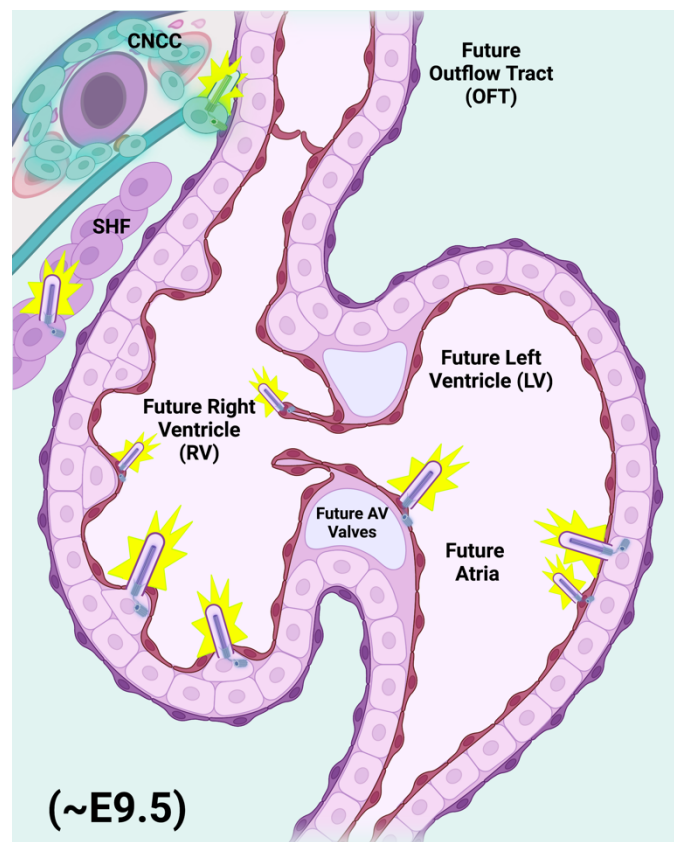


Figure 1.3 Primary cilia within the embryonic heart process Hedgehog signaling that in turn directs heart development. E9.5 embryonic heart depicted undergoing linearization, elongation and folding, prior to septation. A general, representative approximation of the distribution of primary cilia (purple rods) from the CNCC and SHF progenitor populations as well as the endothelial/endocardial cells and embryonic cardiomyocytes within the developing heart chambers.

1.2.2 Establishment of the primitive streak, cardiac crescent and the primitive, heart tube

Early blastocyst formation and subsequent gastrulation phases of development leads to the establishment of three critical germ layers of embryonic tissue, the outer

ectoderm layer, the middle, mesoderm layer (including the hematopoietic, atrial and ventricular cardiac mesoderm), and the inner endoderm layer (Kojima, Tam, & Tam, 2014). The first, formal structural scaffold of the mammalian heart begins approximately seven days into mouse gestation (E7.0) with the formation of the cardiac crescent. Finalization of the cardiac crescent by mouse embryonic day E8.0, envelopes a combination of a more mature, pharyngeal endoderm, and two rapidly proliferating cardiac progenitor populations, the first heart field (FHF) and the second heart field (SHF). The FHF is the first to establish an organized cardiac structure(s) referred to as the primitive heart tubes, which form bilaterally from the cardiac crescent and then merge to form a singular, elongated heart tube by ~E8.0. Contributions from the SHF assist in the early formation of the cardiac outflow and inflow tracts, also visible by ~E8.0 (Meilhac, Lescroart, Blanpain, & Buckingham, 2014).

1.2.3 Linearization of the heart tube, cardiac looping and outflow tract formation

Linearization of the heart tube refers to the merging/elongation of the singular cardiac tube which results in the alignment of the cardiac tube to form the developing cardiac outflow tract (OFT), early right and left ventricles, and primitive right and left atrial chambers by ~E8.5. At this critical stage (~E9.0-E9.25), the developing heart begins to receive contributions from a highly-specialized, migratory group of cardiac progenitor cells known as the cardiac neural crest. Cardiac neural crest cells (CNCC) are a subcategory of neural crest cells which originate from the neural ectoderm, surrounding the dorsal aspect of the developing neural tube (Figure 1.3). CNCC migrate

ventrally toward the developing heart, reaching their primary destination (the cardiac OFT) by E9.5-E10.5. (Figure 1.3, Figure 1.4)

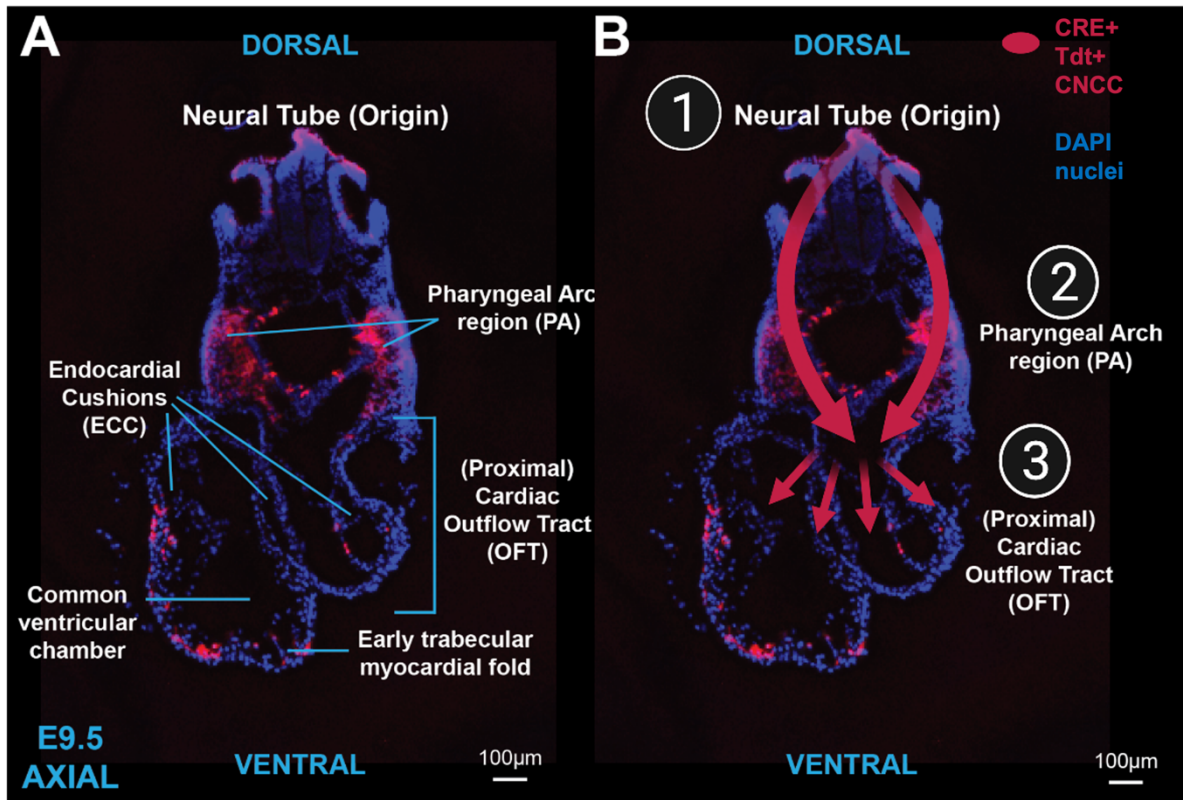


Figure 1.4 The Cardiac Neural Crest. (A-B) The above images depict the developing mouse embryo at E9.5, where all neural crest cells (*Wnt1:Cre+*) are tagged with a fluorescent, Td-tomato reporter (indicated in red). Cardiac neural crest cells are indicated in the central and ventral portions of the embryo, where they can be seen throughout the pharyngeal arches as well as throughout the cardiac region (outflow tract), indicated by the magenta arrows. As a highly-specialized, subpopulation of migratory neural crest progenitor cells, the cardiac neural crest are primarily responsible for migrating ventrally from the neural tube (B1), through the pharyngeal region (B2), and toward the cardiac region beginning around E8.5. CNCC reach the heart ~E9.5 and populate the developing outflow tract ~E10.0 (B3). *Wnt1:Cre+/Tdt+* terminology will be discussed in *Chapter 2, Experimental Design*.

Along with additional contributions from the SHF to the OFT and developing ventricular chambers, the looped heart then undergoes a series of cellular expansions (proliferation) in an elegantly-orchestrated phase of cardiac development referred to as the four-chambered septation phase (Meilhac et al., 2014).

1.2.4 Cardiac septation, four-chamber remodeling, and maturation of the ventricular myocardium

As indicated by name, the septation phase is the phase of cardiac development whereby the previously patent heart tube, becomes physically separated into the four, distinct cardiac chambers characteristic of the adult mammalian heart: the right and left atrial and ventricular chambers which will eventually separate pulmonary from systemic circulation during the early postnatal transition (Dunwoodie, 2007). With proper orientation of the major chambers, the E11.0 embryonic heart begins to undergo septation and four-chamber maturation to form both right and left atrial and ventricular chambers. These segmentations are formed from the endocardial cushions (s), which separate superiorly to form the future interatrial septum, and inferiorly to form the future interventricular septum (Dunwoodie, 2007).

Once the four-chambered heart has been established, the final phase of embryonic heart development involves the compaction and maturation of the ventricular chambers, which also includes angiogenesis of the coronary vasculature along with the formation and organization of the primitive cardiac ventricular conduction system (Gittenberger-De Groot, Bartelings, Deruiter, & Poelmann, 2005). Ventricular maturation and modification of coronary vasculature and cardiac conduction system components continues through the early postnatal period (up to P7.0), due primarily to the abrupt transition from the singular prenatal circulatory network to the more sophisticated and semi-independent pulmonary and systemic circulatory networks characteristics of the postnatal cardiovascular system (Padula et al., 2021; Sedmera, Pexieder, Hu, & Clark, 1998).

1.2.5 Ventricular Maturation and Compaction

The final and arguably most arduous stage of cardiac development occurs in the final stages of gestation, where the muscular, ventricular portion of the heart undergoes a series of morphological changes, most often referred to as “cardiac chamber maturation”. Genetic and/or environmentally-induced congenital abnormalities of the developing ventricular myocardium will differ in phenotype depending on the temporal aspects of such disruptions (Sedmera, Pexieder, Vuillemin, Thompson, & Anderson, 2000). For example, problems occurring during the initial phases of ventricular maturation (i.e. trabeculation) will most often present distinctly, phenotypically different from congenital disruptions occurring the later stages of ventricular development (i.e. compaction of the ventricular myocardium). Specific examples will be discussed in the sections that follow. Of critical, translational relevance, congenital abnormalities of the ventricular myocardium, are highly-correlated with postnatal ventricular arrhythmias in both patients with known CHD as well as in patients with subclinical or undiagnosed aberrancies in ventricular morphology (Towbin & Jefferies, 2017).

1.2.6 Trabecular Emergence & Expansion

Cardiac chamber formation begins earlier on in embryonic development at approximately E9.5, where the common ventricular chamber compartment undergoes the “Emergence” phase of maturation (Moorman & Christoffels, 2003). This stage involves the initial formation of thin, muscular processes termed “trabeculae,” which extend toward the flow of blood through the heart for the purposes of maximizing

cardiac output, providing a mechanism to perfuse and provide nutrients to the developing myocardial cells, and to accomplish these tasks *without* increasing the overall size of the heart itself (Samsa, Yang, & Liu, 2013). One critical aspect of ventricular chamber formation that occurs during trabecular emergence is the organization of CM and associated progenitor populations. More specifically, Sedmera *et al.*, among others (Gustafsson *et al.*, 2005; Samsa *et al.*, 2013; Sedmera *et al.*, 2002; Y. Zhang *et al.*, 2010), have described the organization of cells along the longitudinal axis within individual trabecular projections, is the fact that cells located more towards the lumen of the ventricle are more/further differentiated (mature) than cells which are located more towards the mural aspect (compact ventricular myocardial wall) (Sedmera & Thompson, 2011). This hierarchical arrangement of cardiac chamber progenitors is highly relevant to the context(s)/capacity of cells within the ventricular myocardium to potentially retain their progenitor status. Excessive and/or inappropriate presence of cardiac progenitors (i.e. cells of CNCC, SHF, FHF populations) could theoretically affect the general morphology of the ventricle itself, but also its physiological and regenerative capacity (or not) during the postnatal period (Yamashita, 2016; Y. Zhang *et al.*, 2010). Congenital malformations of the ventricular myocardium at this stage in heart development, are thus almost exclusively characterized by either under-trabeculation or excessive trabeculation (Samsa *et al.*, 2013; Sedmera *et al.*, 2000), also termed “hypertrabeculation”. Mechanistically speaking, prolongation or failure of the trabecular myocardium to cease expanding delays, impairs and/or can completely attenuate consolidation and compaction of the myocardium itself, which affects the subsequent formation and maturation of the coronary vasculature as well as the cardiac conduction

system (CCS)(Ichida et al., 1999; Miquerol et al., 2010), discussed in the sections to follow. Of note, there is still a division in the scientific community regarding the timing and mechanisms of the compaction process, and specifically, whether failure of the ventricle(s) to compact represents a persistence of the expanded trabecular network characteristic of the embryonic ventricular myocardium that was once required for adequate perfusion. The most probable explanation will likely involve a combination of both persistence of embryonic myocardial dynamics as well as mechanistic failures involving a separate and/or codependent series of processes involved in consolidating of the trabecular layer as well as expansion and consolidation of the compact myocardial portion.

1.2.7 Thickening of the Compact Myocardium

Following the emergence and expansion of the preliminary trabecular myocardium, which is completed by approximately E13.0 in the mouse, the latter portion of ventricular maturation is initiated, continuing through embryonic/fetal development up to the first week of postnatal development (Grego-bessa et al., 2007; Sedmera et al., 2000). Thought to be primarily carried out by a tightly regulated communication between the developing endocardium and the ventricular myocardium lying beneath it, compaction of the ventricular myocardium requires a series of dynamic, and still relatively mysterious molecular process (W. Zhang, Chen, Qu, Chang, & Shou, 2013). What is known about ventricular compaction is that the mature, compacted ventricle requires a reduction in thickness of the inner/spongy trabecular myocardium along with expansion and thickening in the outer, compact ventricular myocardium. This is

achieved primarily through a collapsing process which occurs at the deepest point of a trabecular recess concurrently with a proliferative expansion of the compact myocardial and epicardial layers, therefore easing the previously-distinct border between compact and trabecular layers of the ventricle (Samsa et al., 2013). Aesthetically speaking, a cross-section of a properly-compacted ventricle should display a ventricular wall of adequate thickness, where the border between the condensed (compact/outer) and spongy (inner/trabecular) layers are virtually indistinguishable.

1.2.8 Ventricular Compaction and the Formation of the Coronary Vasculature and Cardiac Conduction System

Ventricular compaction is essential for proper cardiac maturation for a number of reasons. Of the most critical, proper ventricular compaction maximizes an adequate volume of cardiac muscle mass, and in particular, muscle mass which is, both functionally and organizationally-speaking, capable of sufficient but also efficient force production (Pieperhoff, Bennett, & Farrell, 2009; Sedmera, Pexieder, Rychterova, Hu, & Clark, 1998; Sedmera et al., 2000; Wessels & Sedmera, 2004). Ventricular contraction in both the pre- and postnatal heart, is the source of muscle force production necessary for pumping blood against the forces of gravity through the entire circulatory network (Krishnan et al., 2014). From the right ventricle, this means pumping blood out to the lungs to receive oxygen via pulmonary circulation. From the left ventricle, ventricular muscle force production must push the oxygenated blood upwards and outwards of the heart itself and through systemic circulation to perfuse working cells, tissues and organs.

In addition to its mechanical capacity, ventricular compaction also serves as a rate-limiting process permitting the proper formation and organization of both the coronary vasculature as well as the cardiac conduction system (especially the ventricular portion). With regards to the development of the coronary vasculature, collapse of the trabecular recess border both permits as well as encourages the invagination and subsequent formation of the endo-myocardial capillary formation, which serves as the vascular pipeline for oxygen and nutrient delivery to the working ventricular CM(Samsa et al., 2013) [Samsa 2013]. Cardiac defects occurring at this stage, are typically characterized by noticeably long and/or thin trabeculae, accompanied by trabecular recesses which protrude noticeably deeper than those observed in a properly compacted (or compacting) ventricular myocardium(Samsa et al., 2013; Sedmera et al., 2000).

Collapse of trabecular recesses are also important to permit proliferation and expansion of the cardiomyocytes present in the compact myocardium. As mentioned in the previous section, the cells present at the distal-most portions (i.e. the mural side) of the trabecular extensions are less-differentiated, more likely to have retained progenitor status and are therefore, more likely to have retained the capacity for more rapid proliferation. Along with proliferation/expansion of compact CMs, there is also a concurrent (though transient) protrusion of the epicardial (outer-most) layer of the ventricle, which forms the major vessels of the coronary vasculature and which is also known to contribute fibrocytes within the compacting myocardial wall (Von Gise & Pu, 2012).

It is known that proper formation and function of the cardiac conduction system is also highly-dependent upon completion of the ventricular compaction process, and in particular, the Purkinje fiber network (PFN) and the peripheral ventricular conduction system (PVCS) components (Samsa et al., 2013). Unfortunately, scientists still cannot agree on the exact origins of the Purkinje-associated conduction cells, and whether they are endocardial, epicardial and/or potentially even myocardially-derived (Liang et al., 2013; Miquerol, Beyer, & Kelly, 2011; Miquerol et al., 2010). What is clear, is the fact that the sheer proximity of PFN and PVCS within the muscular portion of the ventricular wall make it nearly impossible for malformations of myocardium *not* to impact the integrity and function of PFN/PVCS. Of particular relevance, malformations of PFN/PVCS have been closely linked with cardiac phenotypes involving noncompaction of the ventricular myocardium, trabecular disease, and subsequent manifestations of postnatal, cardiac ventricular arrhythmia (Koizumi et al., 2015; Miquerol et al., 2010; Moorman & Christoffels, 2003).

1.2.9 ErbB Signaling in the Developing Ventricular Myocardium

Despite debates within the scientific community on the exact mechanistic dynamics involved in ventricular chamber morphogenesis and ventricular compaction processes, there is a general degree of agreement in the signaling mechanisms most relevant to these processes, most notably, the ErbB signaling pathway in mammals (Crone et al., 2002; Liu et al., 2010; Odiete, Hill, & Sawyer, 2012; Y.-Y. Zhao et al., 1998), summarized in Figure 1.5.

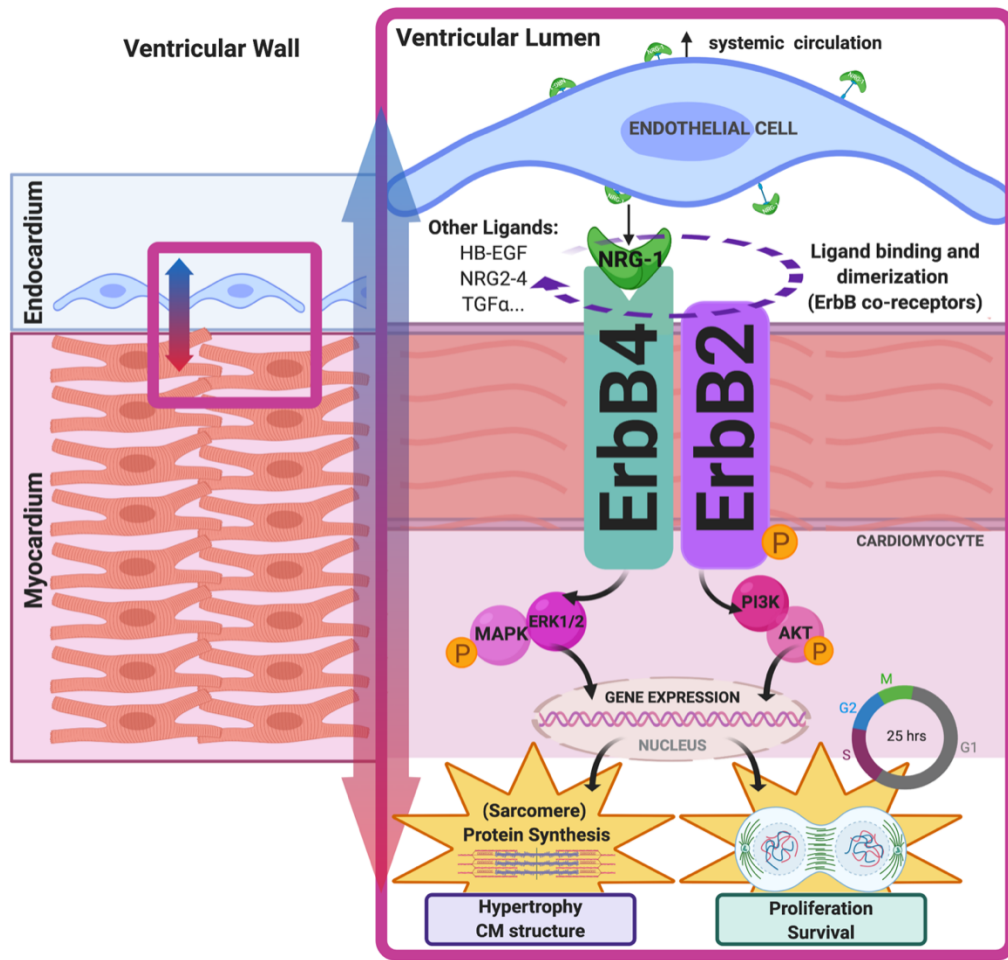


Figure 1.5 ErbB-mediated mechanisms of ventricular maturation and compaction. Cardiac morphogenesis of the ventricular myocardium is dependent upon mechanisms of cell signaling communication between the developing endocardium (EC) and the (ventricular) myocardium beneath the EC. During the compaction process, under normal circumstances, NRG-1 ligand secretion from the inner endocardium, binds to the extracellular, ligand-binding domain of the ErbB4 receptor(s). NRG-1 signaling may also involve activation of ErbB2 receptor, via ErbB2 dimerization with ErbB4. Activation of ErbB signaling mediates proper compaction of the ventricular myocardium via phosphorylation of PI3K/AKT and/or ERK1-2/MAPK, leading to increased synthesis of CM sarcomeric proteins, and increased proliferation and/or survival of embryonic CM.

As previously mentioned, maturation of the ventricular myocardium is primarily characterized by the cell-to-cell communication that takes place between the endocardial and myocardial layers of the ventricle. The dynamics of this interaction rely heavily upon ErbB signaling, where Neuregulin-1 (NRG-1) ligand is produced and

secreted by the single-celled layer of the endocardium, which binds to ErbB2/4 receptors present in CM of the myocardial layer (Figure 1.5). The ErbB2 receptor is of particular interest, as it does not contain the extracellular, ligand-binding domain through which to bind to NRG-1 directly. Instead, ErbB2 activates signal transduction via neighboring ErbB3/4 and EGF heterotrimers (Garratt, Özcelik, & Birchmeier, 2003). ErbB's role in the development of mammalian heart was concurrently identified as primary mediator of anthracycline-induced cardiotoxicity (J. Chen et al., 2012; Unverferth, Magorien, Balcerzak, Leier, & Unverferth, 1983) and, subsequently, trastuzumab-mediated (Bowles et al., 2012; SPARANO, 2001) mechanisms of cardiotoxicity in patients receiving chemotherapy for various forms of breast cancers.

As our understanding of the plasticity and reversibility of ErbB-mediated ventricular disease expanded, much of our mechanistic understanding of ErbB-mediated mechanisms of ventricular plasticity were then better understood in the context of ventricular development and maturation, and vice versa (Odiete et al., 2012; Y.-Y. Zhao et al., 1998). One study in particular, by Staudt *et al.*, used a highly-sophisticated, high resolution imaging modality to study the mechanics, cell behavior and general morphological aspects of trabecular formation and expansion in the developing ventricular myocardium of the mouse (Liu et al., 2010; Staudt et al., 2014). Results from this study substantiated our mechanistic understanding of ErbB2-mediated mechanisms of trabeculation, revealing that loss of ErbB expression (via an ErbB2 knockout model) lead to the formation of fewer trabecular protrusions. However, many aspects of NRG1/ErbB signaling and cardiac chamber maturation remain a mystery, justifying further studies to explore further dynamic aspects of this pathway in both

cardiac development as well as in maintenance of postnatal cardiac tissue and in the pathogenesis of numerous cardiac pathologies involving the ventricular aspects of the postnatal heart.

1.3 Primary Cilia of the Developing Heart

1.3.1 Primary Cilia and Hedgehog Signaling: A Long-Standing History

The best-documented consequence of removing or altering primary cilia function in the body is perturbation of signaling pathways that are dependent on primary cilia, such as the Hedgehog signaling pathway (Figure 1.3, Figure 1.6).

The Hedgehog signaling pathway involves the use of Patched 1 (Ptch1) receptor that is initially located on the primary cilium, where it prevents the Smoothed (Smo) receptor from entering the cilium (Rohatgi, Milenkovic, & Scott, 2007). The binding of Hedgehog to Ptch1 inhibits this repression of the Smo receptor, allowing it to accumulate on the cilium's membrane (Corbit et al., 2005). The loss of a primary cilium from the cell results in a loss of Hedgehog signaling. Activation of the Smo receptor leads upregulation of activator *Gli1*, and therefore activation of the Hedgehog pathway (Robbins, Fei, & Riobo, 2012).

In mammals, there are three members of the Hedgehog gene family: Sonic hedgehog (Shh), Indian hedgehog (Ihh), and Desert hedgehog (Dhh), in contrast to invertebrates, while there is only one known Hedgehog ligand ("Hh")(Pathi et al., 2001). Shh controls left-right asymmetry and development of the lung and heart (Bonnafe et al., 2004; Francis, Christopher, Devine, Ostrowski, & Lo, 2012; Tsukui et al., 1999; X. M. Zhang, Ramalho-Santos, & McMahon, 2001). Ihh mainly functions in the growth and

differentiation of chondrocytes and the development of the endochondral skeleton (Haycraft et al., 2007; Z. Wang et al., 2016; Whitfield, 2008). Dhh is an important element in spermatogenesis and also has a role in the development of the perineural sheath of peripheral nerves (Parmantier et al., 1999; Pathi et al., 2001; X. M. Zhang et al., 2001). The following data together indicate that cardiac cilia and associated Hedgehog signal cascades are clearly essential for normal heart development. The following sections will focus on specific components of the embryonic heart in which primary cilia have been shown to be important. However, many of the developmental and compensatory mechanisms involved in the observed cardiac defects remain poorly understood.

1.3.2 Primary Cilia of the Embryonic Node

Nodal cilia are specialized embryonic cilia that are important in directing laterality of the organs of the thorax and abdomen (Bonnafe et al., 2004). When the cilia are dysfunctional or dysmotile positional defects can be observed, as seen in *Dnaic1* mutants. It has been found that *Dnaic1* mutants display lower rates of situs solitus, and higher rates of situs inversus and heterotaxy (Francis et al., 2012). In the *Dnaic1* mutants with heterotaxy there was also abnormal liver lobation and randomized stomach situs (Francis et al., 2012). In total, the *Dnaic1* mutants showed a range of defects, but the heterotaxy mutants all exhibited structural heart defects including but not exclusive to mispositioning of the OFT. For all the *Dnaic1* mutants there was an observed majority of L-looped hearts, while the normal development of the heart is for dextral looping. Further OFT defects were noted in the *Dnaic1* mutants including

heterotaxy mutants with mispositioning of the aorta and pulmonary trunk as well as abnormal arrangement of the semilunar valves. There were also abnormal ventriculoarterial connections and septation defects noted. The ventriculoarterial defects were only seen in heterotaxy mutants but septation defects were noted in the situs solitus and situs inversus mutants, to a lesser degree than the heterotaxy mutants. Based on the evidence, a role for nodal cilia in proper development can be suggested. While the heterotaxy mutants are not viable postnatally, the situs solitarius and situs inversus mutants are, which provides evidence for a variability in the degree of severity in the defects (Francis et al., 2012). From a clinical and translational perspective, human CHD patient populations with heterotaxy face significantly greater morbidity and mortality risks (Garrod et al., 2014; Nakhleh et al., 2012).

In an analysis of patients with known variations of heterotaxy and primary cilia dyskinesia (PCD), a study found that there were notable ciliary motion defects of the patients with a ciliopathy (Nakhleh et al., 2012; Parmantier et al., 1999). The defects found in patients with PCD were different than those identified with heterotaxy, however. Both showed immotility, stiff or dyskinetic beats, while the heterotaxy samples also showed an incomplete stroke, wavy stroke, and/or an asynchronous beat. Of note, there was one patient in the heterotaxy group who did not have any identifiable cilia at both 5.5 month and 1.4 year of age at examination. Examination with electron microscopy showed no defects in the heterotaxy patients, while ultrastructural defects were found in PCD patients (Nakhleh et al., 2012; Parmantier et al., 1999). Patients with ciliary defects above the age of 6 are more likely to experience respiratory symptoms when they have heterotaxy compared to PCD. It was suggested this difference is both age related and

related to the nature of heterotaxy as neonatal respiratory complications were found only in heterotaxy patients with ciliary dysfunction. Investigators attribute this finding to respiratory complications, such as bronchiectasis are complications that occur over time, and would present when the patient is older (Nakhleh et al., 2012).

1.3.3 Primary Cilia of the Migratory CNCC & Progenitor Populations

In order to investigate mechanisms of CNCC cilia and CNCC-mediated CHD, Willaredt *et al.*, used the cobblestone (*cbbs*) allele to implement a primary cilia hypomorph mouse model where cilia were globally eliminated in the developing mouse heart (Marc August Willaredt et al., 2012). In the *cbbs* allele, expression of a normal IFT88 protein is reduced to 25% of wildtype levels. Examination of CNCC migration in the absence of primary cilia revealed that p75-positive migratory CNCC cells were unaffected by the loss of primary cilia, and were able to populate within the developing pharyngeal arches and cardiac OFT in the *cbbs*^{-/-} mutant animals. By contrast, elaboration of primary cilia was required for subsequent septation and maturation of the developing heart (OFT), where *cbbs*^{-/-} mutants displayed a severe CHD phenotype, including formation of a single OFT (PTA), AVSD, enlarged pericardial sac, dilated atrial chambers, and embryonic lethality by ~E13.5 (Marc August Willaredt et al., 2012). Interestingly, a diverse array of great vessel defects was revealed, including transposition of the great vessels, double aortic arch, and arteria lusoria. Examination of Shh expression revealed no changes in homozygous mutants, but both Gli1 and Ptch1 Hedgehog-pathway readouts were substantially reduced in the pharyngeal

mesenchyme of the mutants, indicating a reduction in Hh signaling (Marc August Willaredt et al., 2012).

1.3.4 Primary Cilia of the Endocardial Cushions

The developing heart valves are referred to as endocardial cushions, because of their sac-like appearance within the developing heart. Over 20 years ago it was reported that mitral valve regurgitation and prolapse are common in patients with polycystic kidney disease type I (Lumiaho et al., 2001). More recent findings have suggested a key role of primary cilia in development of the mitral valve. Firstly, mutations in the Filamin-A gene cause Familial Cardiac Valvular Dystrophy (Matthew Adams et al., 2012; Kyndt et al., 2007). Filamin A turns out to localize to the basal body and works with MKS3 to promote ciliogenesis (Matthew Adams et al., 2012). Secondly, the ciliary protein DCHS1 has been shown to cause mitral valve prolapse in humans (Durst et al., 2015). Thirdly, a series of elegant studies have examined the DZIP1 protein, which localizes to the centrosome (Toomer et al., 2019). Specifically, it has been found that a loss of primary cilia during embryonic development has led to mitral valve leaflet enlargement, characterized by an expansion of the extracellular matrix and histological disruption, present at birth. This led to an adult myxomatous valve pathology comparable to that seen in mitral valve prolapse (Toomer et al., 2019). Crucially, the authors employed both a conditional knock-out of *Ift88* as well as a mouse mutant in the *DZIP1* gene, bearing a mutation seen in patients with mitral valve prolapse, showing a brilliant complementary usage of the two species to elucidate CHDs at the translational level. Interestingly, the Hedgehog ligand controlling this process is Desert hedgehog, marking

a distinct exception to the rule that Sonic hedgehog is controlling most of the processes in cardiac development (Fulmer et al., 2020). The presence of cilia in regards to valve development has been connected to the type of extracellular matrix that was produced, and has been well-characterized by Toomer and colleagues (Fulmer et al., 2020; Toomer et al., 2019). Cilia were specifically found most abundantly where there was proteoglycan-rich regions of extracellular matrix, suggesting a role or connection to the composition of the extracellular matrix during stages of development (Toomer et al., 2019).

There is also evidence that the presence of cilia on the heart valves is key during embryonic development, but that cilia disappear after birth. This work by Toomer *et al.*, (Toomer et al., 2019), in addition to that of Li and colleagues (Y. Li et al., 2015), have further connected ciliopathies identified in murine hearts to human genes. Together along with others, the body of evidence supports a direct role for primary cilia in the pathogenesis of CHD (Burnicka-Turek et al., 2016; Fulmer et al., 2020).

The most common birth defect, and thus also the most common CHD, is a bicuspid aortic valve (BAV), at roughly 1-3% of births. This condition has been associated once before with Joubert syndrome, one of the best studied ciliopathies (Karp, Grosse-Wortmann, & Bowdin, 2012). Primary cilia have been found to be present on the interstitial cells of developing OFT cushions at E11.5 and E13.5 and rarely, on the valve endocardium (Toomer et al., 2017). *Ift88* conditional knockout mice were found to display a BAV phenotype with 68% penetrance, indicating that primary cilia on aortic valves are both present within and play a crucial role in aortic valve morphogenesis (Toomer et al., 2017). The authors demonstrated a unique

spatiotemporal arrangement of cilia on the valves, consistent with what has been previously described to the presence of cilia in areas of low-grade shear stress (Toomer et al., 2017). Interestingly, a later study using genome-wide association protocols in BAV patients revealed single-nucleotide polymorphisms in genes that regulate ciliogenesis through the exocyst, which brings ciliary cargo to the plasma membrane. In humans, defects in this process leads to both BAV as well as valvular stenosis and calcification (Fulmer et al., 2019). Doubtless, mouse models of these mutations will allow for a clear mechanistic explanation of the link between exocyst function and the downstream signal cascades leading to BAV.

1.3.5 Primary Cilia of the Atrioventricular Septa

1.3.5.1 Atrial Septation

Hofmann *et al.* have kept track of the location of Hedgehog-responding cells with time (Hoffmann, Peterson, Friedland-Little, Anderson, & Moskowitz, 2009). Their data show a migration of the Hedgehog-receiving cardiac progenitors from the posterior second heart field splanchnic mesoderm into the atrial septum between embryonic ages E9.5 and E11.5 (Hoffmann et al., 2009). Further observations in the cardiac OFT have revealed that, again between the ages of E9.5 and E11.5, migration of Hedgehog-receiving cardiac progenitors occurs from the pharyngeal mesoderm into the pulmonary artery. In the same study, mice with a conditional allele of *Smo* were used in order to investigate the importance of Hedgehog signaling in atrial septation. Deletion of *Smo* in Hedgehog-responding heart progenitors with a tamoxifen-inducible *Gli1::Cre* transgene revealed that all mutant embryos showed ASD and atrioventricular septal defects

(Hoffmann et al., 2009). Together, these results are in keeping with the ASD seen in the *Shh* knock-out (Smoak et al., 2005) and *Ift88* hypomorph (Marc August Willaredt et al., 2012), but not with the VSD seen in *Shh* (Smoak et al., 2005), *Ift88* (Marc August Willaredt et al., 2012), or *Pkd1* and *Pkd2* (Boulter et al., 2001; Wu et al., 2000) mutant mice.

1.3.5.2 Ventricular septation

Ventricular septation defects are not only the most common CHD but one of the most common congenital defects known to our species. VSDs have been recorded in many cilia mutants in the mouse (Koefoed et al., 2014), and we will focus only on two examples here. It has been found that a mutation in *Dnah11* (the *Dnah11avc4* allele) caused atrioventricular septal defects (AVSDs) (Burnicka-Turek et al., 2016). Mutations in the *Mks1* gene have also been found to cause AVSD. Data shows that *Dnah11* signaling did not occur in the second heart field or the heart tube (Burnicka-Turek et al., 2016). *Mks1* signaling was identified in the second heart field and mutant embryos had decreased expression of Hedgehog signaling. This suggests that cilia have a role in proper atrioventricular septal development and left/right symmetry formation. Data was also suggestive that it is specifically primary cilia that are required for Hedgehog signaling in the second heart field (Burnicka-Turek et al., 2016).

Investigations into the cilia-exclusive protein *Fantom* (*Ftm*) revealed that *Ftm*^{-/-} mutant mice showed ventricular septal defects as well as thinner ventricular septal myocardium, and no membranous lining in the ventricular septum (Gerhardt, Lier, Kuschel, Rü, & Rütger, 2013). It was found that there were no cilia present in the

ventricular septum from E10.5 to E12.5, but there were also no observed atrial septal defects between the *Ftm*^{-/-} and WT mice. A downregulation of Shh was found, but data suggests that *Ftm* is signaled downstream of Shh (Gerhardt et al., 2013). The *Pdgfr*-alpha signaling pathway was also identified, but data are suggestive that Shh mediates *Pdgfr*-alpha signaling. Investigators also noted that *Ftm* genetic mutations in humans have been observed in various ciliopathies, including patients with Meckel-Gruber syndrome, Joubert syndrome and nephronophthisis (Gerhardt et al., 2013). This data suggests that cardiac primary cilia have a role in ventricular septum development and is mediated through Shh signaling.

1.3.6 Primary Cilia of Cardiac Fibrocytes

Primary cilia have been suggested to have a key role in fibrosis of the heart (Villalobos et al., 2019), but the lineage of the necessitates additional confirmation. While primary cilia are present in fetal murine hearts as early as E9.5, and as late as E15.5, there is evidence to suggest that primary cilia elaborations present do not necessarily correspond to cardiomyocytes. This finding has been replicated in fetal rat hearts as well, suggesting that the role primary cilia have in development involve a different cell type. Villalobos *et al.*, exposed adult, infants, and neonatal rodent hearts to myocardial injury in order to further examine how the collective ventricular myocardial cells/tissue, respond to ischemic injury (Villalobos et al., 2019). A 45-minute bout of experimentally-induced ischemia followed by reperfusion, revealed a transient increase in ciliated fibroblasts when compared to the control group. Similarly, when 7-day old mice were given an apical resection surgery there was an observed increase in ciliated

cells 7 days post-operation. It was confirmed that these ciliated cells were not cardiomyocytes. Similar investigations post myocardial infarction of adult murine hearts showed similar findings as well as a suggestion that the increase in cilia is originating from an increase in fibroblasts present in the proliferative healing phase (Villalobos et al., 2019). Similar results were replicated in rat hearts as well as a suggestion that the PKD1, PKD2, and KIF3A proteins are localizing to neonatal rat cardiac fibroblasts. These results all suggest a diverse role of primary cilia in both development and further in wound repair of the post-embryonic heart as well. There was also evidence to suggest that the proteins PKD1 and KIF3A are required for TGF β -1 induced collagen biosynthesis showing a specific functional role for the primary cilia (Villalobos et al., 2019).

1.3.7 Primary Cilia of the Endocardium

Primary cilia have vital roles in heart development, including allowing different areas of the embryonic heart to communicate and coordinate appropriately. It has been established that the signaling interactions between the endocardium and the myocardium in later development contributes to proper development of the heart valves and the trabeculation of the ventricles (Saint-Jean et al., 2019). Different signaling pathways, including the bone morphogenic pathway, are involved in this communication. Many of these pathways are directly dependent on primary cilia for proper functioning. Endocardial cells are defined as specifically-localized endothelial cells; they express proteins that make them identifiable as endocardial cells, including CD31, fibronectin, and NFATc1(Nakhleh et al., 2012).

Endocardial cells, specifically, have been found to send regulating signals to the myocardium which affect the growth and maturation (Artap et al., 2018). Specifically, the signals sent from the endocardium have been found to have key roles in the development of ventricular trabeculations. It has been found that the Notch ligand, transcribed in the ventricular endocardium, is key to proper trabeculation in zebrafish. It is the endocardium-specific notch1b, which requires the presence of primary cilia, that induces the downstream expression of ephrinb2a and neuregulin (Artap et al., 2018; Samsa et al., 2013). These proteins together are key regulators of trabeculation in zebrafish (Artap et al., 2018; Samsa et al., 2013).

The primary cilia specific to cardiomyocytes and the developing heart are known as cardiac primary cilia. The cardiac primary cilia are involved in regulating signaling pathways which influence differentiation, morphogenesis, and the maturation of the heart. Throughout heart development, the primary cilia emerge in different tissues according to the embryonic time point. At embryonic day E9.5, the primary cilia line the endothelium of the atria primordia, endocardial cushions, and what will form into the trabeculations of the ventricles (Koefoed et al., 2014). E 12.5 is a timepoint where primary cilia are found in both the epicardium and in the endocardial cushion's mesenchymal cells. At this timepoint the once ciliated atria primordia begin to de-ciliate with the endothelium lining of the endocardial cushion completely de-ciliated. The trabeculations of the ventricles are still ciliated at this time (Koefoed et al., 2014).

It has been shown that the loss of Smo results in severe heart defects that suggest a vital role of Hedgehog signaling in heart development (Samsa et al., 2015; X. M. Zhang et al., 2001). It has been documented that mutations in Shh led to

developmental defects in the OFT and right ventricle. These defects are known to cause septation defects and a common ventricular outlet (Samsa et al., 2015). It has also been found that *Ihh/Shh* double mutants have heart defects that are more severe than the mutants with just a *Shh* knockout (Smoak et al., 2005). This finding suggests that *Ihh* and *Shh* have a combined role in the development of the heart. In addition, Hedgehog signaling is necessary for neural crest cell survival in the pharyngeal region, for OFT septation, and in the pharyngeal endoderm to regulate signals influencing second heart field survival (Rochais, Mesbah, & Kelly, 2009).

1.3.8 Primary Cilia of the Ventricular Myocardium

Primary cilia have been documented and visualized in nearly all eukaryotic cell types (Wheatley, Wang, & Strugnell, 1996). Primary cilia of terminally differentiated, adult ventricular cardiomyocytes, on the other hand, are a cell type whose ability to elaborate a primary cilium remains a topic of much ongoing debate (Villalobos et al., 2019). Primary cilia of murine, embryonic atrial and ventricular cardiomyocytes has been relatively well-documented using primary antibodies against primary cilia-specific proteins like *ARL13B*, *Ift88* and Acetylated alpha-tubulin and visualized with immunofluorescence microscopy (Diguet et al., 2015; Wheatley et al., 1996). However, the appearance and number of cilia present in the ventricular myocardium appears to shift dramatically in the early-postnatal period (Diguet et al., 2015). There seems to be a pronounced loss in ciliation of ventricular cells following the first week of life, whereas a “resurrection” of cilia appears to occur in response to ischemia, hypoxia, and

mechanical stress and/or changes in hemodynamics associated with disease and aging (Hoffmann et al., 2009; Villalobos et al., 2019).

The presence, length, orientation and integrity of primary cilia can be highly transient in nature, and can vary greatly by species, tissue and cell and type. Importantly, these factors can also be highly varied in embryonic vs postnatal tissue, in healthy vs disease states, and can present a significant challenge to visualizing and/or confirming the presence of primary cilia of ventricular cardiomyocytes (Diguët et al., 2015). In general, ciliogenesis of the primary cilium in mammalian cells can vary highly, but generally begins during the G0 (quiescence) or G1 (cell growth) phase, where elongation of the primary ciliary axoneme continues through the S stage (DNA synthesis) stage of the cell cycle, or until the duplication of the centrosome components of the basal body have completed and prior to entry into the M phase (mitosis), during which the cilium is resorbed (L. X. Li & Li, 2021). As dictated by the fundamental ciliary ultrastructure, the anchoring of the primary cilia axoneme to the cytoplasm is maintained by the basal body complex, which is composed of both mother and daughter centrioles. This means that, prior to cell division, the cilium must be dis-assembled. However, “disassembly” of the primary cilium involves multiple biological processes, but occur primarily via absorption of the primary cilium via expulsion/”shedding of” the axoneme and/or ciliary tip (“cap”) into the extracellular space (Mirvis, Siemers, Nelson, & Stearns, 2019). Thus, in more ways than one, the primary cilium is a key mediator of the cell cycle itself. However, in a population of cells that is post-mitotic and terminally differentiated, rapid cell division is not typically a feature of the mature ventricular myocardium following embryonic development and maturation.

Because of the well-documented capacity of the primary cilium to function as a mechanosensory organelle in the articular cartilage of bone (Whitfield, 2008), kidneys (Hofherr & Köttgen, 2016; Mirvis et al., 2019; Praetorius & Spring, 2001), and as sensors of sheer stress in arterial vasculature (Nauli et al., 2013), consideration for a mechanosensory role of the primary cilium in ventricular cardiomyocytes and their neighboring cell types is a concept that seems not only feasible, but likely (Pala, Jamal, Alshammari, & Nauli, 2018). Investigations looking into the relevance and susceptibility of the embryonic ventricular myocardium to mechanical stimuli performed in chick (Ma et al., 2016; Pala et al., 2018), mouse (Goenezen, Rennie, & Rugonyi, 2013; Sedmera, Pexieder, Hu, et al., 1998), and zebrafish (Samsa et al., 2013; Sedmera, Pexieder, Hu, et al., 1998) embryonic model organisms has provided ample evidence to support a significant role for the biomechanics of embryonic blood flow (hemodynamics), as well as for primary cilia themselves, in helping to shape and promote adequate maturation in the healthy ventricular myocardium (Ma et al., 2016; Paige SL, Plonowska K, Zu A, Paige, Plonowska, Xu, & Wu, 2015; Slough et al., 2008). In the embryonic mammalian heart, primary cilia have been observed in ventricular cardiomyocytes of both rat and mouse model organisms (Diguët et al., 2015; Lindsey, Butcher, & Yalcin, 2014). Primary cilia have also been documented in cardiomyocytes of the developing zebrafish heart (Samsa et al., 2015). Primary cilia of human cardiomyocytes remain a topic of ongoing debate. At present, it is known that human embryonic stem-cell derived cardiomyocytes elaborate primary cilia *in vitro* (Vestergaard et al., 2017), and that human postnatal cardiomyocytes in individuals with existing cardiovascular disease can display primary cilia (Fulmer et al., 2020; Toomer et al., 2019). However, differentiating the capacity of

an adult postnatal cardiomyocyte to elaborate a primary cilium from the actuality of adult cardiomyocytes utilizing the sensory functions unique to this specialized organelle remains unclear, and should be considered in future investigations.

Recent work by Villalobos *et al.*, (Villalobos et al., 2019) provided a thorough analysis of primary cilia present in the ventricular myocardium, where the authors observed the presence of cilia in the neonatal and adult heart. Despite this, further analysis led the authors to conclude that cilia were only elaborated from cardiac fibroblasts, and not from cardiomyocytes them-selves. However, although less abundant in number, cardiac fibroblasts and their primary cilia were shown to be essential for mediating appropriate fibrosis and cardiac remodeling to preserve/optimize cardiac structure/function in the context of aging and disease. Specifically, polycystin 1 (PKD1) exclusive to primary cilia of cardiac myofibroblasts, was shown to initiate appropriate fibrotic cellular responses like activation of transforming growth factor β -1 (TGF- β -1)-SMAD3 activation, production of extracellular matrix proteins, and maintenance/preservation of myocardial contractility following myocardial infarction cardiac injury (Villalobos et al., 2019).

1.4 Hedgehog Signaling Pathway in Cardiac Development and Pathophysiology

Hedgehog ligands function as potent and effective morphogen/growth factor for healthy heart development. Both primary cilia and Hedgehog signaling function as independent and co-dependent mediators of mammalian heart development (Figure 1.3, Figure 1.4). However, because of the dynamic nature of this growth factor, Hedgehog gradients and signaling threshold must be carefully and temporally regulated

at the level of the primary cilium. Regulation of Hedgehog thresholds involves consideration for short and long-range acting capacity of the ligand, resilience nature/preservation of this pathway, and also the type of pathway utilized (i.e. canonical vs noncanonical). Because primary cilia and Hedgehog signaling play such a critical role in the development and maturation of the mammalian heart, the potential capacity for activation and repression of Hh signaling and primary cilia of different cardiac cell populations may offer novel mechanistic insights into cardiac congenital and acquired disease pathogenesis, as well as the potential for innovative therapeutic targets in the detection, treatment, and prevention of both CHD and acquired cardiovascular disease.

1.4.1 Canonical vs. Noncanonical Hedgehog Signaling

Although the complexities of the developing mammalian heart require multiple combinations of local and circulating growth factors at multiple, cell type- and cell fate-specific timepoints, Sonic Hedgehog (Shh) continues to be one of the primary mitogens critical to multiple aspects of mammalian heart development. Genetic and functional aberrancies in Hedgehog pathway genes independent from and along with protein expression profiles have been closely linked with nearly all anatomical manifestations of CHD, including OFT defects, atrio-ventricular septal defects, cardiac arrhythmia, cardiac hyperplasia and multiple cardiomyopathies (Fulmer et al., 2020; Günthel, Barnett, & Christoffels, 2018). Shh functions as a unique growth factor, in the sense that the biological effects of the ligand's activity are not only con-textually dependent, but are also highly sensitive to deviation from normal gradients (Caspary, Larkins, & Anderson, 2007). Both overexpression/upregulation as well as under-expression/downregulation of

the Hedgehog signaling pathway components lead to the propose that Hedgehog requirements of the developing heart are so tightly mediated, that proper heart development requires what we describe as “a Goldilocks Phenomenon.” Hedgehog thresholds (like porridge in the fairy tale) are required in a dosing capacity that is “just right” for the circumstances of a given moment. In other words, too much Hedgehog (e.g. Hh overexpression, *GoF*, etc.) leads to the formation of CHD. Too little Hedgehog also results in CHD. Thus, building a healthy heart requires an elegant titration of Hh signaling to meet the near-instantaneous cellular and tissue demands of embryonic tissue.

The Hedgehog gene/signaling pathway was first discovered in *Drosophila melanogaster* 45 years ago, where fruit fly embryos with mutations in the Hedgehog gene failed to develop correctly, lacking wings and properly organized denticles (E. B. Lewis, 1978). The disorganized and bunched-up denticles closely resembled the morphology of the spikes on a hedgehog, and the Hedgehog gene family was eventually determined to be important mediator genes involved in the tissue patterning, polarity, and laterality of nearly all metazoan embryos (Wood et al., 1980). Subsequent discoveries revealed three Hedgehog genes in mice and humans, including Shh, Desert Hedgehog (Dhh) and Indian Hedgehog (Ihh) homologues. In mammals, Dhh expression remains restricted to a few tissue types [40]. Indian hedgehog is primarily expressed in chondrocytes and is a known mediator of bone and cartilage development (Haycraft et al., 2007; Z. Wang et al., 2016; Whitfield, 2008).

Like many growth factors critical to development, the Shh signal cascade can be categorized broadly into canonical and noncanonical mechanisms. Canonical Shh

signaling involves secretion of the ligand from one cell and activation of the Hedgehog signaling cascade when Shh binds to one of its receptors, Patched-1 (Ptch1), located on the axoneme of the primary cilium on an adjacent cell (Rohatgi et al., 2007). Upon binding/activation, Ptch1 translocates just outside the base of the primary cilium, permitting its co-receptor, Smoothed (Smo), to translocate up within the primary cilium (Corbit et al., 2005), where a downstream family of glioma-associated (GLI) transcription factors acts to further activate or repress variety of biological processing including proliferation, differentiation, polarity/organization and migration within the cell itself (Figure 1.6) and/or of neighboring cells/tissues (Alexander et al., 2019; Echelard et al., 1993).

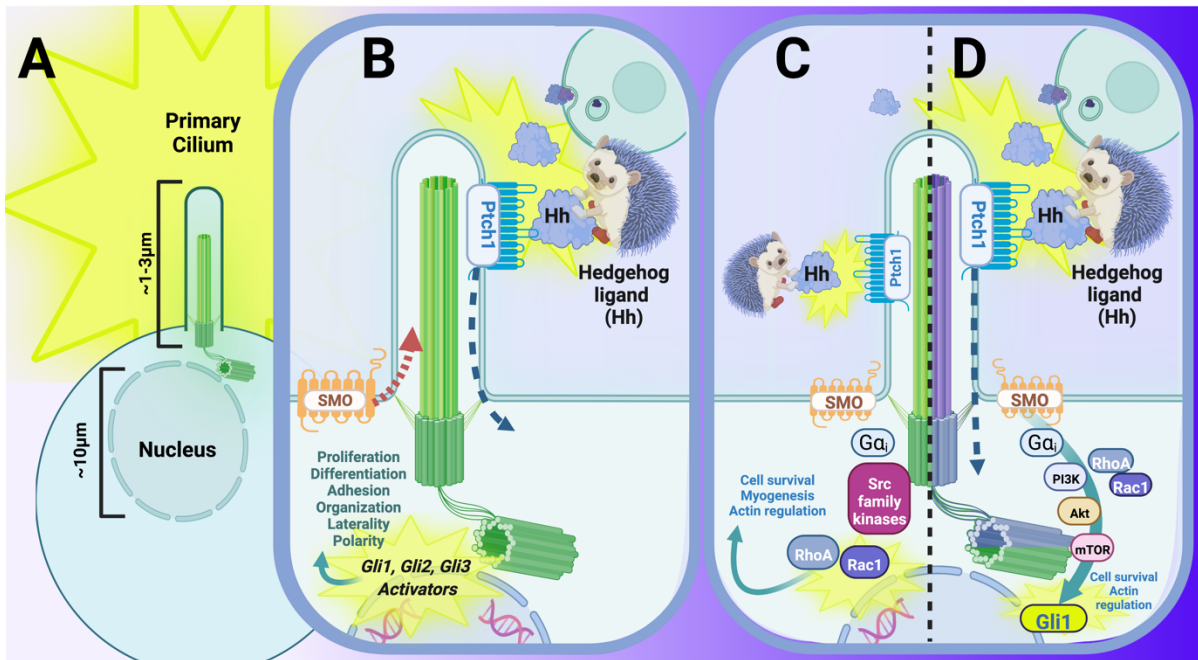


Figure 1.6 The primary cilium and its interaction with canonical and noncanonical Hedgehog (Hh) signal transduction is critical to many aspects of the developing mammal and maintenance of postnatal mammalian tissue. **(A)** Primary cilia extend approximately 1-3 micrometers (μm) into the extracellular environment and function as a highly specialized sensory organelle which interpret changes in the surrounding environment in nearly all mammalian cell types. **(B-C)** The Hh signaling pathway is the pathway most-closely associated with, and potentially dependent upon an intact primary cilium in mammals. **(B)** Traditional (canonical) Hh signaling involves the secretion of Hh ligand from a Hh-secreting cell, which is received by Patched-1 (Ptch1), a 12-pass transmembrane receptor. Binding of Hh ligand to Ptch1 initiates a conformational change which leads to translocation of the Hh-Ptch1 complex just outside of the ciliary axoneme while also permitting its 12-pass transmembrane co-receptor, Smoothed (SMO), to translocate within the ciliary axoneme. Permissive relocation of SMO into the primary cilium concurrently allows Gli activators to enter into the nucleus for transcriptional activation and/or further upregulation of Hh signaling. **(C-D)** Noncanonical pathways for Hh signaling are best-characterized by their functions independent from either a traditional Hh receptor (or co-receptor; e.g. via SMO/Cdo; **C/Type I Noncanonical**), Hh functioning independently from one (or all) of the Gli transcription factors **(C)**, or a non-traditional route of activating Gli targets **(D, Type II Noncanonical)**. **(C)** One example of noncanonical Hh signal transduction can occur in the presence of Hh ligand, where activation of the pathway is achieved via SMO and Hh coreceptors CDO, BOC and GAS1, and the subsequent initiation of RhoA/Rac1-mediated mechanisms of proliferation, cell adhesion and/or migration. **(D)** Another example of noncanonical Hh is brought about in the presence of Hh ligand, where binding to Ptch1 activates a SMO-mediated, G-protein coupled receptor-like activation of PI3K (via G α i) and the subsequent initiation of Gli1 transcriptional activation.

The Hedgehog co-receptor, SMO, is classified as a member of the Frizzled family of G-protein coupled receptors (GPCRs; Class F) (Alexander et al., 2019). The SMO protein contains several components characteristic of GPCRs, including seven

transmembrane domains, an amino-terminal cysteine rich domain, three intra- and extra- cellular loops, and an intercellular carboxyl-terminal tail. These features enable SMO GPCR signaling, with an expanding understanding of regulatory contributions from alternate functional domains beyond the post-translational modification potentials of the SMO carboxyl tail.

Noncanonical Hedgehog signaling, by contrast, describes activation of Shh in the absence of the activation of GLI transcription factors, also known as “the Gli-independent responses (Brennan, Chen, Cheng, Mahoney, & Riobo, 2012),” which can be further broken down into Type 1 and Type 2 two subtypes (Figure 1.6, C-D). Type I noncanonical Hedgehog signaling (Figure 1.6, C) is described as activation of the Hedgehog/GLI pathway independent of the Ptch1 receptor, potentially via CAM-related/downregulated by oncogenes (CDO), brother of CDO (BOC) and/or Growth arrest-specific-1 (GAS1) (M. H. Jeong et al., 2016). This particular route of Hedgehog activation is relevant given that BOC, CDON, and GAS1 have been shown to promote cardiogenesis in pluripotent stem cells (M. H. Jeong et al., 2016), (Figure 4, Ci), and may also play co-mediator roles in regulation of the pathways critical to apoptosis, CREB/ERK/GPCR, and general promoters of myogenesis and axon guidance (Allen, Tenzen, & McMahon, 2007; Martinelli & Fan, 2007; Sigafos, Paradise, Fernandez-Zapico, & Stecca, 2021; Tenzen et al., 2006). While noncanonical Hedgehog signaling is less critical during embryogenesis, this is often the signaling cascade involved in disease initiation and progression, and reactivation of developmental regulatory pathways (Pietrobono, Gagliardi, & Stecca, 2019; Sigafos et al., 2021). Specifically, upregulation of the Hedgehog signaling pathway and activation of the GLI transcription

factors independent of both SMO activation and even of the ligand itself, has been previously identified as one of the primary drivers of disease (Pietrobono et al., 2019; Sigafos et al., 2021).

Type 2 noncanonical Hedgehog signaling is dependent on SMO, but not on activation of GLI transcription factors to carry out a specific biological response (Figure 4, D). Rather, Hedgehog ligand binding to PTCH1 activates the functional GPCR properties of SMO, where its heterotrimeric Gi proteins are responsible for the downstream activation of phosphoinositide 3-kinase (PI3K), Ras homologous family member A (RHOA) and Ras-related C3 botulinum toxin substrate 1 (RAC1) (Polizio, Chinchilla, Chen, Manning, & Riobo, 2011) (Figure 4, D).

The data discussed in the following sections indicate that cardiac cilia and associated Hedgehog signal cascades are clearly essential for normal heart development. The individual sections will focus on specific components of the embryonic heart in which primary cilia have been shown to be important. However, many of the developmental and compensatory mechanisms involved in the observed cardiac defects remain poorly understood. Broadly speaking, type-2 noncanonical Hedgehog signaling is dependent on Smo, but not on activation of Gli transcription factors to carry out a specific biological response. Rather, Hedgehog ligand binding to Ptch1 activates the functional GPCR properties of Smo, where its heterotrimeric Gi proteins are responsible for the downstream activation of Phosphoinositide 3-kinase (PI3K), Ras homologous family member A (RhoA) and Ras-related C3 botulinum toxin substrate 1 (Rac1), (Polizio et al., 2011).

1.4.2 Hedgehog Signaling and Progenitor Cells of Mammalian Heart Development

Shh serves multiple influential but also critical roles in the developing mammalian heart that can be categorized further into extracardiac and intracardiac mechanisms of action (Robbins et al., 2012). Early expression of Shh most relevant to heart development is seen during early somite formation (E8.0; 8 days post coitus) and by E9.5, Shh expression can be seen along the dorsal aspect of the head/future spine. At this stage, Shh expression extend anteriorly along the ventral midline and within the prechordal plate mesoderm (pharyngeal mesoderm), (Martí, Takada, Bumcrot, Sasaki, & McMahon, 1995). From an axial perspective, Shh expression can be seen primarily along the floor plate of the murine notochord (future spinal cord), just dorsal to the cardiac region of the mammalian embryo (Martí et al., 1995). Production and secretion of Shh ligand from this region then expands, concentrating within the pharyngeal arches (and specifically, the endodermal portion), subsequently extending a Shh gradient spanning from the pharyngeal endodermal region to the more the ventral aspect of the cardiac region of the developing embryo (Caspary et al., 2007; Goddeeris, Schwartz, Klingensmith, & Meyers, 2007).

Following formation and elongation of the primitive heart tube, Sonic hedgehog ligand is produced and secreted from the pharyngeal endoderm of branchial arches 3, 4, and 6. From the extensive studies of Shh and its influence on neural progenitors (Robbins et al., 2012), we know that Shh produced in this region is strategically positioned to help guide the migratory path, proliferation, polarity and differentiation of the cardiac neural crest cells (CNCC) on their way to populate the OFT of the developing heart (Epstein et al., 2000).

CHD is a known consequence when the pharyngeal Shh gradient deviates from the norm or if the ability of the migratory CNCC to recognize and response to Shh is damaged, by downregulation of primary cilium function, for example (Clement et al., 2009; Dyer & Kirby, 2009; Meilhac & Buckingham, 2018). Smoak *et al.*, provided an early characterization of the cardiac phenotype resulting from the conditional elimination of Shh from CNCC using the Tg(P0-Cre)1Ky Cre driver, which drives recombination in migratory neural crest progenitor cells (Smoak et al., 2005). Given the temporal aspects of this Cre driver, investigators were able to focus primarily on early OFT formation (E8.5-E10.5). Authors demonstrated that at this earlier stage, Shh did not act directly on CNCC progenitors, and specifically, acted to restrict/refine the expansion of neural crest populations to that of the cardiovascular and craniofacial domains (Smoak et al., 2005). This phenomenon contrasts from what we know about Shh's potential to act directly on differentiated CNCC, where Shh does act directly on these cells to promote cell survival and proliferation during the later stages of heart and OFT development (>E10.5-E12.5), (Smoak et al., 2005). In a subsequent series of experiments, Goddeeris *et al.*, confirmed that Shh produced in the pharyngeal endoderm was required to direct CNCC to survive and proliferate within the endocardial cushions of the developing OFT (Goddeeris et al., 2007). More specifically, conditional elimination of Shh from Nkx2.5+ cells of the secondary heart field (SHF; formerly Anterior heart field 'AHF') not only led to loss of *Shh* mRNA and Shh expression from the pharyngeal endoderm, but also subsequently led to failure of the OFT to septate, resulting in formation of a singular OFT CHD known as persistent truncus arteriosus (PTA), (Goddeeris et al., 2007).

Concurrently with CNCC, cellular influxes from the secondary heart field (SHF) begin to populate the dorsal and inferior aspects of the embryonic heart, including the OFT and right ventricular chamber as early as E10.5 (Meilhac & Buckingham, 2018). In these complimentary and similarly migratory population of progenitor cells, Shh produced/secreted from both the pharyngeal endoderm and possibly, the pharyngeal mesoderm, functions to maintain an appropriate balance of proliferation (Briggs et al., 2016; Christ, Marczenke, & Willnow, 2020; Dyer & Kirby, 2009). Specifically, SHF cells present within the OFT and right ventricle differentiate into cardiomyocytes vascular smooth muscle cells which require Shh to direct appropriate levels of proliferation during the expansion, elongation and septation of both OFT and ventricular portions of the heart (Dyer & Kirby, 2009). Goddeeris *et al.*, demonstrated that by conditionally eliminating Shh from *Nkx2.5/Cre+* (SHF) expressing cells, there was a noticeable disruption to both endocardial cushion formation as well as the subsequent ability of these cells to communicate with cardiomyocytes derived from the first heart field (FHF), (Goddeeris et al., 2007). Taken together with subsequent experiments, investigators concluded that Shh produced internally within the dorsal mesocardium as well as Shh produced in the dorsal mesenchymal protrusions (“extracardiac”) were both required for cellular processes and communications necessary for OFT and atrial formation and septation (Balaskas et al., 2012; Meilhac & Buckingham, 2018).

One key regulator of both Shh and progenitor cell contributions in the developing heart is the low-density lipoprotein receptor related protein-2 (LRP2), a multi-ligand receptor that is highly expressed throughout the developing OFT in a specialized niche of cardiac progenitor cells in SHF (Christ et al., 2020). Under normal circumstances,

LRP2 expression in these SHF cells promotes sustained progenitor cell fate, which is required for complete septation of the cardiac OFT. In LRP2-deficient mouse embryo experiments, loss of LRP2 led to premature differentiation of Shh-dependent progenitor cells into cardiomyocytes within the OFT. Loss of Hedgehog sensitivity in these cells combined with inappropriate differentiation led to shortening of the OFT, which developed fully into a common arterial trunk CHD in mutant hearts (Christ et al., 2020).

1.4.3 Hedgehog Signaling in Pre- and Postnatal Cardiomyocytes

Despite current debates regarding the presence, role, and distribution of primary cilia found in ventricular myocardium, an expanding body of literature supports a role for Shh in the proliferation and tissue homeostasis of both pre- and postnatal ventricular myocardial tissue. From the early stages of heart development, short and long-range Hedgehog signaling gradients are required for proper migration and differentiation of cardiac progenitor cells, including maintenance of progenitor status and appropriate proliferative responses of cardiac neural crest and second heart field cell populations (Abdul-Wajid, Demarest, & Yost, 2018; Briggs et al., 2016; Tang, Martik, Li, & Bronner, 2019). Although CNCC contribution to the ventricular myocardium is accepted in the zebrafish model organism (Bookman, Redmond, Waldo, Davis, & Kirby, 1987; Kelly, Buckingham, & Moorman, 2016), it is widely debated whether this phenomenon is consistent across mammalian species (Cheng et al., 2018; Goenezen et al., 2013; Hoffmann et al., 2009). SHF contributions to the ventricular myocardium have long-since been confirmed (Meilhac & Buckingham, 2018; Torrisi et al., 2021). Later in cardiac development, Hedgehog signaling has been identified as a primary regulator of

both atrial and ventricular septation processes, both of which must be fully septated in order to achieve and isolate right-heart (future pulmonary circulation) from left heart (systemic) circulation networks (Goddeeris et al., 2008).

Hedgehog signaling-based mediation of the electrophysiology of postnatal cardiomyocytes has also been documented, where upregulation of Hedgehog signaling via Smo can reduce potassium sensitivity and function in cardiomyocytes (Cheng et al., 2018). Decreased potassium sensitivity can lead to prolongation of the cardiac action potential duration, subsequently predisposing ventricular cardiomyocytes to life-threatening forms of ventricular arrhythmias (Cheng et al., 2018). In addition to Hedgehog effects on cardiomyocyte-selective ion transport, it is also possible that Hedgehog signaling changes during heart development may also affect the integrity and organization of gap junction proteins like Connexin-40 (Cx40) and Connexin-43 (Cx43), both of which are critical for propagation of cardiac action potential within the distal, ventricular portions of the cardiac conduction system (Kirchhoff et al., 2000). Although the majority of evidence to support this hypothesis has primarily been documented in chondrocytes/bone (Wann et al., 2012) and neural tissue (Torrissi et al., 2021) outside of the heart, the influence of Hedgehog signaling pathways on formation, patterning and integrity of Connexin gap junction proteins in cells and tissues most relevant to cardiac function continue to support the feasibility of this hypothesis (Kawagishi et al., 2018; Paulis et al., 2015).

In addition to Hedgehog influence on the cardiac electrophysiological structures and function, there continues to be a growing interest in the potential roles for Hedgehog in pathogenesis and/or remediation of ischemic cardiac injury (Y. Wang, Lu,

Zhao, & Sheng, 2017). Paulis *et al.*, demonstrated that upregulation of the Shh pathway via multiple pharmacological interventions prior to induced ischemia-reperfusion injury resulted in a pronounced reduction in size and arrhythmogenic capacity of the resulting cardiac infarct (Paulis et al., 2015). The authors concluded that supplementation with Shh ligand prior to this model of ischemic injury, via increase of cardiomyocyte potassium sensitivity, could prophylactically prevent or reduce the likelihood and severity of ventricular repolarization defects (Paulis et al., 2015). Another study by Kawagishi and colleagues found that activation and upregulation of Shh ligand expression regulated the cardiac regenerative response to the neonatal mouse heart in response to apical resection performed on the first postnatal day (Kawagishi et al., 2018). Furthermore, these authors provided a comprehensive characterization of Shh ligand production within the myocardium. Although Shh ligand was determined to be produced and secreted by non-myocyte cells, this study provided convincing evidence to support regulation of cardiomyocyte proliferation as well as influencing inflammatory immune response to injury via recruitment of monocytes and macrophages to the site of damaged tissue (Kawagishi et al., 2018). We propose the hypothesis that the Hedgehog signaling-mediated phenomena described here are dependent upon primary cilia elaborated by postnatal, adult myocardial cells. Doubtless experiments are underway in which primary cilia are genetically ablated from mature myocardial tissue to avoid the predictable complications that could arise if cilia are removed during development of the myocardium.

CHAPTER 2

EXPERIMENTAL DESIGN & METHODS (PART I)

2.1 Neural Crest-Specific Conditional Elimination of Primary Cilia (*In Vivo*)

It has long since been established that CHD results from genetic and/or environmental problems affecting CNCC cardiac progenitors (Kirby & Waldo, 1995). It has also been well-documented that defects in primary cilia-specific and/or primary cilia-associated genes lead to many different forms of CHD, which can manifest independently as well as concurrently, in the context of many ciliopathic syndromic congenital disorders (Badano et al., 2006; Marc August Willaredt et al., 2012; Williams, Carson, & Lo, 2019). However, examination into the possibility that CNCC-mediated CHD may be carried out via the primary cilium specifically, has yet to be investigated. Thus, the purpose of the investigations to follow aim to first ask the question if primary cilia of CNCC are involved in the pathogenesis of CHD, and second, probe further into the mechanistic aspects supporting a role for CNCC primary cilia in the pathogenesis of CHD.

2.1.1 Experimental Animals and IACUC Statement of Compliance

All animal experiments were conducted in compliance with the regulations of the Institutional Animal Care & Use Committee (IACUC) for the University of New England, Biddeford, ME, USA).

Multiple neural crest specific *Wnt1:Cre*-drivers (B6.Cg-*H2az2^{Tg(Wnt1-cre)}11Rth*; Jax stock #009107 (Danielian, Muccino, Rowitch,

Michael, & McMahon, n.d.); B6.Cg-E2f1Tg(Wnt1-cre)2Sor/J; stock #022501 (A. E. Lewis, Vasudevan, O'Neill, Soriano, & Bush, 2013), were crossed with the *Ift88* floxed construct (Haycraft et al., 2007) as well as a *Kif3a* floxed mouse (B6.129/Kif3atm1Gsn/J; stock #003537) (Marszalek et al., 2000), to generate two independent models with conditionally-activated loss of primary cilia in the CNCC population (Figure 2.1, Table 2.1).

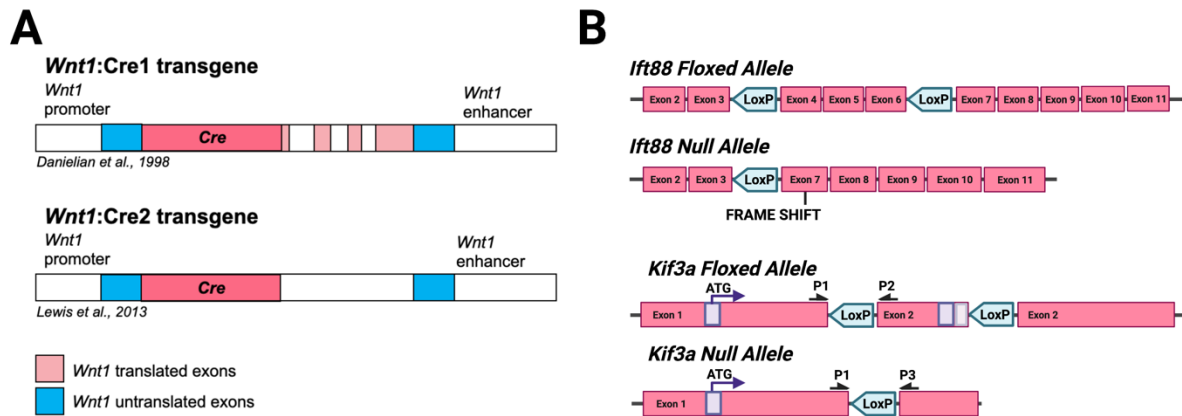


Figure 2.1 Illustrative overview of relevant genetic components for the *in vivo* elimination of primary cilia from CNCC in the developing mouse embryo. (A) Primary cilia of CNCC were genetically eliminated using multiple, *Wnt1*:Cre (Neural crest-specific) Cre-drivers crossed with animals homozygous for (B, top) the *Ift88* floxed and/or null allele(s) (Haycraft et al., 2007) or animals homozygous for the (B, bottom) *Kif3a* floxed and/or null allele(s) (Marszalek et al., 2000). (A) The original *Wnt1*:Cre-1 driver (Danielian et al., 1998.) was designed by inserting the Cre cDNA/transgene under the control of the *Wnt1* expression domain. Use of a Tdtomato reporter confirmed activation of this Cre recombination at ~E7.5 in the dorsal aspect of the neural tube region. (A, bottom) A secondary *Wnt1*:Cre-2 neural crest-specific Cre driver (A. E. Lewis et al., 2013) was also crossed with animals homozygous for the *Ift88* or *Kif3a* mutant alleles (B). The *Wnt1*:Cre-2 was used as the primary Cre-driver for the majority of experiments given its improved efficiency and specificity, attributed to a decreased number of translated exons within the *Wnt1* promoter domain. (B, top) The targeted *Ift88* allele was generated by inserting *loxP* sites flanking exons 4-6, leading to the disruption of *Ift88* following the introduction of Cre recombinase and the subsequent translational frame shift mutation leading to *Ift88* complete loss of function, comparable to the floxed allele-mediated germline mutation (*Ift88* null). (B, bottom) A *Kif3a* conditional knockout was also used to eliminate CNCC primary cilia, where *loxP* sites were positioned within the intron sequence flanking exon 2 (protein coding). Introduction of the neural crest-specific Cre-driver lead to recombination and translation of either the *Kif3a* floxed allele or deletion of DNA resulting in the *Kif3a* null allele.

The *Ift88* floxed allele was introduced into *Wnt1*:Cre-positive mice, which were then crossed to another heterozygous mouse to generate a litter of offspring that contained

control, heterozygous (*Ift88flox/wt*) and homozygous (*Ift88flox/flox*) mice. A Td-tomato (Tdt) reporter (B6.Cg-Gt(ROSA)26Sortm14(CAG-tdTomato)Hze/J Strain #:007914; Ai14), (Madisen et al., 2010), was used to track and quantify CNCC in the developing embryo (Table 2.1; Figure 2.2, A).

Table 2.1 Mouse lines used to investigate and model congenital heart disease (*in vivo*) resulting from the loss of primary cilia in cardiac neural crest progenitor cells.

Cre-Driver (Promoter)	Background Source/Stock #	Allele Type	Generation/Description
Wnt1:Cre-1 <i>Wingless-related MMTV integration site 1 (Wnt1)</i>	B6.Cg-H2az2Tg(Wnt1-cre)11Rth Tg(Wnt1-Gal4)11Rth/J; Stock#009107	Congenic/transgene	Co-insertion of Wnt1-Gal4 and Wnt1-Cre transgenes to generate transgenic mice; Cre expression/recombination is directed under the expression/regulatory sequence of Wnt1; recombination begins ~E7.5 and is present in the midbrain and developing neural tube (Neural crest cells)
Wnt1:Cre-2 <i>Wingless-related MMTV integration site 1 (Wnt1)</i>	B6.Cg-E2f1Tg(Wnt1-cre)2Sor/J; stock#022501	Congenic/transgene	Cre expression/recombination is directed under the expression of both promoter and enhancer sequence of Wnt1; recombination begins ~E7.5 and is present in the midbrain and developing neural tube (Neural crest cells)
cTnT:Cre <i>Cardiac troponin-T (cTnT)</i>	Tg(Tnnt2-cre)5Blh/JiaoJ; stock#024240	Congenic/transgene	Cre expression/recombination is directed under the expression of the rat cardiac troponin-T promoter; recombination begins ~E7.5 and is active early in cells with cardiac-lineage commitment (i.e. cardiomyocytes)
Conditional knockout	Background Source/Stock #	Allele Type	DESCRIPTION
<i>Ift88</i> <i>floxed</i>	B6.129P2-Ift88tm1Bky/J; stock#022409	Congenic/Targeted mutation	Targeting vector used to insert <i>loxP</i> sites flanking exons 4-6 of the <i>Ift88</i> flox allele; introduction of Cre recombination initiates a frame shift mutation leading to <i>Ift88</i> LoF
<i>Kif3a</i> <i>floxed</i>	B6.129-Kif3atm1Gsn/J; stock#003537	Congenic/Targeted mutation	Targeting vector used to insert <i>loxP</i> sites flanking 2 protein coding regions of the intron between exon 1 and exon 2 of the <i>Kif3a</i> flox allele; introduction of Cre recombination initiates a deletion leading to <i>Kif3a</i> LoF
Fluorescent Reporter	Background Source/Stock #	Allele Type	DESCRIPTION
<i>Tdtomato</i> R26 w/ Ift88 <i>floxed</i>	B6.Cg-Gt(ROSA)26Sortm14(CAG-tdTomato)Hze/J Strain #:007914; Ai14	Congenic/ Gene trap/ Targeted mutation	Cre reporter strain with a <i>loxP</i> -flanked STOP cassette preventing transcription of a CAG promoter-driven red fluorescent protein variant (tdTomato); located within the <i>Gt(ROSA)26Sor</i> locus; expression of Tdt fluorescence is activated following introduction of Cre recombination
Hedgehog Gain-of-Function	Background Source/ Stock #	Allele Type	DESCRIPTION
<i>SmoM2</i> CAG/YFP+ R26 <i>SmoM2</i> <i>floxed</i>	Gt(ROSA)26Sortm1(Smo/EYFP) Amc/J; stock#005130	Targeted mutation	Targeted mutation leading to the constitutive expression of the <i>Smo/EYFP</i> fusion gene; introduction of Cre recombination activates unrestrained Hedgehog signaling (Hh GOF) in Cre-expressing cells/tissues

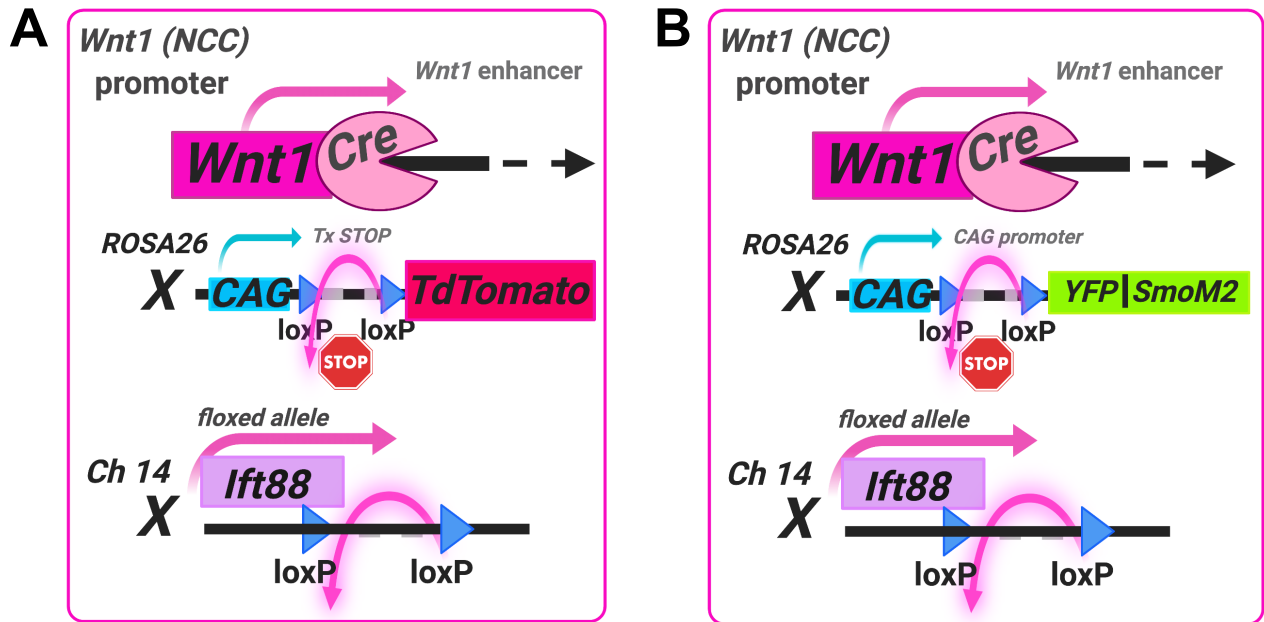


Figure 2.2 Experimental, genetic manipulation of conditional knockout. **(A)** Illustrative schema of *Wnt1*:Cre-Lox-mediated neural crest-specific, conditional knockout of primary cilia using the *Ift88* floxed allele (murine) located at chromosome 14 **(A)** Neural crest-specific elimination of primary cilia using multiple, *Wnt1*:Cre drivers introduced into C57BL6-J mice homozygous for the *Ift88* floxed allele. Cre-positive, *Ift88* heterozygous animals were crossed with homozygous *Ift88* floxed animals to produce MUT (*Cre+//Ift88^{lox/lox}*), HET/CON (*Cre+//Ift88^{lox/+}*), and littermate CON (*Cre+/-//Ift88^{+/+}*). A Td-tomato reporter was used to track and quantify CNCC and subsequent loss and/or maintenance of primary cilia. **(B)** Additional experiments utilized a HH GoF model (via *SmoM2*) introduced into the original CNCC conditional elimination of primary cilia mouse model.

To investigate potential roles of Hedgehog signaling in myocardial maturation of *Ift88*-homozygous mutants, we expressed a constitutively-active Hedgehog receptor, *Smoothened-M2* (*Smo-M2;Gt(ROSA)26Sortm1(Smo/EYFP)Amc/J; Jax stock #005130*) (J. Jeong, Mao, Tenzen, Kottmann, & McMahon, 2004), where recombination was activated by the NCC-specific Cre-driver, *Wnt1*:Cre (Table 2.1; Figure 2.2, B).

2.1.2 Breeding, Timed Matings, Euthanasia and Collection of Embryonic Tissue

Timed matings were set up between *Wnt1*:Cre+/*Ift88^{lox/+}* female animals and the appropriate male genotype corresponding to the designated experiment. Animals were

checked every morning at a similar time of day and females were gently probed to examine the vaginal opening for the physical/visual presence of a sperm plug, indicating that coitus had occurred as well as beginning the gestational timeline determined at E1.0. Following positive identification of a sperm plug, females were then removed from the breeder cage and their weight (grams) was recorded on the corresponding mouse ID card. Follow-up weights were collected no sooner than E7.0 to determine if insemination had occurred, indicating pregnancy status. In general, the female was determined to be pregnant if her weight increased by a minimum of 1.5 grams at E7.0. Other positive indicators of pregnancy in addition to weight gain included animal age, size & shape of the animal's abdomen and breeding history. More specifically, animal age was considered relevant due to the fact the older females and/or only recently sexually mature females may be less-likely to have a successfully pregnancy take place. Enlarged, especially rounded abdomen regions with notable distinction (i.e. darkening) of the nipple tissue was also considered to be indicative of pregnancy. Mating history was considered primarily in the context of the younger/recently sexually mature females, where successful previous mating would increase the likelihood that pregnancy would occur following the most recent plug discovery. Following determination of relevant embryonic timepoint for dissections, female mice were euthanized and embryos were dissected out for tissue collection.

2.1.3 Genotyping

Mouse matings were checked daily, where twelve noon of the day of vaginal plug discovery was designated as embryonic day 0.5 (E0.5). Genomic DNA was isolated

from embryonic and adults tail tissue samples as previously described (Marc August Willaredt et al., 2012). PCR genotyping was performed using the following primers (Table 2.2).

Table 2.2 Primers and primer pairs used for animal genotyping

Gene	F Primer (5'-3')	Reverse Primer (5'-3')
Cre	<i>En1Cre (F)</i> TAA AGA TAT CTC ACG TAC TGA C	<i>En1Cre (R)</i> TCT CTG ACC AGA GTC ATC CTT AGC
Ift88	<i>BY598 (F)</i> GCC TCC TGT TTC TTG ACA ACA GTG	<i>BY919 (flox)</i> GGT CCT AAC AAG TAA GCC CAG TGT T <i>BY956 (Δ/null)</i> CTG CAC CAG CCA TTT CCT CTA AGT CAT GTA
Kif3a	<i>K2 (F)</i> AGG GCA GAC GGA AGG GTG G	<i>K1 (flox)</i> TCT GTG AGT TTG TGA CCA GCC <i>K3(Δ/null)</i> TGG CAG GTC AAT GGA CGC AG
Tdtomato	<i>oIMR9105</i> CTG TTC CTG TAC GGC ATG G <i>oIMR902</i> AAG GGA GCT GCA GTG GAG T	<i>oIMR9103</i> GGC ATT AAA GCA GCG TAT CC <i>oIMR9021</i> CCG AAA ATC TGT GGG AAG TC
SmoM2 CAG/YFP	<i>R26SMO/YFP (F)</i> CCT CGT GAC CAC CTT CG	<i>R26SMO/YFP (R)</i> TTG ATG CCG TTC TTC TGC

PCR products were run out on a 2% agarose gel (Figure 2.3). Expected band length for the *Ift88* floxed allele 370 bp, 270 bp for the null (Δ) allele, and 350bp for the *Ift88* WT allele.

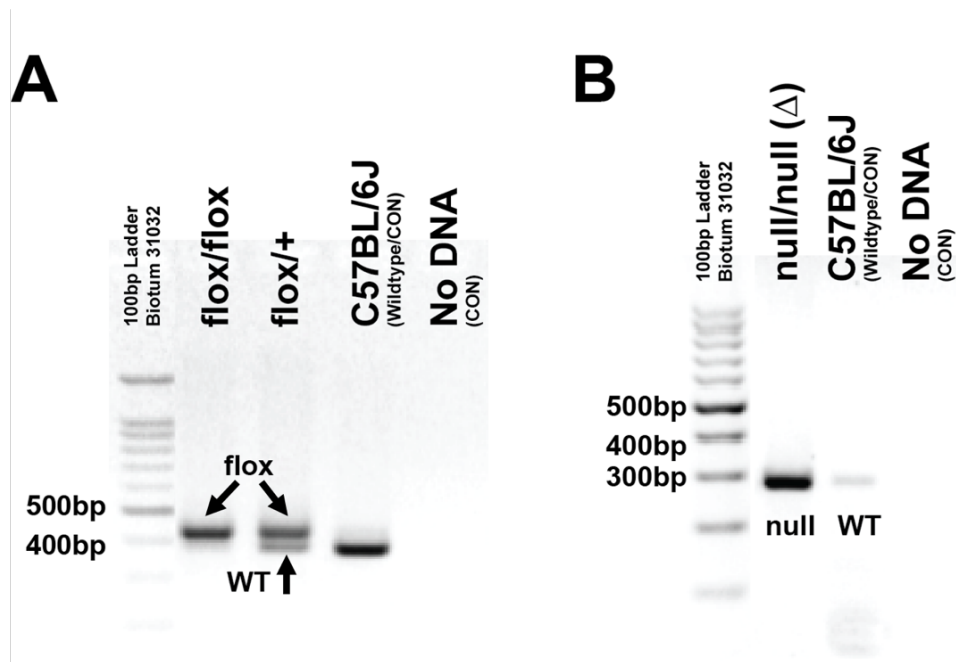


Figure 2.3. Genotyping mice and embryos for the *Ift88* floxed allele. Representative gel image from genotyping results of (A) *Ift88* MUT (*flox/flox*), HET (*flox/+*), C57BL/6J WT CON alleles (A), as well as a NO DNA negative loading control. (B) Representative gel image from genotyping results of the *Ift88* null (*delta/Δ*) allele, C57BL/6J WT CON alleles (A), as well as a NO DNA negative loading control.

2.2 Histological Characterization and Analyses

2.2.1 Histology: Hematoxylin & Eosin (H&E) Staining

Mouse embryos and whole hearts of different stages (E12.5 to P1.0) were immersion-fixed overnight in freshly-prepared 4% paraformaldehyde (PFA) in 0.1 M PBS (1X PBS) at room temperature (RT), followed by a dehydration series of 10%, 20%, and 30% ethanol in distilled H₂O (dH₂O) and embedded in paraffin. Serial paraffin sections (ranging from 5 to 10 μm thickness) were collected through the developing heart and outflow tract and were treated for 2x 5 minutes with xylol, rehydrated in a descending ethanol series, and washed with distilled H₂O (dH₂O). The sections were then stained

with hematoxylin for 8 to 10 minutes, rinsed briefly in dH₂O, and 15 minutes in tap water. The sections were briefly rinsed in dH₂O before staining in 0.1% Eosin, rinsed several times in dH₂O, dehydrated in an ascending ethanol series, treated for 2x 5 minutes with xylol, and mounted with (Surgipath® MM 24 Mounting Media, Leica Microsystems).

2.2.2 Ventricular Myocardial Assessments for Noncompaction Cardiomyopathy using Axial H&E Paraffin Sections

Transverse (axial), H&E-stained serial sections of E14.5, E18-20.5 and P1.0 embryos were photographed (BZ-X800 All-in-One Fluorescence Microscope, Keyence Co., USA) and tiff files were imported into Fiji/Image J. A total of three serial sections were selected from each heart at the widest portion of the ventricular myocardium (atrio-ventricular level). Trabecular and compact myocardial thickness were measured radially, and perpendicular to the interventricular septum (Figure 2.4).

NORMAL

NON-COMPACTION

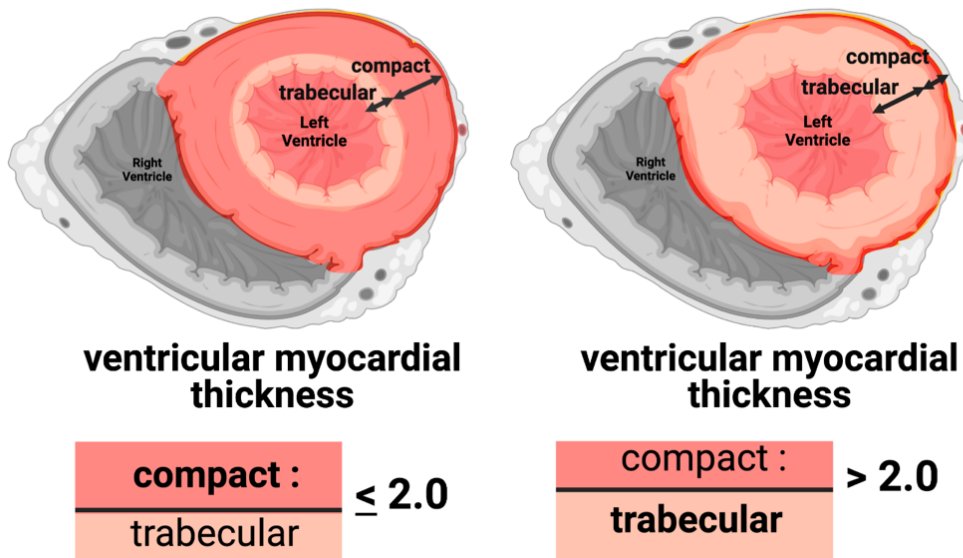


Figure 2.4 Diagnostic Evaluation of Ventricular Noncompaction (LV). Illustrative depiction showing distribution of trabecular and compact ventricular, myocardial wall thickness in a normal LV (left), compared to an LV which displays noncompaction of the ventricular myocardium (right). From a clinical perspective, noncompaction of the ventricular myocardium is considered to be diagnostically relevant if/when the ratio of the thickness of the trabecular myocardium is greater than 2.0.

The distance between the most medial trabecular fold and the deepest trabecular recess was classified as trabecular thickness (mm), and the distance from the base of the deepest trabecular fold to the outermost surface of the ventricular was determined as the compact myocardial thickness (mm), as summarized by Almeida & Pinto (2013) (Almeida & Pinto, 2013). The ratio of trabecular thickness to compact thickness (termed “NCC ratio) was calculated from an average of 6 ventricular wall thickness measurements performed by 2 blinded technicians. As in humans, a ratio of ≥ 2.0 was classified as diagnostically-significant NCC (Almeida & Pinto, 2013).

2.2.3 Histology: Immunohistochemistry and Immunofluorescence

Mouse embryos and whole hearts aged E9.25 to P1.0 were collected in 0.1 M PBS, and embryonic tail samples were collected separately for DNA extraction and genotyping. Embryos were fixed overnight (ON) at 4°C in 4% PFA in 0.1 M PBS, followed by a rinse in 0.1 M PBS for 60 minutes. Embryos were then transitioned through an ascending sucrose series (10%, 20%, and 30% in 0.1 M PBS) and embedded in optimal cutting temperature (OCT) embedding medium (VWR International) and frozen on dry ice. Individual embryos and whole hearts were cryo-sectioned at 7-12µm thickness (Leica Microsystems, Wetzlar, Germany) in both axial (transverse) and sagittal planes and were stored at -80°C. Frozen tissue sections were thawed at room temperature and blocking was performed using 0.25% Triton X-100 in blocking buffer containing 1% Bovine Serum Albumin (BSA), 5% Normal Goat Serum (NGS) and 0.1M PBS. Tissue incubated in blocking buffer (w/ Triton X-100) at RT for 60 minutes in a humid chamber. Sections were then stained with the following primary antibodies, summarized in (Table 2.2): Anti-ADP-ribosylation factor-like 13B (Arl13B; Cat#17711-1-AP, rabbit polyclonal, Proteintech) 1:1000; anti-lft88 (Cat#13967-1-AP, rabbit polyclonal, Proteintech) 1:100; anti-acetylated alpha tubulin (clone 6-11B-1, Cat#MABT868, Sigma, Munich, Germany) 1:1000; anti-gamma tubulin (clone GTU-88, Cat# T5326 Sigma) 1:1000; anti-phosphorylated histone H3 (Ser10, rabbit 06 -570; Millipore Corporation, Schwalbach am Taunus, Germany) 1:200; anti-cleaved caspase-3 (Asp175, #9661, Cell Signaling Technology, Danvers, Massachusetts, USA) 1:200; anti-CD-31 (PECAM-1; clone MEC13.3, Cat#553370, rat Lewis IgG2a, κ; BD Biosciences) 1:1000; or anti-Neuregulin-1 (NRG-1; clone 7D5, mouse monoclonal IgG2a, Cat#MA5-12896, Invitrogen)) 1:400. Incubation with primary

antibodies was performed in a humid chamber at RT for 60 minutes or was stored overnight at 4°C. Slides were then washed for 3 minutes with 0.1M PBS and incubated with secondary antibodies for 60 minutes at RT in a humid chamber.

Table 2.3. Primary antibodies used for IHC/Immunofluorescence.

1° Antibodies/Immunofluorescence						
Antibody/Target	Source	Cat#	Species/clonality	Isotype	Working Dilution	[Working]
αArl13B	Proteintech	17711-1-AP	Rabbit pAb	IgG	1:1000	0.9 µg/mL
αArl13B	Proteintech	66739-1-Ig	Mouse mAb	IgG2a	1:200	5.0 µg/mL
αAcetylated α-tubulin	Sigma	T7451	Mouse mAb (clone6-11b-1)	IgG2b	1:1000	0.1 µg/mL
αGamma-tubulin	Sigma	T6557	Mouse mAb (clone GTU-88)	IgG1	1:1000	0.1 µg/mL
αCardiac Troponin-T	Invitrogen	MA5-12960	Mouse mAb (clone 13-11)	IgG1	1:300	1.5 µg/mL
αPhosphorylated histone H3	Invitrogen	PA5-17869	Rabbit pAb	IgG	1:400	2.0 µg/mL
αPECAM-1 (CD-31)	Abclonal	A4900	Rabbit mAb	IgG	1:200	5.0 µg/mL
αNRG-1	Invitrogen	MA5-12896	Mouse mAb (clone 7D5)	IgG2a	1:100	10.0µg/mL
αShh	Bioss	bs1544R	Rabbit pAb	IgG	1:100	10.0µg/mL
αPtch1	ABclonal	A0826	Rabbit pAb	IgG	1:100	10.0µg/mL
αGli1	Abcam	Ab217326	Rabbit pAb	IgG	1:200	5µg/mL
αGli3	Abcam	[EPR4594] Ab181130	Rabbit mAb	IgG	1:200	5µg/mL
αSmo	Proteintech	20787-1-AP	Rabbit pAb	IgG	1:200	4µg/mL
αSox2	Santa Cruz	Sc-17320	Goat pAb	IgG	1:200	5µg/mL

The following secondary antibodies were matched to antigen of the corresponding primary antibody (Table 2.3): Alexa 488 (Goat anti-rabbit), : Alexa 488 (Goat anti-mouse), Alexa 488 (Goat anti-rat), Alexa 555 (Goat anti-rabbit), Alexa 555 (Goat anti-mouse), Alexa 647 (Goat anti-mouse), Alexa 647 (Goat anti-rabbit) Alexa 647 (Donkey anti-rabbit), and Alexa 647 (Goat anti-rat). Co-labeling experiments to detect cilia using the anti-acetylated alpha tubulin and the anti-gamma tubulin antibodies were detected with isotype-specific anti-mouse immuno- globulin G1 (IgG1) and IgG2b secondary antibodies, respectively (Table 2.3).

Table 2.4 Secondary antibodies used for Immunofluorescence.

2° Antibodies/Immunofluorescence				
Fluorophore	Cat#	Immunogen	Species/ Clonality & Isotype	Application; [Working]
Alexa 488	Ab150077	Goat IgG	αRabbit IgG (H+L)	1:1000 (0.1µg/mL)
Alexa 488	A32731	Goat IgG	αRabbit IgG (H+L)	
Alexa 488	A11006	Goat IgG	αRat IgG (H+L)	
Alexa 488	Ab150113	Goat IgG	αMouse IgG (H+L)	
Alexa 488	A21121	Goat IgG	αMouse IgG1	
Alexa 488	A21131	Goat IgG	αMouse IgG2a	
Alexa 555	A21422	Goat IgG	αMouse IgG (H+L)	
Alexa 555	A21127	Goat IgG	αMouse IgG1	
Alexa 555	Ab150078	Goat IgG	αRabbit IgG (H+L)	
Alexa 555	A21147	Goat IgG	αMouse IgG2b	
Alexa 568	Ab175710	Goat IgG	αRat IgG (H+L)	
Alexa 647	A21247	Goat IgG	αRat IgG (H+L)	
Alexa 647	A21244	Goat IgG	αRabbit IgG (H+L)	
Alexa 647	A21235	Goat IgG	αMouse IgG (H+L)	
Alexa 647	A21242	Goat IgG	αMouse IgG2b	
Alexa 647	A21446	Rabbit IgG	αGoat IgG (H+L)	

Secondary antibodies were all used at 1:1000 dilution (0.1 µg/mL). Following incubation with secondary fluorophores, tissue was rinsed 3x3 minutes with 0.1 M PBS and briefly immersed in dH₂O, followed by cover slipping with *Fluoroshield* Mounting Medium with DAPI (ab104139, Abcam) and storage at 4°C. Individual sections were imaged using confocal microscopy (Leica Microsystems, Mannheim, Germany) and images were formatted using Fiji/Image J (Schindelin et al., 2012). For a detailed, step-by-step protocol for IF procedures, please see complete protocols included as Supplementary Protocols in Appendices C-D.

2.2.4 Characterization of Primary Cilia: Integrity, Length, and Morphology

Quantification of cilia length and qualitative assessments of cilia morphology were performed using serial z-stacks of confocal microscopy datasets from frozen tissue sections stained with antibodies targeting primary cilia and the basal body (α Ar113B, α gamma-tubulin, respectively) and ciliary length was calculated using the Pythagorean Theorem (PyT Method), validated by Dummer and colleagues (Dummer, Poelma, DeRuiter, Goumans, & Hierck, 2016), (Figure 2.2.4).

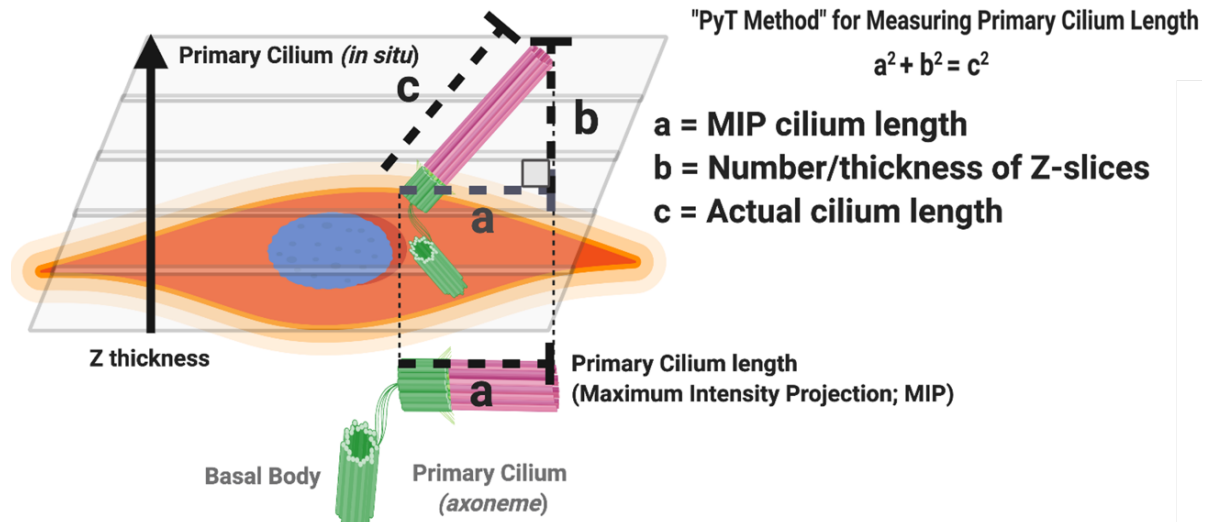


Figure 2.5 Overview of PyT Method for Measuring Primary Cilia Length. Visual depiction demonstrating the appearance and orientation of a primary cilium with intact basal body. Quantification of primary ciliary length was calculated using the validated PyT method.

Presence or absence of cilia as well as ciliary length from Tdt+ and Tdt- cells were quantified using Fiji/Image J from z-stack files. Each of these variables were collected from the following regions: Pharyngeal arch region (PA), outflow tract/endocardial cushions (OFT/ECC), and the ventricular myocardium (vMyoC); and were quantified at E9.25-E9.5, E10.5, and E11.5.

2.3 Micro-Magnetic Resonance Imaging and 3D Reconstructions

2.3.1 Preparation of Embryos for μ MRI

Embryos were submerged in an ice-cold 4% paraformaldehyde (PFA) combined with a 4 mM gadoliniumdiethylene triamine pentaacetic acid (Gd-DTPA) and placed on a rocker for fixation. Following two weeks of fixation, embryos were removed from the PFA/Gd-DTPA solution and embedded and prepared in a 50-mL Falcon tube, containing a 1% agarose gel and 4 mM Gd-DTPA solution for imaging. In order to optimize

embryonic fixation for μ MRI, approximately 2-3 embryos were combined in each tube, which varied depending on the degree of variation in size between individual CON and MUT embryos. Embryos were stored at 4°C prior to μ MRI imaging, which took place in a single session following successful collection of the adequate number of samples (CON, n=4; MUT, n=4).

2.3.2 μ MRI Acquisition and Data Collection

Embryos were scanned using a BRUKER PharmaScan 7.0 T horizontal-bore system (BRUKER, Billerica, MA USA). All imaging preparation, quality control and implementation were performed by our collaborator, Dr. Ilka Pinz, Director of the Small Animal Imaging Core facility at Maine Medical Research Institute (MMCRI; Scarborough, ME USA). Dr. Pinz acquired quality μ MRI scans using a standardized protocol for *in-vivo* mouse embryos, which was optimized for consistency between scans (Yang et al., 2010) MRI parameters were chosen as originally described by O’Cleary *et al.*, with slight modifications to account for the lower magnetic field in our system (Cleary et al., 2009).

2.3.3 Measurement and Analysis of Anatomical Parameters

Two-dimensional sagittal slices from tail to head were obtained and analyzed for anatomical aberrancies. While μ MRI was performed on whole-embryo samples, we focused our analyses primarily on the developing OFT and atrial/ventricular chamber portions of MUT and CON embryos at E14.5. Subsequently, 2-D images will be compiled to construct a 3-D model depiction of a sample selection on mutant and WT embryonic hearts. The construction of 3-D models was used to further characterize the phenotypic

aspects of the OFT of mutant and WT mice, with particular advantages seen in the arrangement of the great vessels of the OFT. Of additional relevance, investigators compiled both 2-D and 3-D images to explore the individualized variation(s) in phenotypic characteristics of OFT and great vessel defects between individual embryos as well as between CON and MUT.

2.4 Relative Gene Expression Using Quantitative, Real-Time PCR

Whole heart RNA was extracted from E9.5-E12.5 embryos using the PureLink RNA Mini Kit (Invitrogen) according to the manufacturer's instructions. 200ng-1ug of RNA was transcribed into cDNA using SS Vilo MasterMix (Cat#11755050/Invitrogen). Quantitative real time PCRs were performed with the ABI Prism 7000 Detection System (Applied Biosystems) using FG Power SYBR Green Mastermix (Cat#4367659; Invitrogen) and 1µl of cDNA (generated from 5 ng of whole RNA input). The following primer pairs were used to detect gene expression in mouse: *Shh* (Forward: 5' -GAT GAC TCA GAG GTG CAA AGA C- 3'; Reverse: 5' -CTC GAC CCT CAT AGT GTA GAG AC- 3'), *Ptch-1* (Forward: 5' -TCA AAG GTG GAG GTC ATA GAG- 3'; Reverse: 5' -AAG CAG TTC TGG AAA GAG GT- 3'), *Gli1* (Forward: 5' -CTC AAA CTG CCC AGC TTA ACC- 3'; Reverse: 5' -GCT GAC TGT GTA AGC AGA GC- 3'), *YFP/SmoM2* (F: 5' - CCT CGT GAC CAC CTT CG- 3'; R: 5' - TTG ATG CCG TTC TTC TGC- 3'), and *GAPDH* (Forward: 5' AAT GGT GAA GGT CGG TGT G- 3'; Reverse: 5' -GTG GAG TCA TAC TGG AAC ATG TAG- 3'), all summarized in Table 2.4.

Table 2.5. qRT-PCR targets & primer sequences.

Target (Mouse)	Forward Primer (5'-3')	Reverse Primer (5'-3')
<i>GAPDH</i>	AAT GGT GAA GGT CGG TGT G	GTG GAG TCA TAC TGG AAC ATG TAG
<i>Shh</i>	GAT GAC TCA GAG GTG CAA AGA C	CTC GAC CCT CAT AGT GTA GAG AC
<i>Ptch1</i>	TCA AAG GTG GAG GTC ATA GAG	AAG CAG TTC TGG AAA GAG GT
<i>Gli1</i>	CTC AAA CTG CCC AGC TTA ACC	GCT GAC TGT GTA AGC AGA GC
<i>Gli3</i>	GGGTGAACAGCATCAAAAATGGAG	TCCGATAGCCATGTTGGTGG
<i>SMO</i>	CCT CGT GAC CAC CTT CG	TTG ATG CCG TTC TTC TGC
<i>YFP/ SMO M2</i>	CCT CGT GAC CAC CTT CG	TTG ATG CCG TTC TTC TGC

The standard quantification protocol was applied with the following cycles: 2 min at 50°C, 10 min at 95°C, followed by 45 cycles: 15 s at 95°C and 1 min at 60°C. Each individual reaction was performed in triplicate. GAPDH primers were used to normalize results. The $2^{-\Delta\Delta C_T}$ method was used to calculate relative gene expression from qRT-PCR results (Livak & Schmittgen, 2001).

2.5 Quantitative FLOW Analysis

2.5.1 Tissue Extraction & Processing

Embryonic whole hearts were excised/dissected out at timepoints E10.5-E14.5 and dissociated as previously described (Muthukrishnan, Ryzhov, Karolak, & Oxburgh, 2018). Briefly, whole hearts were minced and digested at 37°C for 45 minutes using

10mg/mL collagenase IV (Life Technologies; 10 mg/ml dissolved in DMEM), and were briefly vortexed every 15 minutes to minimize tissue clumping.

2.5.2 Single-Cell Suspension Preparation and Quantitative Flow Analysis

Digested tissue solutions were then passed through a 70 μ m nylon filter (Miltenyi Biotec) into individual wells of a 6-well tissue culture plate containing DPBS buffer (Ca⁻, Mg⁻). Plates remained on ice for ~2 min to quench enzymatic activity. Filtrate containing single cells was centrifuged for 5 min at 500 g, and resuspended in FACS buffer containing 0.5% BSA and 2mM EDTA in 0.1M PBS. Samples were then transferred to a 2.0mL conical tube, where they remained stored on ice prior to analytical FACS. Full protocol for cell preparations for quantitative Flow cytometry analyses is included in Appendix A1. Conjugated primary antibodies used for Flow analysis are detailed below in Table 2.6.

Table 2.6. Conjugated Antibodies used for Quantitative Flow Analyses.

Quantitative Flow Cytometry					
Antibody/Target	Source	Cat#	Species/clonality	Isotype	[Working]
CD29-APC/Cy7	eBioscience	Clone:HMB1-1;	Hamster mAb	IgG	0.5µg/test
CD45-FITC	eBioscience	Clone: 30-F11; # 11-0451-82	Rat mAb	IgG2b κ	0.125µg/test
PECAM-1(CD31)	Invitrogen	Clone: 390	Rat mAb	IgG2a κ	0.25µg/test
PeCy7 VCAM-1	Fisher Scientific/Novus Bio	Clone:429; #NB007703	Rat mAb	IgG	
PE αCardiac Troponin T	BD Pharmingen	#564767	Mouse mAb	IgG1κ	5µl/test
ErbB2	Invitrogen	e2-4001 #MA5-13105	Mouse mAb	IgG1	1µg/test
ErbB3	Invitrogen	RTJ2 #MA1-860	Mouse mAb	IgG1	1µg/test
ErbB4	Invitrogen	H4.77.16 (Ab77) #MA5-12888	Mouse mAb	IgG1	0.5µg/test

2.6 Protein Expression & Quantification

2.6.1 Western Blot

Individual embryonic bi-ventricular myocardial chambers were dissected at E12.5 over 1X PBS and excised at the atrioventricular junction. Embryonic ventricular tissues designated for protein quantification were flash frozen immediately following dissection and stored at -80C. In preparation for Western Blot quantification of protein, ventricular samples were removed from storage at -80C and thawed on ice. RIPA buffer was freshly prepared, containing 50mM Tris-HCl (pH8.0), 150 mM NaCl, 0.5% Triton-X-100, 0.5% Na Deoxycholate, and 1% SDS, while ventricular tissue continued to thaw on ice. Immediately prior to tissue lysis, one cOmplete™ protease inhibitor cocktail tablet (per

50mL RIPA; Roche; Cat# 11697498001, purchased from Millipore Sigma, USA) as well as 50µL of Halt Protease Inhibitor Cocktail (100X; per 50mL RIPA buffer Cat#78430, Thermo Scientific) were added to the RIPA buffer. Ventricular tissues contained in 1.7µL microcentrifuge tubes were subsequently lysed using 50µL cold RIPA Buffer (containing protease and phosphatase inhibitors) and homogenized using a motorized pestle while tissues remained on ice. Mixtures remained incubating on ice for 15 minutes and were removed briefly for vortexing every 5 minutes. Sample tubes were centrifuged for 15 minutes at 140000xg at 4 degrees Celsius and then transferred to fresh, pre-chilled tubes, where protein concentration of individual samples was determined using a QuantiPro BCA Assay Kit (Cat#QBPCA; Sigma Aldrich), following the manufacturer's protocol.

Protein lysates of equal concentration (15µg total) were combined with equal volumes of 2X Laemmli buffer (Bradford Reagent, Sigma cat#6916) and boiled for 8 minutes at 95°C, after which, samples were immediately removed and placed on ice. Western blot quantification of protein expressions was performed using 4–20% precast polyacrylamide gels (Cat#4561094; Bio-Rad). Running buffer was diluted to a 1X concentration from a 10X stock containing 25mM Tris, 190 mM glycine and 0.1% SDS. Gel electrophoresis was performed for 40 min at 190V prior to transfer onto a nitrocellulose membrane (Bio-Rad) in 1X TBS transfer buffer containing 5% (weight/volume) nonfat dry milk and 0.1% Tween 20 (60 minutes at 30V). Membranes were incubated overnight at 4°C with the following primary antibodies: Anti-Neuregulin-1 (NRG-1; Cat#AF377 R&D Systems/biotechne; goat polyclonal [1:500] anti-GAPDH (Cat# 60004-1-Ig, Proteintech; Mouse monoclonal [1:10,000]) and anti-alpha-tubulin

(Rabbit polyclonal; Cat#11224-1-AP, Proteintech; [1:2000]). Secondary antibodies IRDye® 800CW, 680RD, or 680LT against mouse, rabbit and goat species, respectively; Licor; [1:15,000]). Blots were imaged using the Odyssey Infrared Imaging Systems (Licor) and fluorescence signal intensity was quantified using FIJI/ImageJ. Each sample was normalized to the lowest mean fluorescence intensity value (IntD) of the control antibody, and each data set was normalized to the lowest control value prior to statistical analysis.

2.6.2 Quantitative Immunofluorescence

Quantification of protein expression from immunofluorescence analysis was performed as previously described and optimized by Tenbaum and colleagues (Tenbaum et al., 2012). Briefly, standard immunofluorescence analysis protocols were performed with primary antibodies against a single protein of interest along with a secondary antibody/fluorophore to correspond to a species raised against that of the primary antibody antigen. Nuclei were counter-stained with mounting medium containing DAPI (Abcam). Stained tissues were imaged using confocal microscopy using a predetermined number of frames relative to the individual tissue section thickness. Image files were analyzed using FIJI/IMAGEJ software, where the Region of Interest (ROI) was selected using the Freehand Tool, and cross-verified using the Polygon tool for each channel, including DAPI. Integrated Density Value (IDV) was determined from the indicated ROIs. Three IDV values were calculated per ROI and compared at the individual cellular level to the nuclear expression of DAPI as well as at the level of a given tissue ROI to a positive or negative-control ROI within the same

tissue section. A unique, statistical analysis for comparison of mean cell/tissue IDV was performed using a non-parametric Kruskal-Wallis test three or more groups of unpaired values. Post hoc analysis included a Dunn's multiple comparison post-test to determine corresponding p-value(s) of differences in the rank sums between each pair of grouped values (Tenbaum et al., 2012).

2.7 Early Postnatal Cardiac Electrophysiology

2.7.1 Electromyography Technology Modified to Measure Cardiac ECG

Perinatal electrocardiography (ECG) was first attempted using an adapted setup of the Power2/26 Device (AD Instruments), modified from its default EMG setup for surface detection of cardiac electrocardiography. Data was collected during the first postnatal day (P1.0), where mice remained conscious in the prone position. Modified gel-coated ECG electrodes were placed in the right axilla and the left lower quadrant of the abdomen, allowing for a two-lead electrophysiological evaluation. ECGs were collected for a total of 5 minutes, after which, pups were euthanized for further histological evaluation. ECG analysis included heart rate (HR; minimum, maximum and mean), QRS duration, P wave presence, PR interval. These values along with overall ECG interpretation was analyzed using LabChart Reader and Labscribe (ADInstruments).

2.7.2 Novel, Non-invasive ECG Developed for Neonatal Mice

Neonatal mouse ECG data was collected using a custom-made device, the Neonatal mouse ECG and Respiratory System (iWorx; Dover, NH, USA). This system is a non-invasive, USB powered ECG and respiratory measurement system which involves

the prone placement of the neonate mouse, covering 4 silver wire electrodes covered with conductive electrode gel and designed to measure electrophysiology transcutaneously through the mouse's ventral thoracic wall. Flanking silicone bumpers secured the pup in place, after which a fifth "grounding" electrode was placed on the mouse's dorsal surface and held in place with a dorsally-positioned silicone bumper. The mouse pup, silicone bumpers, and platform were placed inside an aluminum Faraday cage and allowed to acclimate to its position for a few minutes, after which ECG data was collected for a total of 5 minutes and pups were euthanized for further histological evaluation. ECG analysis included heart rate (HR; minimum, maximum and mean), QRS duration, P wave presence, PR interval, and overall ECG interpretation.

A full-length manuscript description of this method can be found in the proceeding Chapter 3 (*METHODS (PART II): IN VIVO ANALYSIS OF POSTNATAL CARDIAC ELECTROPHYSIOLOGY*)

2.8 Statistical Considerations and Analyses

Initial data collection, descriptive statistics and Student's t-test of paired datasets were performed using Microsoft Excel (v 16.16.25 200810). Further descriptive characteristics, normality tests, statistical analyses and figures were generated using GraphPad Prism (v 8.4.3; 2020). All outcome variables are expressed as mean values \pm standard error of the mean (SEM), unless otherwise indicated. A Kolmogorov–Smirnov test for normality was performed for nonparametric datasets, to determine whether individual datasets were normally distributed. For instances where data was normally

distributed (as determined by Kolmogorov–Smirnov test $p \leq 0.05$), a Student's t-test of paired and unpaired data was performed to compare mean MUT values to that of CON. In cases where data were not normally distributed (e.g. VCAM+/ErbB3+ expression, Figure 4.9), a nonparametric Mann-Whitney or a Welch's t-test was employed to compare mean values of unpaired data. In cases where comparison of outcome variables were normally distributed, but which included multiple, mixed model components, One-Way Analysis of Variance (ANOVA) was used to compare mean outcome values on experimental variable compared to CON values, Tukey's post hoc multiple comparisons test was implemented to compare mean values between/within CON and MUT/experimental data. Confidence interval was set at 95% (CI of diff) and statistical significance was set at $p \leq 0.05$.

CHAPTER 3
METHODS (PART II):
IN VIVO ANALYSIS OF POSTNATAL MAMMALIAN CARDIAC
ELECTROPHYSIOLOGY*

**Re-formatted/modified from Fitzsimons et al, 2020 (Fitzsimons, Brewer, Forrester, Moran, & Tucker, 2020)*

Electrocardiography (ECG) has long been relied upon as an effective and reliable method of assessing cardiovascular (and cardiopulmonary) function in both human and animal models of disease. Individual heart rate, rhythm, and regularity, combined with quantitative parameters collected from ECG, serve to assess the integrity of the cardiac conduction system as well as the integrated physiology of the cardiac cycle. This protocol provides a comprehensive description of the methods and techniques used to perform a noninvasive ECG on perinatal and neonatal mouse pups as early as the first postnatal day, without requiring the use of anesthetics. This protocol was designed to directly address a need for a standardized and repeatable method for obtaining ECG in newborn mice. From a translational perspective, this protocol proves to be entirely effective for characterization of congenital cardiopulmonary defects generated using transgenic mouse lines, and particularly for analysis of defects causing lethality at or during the first postnatal days. This protocol also aims to directly address a gap in the scientific literature to characterize and provide normative data associated with maturation of the early postnatal cardiac conduction system. This method is not limited to a specific postnatal timepoint, but rather allows for ECG data collection in neonatal

mouse pups from birth to postnatal day 10 (P10), a window that is of critical importance for modeling human diseases in vivo, with particular emphasis on congenital heart disease (CHD).

3.1 Utility and Translational Relevance of Perinatal ECG in mouse

Cardiac function can be measured in different ways, the most common of which includes the use of electrocardiography (ECG) to analyze the conduction of electric current through the heart as well as its overall cardiac cycle and function (Pappano, Achilles J., 2019). Electrocardiography continues to be a useful diagnostic tool for identifying and characterizing cardiac anomalies in both human and animal models of disease electrocardiogram reading can be found in abnormal cardiac development (i.e., congenital heart disease (CHD)), and can include arrhythmias manifesting as changes in heart rate (e.g., bradycardia), and rhythm (e.g., “heart blocks”), suggestive of defects in the integrity and/or function of the underlying myocardium (Kaese & Verheule, 2012; Pappano, Achilles J., 2019). Changes such as these may predispose patients to life-threatening cardiac dysfunction (e.g., congestive heart failure and/or cardiac arrest) and increased mortality standardized and repeatable method for collecting ECG during this early postnatal period is critical (Rudy & London, 2001; Sisakian, 2014). Given the high rates of mortality with severe and untreated CHD, developing a standardized and repeatable method for collecting ECG during this early postnatal period is critical.

Although we are not the first to address this problem, previous methods of collecting ECG on a mouse pups have traditionally included invasive procedures (subcutaneous needle or wire electrodes) and/or the use of anesthetics (Cao et al.,

2014; Zehendner, Luhmann, & Yang, 2013; Y. Zhao et al., 2015). Advantages of performing noninvasive ECG analysis include minimizing pain and undo stress on the animal. While the experimenter must still be cautious about causing the pup stress, the device is designed to avoid common stressors in order to produce accurate data. In the context of evaluating cardiac function, introducing anesthesia to animals that may have cardiopulmonary abnormalities could potentially mask or even exacerbate underlying conditions. Anesthetics may affect the electrical conduction by altering depolarization and/or repolarization of the cells. Finally, the use of anesthesia can put the newborn pup at an increased risk for hypothermia, which could further confound any inherent pathology. The following protocol does not introduce any anesthetics, invasion, or pronounced discomfort to the pup. Once equipment setup is finalized, device setup and data collection involving the animal can be completed efficiently, after which the pups can be returned to their mother. Additionally, this system allows for repeat and/or serial analyses to be performed, which is ideal for experiments requiring analysis over time, introduction of pharmacological therapies, etc.

3.2 Protocol

The following protocol follows the standards of the Institutional Animal Care and Use Committee of the University of New England. Close observation of the protocol should deliver satisfactory ECG reads in all examined neonates ($n > 70$).

Device preparations

1. Plug the device into the USB port of a computer with the ECG software downloaded on it. The measuring device will automatically

begin heating up to (37 °C/98.6 °F). The internal heating unit is contained within the measuring unit and heats only the plastic surface. The silver wire electrodes are not heated.

2. Allow approximately 15 min for the surface to reach the temperature. Use this time to gather and set up animals.

NOTE: The protocol may be paused at this point and the platform can remain plugged in and heating for an extended period of time. In the absence of a self-heating electrode platform, an animal safe heating pad may also be used to keep mother and pups from becoming hypothermic.

Animal preparations

1. Collect the mother and pups and keep within the housing cage until ready to collect.

2. Once the measuring unit has heated to the temperature, remove the mouse pup from the cage and wipe the thorax with 70% ethanol sprayed on a wipe. Place the pup on the heated surface of the plastic.

3. Allow the mouse to acclimate to the surface in the dark for approximately 2-5 minutes.

Mouse and electrode platform setup (electrode application)

1. Use a metal spatula, probe, or wooden dowel to collect a small droplet of adhesive, electrical conducting gel (a quick-drying high-conductivity electrode gel commonly used for placement of rodent electrodes). NOTE: Any nonfibrous, solid object can be used to apply the conducting gel, as long as the object will not leave behind synthetic fibers or similar material on the electrodes that could interfere with the quality of the electrical signal.

2. Using the spatula/dowel, gently touch the top of each of the four, flattened electrode surfaces by pressing gently down and pulling the conducting gel at an oblique angle away from the center of the electrode construct. Make sure that each individual electrode is completely covered with the gel. CAUTION: This step is extremely important to ensure that the conductive, electrode gel does not adhere to more than a single electrode. Adhesive strands that form between electrodes can conduct charge and potentially interfere with or short out the desired electrical signal. The protocol should not be paused at this time as the gel will begin to solidify and become adherent. Make sure to set up the mouse to the platform within 5-10 minutes of applying conducting gel (or equivalent conductive electrode gel substitution).

3. Place the metal spatula or wooden dowel with the remainder of the gel to the side.

4. Place the neonatal mouse pup sternum down and prone with the head of the pup facing the outgoing USB edge of the platform. Make sure that a portion of the pup's chest is covering each of the four electrodes. Gently restrain the pup's forearms by their side while simultaneously holding down for approximately 1 min to allow the conducting gel to set.

5. Place rubber silicone bumpers on the right and left sides of the pup. Bumpers should secure the pup on each side and provide stability to prevent excessive movements of the mouse but should NOT prevent all movement of the mouse. Once installed, watch the mouse for a moment and adjust bumper placement as needed. CAUTION: Do not compress the mouse too tightly as this can interfere with respiratory mechanics and respiratory rate.

6. Use the dowel that was set aside to apply remaining conducting gel to the grounding tail electrode and place on the rump of the pup. Apply gentle pressure to allow the gel to set before releasing the pup.

7. Place the final silicon bumper on top of the rump of the mouse to hold the grounding electrode in place. CAUTION: Do not apply excessive force while placing the final bumper as this could cause discomfort to the pup and/or displace the grounding electrode.

8. Grab ahold of the entire platform and gently place inside the Faraday cage. CAUTION: Use caution and ensure the top silicone bumper does not become displaced once the Faraday cage is in place.

9. Prior to recording, make sure the mouse pup is not moving excessively and make sure the body and head of the mouse appears secure. CAUTION: Make sure the mouse pup's head is able to move somewhat freely within the bumpers and is not completely snout down into the platform. The raised platform is designed to elevate the mouse thorax slightly and prevent suffocation, but this should be closely monitored.

3.3 Representative Results

An ideal ECG would have a clear, prominent signal that allows all waves to be analyzed in several different time frames (Figure 3.1).

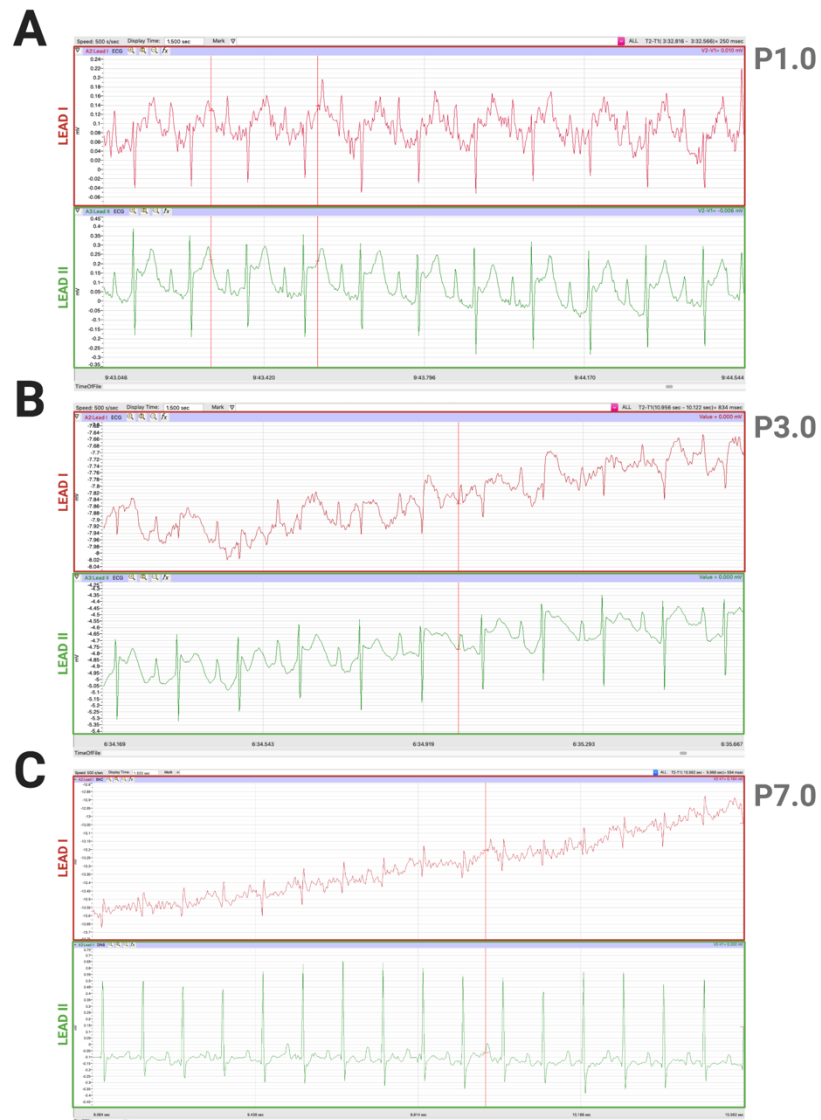


Figure 3.1. Representative electrocardiographic reads from neonatal mice on the first (A, P1.0), third (B, P3.0), and seventh (C, P7.0) postnatal day. **(A-C)** Images represent examples of good quality ECG tracings using the 2-lead, noninvasive device, captured in a 1.5 s frame of the reading. Notable characteristics of good ECG reads include clear, discernable beats, as described collectively by the presence of consistent P-waves followed by a QRS complex and subsequent T-waves, visible in both Leads I-II of each postnatal time point. Examples also include a low signal- to-noise ratio (minimal artifact) and a discernable isoelectric line. Top ECG strip (red): Lead I; bottom ECG strip (green): Lead II.

The laboratory initially employed a custom application of an electromyography apparatus to produce ECGs of an unsatisfactory quality, which only allowed us to

analyze basic parameters such as heart rate (Figure 3.2). This inspired work with a company to develop a novel prototype ECG device specifically for the analysis of early postnatal mouse pups.

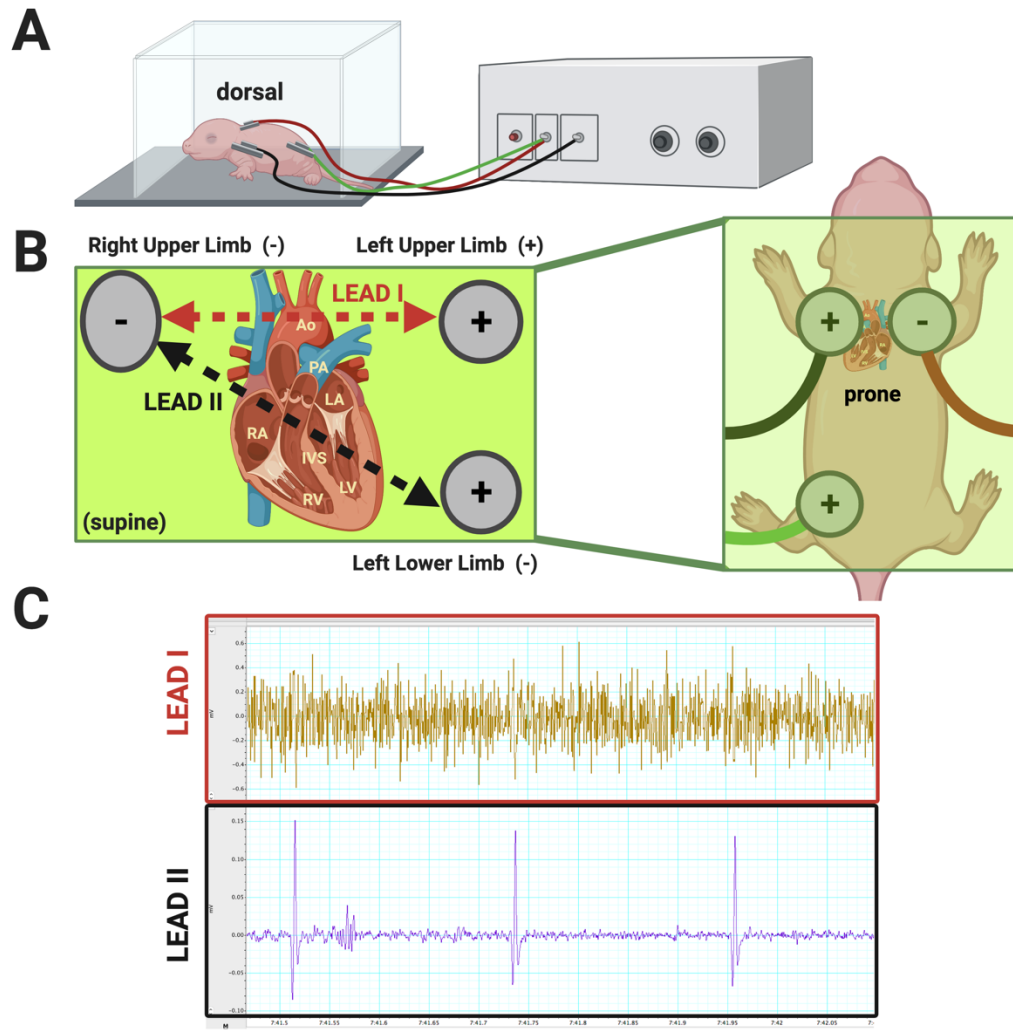


Figure 3.2 Illustration of traditional limb lead electrodes for noninvasive collection of early postnatal ECG. (A, left) Lateral view of mouse and electrode placement within Faraday cage (box). (B) Traditional self-stick skin electrodes are positioned on the dorsal surface of the pup. (A, right) ECG-like signal may be interpreted with the use of traditional electromyography transducer to produce a minimalistic ECG tracing discernable only in Lead II (C, bottom). (B-C) Electrode placement, chest lead directionality, and corresponding, representative ECG tracing from a neonatal mouse pup at P1.0 (Lead II; purple).

A poor-quality reading has no discernable beats, shows clear interference, and has waves or inconsistency across the reading (Figure 3.3).

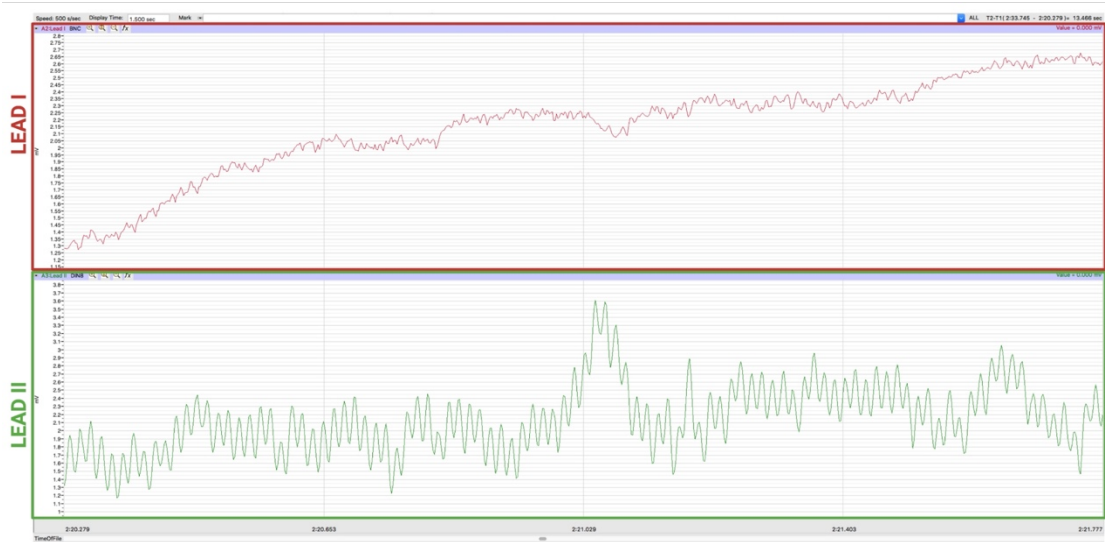


Figure 3.3: Representative ECG read with complications. This image is representative of a poor-quality ECG reading using the 2-lead, noninvasive device on the first postnatal day (P1.0). The above images were captured in a 1.5 s reading frame. Poor quality ECG tracings are characterized by the absence of discernable beats (and specific cardiac cycle waveforms), along with pronounced artifact (high signal:noise ratio), and notable inconsistencies between Leads I and II from a given mouse pup. To improve this ECG, both the device and the silicone bumpers securing the pup would require repositioning within the Faraday cage. To minimize electromagnetic interference, removal of all moving devices near the apparatus would need to be carried out. The final troubleshooting measure would involve repositioning of the mouse pup on the device electrodes and/or more conductive gel would need to be (re-)applied. Top ECG strip (red): Lead I; bottom ECG strip (green): Lead II.

To achieve the highest quality ECG, follow instructions carefully. Use caution with application of conducting gel, as it is moderately adhesive, and may require additional time to allow the mouse to accommodate to the device. By doing this, it lowers the risk of the mouse moving, there being a shorting out of electrodes, and for correct use of the device. Mice should be placed on the device so the head is facing the cords that connect the device to the USB-port and in a prone position (Figure 3.4).

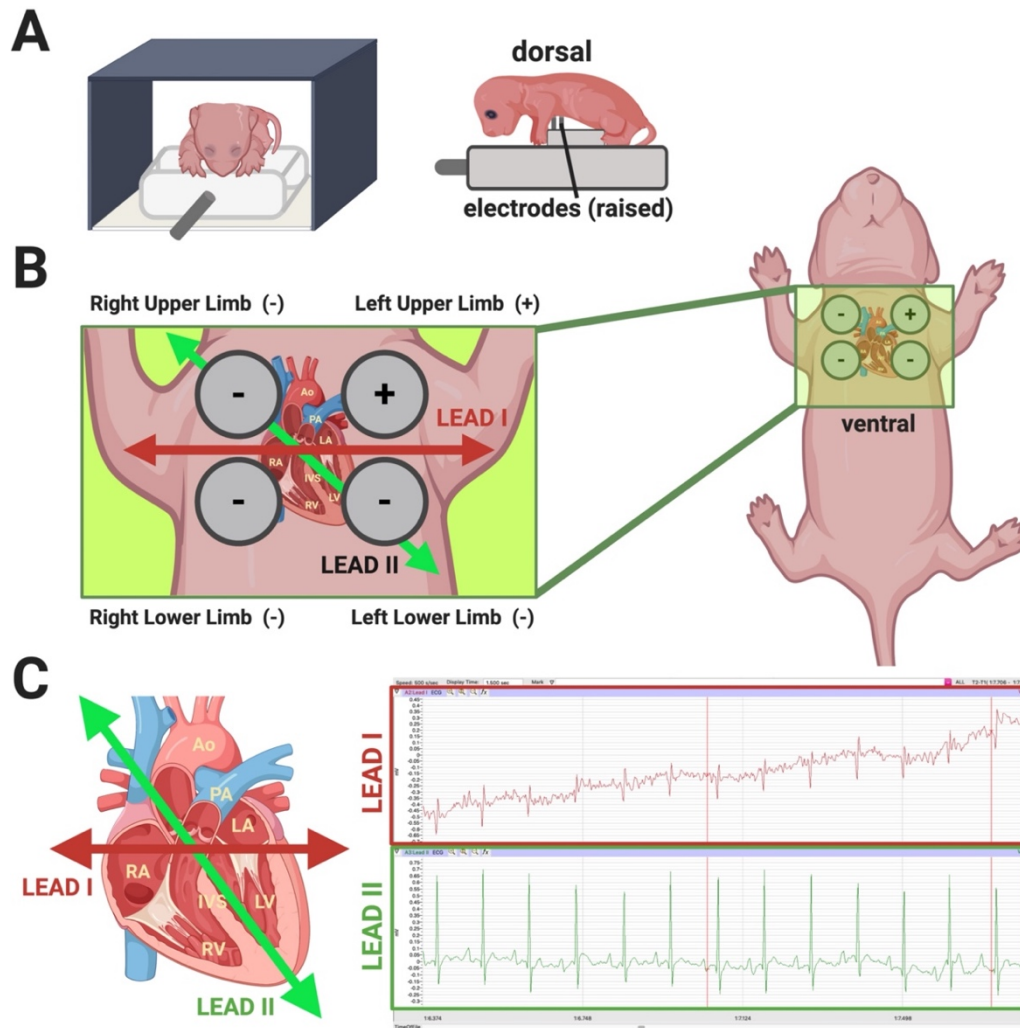


Figure 3.4 Placement of the mouse pup and limb lead electrodes for collection of early postnatal ECG. (A) Left: Anterior perspective of mouse placement on electrode platform within the Faraday cage (black). Right: Lateral view illustrating proper mouse placement on top of raised electrodes/platform; supportive silicone bumpers (not pictured) are placed to either side and across the top of the mouse pup within the Faraday cage. (B) Bipolar limb leads and electrode placement on the neonatal mouse. Illustration depicts the point of contact for each raised electrode on the ventral thoracic surface of the mouse pup. (B,C) Electrode placement, chest lead directionality, and (C) corresponding, representative ECG tracings from a neonatal mouse pup at P1.0 (Lead I (red); Lead II (green)).

The mouse should be secured by rubber bumpers to hold them securely in place, with two on the side and one on the top (Figure 3.4). These bumpers should secure the mouse, but should not inhibit the mouse from moving its head. The layout of the mouse

is important for the reading, as the leads are stationary. The leads are set up so that the front two electrodes are Lead I (Figure 3.4). The rear two electrodes are Leads II and III, with the ground electrode being on the rump of the pup (Figure 3.4). Setting the mouse up in this way will allow for better results.

The program used allows for the analysis of the ECG in the program. This provides analysis of key aspects including heart rate, R-R intervals, QRS complex interval, QT interval, and PR interval. Given this ability, it was possible to establish a data set of normative values for a perinatal mouse (Table 3.1).

Table 3.1 Representative results of ECG measurements for the average perinatal mouse pup P1, P3, P5, and P7.

Pup Age	Ave/STDEV	Heart Rate	R-R Interval	PR Duration (ms)	QRS Duration (ms)	QT Duration (ms)	ST Duration (ms)	T Duration (ms)	P Duration (ms)
P1	Averages	357.2	169.1	36.3	16.9	45.4	16.4	18	12.8
	Standard Deviation	36.3	20	10.9	5.8	16	7.4	7.2	3.1
P3	Averages	412.4	149.2	46.4	14.5	53	22.3	16.2	14.8
	Standard Deviation	55.4	21.4	6.8	11	12.2	6.9	4.6	3.1
P5	Averages	505.5	119.2	46.7	11.7	51.3	20.8	18.8	14.2
	Standard Deviation	19.2	4.6	13.3	5.8	8.1	11.4	4.6	2.3
P7	Averages	555.3	108.7	40	9.5	43.6	20.3	13.7	14
	Standard Deviation	34.2	7	2.5	0.6	6	7.1	3.2	2.7

These normative results were based off mice who were analyzed within one day after birth. It was found that an average heartbeat was 357.2 beats per minute.

The average R-R, QRS, QT, and PR intervals were 169.1, 16.9, 45.4, and 36.3 milliseconds (ms), respectively (Table 3.1). Importantly, the setup can be used to analyze ECG patterns from neonatal mice suffering from congenital heart defects (Figure 3.1).

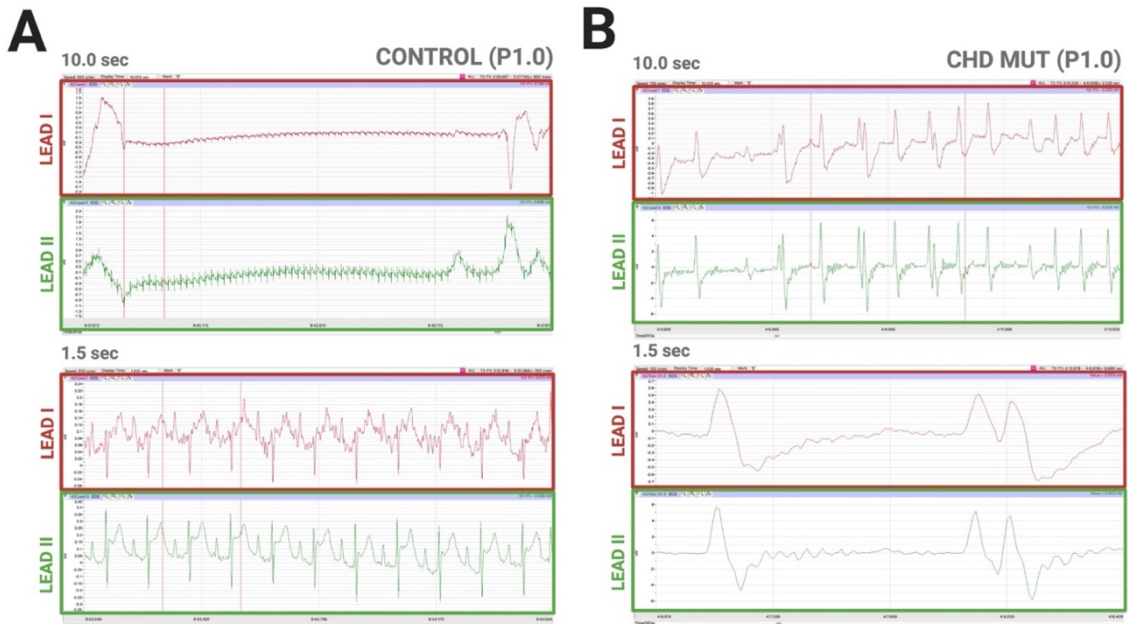


Figure 3.5 Comparative electrocardiographic reads from littermate control pups and mutant pups with congenital heart disease on the first postnatal day (P1.0). **(A,B)** Images represent examples of good quality ECG tracings from healthy neonatal pups **(A, CONTROL)** compared to pups born with CHD **(B, CHD MUT)** at P1.0. The 2-lead, noninvasive device was used to capture ECG tracings at 10.0 **(A,B, top)** and 1.5-second intervals **(A, B, bottom)**. Noticeable differences in heart rate are apparent in the CHD MUT **(B)**, as visualized by the decreased number of cardiac cycles (complexes) visible in the given time frame. Comparison also reveals irregularities in the general morphology of QRS waveforms, frequency, and overall regularity of cardiac cycles in the CHD MUT **(B)** when compared to the control **(A)**. Lead I (red); Lead II (green).

3.4 Discussion

The data points collected in perinatal day 1 mouse pups are slightly below the average expected values for adult mice (D. Ho et al., 2011) (500-700 beats per minute). There is an increase in heart rate as the mouse ages, which falls more in line for the expected values (Table 3.1). However, it is important to emphasize that neonatal values were on the lower end of this range, supporting the idea that normative values should be documented in an age-specific manner. This method is different than other electrocardiogram protocols in that there is no physical trauma to the mouse. The protocol is totally noninvasive, does not require the use of anesthesia, and is optimal for

mice immediately after birth. No other electrocardiogram device allows for pups this young to be analyzed in this manner (Chu et al., 2001; Heier & DiDonato, 2015; Heier, Hampton, Wang, & DiDonato, 2010). This protocol aims to establish a reliable reference method to generate normative data specific to the neonatal mouse population, but applicable to human pediatric populations.

When performing an electrocardiogram on such a small animal, it is important to be cautious with all steps. However, there are a few key steps that can change the quality of the results. The first is applying the conductive gel. If there is too much gel, there will be a higher chance for the electrodes to connect and short. If there is not enough gel, there will not be a secure connection. The best method to apply the gel is to approach the electrode from the outside corner and roll the gel over the top of the electrode. It is very important that extreme caution is taken to assure there are no threads between electrodes, which would interfere with the presence and/or quality of the electrical activity. It may be useful to take a thin tool (e.g., forceps), and run it between the electrodes to collect any stray threads which may not be apparently visible. While not formally required as part of the protocol, this extra step could serve as an additional precaution to ensure optimal conduction and minimal noise.

If the presence of noise of static causes the ECG to be unreadable (Figure 3.5), it may be useful to remove all electronic devices from the immediately (table-top) vicinity. This is especially helpful if any of the electronic devices present nearby are moving, as this movement can be picked up by the ECG recording device (Patel & Souter, 2008). It is also important not to introduce any outside movements during data collection. Outside movements that could interfere with the quality of the ECG could include setting

objects down on the same nearby surface, and must be avoided until after the reading is complete. In addition to outside devices, very active mouse pups may also cause electrical interference associated with excessive body movements. The likelihood of this type of musculoskeletal interference increases as the pups mature, which should be considered when selecting ages for data collection. In the event that the pup shifts from the electrodes in a way that significantly compromises the quality of the ECG reading, repositioning of the pup should be considered. Repositioning the mouse before opting to reapply the electrode gel can provide improved results in most cases and save additional time and reagents. Before repositioning the pup, select the pause button in the software. Pausing the run will stop active recording of the ECG but will continue to track time. Of note, when the recording is resumed, the ECG will appear at a later time than paused at. Slide the device platform out from the Faraday cage with the mouse still positioned between the bumpers. Remove the bumpers surrounding the mouse, and gently lift the pup off of the electrodes. Reposition pup on the electrodes following the same protocol of gently holding the mouse in place for 1 min for gel to adhere (step 3.4-3.5). Try to reposition the mouse so that the electrodes are on the thorax between the upper limbs (Figure 3.4). While designed as an ideal, noninvasive method for collecting ECG in neonatal mice, one limitation associated with this protocol would be the increased mobility associated with data collection on an un-anesthetized mouse, as the mouse may also move and shift on the device which will affect the quality of the reading. While movement may be limited with positioning of silicone bumpers, this cannot be prevented without the use of sedation or anesthesia.

In a situation where the ECG recording comes with heavy interference (Figure 3.3) despite having minimized all electrical interference, the next step that should be taken is to reposition the external wiring connecting the recording platform to the Faraday cage. It is very important that the external wiring remains properly connected to the recording platform during data acquisition. If external wiring is repositioned, be sure to reattach this wiring carefully at both ends, until a clearer recording can be obtained. If the use of the Faraday cage provided with the device is not suitable, the device can be used in other Faraday cages. If the recording is not clear or the mouse has moved from the electrodes, remove the mouse from the device and clean the electrodes by taking forceps and removing all the conductive gel. Because the conducting gel is water-soluble, one can also use warm water to gently remove excess gel from the skin of the pup. Reapply the gel and reposition the pup. To obtain the best results make sure the device is properly cleaned before and after each use. The gel does dry and can be removed using forceps to pull it from the device, but the gel is water soluble, so a damp cloth can be used to clean the electrodes of the recording platform. Older mice have been more active in the recording process, so it is important to closely monitor them as they often move from the electrodes and can even move off the device platform. While a clear read may not happen right away, with troubleshooting and repositioning, there has been success in getting usable recordings with this device (Figure 3.4). Active mice may need to be returned to their mother and reanalyzed after a break. They can also be held in the palm of a hand and gently covered to provide heat and darkness until the pup settles down. This device is designed to collect ECG data on mouse pups from the age of birth to P10 (Figure 3.6).

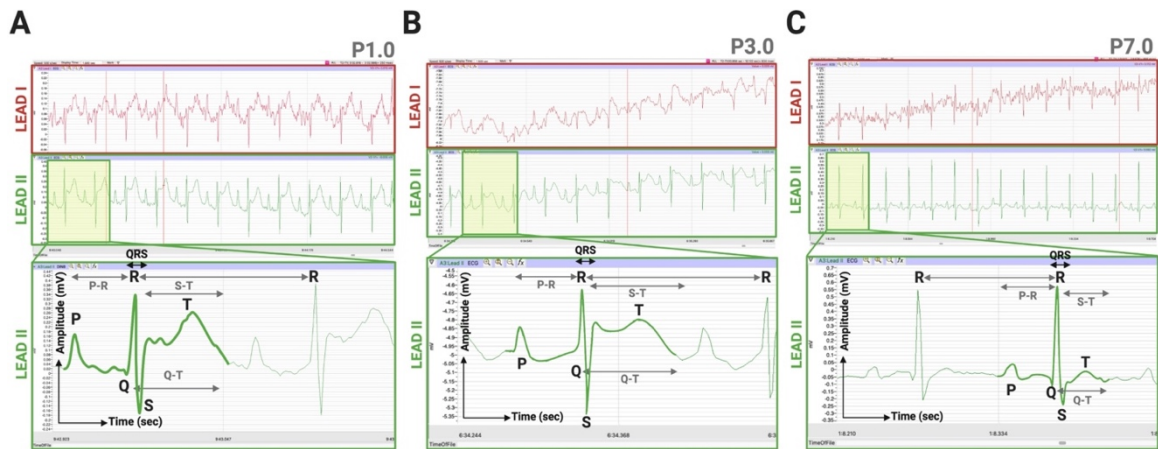


Figure 3.6 Representative ECG tracings of neonatal mice at multiple postnatal time points. Representative ECG reads (top 2 traces) and illustrated cardiac cycles (bottom row) from neonatal mouse pups on the first (A, P1.0), third (B, P3.0), and seventh (C, P7.0) postnatal day. Each image represents an exemplary ECG tracing using the 2-lead, noninvasive device, captured in a 1.5 second frame of the reading (A-C, Lead I (top/red); Lead II (bottom/green)). While individual waveforms do appear to undergo morphological changes with increasing age, notable and consistent characteristics include clear, discernable beats, as described collectively by the presence of consistent P-waves followed by a QRS complex and subsequent T-waves, visible in both Leads I-II of each postnatal time point.

Pups older than P10 will likely not be able to fit into the device with the Faraday cage, an essential component to maximizing signal to noise ratios. Even at P10, positioning adjustments will likely need to be made to accommodate a larger body size into the device. Use extreme caution when moving the device into and out of the Faraday cage. Removal of the top bumper will allow the mouse to lay on the electrode platform with the surrounding Faraday cage. Given that the mice at this age are more active, they are more apt to move off the electrodes without the stabilization of the top bumper. The top bumper can also be placed in front of the pup to help discourage the pup moving off the device. The novelty of this device and corresponding protocol include optimization for use immediately after birth, the ability of the system to accommodate a broader age range (P1-P10) and the need addressed by this method to expand the translational

applications of in vivo research methods in the field of cardiovascular physiology and beyond. Although sophisticated devices utilizing echocardiography to quantify cardiac cycles in neonate mice are available (Castellan, Thomson, Moran, & Gray, 2020). One great advantage of this protocol is that it allows for a relatively simple and affordable means to address basic electrophysiological parameters, which is very attractive in the current parlous scientific funding environment.

3.5 Disclosures

The authors report no conflicts of interest.

3.5.1 Acknowledgments

The authors acknowledge generous support from the Saving tiny Hearts Society (KLT), the UNE COBRE Program (NIGMS grant number P20GM103643; Pricipal Investigator, Ian Meng), and the SURE Fellowship Program at the University of New England (VLB), as well as patient technical support from Ashish More (iWorx, Dover, NH). Figure 3, Figure 4, and Figure S1 were created with BioRender software.

3.5.2 References

References cited in Chapter 3 have been incorporated sequentially into the larger body of the dissertation. Numbered citations reflect works cited in the *REFERENCES*.

CHAPTER 4

LOSS OF CNCC PRIMARY CILIA CAUSES CONGENITAL HEART DEFECTS VIA UPREGULATION OF HEDGEHOG SIGNALING

4.1 Neural Crest Cells Elaborate Primary Cilia Necessary for Cardiogenesis

Primary cilia are known to be essential to many processes of cellular, tissue and organogenesis (Goetz & Anderson, 2010; Tasouri & Tucker, 2011) and have been documented in nearly all mammalian cell types (Satir, Pedersen, & Christensen, 2010). However, characterization of both sensory and mechanical roles of cilia in many cell types lacks complete characterization of the functional/physiological roles played by the cilium, and consequently, problems that may arise resulting from damage to and or loss of the cilium from many of these cell types (Pan, Wang, & Snell, 2005; Wong et al., 2009). In the developing heart, primary cilia have been found in nearly all progenitor cell populations required for proper embryonic heart formation, including but not limited to cells of the first and second heart fields, as well as CNCC populations (Burns et al., 2019; Kaur, McGlashan, & Ward, 2018; Klena, Gibbs, & Lo, 2017; Marc August Willaredt et al., 2012). As these cardiac progenitors mature and differentiate, primary cilia can further be observed in cell types such as endocardial cells (Samsa et al., 2015), epicardial cells (Koefoed et al., 2014), mesenchymal cells of the developing endocardial cushions (Toomer et al., 2017), and in some cases, cardiomyocytes (Clement et al., 2009; Diguët et al., 2015; Villalobos et al., 2019).

4.1.1 Conditional Elimination of Primary Cilia from CNCC Leads to Global Congenital Heart Defects

Primary cilia of CNCC were conditionally eliminated using multiple *Wnt1:Cre* drivers flanking *Ift88 loxP* at Chromosome 14 (Table 4.1). A td-tomato (*Tdt*) reporter was used to track neural crest migration following activation of the *Wnt1-Cre* at approximately E7.5 (Table 4.1). Quantification of both *Cre⁺/Tdt⁺* CNCC cells and non-CNCC cells (*Tdt⁻/Cre⁻*) as well as the presence/absence of primary cilia was performed at multiple embryonic timepoints, beginning at E9.5, in the pharyngeal region (pharyngeal arch region; PA), the developing outflow tract and endocardial cushions (OFT(ECC)), as well as the primitive ventricular myocardium (vMyoC; Figure 4.1). A “ciliated cell” was defined as a nucleus (DAPI) in proximity to the presence of both an intact primary cilium axoneme (anti-Arl13B/ anti-acetylated alpha-tubulin) as well as its corresponding basal body component (anti gamma-tubulin) using immunofluorescence analysis of frozen tissue sections. We further assessed ciliation as an independent variable by anatomical region, specifically in the pharyngeal region, the endocardial cushions of the developing outflow tract (OFT/ECC), as well as in the developing ventricular myocardium (vMyoC). Primary cilia are shown to be present on both CNCC (td-tomato-positive; *Tdt⁺*) and non-CNCC (td-tomato-negative; *Tdt⁻*) cell populations of WT CON, *Tdt⁺* (*Cre⁺*) controls (*Tdt⁺/Cre⁺CON*; “CON”) and homozygous MUT embryos at E9.5 in PA, cardiac OFT and vMyoC (Figure 4.1; A, C). Qualitative analysis of these same regions at E11.5 revealed a noticeable loss of primary cilia axonemes (anti-Arl13B+) in *Tdt⁺* CNCC of *Tdt⁺MUT* when compared to CON (*Tdt⁺CON*; Figure 4.1B). Loss of primary cilia (expressed as percent ciliation; % ciliation) from *Tdt⁺*

(Cre+/CNCC) and Tdt- (Cre-/non-CNCC) cells in the homozygous mutant was observed beginning at E9.5 (Figure 4.1; A, C). Two-way ANOVA statistical analysis was performed with Tukey's post-hoc analysis to compare PA %ciliation of Tdt+/CRE+ (CNCC) between CON and MUT at E9.5 (Figure 4.1, Panel C).

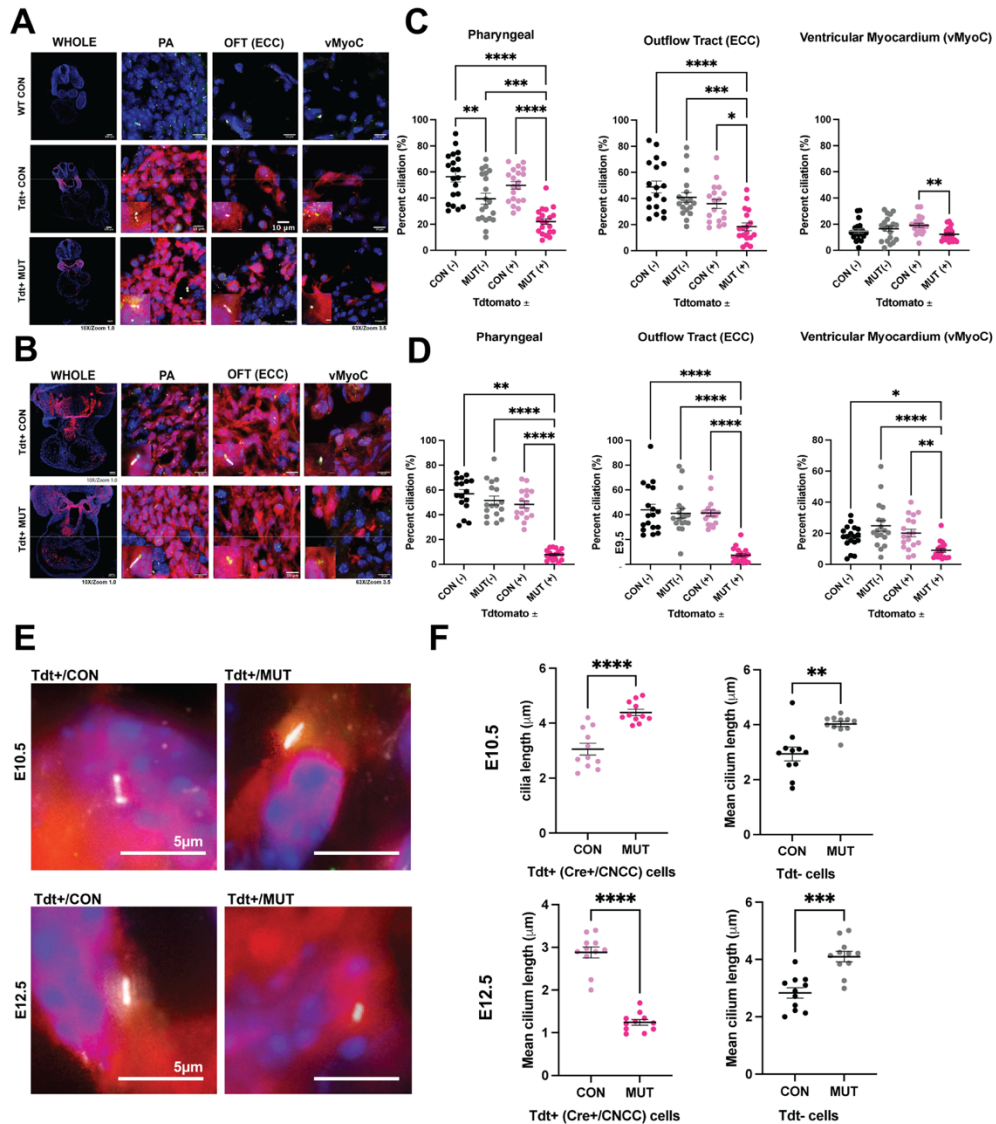


Figure 4.1. Tracking and quantifying loss of primary cilia of CNCC during heart development using a td-tomato reporter. (A-D) Tracking and quantifying loss of primary cilia of CNCC during heart development (E9.5-E11.5) using a Tdt reporter. Representative confocal immunofluorescence images illustrating the regional presence of the intact primary cilia axoneme (α Arl13B/white) and basal body complex (α -tubulin/green) on both CNCC (Wnt1:Cre+/Tdt+;red) and non-CNCC cells (Wnt1:Cre-/Tdt-; DAPI/blue) in the pharyngeal arches (PA), endocardial cushions (OFT(ECC)) and the ventricular myocardium (vMyoC) regions of wildtype control (WT CON/Tdt-; **A, top**), Tdt+CON (Wnt1:Cre+/Tdt+/lft88+/+; **A, middle**) and Tdt+MUT (Wnt1:Cre+/Tdt+/lft88flox/flox; **A, bottom**) embryos at E9.5 (A) and E11.5 (B) dpc. (C-D) Presence of intact primary cilia (axoneme and basal body) were quantified and expressed as percent ciliation (% ciliation) in Tdt+ and Tdt- cells of CON and MUT embryos in the PA, OFT/ECC and vMyoC regions of interest at the indicated embryonic time points. A two-way ANOVA was used to compare % ciliation between and among CON and MUT tissue. (E) Representative immunofluorescence images indicated the axoneme of the primary cilium of Tdt+ cells of the OFT/ECC CON (E, left) and MUT (E, right) at E10.5 and E12.5, respectively. (F) Quantitative analysis of individual primary cilia length (μ m) of Tdt+ (pink/magenta) and Tdt- (black/gray) cells of CON (left) and MUT (right) OFT/ECC at E10.5 (F, top) and E12.5 (F, bottom). * $p \leq 0.05$; ** $p < 0.01$; *** $p < 0.001$; **** $p < 0.0001$

As expected, in comparison of Tdt+ and Tdt- cells of the CON, we observed no statistically significant difference in % ciliation ($p=0.4237$). By contrast, In the homozygous mutant, % ciliation in the targeted Tdt+/CNCC decreased significantly by $17.6\pm 4.30\%$ when compared to the non-CNCC cells of the MUT ($p=0.0008$), and decreased by approximately 27.8% (± 4.30 SEM) when compared to CNCC of the CON ($p<0.0001$). Statistical comparison of the % ciliation in non-CNCC (Tdt-) cells, revealed that there was also a significant decrease of $16.81\pm 4.30\%$ in percent ciliation in the MUT compared to CON ($p=0.0014$). In the E9.5 OFT/ECC region, no statistically significant decrease in % ciliation was observed between CON CNCC (Tdt+) cells and non-CNCC (Tdt-) cells ($p<0.09$). Percent ciliation in the MUT decreased significantly by $22.39\pm 5.42\%$ in MUT Tdt+ versus Tdt- cells, and by $17.51\pm 5.42\%$ when compared to CON Tdt+ cells ($p=0.0113$). In the OFT region, we did not observe any statistically significant differences in % ciliation of the Tdt- (non-CNCC) cells of the CON versus MUT ($p=0.452$). Percent ciliation of Tdt+ cells present in the E9.5 future vMyoC region was performed, and revealed a statistically significant differences only in the comparison of % ciliation of Tdt+ cells of MUT to those of the CON, which declined by $6.865\pm 1.93\%$ ($p=0.0041$). Of note, % ciliation in Tdt+ and Tdt- cells of the E9.5 MUT vMyoC did not statistically significantly differ ($p=0.133$).

In the subsequent two embryonic, gestational days (E11.5), the qualitative loss of primary cilia in CNCC/Tdt+ cells was notably pronounced when compared to CON (Figure 4.1, Panel D). Quantification using a two-way ANOVA statistical analysis was performed with Tukey's post-hoc analysis to compare PA % ciliation of Tdt+/CRE+

(CNCC) between CON and MUT at E11.5. Percent ciliation in the PA region decreased drastically by $43.58 \pm 4.511\%$ in the Tdt+ versus Tdt- cells of the MUT ($p < 0.0001$), and decreased by $40.47 \pm 4.511\%$ in the MUT Tdt+ cells compared to those in the CON ($p < 0.0001$). The decrease in % ciliation observed in the Tdt- cells of the MUT versus CON in the E9.5 PA was no longer significantly different by E11.5 ($p = 0.622$). In the E11.5 OFT/ECC region, % ciliation decreased by $33.7 \pm 4.71\%$ in the Tdt+ cells compared to Tdt- cells of the MUT ($p < 0.0001$), and decreased by a similar $33.94 \pm 4.71\%$ when compared to Tdt+ cells of the CON OFT/ECC ($p < 0.0001$). There were no statistically significant differences in % ciliation of the Tdt+ and Tdt- cells of the CON ($p = 0.953$), as well as when comparing Tdt- cells of the MUT to those of the CON ($p = 0.9402$). Final comparison of % ciliation of the E11.5 vMyoC region revealed multiple changes when compared to results from E9.5 vMyoC. Specifically, % ciliation decreased by $15.79 \pm 3.18\%$ in the Tdt+ cells versus the Tdt- cells of the MUT, and continued to statistically significantly decline to $20.13 \pm 3.18\%$ when compared to Tdt+ cells of the CON ($p = 0.0052$). Importantly, no statistically significant differences were observed in the Tdt+ compared to the Tdt- cells of the CON ($p = 0.853$), as well as when comparing Tdt- cells of the MUT to those of the CON ($p = 0.118$).

4.1.2 *In Vivo* Loss of CNCC Primary Cilia Leads to Outflow Tract Defects and Multi-Component CHD

Conditional elimination of primary cilia from CNCC using multiple neural crest-specific Cre-drivers resulted in several CHDs known to be associated with problems with neural crest and/or primary cilia (alignment/laterality), including congenital

abnormalities of the OFT, atrial and ventricular septa, endocardial cushions (future heart valves) solidified by E14.5 (Figure 4.2).

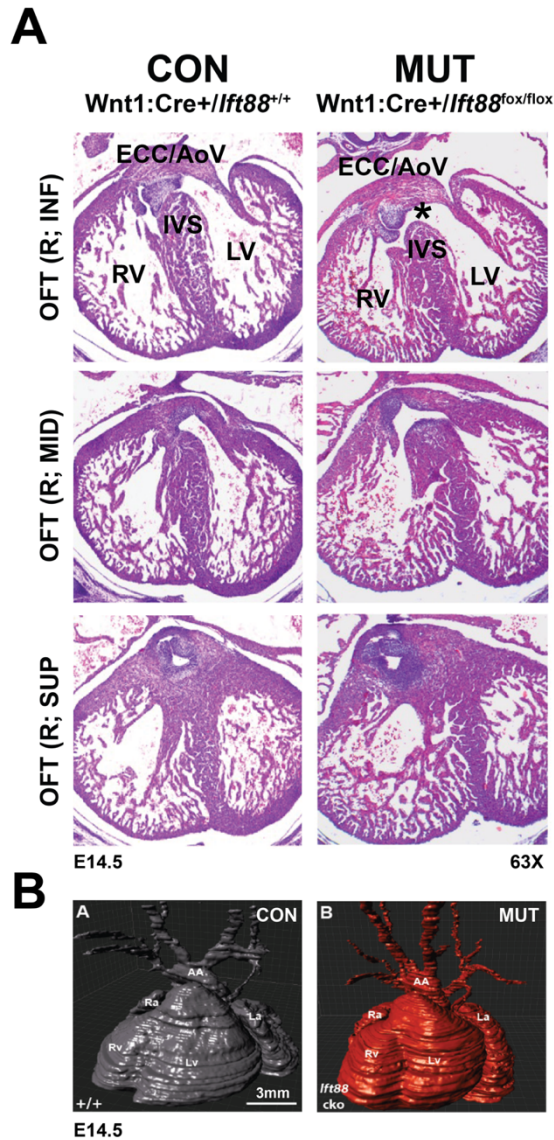


Figure 4.2 CNCC loss of primary cilia impairs proper alignment and septation of the developing outflow tract, leading to outflow tract defects. Serial histological sections illustrating normal embryonic (mammalian) outflow tract (OFT) formation in the CON (**A, Left**) and formation of the double-outlet right ventricle (DORV) in the MUT (**A, Right**) at E14.5. (**B**) Serial sections of two-dimensional H&E images were photographed and compiled using IMARIS software to render a three-dimensional reconstruction of the CON (**B, Left**) and MUT (**B, Right**) embryonic whole heart and OFT at E14.5. Outflow Tract (OFT), right (R), inferior (INF), mid-level (MID), superior (SUP), endocardial cushions (ECC); (future) Aortic valve (AoV), Right Ventricle (RV), Left Ventricle (LV); Interventricular Septum (IVS), Aortic Arch (AA), Right atrium (Ra), Left Atrium (La), *Indicates VSD.

Histological examinations of the CON OFT region at E14.5 illustrates the inferior portion of the proximal, left OFT with an intact, developing aortic valve, which is continuous with an intact interventricular septum (IVS), fully septating the E14.5 right and left ventricles (Figure 4.2, A, Left/OFT (INF)). Ascending sections of the CON illustrate the left OFT shifting further towards the midline of the heart, in line with the fully-intact IVS (Figure 4.2, A, Left). The AoV leaflets and (future) AoV are visible in the CON OFT, where it remains at the midline of the heart, in line with the intact IVS and is appropriately aligned with the aortic vestibule shown (Figure 4.2, A, Left/OFT (INF)).

Serial, ascending sections of the MUT OFT (A, Right/OFT (INF)) reveal the developing ECC/AoV situated in a more exaggerated fashion towards the RV side of the heart, and which is discontinuous with the intramembranous portion of the IVS at E14.5 (Figure 4.2, A, Right). Ascending, serial sections reveal an additional ventricular septal defect in the muscular portion of the IVS as well as the left OFT that remains oriented towards the RV side of the heart and not at the midline (bottom panel; OFT (MID)). The distal, superior aspect of the MUT OFT show the orientation of the left OFT aligning with the RV side of the heart, solidifying the DORV phenotype seen in MUT (Figure 4.2).

Serial, two-dimensional tissue sections of CON and MUT stained with H&E were imaged at 63X and were compiled using the IMARIS software to render a three-dimensional E14.5 embryonic whole-heart and OFT (Figure 4.2, B). On first examination, the MUT 3D rendering (B, Right) does not appear grossly different from the CON (B, Left). However, upon closer examination of the OFT region, it is clear that the general morphology of the MUT OFT appears less robust and potentially smaller, in addition to the fact that it is oriented more anteriorly and laterally (towards the right side

of the heart) when compared to CON (Figure 4.2, B). Additional observations included a smaller (thinner) aortic arch (AA) and what appears to be dilation (or an overall larger size of the left atrium of the MUT compared to CON (Figure 4.2, B).

Following our initial histological characterization of phenotype resulting from CNCC loss of primary cilia, we then sought to expand our phenotypic analysis to include 3D, high-resolution, micro-MRI analysis of CON and MUT both at the whole embryo level in the sagittal plane, as well as a focused, 2- and four-chamber study of the developing mouse at E14.5 (Figure 4.3). We observed no obvious differences in whole-embryo size between CON and MUT embryos were observed at E14.5 (Figure 4.3, A).

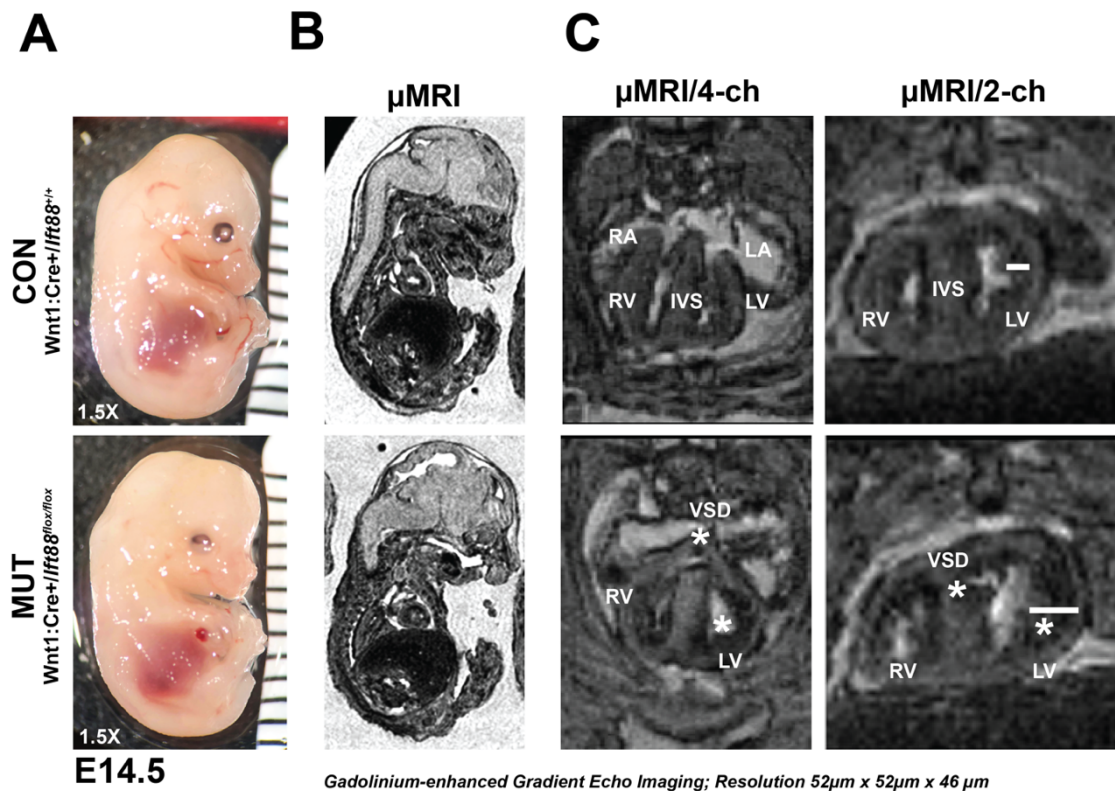


Figure 4.3 Phenotypic analysis of E14.5 CON and MUT embryos using micro-magnetic resonance imaging. **(A)** Elimination of primary cilia in neural crest populations (MUT, bottom) results in a variety of CHDs along with accompanying extracardiac congenital defects, including craniofacial phenotypic abnormalities most pronounced in the MUT by E14.5 when compared to CON (top). **(B)** 3D High-resolution, micro-MRI characterization of individual CON (top row) and MUT (bottom) whole-embryos at E14.5. **(C)** 3D μ -MRI analysis of the embryonic mouse heart utilizing both 4-chamber (left) and 2-chamber (right) perspectives. Resolution at 52 m x 52 μ m x 52 μ m; Images courtesy of MMCRI Small Animal Imaging Core Facility; Right Atrium (RA), Left Atrium (LA), Right Ventricle (RV), Left Ventricle (LV), Interventricular Septum (IVS), Ventricular Septal Defect (VSD); *Indicates congenital cardiac defect not observed in CON; white lines in both CON and MUT 2-chamber views are drawn as an approximation of LV wall trabecular thickness.

Despite the lack of size differences, the MUT phenotype was easily identifiable by E14.5 due to the extent of the severity of craniofacial defects, cleft palate, and hydrocephaly present in MUT when compared to CON (Figure 4.3, A, B). Beneath this exterior, MUT embryos displayed a full array of congenital cardiac defects, including

OFT defects, VSD, and what was *initially* characterized as ventricular hypertrophy, visible with μ -MRI of the cardiac region from the 4- and 2-chamber views (Figure 4.3, C).

Upon closer examination of the MUT ventricular morphology from μ -MRI, and concurrently with our histological analysis of the E14.5 LV myocardium, it became clear that what had initially appeared as hypertrophy of the MUT ventricles, was actually a combination of ventricular dilation, excessive expansion of the trabecular myocardium and thinning of the compact myocardium (NCC) in the MUT when compared to CON (Figure 4.3, C). Surprisingly, this aspect of the MUT ventricular phenotype can also be seen in the whole-embryo μ -MRI images (Figure 4.3, B). Specifically, the cross-sectional view of the CON includes an open lumen (white circle) and a ventricular myocardial thickness that is unremarkable. In the MUT, however, the cross-sectional view of the ventricular chamber does not reveal an obvious and patent ventricular lumen (Figure 4.3, B, bottom). Instead, the MUT ventricular chamber appears clouded by the extent of the trabecular folds protrusions. Most importantly, these and all other described cardiac phenotypic findings discovered with 3D μ -MRI, were also observed using 2D histological analysis with standard H&E staining, further confirming our initial phenotypic characterizations and justifying our subsequent investigations seeking to quantify the novel aspect of the MUT phenotype, noncompaction of the ventricular myocardium.

4.1.3 Persistent, Embryonic and Perinatal Ventricular Myocardial Phenotype Resulting from the Loss of CNCC Primary Cilia *In Vivo*

Most notably, the resultant phenotype consistently displayed a novel and persistent aspect of the mutant phenotype, which included pronounced hypertrabeculation of the ventricular myocardium, a thinning of the compact myocardium, and an overall failure of the ventricular myocardium to fully mature (noncompaction/NCC) when compared to controls (Figure 4.3).

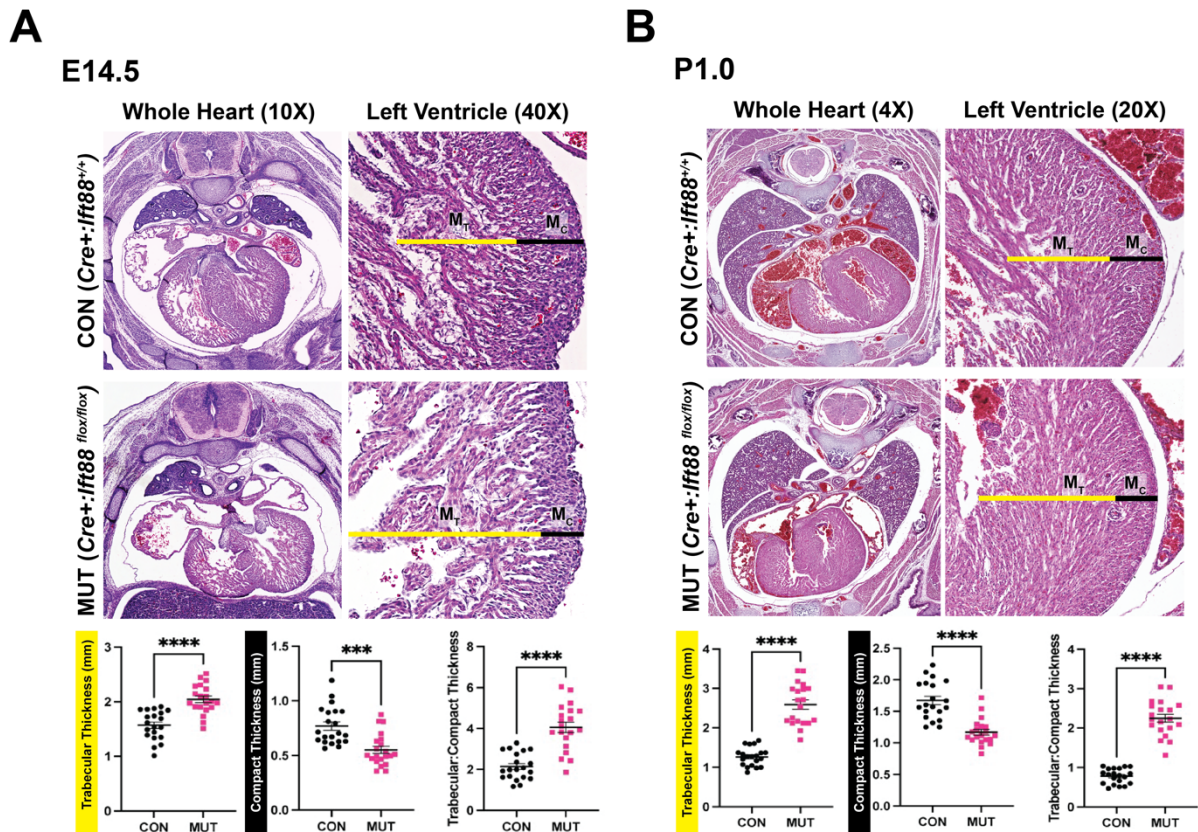


Figure 4.4. Persistent, Embryonic and Perinatal ventricular myocardial phenotype resulting from the loss of CNCC primary cilia *in vivo*. Paraffin-embedded, transverse cross-sections of littermate control (CON; Cre+/*lft88*^{+/+}) and homozygous MUT hearts (Cre+/*lft88*^{lox/lox}) stained with H&E at embryonic time points E14.5 (**A, top**) and postnatal day 1 (P1.0; **B, top**). Comparison of mean ventricular myocardial trabecular (M_T) and compact (M_C) thickness (mm) as well as LV NCC ratios of CON and MUT hearts at E14.5 (**A, bottom**) and P1.0 (**B, bottom**). Quantitations also included assessment of LV NCC ratios, expressed as LV trabecular:compact thickness (mm) from CON and MUT hearts at E14.5 (**A, bottom**) and P1.0 (**B, bottom**). ***Indicated statistically significant differences, p<0.001,****p<0.0001

Changes in the general morphology of the ventricular myocardium, including trabeculation, were first visible by E11.5 in the MUT, and were diagnostically significant at E14.5 (Figure 4.4). Ventricular thickness measurements at E14.5 revealed a statistically significant increase in the trabecular thickness in the MUT when compared to CON ($p < 0.01$). Although only a slight decrease in compact thickness was observed in the MUT, the noncompaction ratio of compact to trabecular thickness was statistically increased in the MUT versus the CON ($p < 0.01$; Figure 4.4, B). The noncompaction component of the ventricular phenotype can be best characterized by the extent of the hypertrabeculation of the ventricular myocardium, which persisted through the first postnatal day (Figure 4.4, C), when perinatal lethality occurred. At P1.0, trabecular thickness remained significantly thicker in the MUT ventricular myocardium ($p < 0.0001$; Figure 4.4, C-D). It was also at this point that compact myocardial thickness became significantly decreased in the MUT compared to the CON ($p < 0.01$), and the differences in noncompaction ratio between the CON and MUT became further exaggerated ($p < 0.0001$; Figure 4.4, D).

4.1.4 Persistent Noncompaction Resulting from CNCC Loss of Cilia Occurs Concurrently with Disruption to the Cardiac Conduction System and Fatal Cardiac Arrhythmia

Cardiac function was assessed using a novel, non-invasive method of ECG collection designed by our lab for the newborn mouse (Figure 4.5). Multi-lead ECG analysis of P1.0 MUT and littermate CON pups revealed pronounced bradycardia, heart rate irregularity, and frequent occurrences of premature ventricular contractions (PVCs)

in the MUT (Figure 4.5). Some MUT pups also displayed ventricular arrhythmias such as junctional rhythms, second degree heart block (BBB), and the appearance of J waves/J wave depression suggestive of early ventricular repolarization (Figure 4.5). Other instances of ventricular irregularities included widened QRS complex, suggestive of defects with ventricular repolarization (Figure 4.5). On several occasions during data collection, MUT pups also experienced bouts of ventricular tachycardia, ventricular fibrillation, and instances of Torsade du Ponte which appeared to be transient in nature and typically resolving within milliseconds (Figure 4.5, Table 4.1).

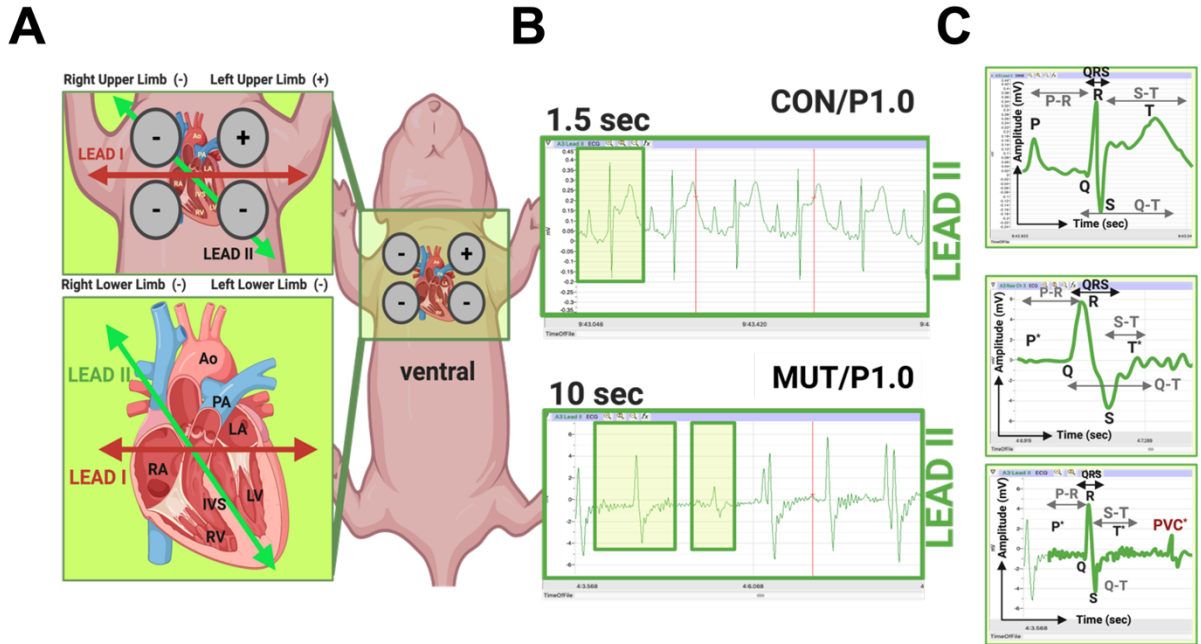
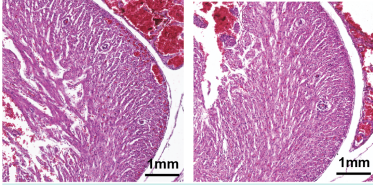
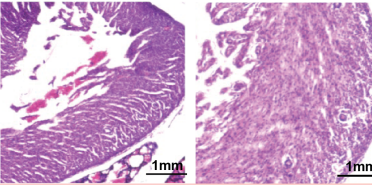
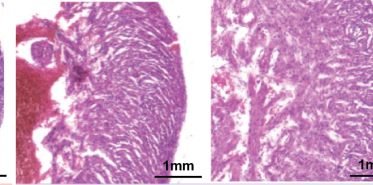


Figure 4.5. CNCC loss of primary cilia impairs ventricular morphology and cardiac function. (A) A novel, non-invasive method of collecting mouse electrocardiograms was developed to characterize and quantify electrophysiological abnormalities in MUT and CON pups on the first postnatal day (P1.0). **(B, top)** Representative ECG strip from Lead II of CON pup, demonstrating heart rate, rhythm, and regularity within normal limits. **(B, bottom)** Representative ECG from Lead II of MUT pup, indicating a grossly abnormal heart rate, rhythm disturbances and a variety of waveform abnormalities. **(C, top)** Enlarged, representative tracing of a single cardiac cycle from a CON pup, demonstrating a the sequential P-wave, QRS complex and subsequent T-waveforms, all with morphology within normal limits. **(C, middle/bottom)** Enlargement of two, representative but abnormal waveforms from a MUT pup, illustrating a barely detectable P-wave followed by a widened QRS complex, ST-segment depression, and minimal formation of a T-wave **(C, middle)**. **(C-bottom)** Additional, abnormal but representative QRS complex and accompanying PVC from a MUT pup.

Table 4.1 Summary of multiple Cre-drivers and primary cilia-specific conditional knockout mouse models and persistence of anatomical and cardiac electrophysiological phenotype

		GENOTYPE/SPECIFICITY					
		Wnt1:Cre-2		Wnt1:Cre-1		Wnt1:Cre-2	
		CON (<i>Ift88^{+/+}</i>)	MUT (<i>Ift88^{flox/flox}</i>)	CON (<i>Ift88^{+/+}</i>)	MUT (<i>Ift88^{flox/flox}</i>)	CON (<i>Kif3a^{+/+}</i>)	MUT (<i>Kif3a^{flox/flox}</i>)
PHENOTYPE	P1.0 LV (H&E)						
	MUT CHD (P1.0)	OFT Defects/DORV (81%; N=26/32) ASD+VSD (100%; N=32/32) >1 VSD (97%; N=30/32) N=42 CON; N=32 MUT *Ventricular NCC (100%; *N=12 total*) *ECG Abnormalities (100%;*N=7 total*)		OFT Defects/DORV (80%; N=8/10) ASD+VSD (100%; N=10/10) >1 VSD (90%; N=9/10) N=13 CON; N=10 MUT *Ventricular NCC (100%; *N=6 total*) *ECG Abnormalities (100%;*N=4 total*)		OFT Defects/DORV (81%; N=3/3) ASD+VSD (100%; N=3/3) >1 VSD (97%; N=3/3) N=5 CON; N=3 MUT *Ventricular NCC (100%; *N=3 total*) *ECG Abnormalities (100%;*N=3 total*)	
	MUT ECG (P1.0)	Bradycardia (100%; N=7/7) Loss of P waves (71%; N=5/7) Widened QRS (100%; N=7/7) Increased QRS Amplitude (100%; N=7/7)		Bradycardia (100%; N=4/4) Loss of P waves (75%; N=3/4) Widened QRS (100%; N=4/4) Increased QRS Amplitude (100%; N=4/4)		Bradycardia (100%; N=3/3) Loss of P waves (100%; N=3/3) Widened QRS (100%; N=3/3) Increased QRS Amplitude (100%; N=3/3)	

4.1.5 Disappearance of CNCC primary cilia disrupts OFT Sonic Hedgehog

Expression

Neural crest cells (including CNCC) migrate ventrally towards the developing cardiac OFT, where future differentiation and proliferation cell behaviors are mediated, in part, by exposure to Sonic Hedgehog (Shh) ligand, which is secreted in abundance from the pharyngeal endoderm, where ligand secretion expands ventrally, forming a Hh gradient up through the developing cardiac outflow tract. At this same embryonic timepoint, isolation of E12.5 ventricular tissue revealed statistically significantly

decreased expression of *Shh* in MUT ($p < 0.01$) and a trend towards decreased *Ptch1* in MUT when compared to CON (Figure 4.6, B).

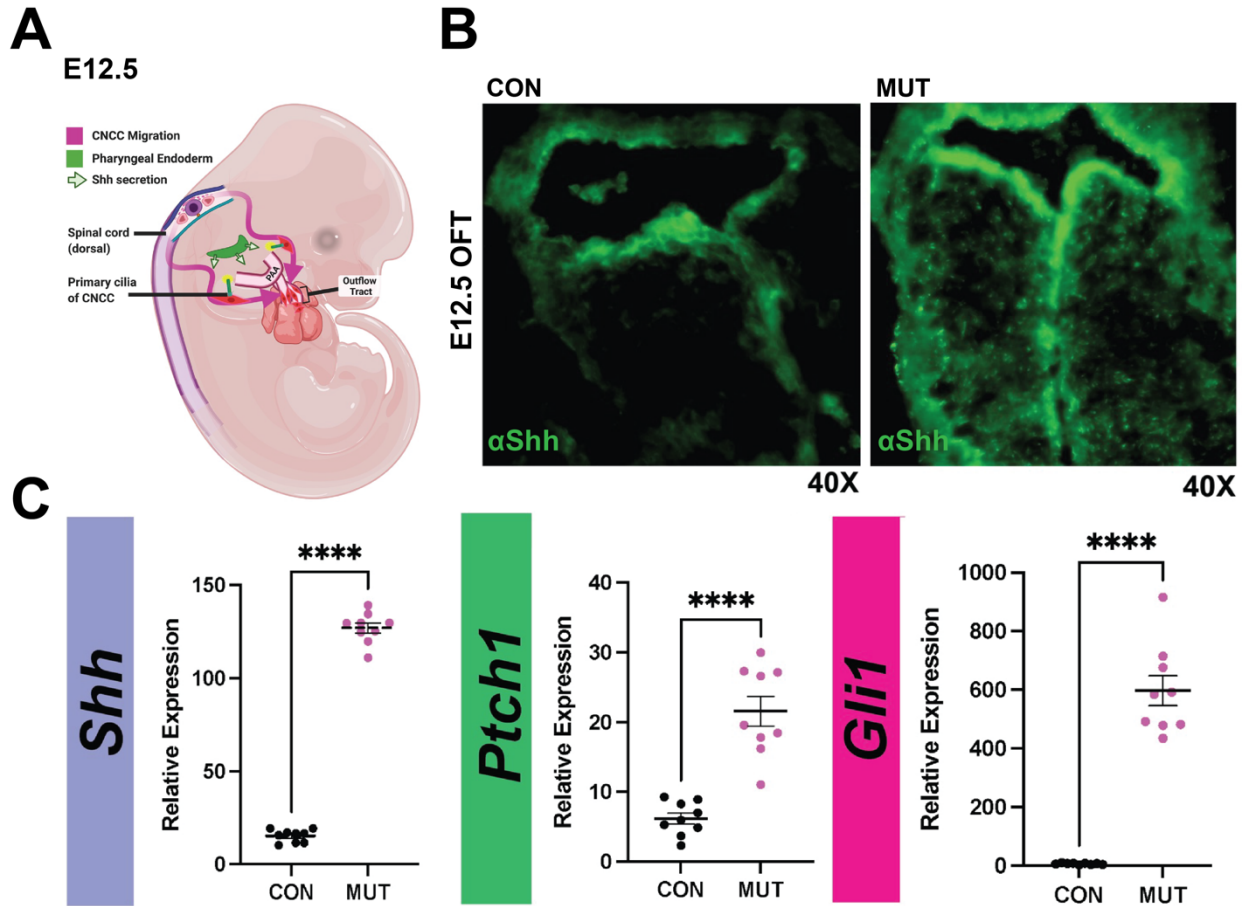


Figure 4.6. OFT Hedgehog signaling is upregulated following CNCC loss of primary cilia. (A) At E12.5, Hh ligand is secreted in abundance from the pharyngeal endoderm, where ligand secretion expands ventrally, forming a Hh gradient up through the developing cardiac outflow tract. (B) Immunofluorescence detection of Shh expression in the endocardial cushions of the proximal aspect of the E12.5 developing OFT of CON (B, left) and MUT (B, right) embryos. (C) Relative expression of *Shh*, *Ptch1*, and *Gli1* isolated from the E12.5 endocardial cushions/OFT. Student's t-tests were performed to compare mean relative expression values of CON (black) and MUT (magenta) E12.5 OFT tissues. Statistical significance was set at $p \leq 0.05$; **** $p < 0.0001$

4.2 Early Disruption to Ventricular Myocardial Organization Coincides with Loss of CNCC Primary Cilia

CNCC conditional elimination of primary cilia reveals a visible phenotype by E10.5 in the MUT. In the MUT E10.5 OFT, there are obvious abnormalities in size and shape of endocardial cushion (ECC) formation/morphology along with noticeable disruption to the cellular organization and structural integrity of the OFT ECC and ventricular endocardium (Figure 4.7, A, C-F).

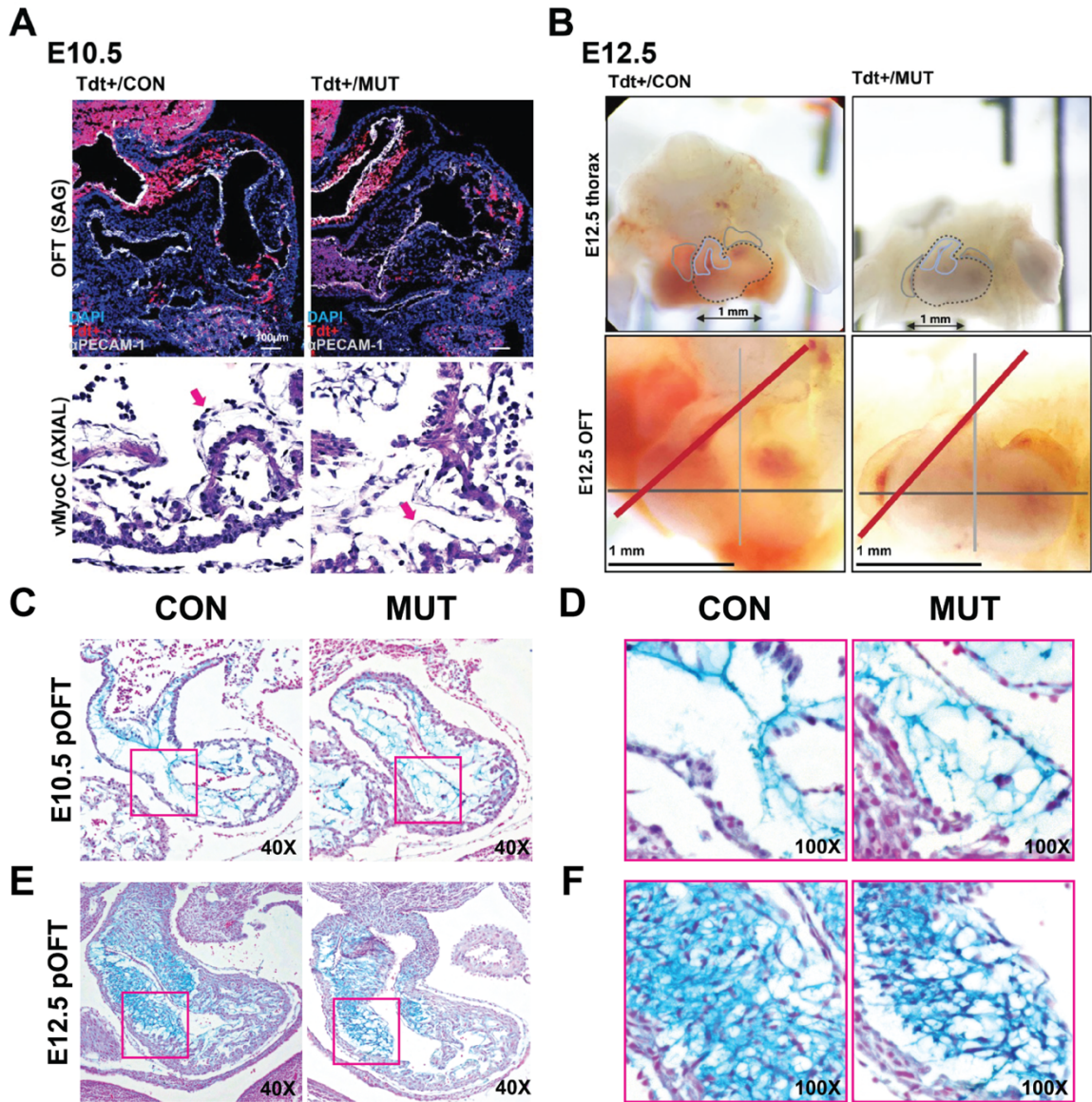


Figure 4.7 Loss of primary cilia in CNCC disrupts ECC formation, OFT alignment and ventricular endocardial organization. **(A)** Global, qualitative analysis of the cellularity, integrity and continuity of the E10.5 endocardium using immunofluorescence analysis of sagittal stained frozen tissue sections of Tdt+ CON and MUT embryos using an anti-CD31 primary antibody (A-top) and standard H&E staining axial sections of the E10.5 ventricular myocardium (A-bottom). **(B)** Brightfield photographs obtained using a dissection microscope to qualitatively assess the gross anatomical length and spatial orientation of the developing embryonic heart and OFT at E12.5 in CON (B-left) and MUT (right). Bottom panel (B-bottom, from L to R) represents a higher magnification photograph of the tissue samples described in B-top. **(B, bottom)** Red lines indicate an approximation of the net direction of bloodflow coming out of the E12.5 cardiac OFT; thin, light blue line indicates an approximation of the the sagittal plane adjusted for the position of the individual embryo; dark blue line indicates approximation of coronal plane, adjusted for the position of the individual embryo; visualization of the E12.5 OFT ECC are outlined in light blue (B, top). **(C-F)** Alcian Blue and Nuclear Fast Red stains of the proximal aspect of the E10.5 **(C-D)** and E12.5 **(E-F)** cardiac OFT in CON and MUT embryos. **(D, F)** Higher magnification inset of ECC cross sections indicated by the magenta boxes of lower magnification images **(C, E)** for both CON and MUT.

Immunofluorescence analysis of sagittal sections with anti-CD31 (PECAM-1; white) of Tdt+, E10.5 embryos revealed a highly discontinuous staining pattern in addition to differences in the cellular organization of the endocardium in the MUT that are not observed in the CON (Figure 4.7, A, top & bottom).

Upon gross examination of the E12.5 cardiac outflow tract, there do not appear to be any pronounced differences in either the orientation and/or laterality of the MUT OFT when compared to the CON (Figure 4.7, B). However, examination of the approximate locations and orientations of the OFT ECC in the MUT appear to be slightly thinner and more elongated when compared to the more substantial, “stump-like” appearance of the CON OFT ECC (Figure 4.7 B).

We then examined the cellularity and extracellular matrix (ECM) deposition of the E10.5 (Figure 4.7, C, D) and E12.5 pOFT (Figure 4.7, E, F) using Alcian Blue stains (with Nuclear fast Red). Alcian blue stains hyaluronic acid, where increased staining density (indicated in blue) is reflective of increased glycosaminoglycan content and increased cartilage formation/development. Conversely, decreased cartilage formation (deposition of ECM) is essential for proper ECC/valve development in the heart. We observed that ECC of the MUT pOFT varied slightly in morphology compared to CON, and specifically in the thickness of the OFT ECC (Figure 4.7, C-F). However, these differences in ECC thickness were not pronounced, and were difficult to interpret in the context of controlling for embryo/tissue alignment in both CON and MUT. Differences in cellularity and distribution of the Alcian Blue stain throughout pOFT ECC in MUT appeared drastically different from that of the CON at both E10.5 (C, D) and

E12.5 (E, F) timepoints (Figure 4.8). Specifically, ECC cross sections of CON at E10.5 (C, D) were primarily characterized by vast areas of a-cellularity, where minimal Alcian blue staining (cardiac jelly) was observed within the ECC “belly.” Rather, ECM/cardiac jelly distribution, as indicated by Alcian blue, was observed mostly surrounding the outside borders of the cushions (Figure 4.7, C, D). In the OFT ECC of the MUT at the same embryonic timepoint, the valvular interstitium was not a-cellular in appearance, where several nuclei were observed (Figure 4.7, C, D). Cells of the MUT ECC valvular interstitium also displayed a webbing-like pattern of staining distribution of the Alcian Blue, likely indicative of the lingering presence of cardiac jelly, consolidated within valvular interstitial region (Figure 4.7, C, D). By E12.5, the CON ECC appear entirely robust in both the thickness and cellular density of the ECC (Figure 4.7, E, F). In the MUT ECC at this same time, the cellular density within the valvular interstitium does not appear to match the CON, in addition to the fact that there are numerous, acellular “pockets” lacking Alcian blue stain not observed in the CON (Figure 4.7, E, F).

4.2.1 CNCC Loss of Primary Cilia Affects Development of Ventricular Myocardium Via Shh-Mediated Increases in Proliferation of Ventricular Cardiomyocytes.

Immunofluorescence analysis of cellular proliferation of the developing ventricular myocardium was performed using a primary antibody against phosphorylated histone-H3, a marker for the M1 (mitosis) phase of the cell cycle. Quantification of proliferation (pH3) in cardiac troponin-T-positive cells (cTnT+) at three embryonic time points (E11.5, E12.5, E14.5) revealed that the percentage of cTnT+ cells did not statistically significantly differ between CON and MUT samples at E11.5

(data not shown). The percentage of cells double positive for cTnT and pH3 (i.e. proliferating ventricular cardiomyocytes) also did not statistically significantly differ when comparing the CON to MUT ventricular myocardium at E11.5 (data not shown). Even when examining overall rates of proliferation (i.e. all pH3+ cells), the CON ventricular myocardium did not differ from the MUT ($P=X$; Figure 4.8A).

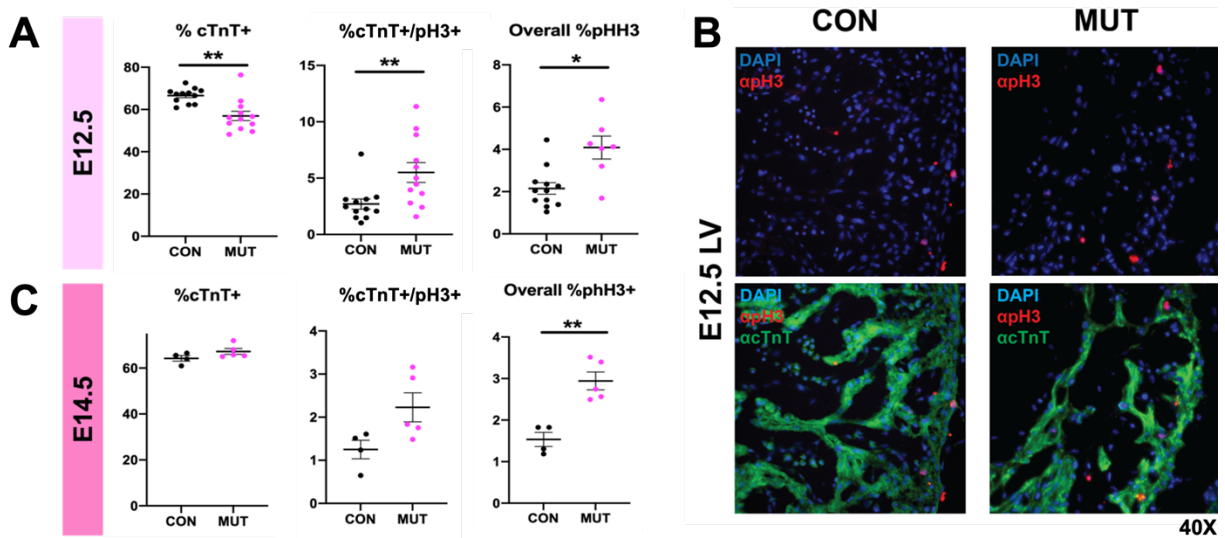


Figure 4.8. Hypertrabeculation aspect of ventricular noncompaction may be explained by increased proliferation of ventricular cardiomyocytes brought about by upregulation in Hedgehog signaling. (A) Quantification of ventricular cardiomyocytes as indicated by cTnT-positive signal (cTnT+; green) with and without pH3-positive (pH3+; red) marker for cell proliferation and expressed as percentage of cTnT+ cells compared to DAPI-positive only nuclei undergoing mitosis in CON (black) and MUT (magenta) left ventricles at E12.5 (A, B) and E14.5 (C). (B) Representative images illustrating the presence and localization of cTnT+ and pH3+ signal in the lateral wall of CON (B, left) and MUT (B, right) left ventricles; * $p<0.05$, ** $p<0.01$

By E12.5, the percentage of ventricular cells staining positive for cTnT, was statistically decreased in the MUT compared to CON ($p<0.01$; Figure 4.8, A). Of note, these results were consistent with analysis of cardiomyocytes using quantitative FLOW analyses of the E12.5 ventricular myocardium (Figure 4.8). However, despite the lower percentage of ventricular cardiomyocytes in the MUT, the percentage of double-positive

cTnT/pH3 in the MUT were statistically increased when compared to the CON ventricular myocardium at E12.5 ($P < 0.01$; Figure 4.8, A). Overall percentage of cells double positive staining for DAPI (nuclear stain) and pH3 was also statistically higher in the MUT versus the CON ($p < 0.05$; Figure 4.8, A).

Distribution and location of pH3+ mitosis marker did not appear to differ between the CON and MUT E12.5 LV (Figure 4.8, B, top). Of note, ventricular cells undergoing proliferation were most-commonly observed within the outer, future-compact myocardial wall, and this did not noticeably differ in the CON compared to the MUT (Figure 4.8, B, top). Qualitatively speaking, the organization of cTnT+/CM appears noticeably different from the CON (Figure 4.8, B). More specifically, the trabeculations of the E12.5 LV wall of the CON display substantial thickness, project radially in a uniform fashion towards the lumen of the LV, and display a robust cTnT+ signal (Figure 4.8, B, bottom). The general integrity and organization of the E12.5 MUT LV wall contrasts from the CON in that the general, overall integrity, continuity, and organization/directionality of the MUT cTnT+/CMs appear distinctly different (Figure 4.8, B, bottom). Of note, the trabecular extensions of the MUT appear thinner, more disorganized, and more sparsely distributed when compared to those of the CON (Figure 4.9, B, bottom).

Percentage of cTnT+ CM equilibrated by E14.5 (Figure 4.8, C), where the percentage of cTnT+ cells did not statistically differ from the CON (Figure 4.9, C). However, despite comparable percentages of CM between MUT and CON, The percentage of CMs undergoing proliferation (cTnT+/pH3+) remained elevated in the MUT when compared to the CON ventricular myocardium, but was no longer statistically significant (Figure 4.8 C). Overall percentage of cells undergoing

proliferation remained statistically greater in the MUT versus CON ($p < 0.01$; Figure 4.8, C).

4.2.2 CNCC Loss of Primary Cilia Leads to Decreased Ventricular Cardiomyocyte Populations and Disrupts ErbB Signaling.

Single cell suspension/isolation was performed using the extracted, biventricular tissue extractions from CON ($n=12$) and MUT ($n=10$) embryonic hearts at E12.5. Quantitative FLOW analysis was used to quantify endocardial and myocardial cells using primary antibodies against PECAM-1 (CD-31) and VCAM-1, respectively. Only a minimal decrease in the percentage of cells positively expressing the PECAM-1 endothelial (endocardial; EC) cell marker of the MUT when compared to CON (Figure 4.8, A-B). When investigating the distribution of VCAM-1-positive cardiomyocytes (CM), there was a statistically significant decrease in the percentage of CM cells in the MUT ventricles when compared to CON ($p < 0.001$; Figure 4.10A-B). Of note, there was a much greater variability between CON samples when compared to those from the MUT. Further analysis was performed to quantify ErbB2, ErbB3 and ErbB4 protein expression in both EC and CM cells of the E12.5 ventricular myocardium. In addition to the negligible differences in EC cell percentages, ErbB2, ErbB3, and ErbB4 expression was unchanged in the MUT ventricles compare to the CON (Figure 4.10C-D). Analysis of VCAM-1/ErbB2 double-positive CMs revealed a statistically significant decrease in ErbB2 ($p < 0.05$) and a notably pronounced decrease in ErbB4 expression ($p < 0.001$) of the MUT compared to the CON (Figure 4.9, E-F). No statistically significant differences

in VCAM-1/ErbB3 double-positive CM cells were observed between the MUT and CON (Figure 4.9, E-F).

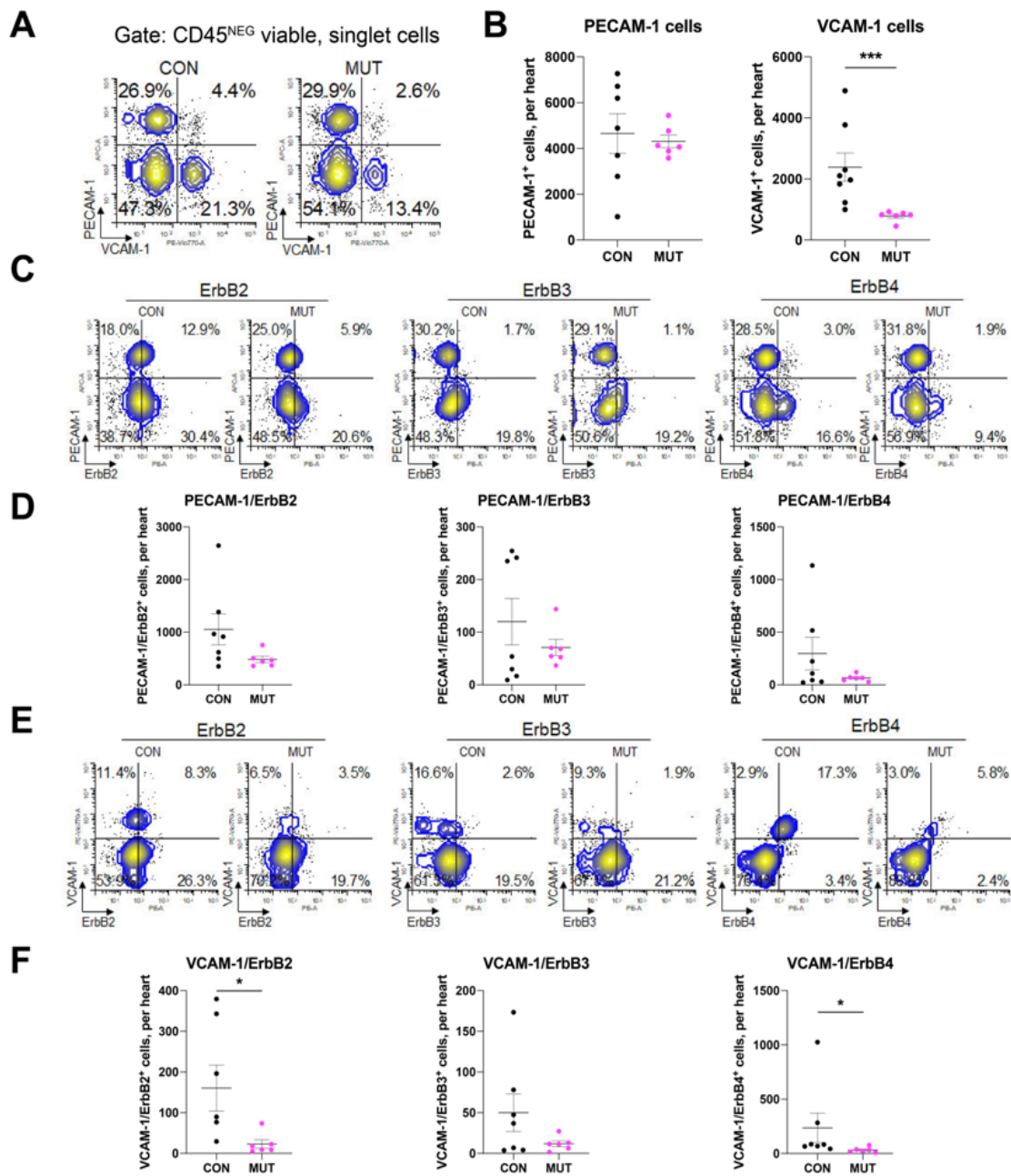


Figure 4.9 Loss of primary cilia “pertErbBs” ventricular compaction. FLOW analysis of cko mutant hearts reveals/shows a decreased cardiomyocyte cell population and disruption to ErbB signaling at E12.5. (A) Representative quantitative FLOW analyses of PECAM-1-positive endocardial cells (EC) and VCAM-1-positive cardiomyocytes (CM) isolated from control (CON) and mutant (MUT) embryonic whole hearts at E12.5. (C, E) Representative quantitative FLOW analysis for expression of ErbB2, ErbB3, and ErbB4 in PECAM-1-positive (C) and VCAM-1-positive (E) heart cells at E12.5. (B, D, F) Graphs indicate absolute number of single-marker (A) and double-marker (C,E) positive cells for the FLOW analyses. (A-F) CON: n=7; MUT: n= 6. *Indicates statistical significance where $p < 0.05$; *** $p < 0.001$

Protein analysis of the ligand upstream to ErbB receptors was performed using multiple, repeated immunofluorescence analyses of Neuregulin-1 (NRG-1) in the ventricular myocardium of E9.5 and E12.5 CON (n= 4) and MUT (n= 3) embryos (Figure 4.10, A).

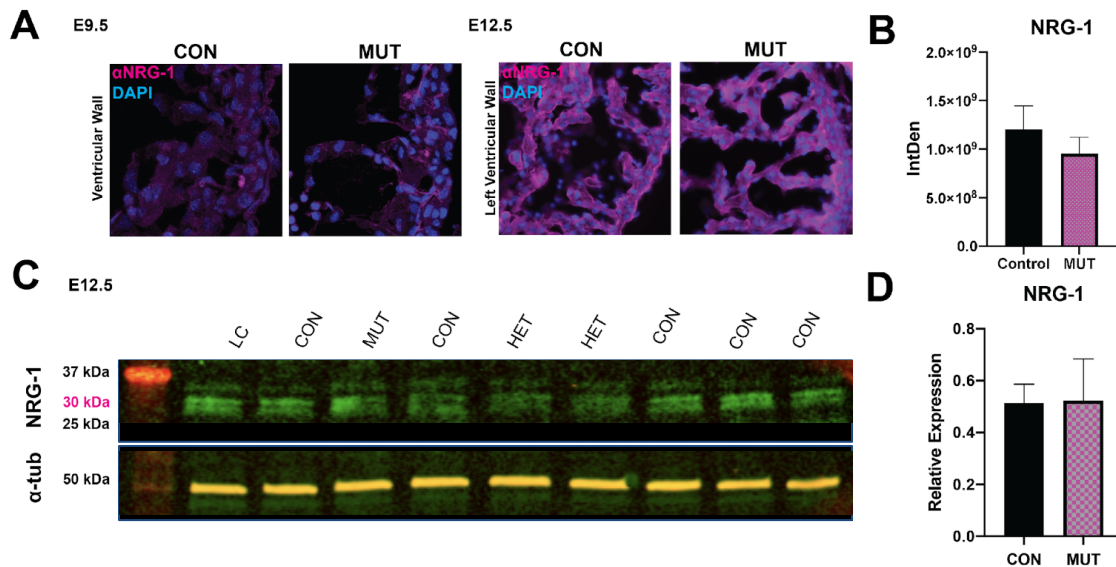


Figure 4.10 CNCC loss of primary cilia does not affect expression of ventricular Neuregulin-1 (NRG-1). **(A)** Immunofluorescence analysis of ventricular NRG-1 was performed comparing the ventricular walls of the homozygous mutant heart (MUT; n=4) to the littermate control (CON; n=4) during initial trabeculation (E9.5/A, left) and prior to the ventricular compaction/ maturation stage (E12.5; A, right). **(B)** Intensity of ventricular anti-NRG-1 signal was quantified at E12.5, and a Welch's t-test was used to compare mean fluorescence intensity (IntDen) between MUT to CON samples ($p=0.528$), and statistical significance was set at $p<0.05$. **(C)** Multiple Western Blot analyses of ventricular NRG-1 protein expression was performed, comparing MUT (n=4) to CON (n=10) and heterozygous tissue (HET; n=6) and a positive loading control (LC) of flash frozen tissue collected at E12.5. **(D)** Expression of ventricular anti-NRG-1 expression (C; top) was quantified using the 30kDa doublet, which was normalized to anti-alpha tubulin (50kDa; C/bottom), and the positive and a test was used to compare mean values, where statistical significance was set at $p<0.05$ ($p=0.904$).

Indirect quantification of ventricular NRG-1 fluorescence signal at E12.5 revealed only a slight decrease in NRG-1 signal in the MUT ventricular myocardium compared to the CON, although this difference was not statistically significant (Figure 4.10, B).

Additional quantification of NRG-1 protein expressing using Western Blot analysis confirmed outcomes observed with immunofluorescence analysis, where NRG-1 expression was statistically unchanged in the CON, HET and MUT ventricles (Figure 4.10, C-D)

4.3 Hedgehog *Gain-of-Function* in CNCC With and Without Intact Primary Cilia.

In order to probe further into the potential mechanisms of primary cilia in modulating ventricular maturation, we introduced a constitutively active Smoothed M2 (SMOM2) mutant receptor (J. Jeong et al., 2004) under the control of the *Wnt1:Cre-2* promoter (A. E. Lewis et al., 2013), (Table 4.1). The resulting phenotypes of interest and for analysis were littermate CON (*Wnt1:Cre+/YFP-/Ift88^{+/+}*; and *Wnt1:Cre-/ YFP+/Ift88^{flox/flox}*), MUT (*Wnt1:Cre+:/Ift88^{flox/flox}*), Smoothed M2 MUT with some intact CNCC primary cilia (“SMOM2+cilia”; *Wnt1:Cre+/YFP+/Ift88^{flox/+}*), and Smoothed M2 MUT with CNCC missing primary cilia (“SMOM2-cilia”; *Wnt1:Cre+/YFP+/Ift88^{flox/flox}*). Embryos were dissected at timepoints corresponding to those most developmentally relevant in the mouse heart, including E12.5 to assess initial phenotype, E14.5 to assess OFT formation and to quantify OFT/chamber septation and ventricular morphology, and E16.5 to assess persistence of possible ventricular phenotypes into the latter embryonic developmental period.

4.3.1 Hedgehog *GoF* in CNCC With Intact Primary Cilia Exacerbates OFT Defects and Ventricular Hypertrabeculation.

Introduction of a constitutively active SMOM2 receptor in CNCC with intact primary cilia (SMOM2+cilia) resulted in the manifestation of a much more extreme version of the original MUT phenotype. The most obvious aspects of the SMOM2 phenotype on a gross scale, included small stature and exacerbated craniofacial defects (e.g. exencephaly, loss of or minimal formation of the mandible/ “jaw bone,” more severe cleft palette, etc.; data not shown). At the level of the developing heart, SMOM2+cilia mutants displayed a singular cardiac OFT (specifically, a Persistent Truncus Arteriosus (PTA)), ASD/VSD that appeared to be much larger than those observed in the original MUT, and finally, and even more pronounced noncompaction of the ventricular myocardium when compared to MUT and CON (Figure 4.11, A-B).

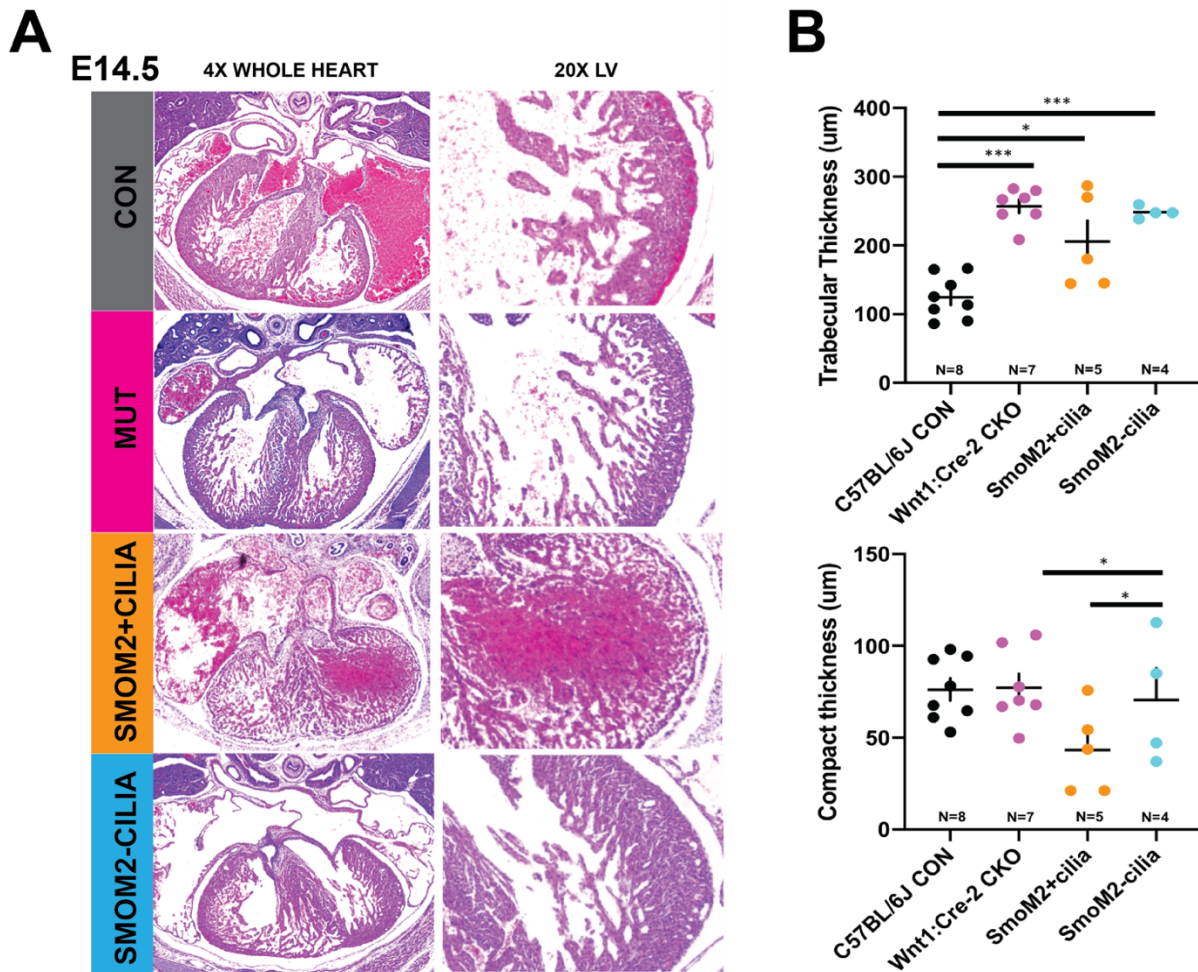


Figure 4.11 Introduction of Hh *GoF* offers new insights into mechanisms for CNCC primary cilia-mediated ventricular maturation. Hypertrabeculation was observed, regardless of the presence of Smo-M2 expression in *Ift88*-homozygous mutants. Notably, expressing Smo-M2 in an *Ift88*-heterozygous background (SMOM2+cilia/orange) resulted in a severe reduction of compact ventricular thickness (**B, bottom**), an observation not seen in the original *Wnt1:Cre-2/Ift88* mutant phenotype (MUT/magenta; **A-B**). As this effect vanished in the *Ift88*-homozygous background, a novel outcome supporting the conclusion that proper Hh signaling is dependent on intact primary cilia in the CNCC population. ***Indicates statistical significance $p \leq 0.001$; ** $p \leq 0.01$; * $p \leq 0.05$.

Interestingly, the SMOM2-cilia also displayed OFT defects (PTA) in addition to an unexpected cardiac phenotype, that included abnormal ventricular chamber morphology, but which was characterized primarily by a pronounced increase in the

thickness of the compact ventricular myocardium (Figure 4.11, B, bottom) accompanying hypertrabeculation (Figure 4.11, B, top).

When specifically referring to the quantitative measurements of trabecular myocardial thickness in the experimental animal groups (MUT/magenta, SMOM2+cilia/orange, SMO-cilia/blue), statistically significant increases in trabecular thickness were observed in MUT (n=7;p<0.001), SMOM2+cilia (n=5; p<0.05) and SMOM2-cilia (n=4; p<0.001) experimental groups when compared to CON (n=8; Figure 4.10, B, top). Interestingly, trabecular thickness in SMOM2+cilia decreased slightly compared to MUT, and, although not statistically significant, included values overlapping with those of the CON when compared to either MUT or SMO-cilia.

When assessing the quantitative assessments of the compact myocardium at E14.5 (Figure 4.11, B, bottom) the most notable observation was that the compact myocardial thickness of each of the MUT, SMOM2+cilia and SMOM2-cilia experimental conditions did not statistically significantly differ from measurements taken in the CON, although the likelihood that this finding has more to do with a small data set is more probable, especially when taking into consideration the outcomes variable quantified in the results and discussions sections that follow. Despite this, we observed a statistically significant increase in compact myocardial thickness in the SMOM2-cilia when compared to SMOM2+cilia (p<0.05; Figure 4.11, B, bottom).

4.3.2 Hedgehog *GoF* in CNCC With Intact Primary Cilia Further Upregulates Hh Signaling and Cardiomyocyte Proliferation.

After assessment and quantification of the cardiac phenotype associated with our Hh *GoF* model, we next sought to investigate and quantify outcomes related to Hh signaling, which also served as a further verification that SMOM2 was, in fact, constitutively upregulating Hh signaling in CNCC (Figure 4.12)

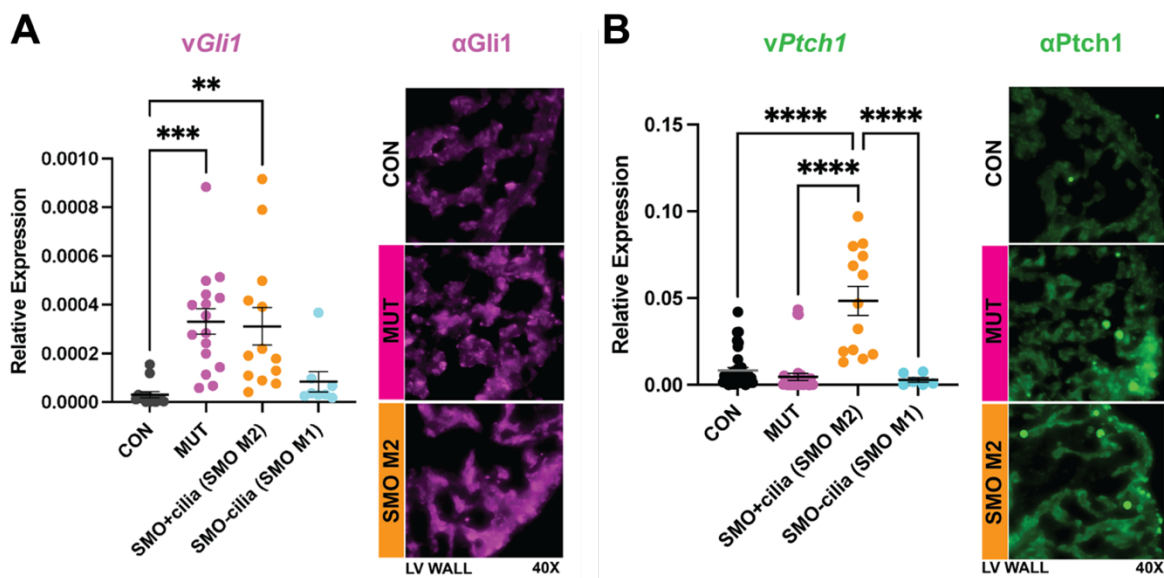


Figure 4.12 Hh *GoF* (via SMOM2) further upregulates ventricular Hedgehog in the presence of partially intact (*Ift88* het) CNCC primary cilia population. Relative expression of ventricular *Gli1* (**A, left**) and *Ptch1* (**B, left**) of CON, MUT and SMOM2 with (orange) and without (blue) intact primary cilia at E12.5. Expression of ventricular *Gli1* (**A, right**) and *Ptch1* (**B, right**) in the LV wall of CON, MUT and SMOM2 at E12.5. ** $p < 0.01$; *** $p < 0.001$; **** $p < 0.0001$

Ventricular expression of *Gli1* (Figure 4.12, A) and *Ptch1* (Figure 4.12, B) Hh signaling components were quantified using qRT-PCR at embryonic time point E12.5, where mean relative expression values were compared between and within CON (black), MUT (magenta), SMOM2+cilia (orange) and SMOM2-cilia (blue) experimental conditions. There was a statistically significant increase in ventricular expression of *Gli1* In both

MUT ($p < 0.001$) and SMOM2+cilia ($p < 0.01$), when compared to CON (Figure 4.12, A), but not when compared to each other ($p =$). SMOM2-cilia ventricular expression of Gli1 did not differ from either CON, or MUT/SMOM2+cilia experimental conditions.

Indirect assessment of ventricular Gli1 protein expression using qualitative immunofluorescence analysis with α Gli1 was used to compare MUT and SMOM2+cilia to CON E12.5 LV (Figure 4.12, A, Right). Ventricular expression of Gli1 appears to be localized in the areas of the trabecular projections and recesses that would likely correspond to the morphology and location of ventricular endocardial cells, although this observation is speculative. Overall Gli1 expression in the MUT appears to be increased compared to the CON, in a pattern that can be described in the MUT as more robust but also more punctuated. Ventricular Gli1 expression in SMOM2+cilia appears to be even further increased when compared to both MUT and CON. Further, the staining pattern of Gli1 in SMOM2+cilia seems to be more diffusely distributed throughout the layers of the ventricular myocardium and trabecular extensions, and appears to lack the prevalence of the punctuate patterning observed in both MUT and CON (Figure 4.12 A, right).

Relative expression of ventricular *Ptch1* at E12.5 revealed a statistically significant increase only in SMOM2+cilia when compared to CON ($p < 0.0001$; Figure 4.12, B). Interestingly, ventricular *Ptch1* in SMOM2+cilia was also upregulated when compared to MUT ($p < 0.0001$) and SMOM2-cilia ($p < 0.0001$; Figure 4.12, B). Of note, ventricular *Ptch1* did not statistically differ from the CON in either the MUT or SMOM2+cilia (Figure 4.12, B).

Immunofluorescence analysis of α Ptch1 in the E12.5 LV revealed staining patterns that were consistent with quantitative measurements *Ptch1* (Figure 4.12, B). In general, ventricular Ptch1 in the MUT did not appear noticeably different from CON, although sporadic instances of what appeared to be a qualitative increase in signal intensity were observed in the outer (presumably compact) portion of the LV wall (Figure 4.12, B). Qualitative assessment of SMOM2+cilia ventricular Ptch1 revealed an obvious increase in both signal intensity as well as overall distribution of fluorescence signal throughout the layers and trabecular extensions of the LV compared to those observed in the CON. Of interest, although this was not quantified, we observed a possible increase in staining specificity and signal intensity in the SMOM2+cilia endocardial edges within the LV trabecular extension that was not apparent in the CON (Figure 4.12, B).

Following confirmation of Hh upregulation in the E12.5 MUT and SMOM2+cilia LV, we repeated our investigation of CM proliferation (Figure 4.13), originally described in CON and MUT LV (Figure 4.8).

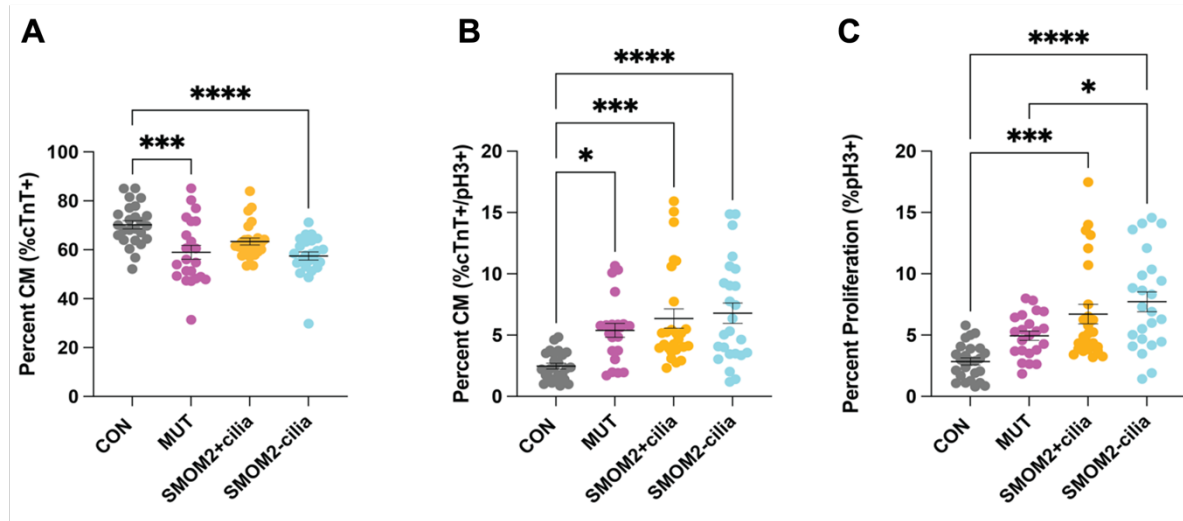


Figure 4.13 CNCC loss of primary cilia and HH *GoF* is associated with changes in cardiomyocyte and overall ventricular myocardial proliferation. **(A)** Percentage of cTnT-positive (cTnT+) ventricular cardiomyocytes (CMs) in the LV of CON (grey), MUT (magenta), SMOM2+cilia (orange), and SMOM2 (blue) at E12.5. **(B)** Percentage of cells double-positive for CM marker cTnT and pH3 marker of mitosis/proliferation in the LV of CON (grey), MUT (magenta), SMOM2+cilia (orange), and SMOM2 (blue) at E12.5. **(C)** Overall percentage of cells double-positive for the nuclear marker, DAPI, and pH3 in the LV of CON (grey), MUT (magenta), SMOM2+cilia (orange), and SMOM2 (blue) at E12.5.

Quantitative analysis of CMs in the E12.5 LV was performed using immunofluorescence analysis with a primary antibody against cTnT (Figure 4.13, A). Percentage of CMs in the E12.5 ventricular myocardium were statistically decreased in both the MUT (magenta; $p < 0.001$) and SMOM2-cilia (blue; $p < 0.0001$) when compared to CON (grey; Figure 4.13, A). Interestingly, despite the NCC phenotype and hypertrabeculation phenotype observed in the SMOM2+cilia, the percentage of CMs did not differ statistically when compared to CON in the E12.5 LV (Figure 4.13, A).

In order to assess and quantify proliferation of CM in the E12.5 LV, we quantified ventricular CM double-positive for cTnT and pH3 mitosis marker and expressed these values as a percentage of the total number of cells (Figure 4.13, B). We observed increased CM proliferation in MUT (magenta; $p < 0.05$), SMOM2+cilia (orange; $p < 0.001$) and SMOM2-cilia (blue; $p < 0.0001$) when compared to CON (Figure 4.13, B).

Quantification of total proliferation was collected as a percentage of DAPI-positive (DAPI+) nuclei also staining positively for the α H3 mitosis marker (Figure 4.13, C).

Overall proliferation in the E12.5 ventricular myocardium did not statistically significantly differ in the MUT (magenta) compared to the CON, but was markedly increased in SMOM2+cilia (orange; $p < 0.001$) and SMOM2-cilia (blue; $p < 0.0001$) when compared to CON (Figure 4.13, C). Of note, SMOM2-cilia overall ventricular proliferation was also statistically significantly increased when compared to MUT ($p < 0.05$; Figure 4.13, C).

4.4 Globally-upregulated cardiac Hh resulting from CNCC loss of primary cilia may be attributed to Non-CNCC primary cilia in a paracrine capacity.

We next sought to explore whether the upregulation in Hh signaling (specifically via increased Gli1 and Ptch1) observed in the MUT was originating from Tdt+/CNCC in the absence of primary cilia, or alternatively, via a compensatory and/or paracrine-mediated response in the Tdt-/Non-CNCC in the OFT of MUT compared to CON embryos at E12.5 (Figure 4.14).

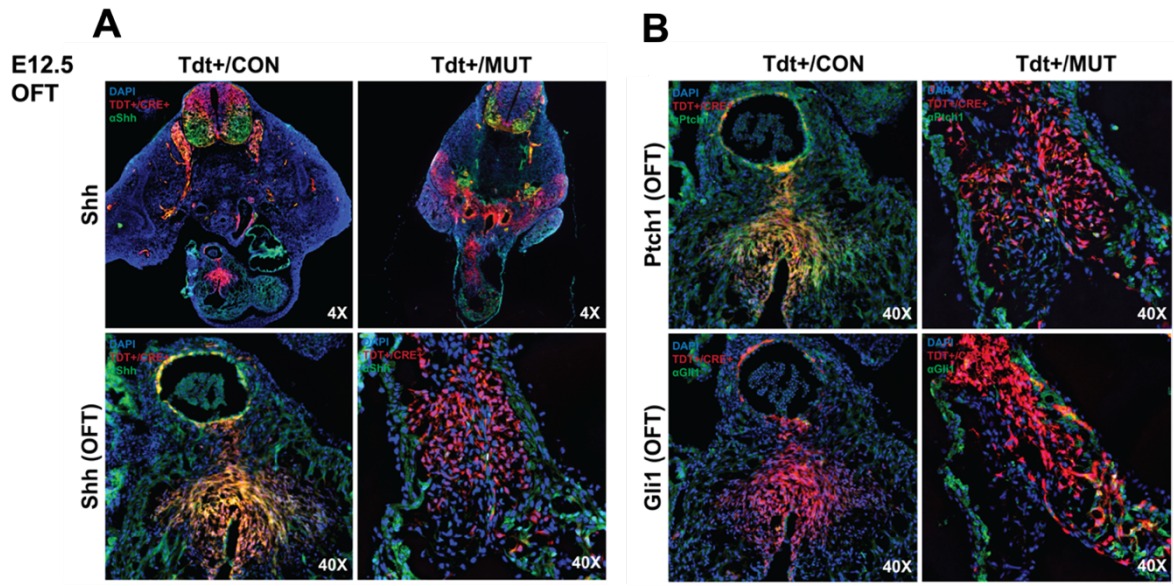


Figure 4.14 Hh OFT Upregulation in Non-CNCC of MUT suggest paracrine and/or compensatory response to CNCC loss of primary cilia. **(A)** Whole-embryo (4X; top) and OFT (40X; bottom) distribution of CNCC/Tdt+/Cre+ and Shh (green) in Tdt+/CON (left) and Tdt+/MUT (right) at E12.5. **(B)** Immuno-fluorescence detection of Ptch1 (top) and Gli1 (bottom) expression in the developing OFT of Tdt+/CON (left) and Tdt+/MUT embryos at E12.5.

Immunofluorescence analysis of Hh signaling in the E12.5 OFT was performed to further examine protein expression of Shh, its receptor Ptch1 and Gli1, its transcriptional activator (Figure 4.14). Qualitative comparison of Tdt+, E12.5 whole-embryo axial sections stained with a primary antibody against Shh, first revealed a noticeable difference in the location, distribution and apparent prominence of Tdt+ signal in the MUT versus the CON (Figure 4.14, A, top). More specifically, Tdt+ signal in CON was highly-specific and localized to the projecting dorsal root ganglia bilaterally from the superior portion of the image (dorsal aspect/notochord region of the embryo) in addition to the abundant signal observed in the ECC of the developing OFT. In the MUT, Tdt+ signal is also evident in the dorsal root ganglia, located bilaterally to the spinal/notochord region of the embryo. However, Tdt+ signal in the mutant, by contrast to CON, is abundantly and less specifically spread throughout the pharyngeal arch region

of the cross section (Figure 4.14 A, top). In the developing OFT of the MUT, Tdt+ signal appears diffusely spread throughout both ECC of the OFT, where Tdt+ cells of the MUT seem to be qualitatively less organized and spread in a thin layer in a slightly more linear pattern throughout what appears to be a slightly more elongated OFT (Figure 4.14 A, top). Consistency in Shh expression at the whole-embryo level was observed in the ventral portion of the developing spinal cord in both CON and MUT, as well as throughout the trabeculae of the ventricular myocardium. Differences in Shh expression at 4X magnification were noted in the noticeable absence of atrial tissue in the MUT, possibly attributed to differences in orientation/alignment of embryonic tissue sections, despite our best efforts to align and match appropriately, corresponding regions of the CON and MUT E12.5 OFT regions (Figure 4.14, A, top). Finally, Shh expression in the MUT is apparent in the notochord region, a pattern that is not apparent in the CON.

Upon examination of the CON and MUT ECC at a higher magnification (Figure 4.14 A, bottom), Tdt+ signal in the CON can be seen nicely concentrated surrounding the luminal borders of the ECC, most prominently located within the mid-level portions of the OFT and surrounding the future pulmonary artery. Expression of Shh in the CON ECC appears most abundantly surrounding within what is presumably the endothelial layer of the future pulmonary artery (Figure 4.14, A, bottom/left). Most relevant, however, is the observation that Shh expression (green) and localization does not seem to localize exclusively to either Tdt+ cells of the ECC or the Tdt- cells in the surrounding myocardial tissue. Examination of the MUT OFT at 40X (Figure 4.14, A, bottom/right) reveals distinctly different findings. More specifically, while Tdt+ contribution in the MUT can be seen in the areas of the ECC corresponding to those observed in CON, Tdt+

distribution is far less concentrated in any one specific region of the ECC (Figure 4.14 A, bottom/right). Upon examination of Shh expression in the MUT OFT, areas with overlapping Tdt+/Shh+ signal were not present, in stark contrast to Tdt+/Shh+ overlap in the CON. Shh expression in the MUT OFT was observed and appeared to be localized in Tdt-/non-CNCC cells present in the outermost portions of the ECC as well as within the trabecular folds present at the OFT transition point where the ECC meet the ventricular myocardium (Figure 4.14, A, bottom/right).

We then compared qualitative expression of Ptch1 in CON and MUT OFT at E12.5 using immunofluorescence. Similar to staining patterns observed when examining Shh expression in CON OFT, protein expression of Ptch1 in the CON ECC was localized to the cell layers surrounding the lumen of the future pulmonary artery as well as within the central regions of the ECC (Figure 4.14 B, top/left). Areas with overlapping Tdt+ and Shh+ expression were apparent, along the luminal portions of the ECC of the CON, but Shh expression did not appear to be localized exclusively to either Tdt+ or Tdt- cells. In the corresponding OFT of the MUT, Ptch1 expression was observed in within the outer edge portions of the ECC/OFT and within Tdt- cells of the transitional trabeculae of the ventricular myocardium (Figure 4.14, B, top/right). Of note, Shh expression observed in the MUT did not appear to coincide/localize with the Tdt+ CNCC within the ECC, suggesting that upregulation of OFT Ptch1 at E12.5 may be originating from Tdt-/non-CNCC cells.

Immunofluorescence analysis of Gli1 in the developing OFT of CON and MUT embryos at E12.5 revealed a general absence of signal and specificity in CON when compared to MUT (Figure 4.14, B, bottom). Gli1 expression in the ECC/OFT of the

As previously discussed, Hh ligand production and secretion at E12.5 is primarily originating from the pharyngeal endoderm, where a Hh gradient is formed, spanning out towards the developing heart and OFT (Figure 4.15, A). Given that this portion of the developing pharyngeal arch region is also abundant in Tdt+/CNCC contributions, we hypothesized that loss of primary cilia from CNCC in this region may also disrupt Hh signaling. Upon closer examination of SMO expression in Tdt+ and Tdt- cells of the pharyngeal region in CON, SMO expression/staining pattern appears dispersed throughout clusters of both Tdt+ and Tdt- cells in a punctuated pattern (Figure 4.15 B, top). Of note, SMO “granule-like” SMO signal appears to localize to the primary cilium and basal body itself (Figure 4.15 B, B/inset) in addition to its distribution in areas not associated with a primary cilium (Figure 4.15 B; A, C/inset). By contrast, SMO signal in the MUT appears to be distributed primarily in the cytoplasmic areas surrounding Tdt- cells (Figure 4.15 B, bottom; B, C/inset). While the *Iff88* cko does not result in complete elimination of all primary cilia of all CNCC, primary cilia that are present on Tdt+ cells do not appear to be associated or overlapping with areas where SMO signal is apparent. (Figure 4.15, B; A-B/inset). Interestingly, the punctuated pattern of SMO granules observed in the CON are not as prominent in the MUT, and/or are overshadowed by the extent of the cytoplasmic localization pattern in the MUT (Figure 4.15, B, bottom, C/inset). Of additional note, primary cilia of Tdt- cells in the MUT appear to be qualitatively longer than those seen remaining in the Tdt+ cells of the MUT (Figure 4.15 B, bottom, C/inset).

CHAPTER 5

LOSS OF CARDIOMYOCYTE PRIMARY CILIA IN THE DEVELOPING HEART

In the developing heart, primary cilia are now recognized as key genetic and cellular targets for the identification, treatment and prevention of congenital heart defects (CHD). However, the presence and function of primary cilia specific to developing cardiomyocytes (CM) and their potential role in the postnatal myocardium has yet to be characterized and represents a topic of ongoing debate.

5. 1 Cardiomyocyte-Specific Conditional Elimination of Primary Cilia in the Developing, Mammalian Heart

The following series of experiments survey an *in vivo*, conditional elimination of primary cilia of murine embryonic CM using a cTnT:Cre (Jiao et al., 2003), *Ift88 floxed* cross (Figure 5.1) and a focused histological analysis characterizing the developing ventricular endocardium and myocardium (Figure 5.1, A).

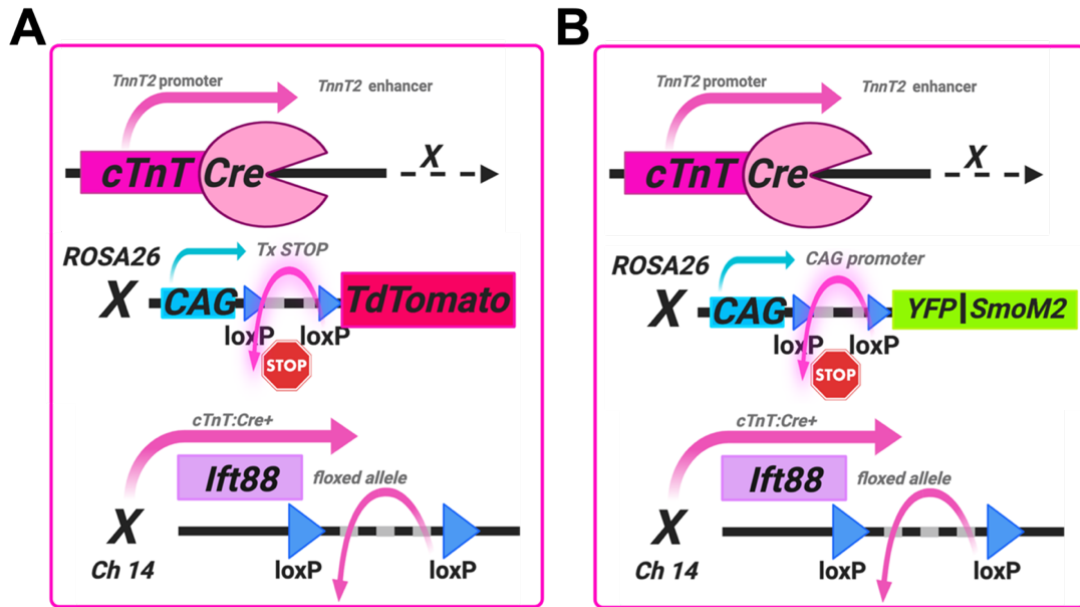


Figure 5.1 Generation of cardiomyocyte-specific, primary cilia conditional knockout mouse model with addition of Hh GoF perturbations. (A-B) Illustrative schema of Cre-Lox-mediated neural crest-specific, conditional knockout of primary cilia using the *Ift88* floxed allele (murine) located at chromosome 14. (A) Cardiomyocyte-specific elimination of primary cilia using a cTnT:Cre driver introduced into C57BL6-J mice homozygous for the *Ift88* floxed allele. Cre-positive, *Ift88* heterozygous animals were crossed with homozygous *Ift88* floxed animals to produce MUT (Cre+/*Ift88*^{lox/lox}), HET/CON (Cre+/*Ift88*^{lox/+}), and littermate CON (Cre+/-/*Ift88*^{+/+}). A Td-tomato reporter was used to track and quantify CM and subsequent loss and/or maintenance of primary cilia. (B) Additional experiments utilized a HH GoF model (via SmoM2) introduced into the original cTnT:Cre+/CM conditional elimination of primary cilia mouse model.

5.1.1 Conditional elimination of cardiomyocyte primary cilia mimics ventricular myocardial phenotypes observed with CNCC loss of primary cilia.

Characterization of the resultant phenotype was performed using standard hematoxylin and eosin staining of E14.5, E16.5, and early postnatal homozygous mutants (MUT; cTnT: Cre+/*Ift88*^{lox/lox}) and control littermates (CON; cTnT: Cre+/*Ift88*^{+/+}). Quantitative analysis of both MUT and CON trabecular (tMyoC) and compact (cMyoC) ventricular myocardial thickness using transverse, paraffin-embedded tissue sections of embryonic and perinatal samples stained with H&E (Figure 5.2).

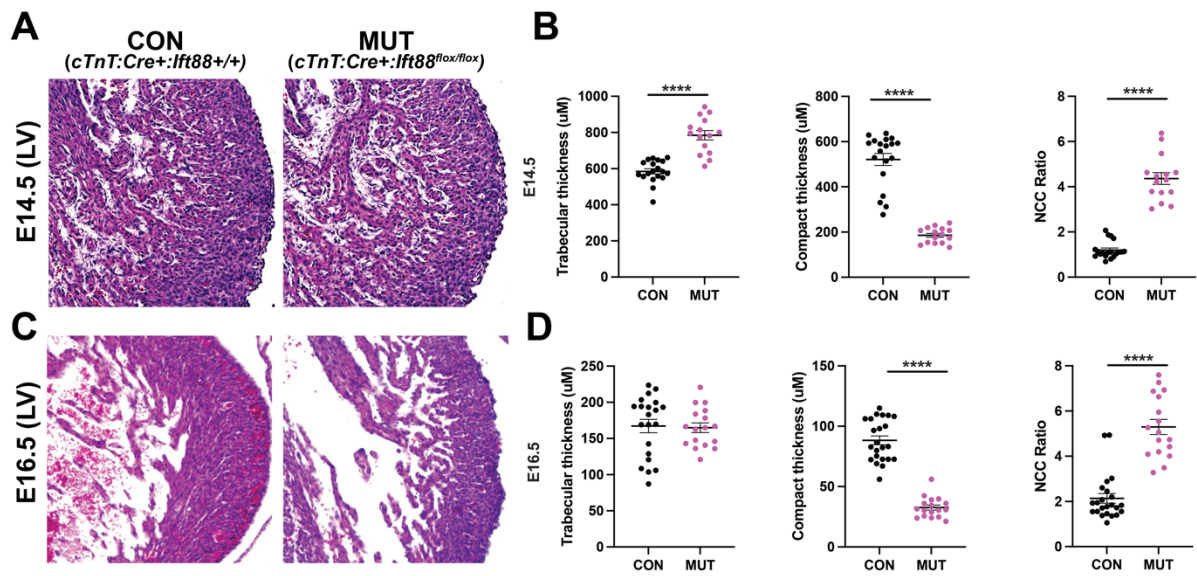


Figure 5.2 *In vivo* loss of CM primary cilia impairs myocardial maturation. *In vivo* loss of CM primary cilia impairs myocardial maturation. **(A)** Loss of primary cilia in CM of the developing heart leads to noncompaction of the ventricular myocardium visible by E14.5 in MUT when compared to CON. **(B)** Quantification of trabecular and compact ventricular myocardial thickness was performed using 2D, axial cross sections of the E14.5 mouse heart. NCC Ratio was calculated and expressed as a ratio of measured trabecular and compact thickness measurements. **(C)** Qualitative and Quantitative **(D)** assessments of MUT ventricular myocardium illustrating the persistence of the NCC phenotype resulting from CM loss of primary cilia. **** $p < 0.0001$

Elimination of primary cilia from embryonic CM leads to a noticeable phenotype characterized primarily by abnormalities in cardiac chamber formation, specifically, noncompaction of the ventricular myocardium, visible by E14.4 (Figure 5.2, A). Quantification of trabecular and compact myocardial wall thickness were performed, revealing a statistically significant increase in trabecular thickness of the MUT compared to CON ($p < 0.0001$), decreased compact thickness in MUT versus CON ($p < 0.0001$), and an NCC ratio that was nearly triple the average of littermate CON at E14.5 ($p < 0.0001$; Figure 5.2, B). Additionally, the MUT endocardium displays increased cellularity and staining intensity when compared to the CON.

Importantly, this MUT ventricular NCC phenotype persisted through the late-embryonic period of ventricular maturation and did *not* result in either embryonic or perinatal lethality (Figure 5.2 C-D). Most notably, characterization of the MUT phenotype repeated at E16.5 revealed a normalization of trabecular myocardial thickness in the MUT that was no longer statistically significantly different from CON (Figure 5.2, C). However, persistence of the NCC phenotype through E16.5 is supported by the repeated decrease in compact myocardial thickness observed in the MUT when compared to CON. Given the persistence and seemingly increased severity of the reduction in compact myocardial thickness observed in the MUT, combined with the fact that NCC and its diagnostic significance is expressed as a ratio, it was not surprising that NCC ratio in the MUT remained statistically significantly more pronounced when compared to CON ($p < 0.0001$; Figure 5.2, C).

Following our initial characterization of the phenotype resulting from conditional elimination of primary cilia from embryonic CM, we performed an immunofluorescence analysis to quantify and confirm the loss of CM primary cilia of the MUT. In this series of experiments, we also incorporated a validation experiment to confirm the specificity of the cTnT:Cre-driver by using a primary antibody against cTnT. Specifically, “true” CM were identified as those cells double-positive for the Tdt+/Cre+ reporter as well as cTnT in addition to the DAPI nuclear marker (data not shown). However, for quantification purposes and aesthetic clarity, representative images of both CON and MUT CM depict *only* the cTnT+ (green) and Arl13B+ (primary cilia marker; red), where the Tdt+ channel has been removed (Figure 5.3)

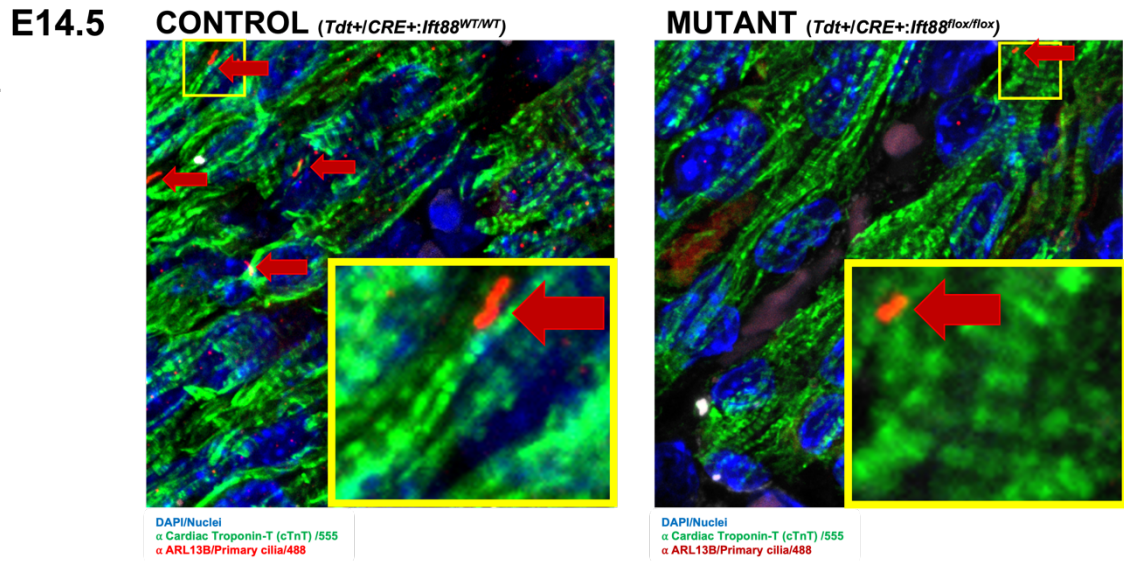


Figure 5.3 Immunofluorescence Analysis of the Loss of primary cilia in embryonic, (ventricular) cardiomyocytes. Primary antibodies against cardiac Troponin-T (cTnT; green) and Arl13B (red) were used to identify primary cilia elaborating from cTnT+ cardiomyocytes in CON (left) and MUT (right). DAPI (blue) was used as a nuclear marker and to confirm cellular localization of a given primary ciliary axoneme. Red arrows indicate confirmation of an intact primary cilium. Small, yellow boxes indicate the origin of the magnified inset image, also outlined in a yellow box.

As illustrated in Figure 5.3, representative qualitative images of CM primary cilia analyzed with immunofluorescence, showing an abundance of intact primary cilia protruding from cTnT+(CM) and correspond to individual nuclei in CON (left). In the MUT (right), by contrast, primary cilia appear noticeably absent from cTnT+/CMs. Of note, although the occasional ciliary axoneme could be found in MUT ventricular CM, these cilia appeared shorter and more “stump-like,” than those observed in CON (Figure 5.3, Left).

5.2 Introduction of Hh *GoF* in Cardiomyocytes with and without Intact Primary Cilia Impacts Ventricular Maturation.

In order to probe further into the Hedgehog (Hh) signaling aspects resulting from the loss of cilia, implementation of an *in vivo* conditional knockout in which cTnT:Cre drives expression of a mutant, constitutively-active Hh receptor in the presence or absence of a functional *Ift88* gene (Figure 5.1, B). Initial, qualitative characterization of the resulting MUT phenotype was characterized by a pronounced thinning of the outer compact ventricular wall, combined with a noticeable expansion in ventricular trabeculations seen in both MUT and SMOM2 phenotypes (Figure 5.4, A).

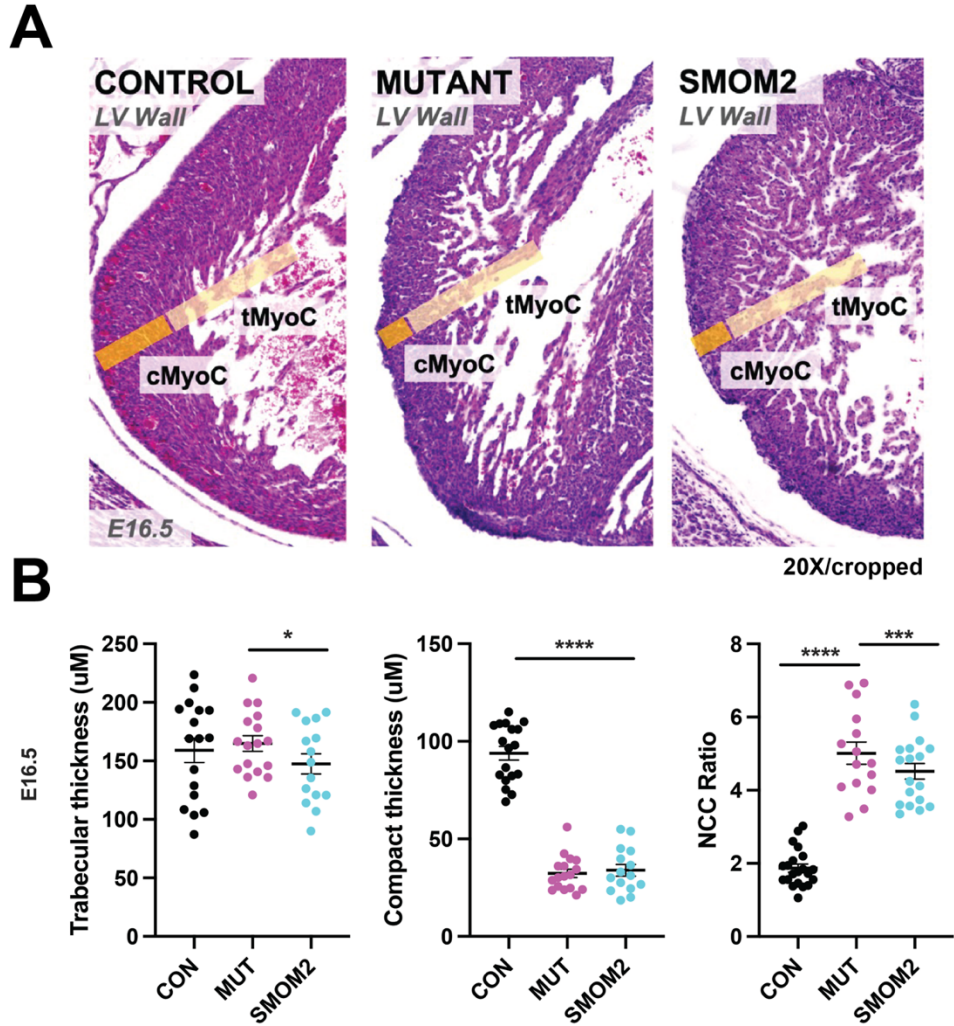


Figure 5.4 Hh *GoF* in ventricular cardiomyocytes with and without intact primary cilia leads to a phenotype characterized by ventricular noncompaction. **(A)** Histological analysis of the LV at E16.5 in CON (cTnT:Cre+/Ift88^{+/+}), MUT (cTnT:Cre+/YFP-/Ift88^{fllox/fllox}), and SMOM2 (cTnT:Cre+/YFP+/Ift88^{fllox/+}). Smaller, gold line indicated an approximation of the compact myocardium (cMyoC) and the trabecular myocardium (tMyoC) of the E16.5 LV. **(B)** Quantification of E16.5 ventricular thickness and corresponding NCC ratios for CON (black), MUT (magenta), and SMOM2 (blue). *p<0.05; ***p<0.001; ****p<0.0001

5.2.1 Hh GoF in Cardiomyocytes with Some Intact Primary Cilia Preserves Trabecular Myocardial Thickness, but Persists in Limiting Adequate Expansion of the Compact Ventricular Myocardium.

Quantification of ventricular thickness measurements at E16.5 revealed no statistically significant differences in thickness of the trabecular myocardium when comparing MUT to CON ($p =$ Figure 5.4, B). Trabecular thickness of SMOM2 was also not statistically significantly different from CON, but was significantly decreased when compared to MUT ($p < 0.05$; Figure 5.4, B). When comparing measurements of the compact myocardial thickness, *both* MUT and SMOM2 displayed ventricles (LV) with statistically significantly decreased compact myocardium when compared to CON ($p < 0.0001$; $p < 0.0001$, respectively; Figure 5.4, B). Despite persistence of the hypertrabeculation phenotype seen at E14.5 (Figure 5.3), loss of primary cilia in embryonic CM with and without the introduction of Hh *GoF* did not lead to a sustained and/or global impairment of ventricular maturation. Surprisingly, CM loss of primary cilia in the presence of SMOM2 resulted in a restoration of normal trabecular myocardial thickness (Figure 5.4, B).

Compact myocardial thickness, by contrast, was drastically affected with CM loss of primary cilia with and without Hh *GoF* and was visible by E14.5, but persisted into the later stages of ventricular myocardial development in the MUT and SMOM2 at E16.5 when compared to CON ($p < 0.0001$, $p < 0.001$, respectively; Figure 5.4, B). Thus, due to the degree to which the LV compact myocardium was reduced in both MUT and SMOM2, NCC values remained statistically significantly greater in MUT and SMOM2 when compared to CON (Figure 5.4, B).

5.3 Characterizing Cardiomyocyte Primary Cilia in Human CHD

5.3.1 Characterizing breadth of cardiomyocytes phenotypes in human, pediatric CHD cases.

In order to probe further into the translational aspects of primary cilia in the developing mammalian heart, we obtained human tissue biopsy samples from pediatric CHD patients. Extensive histological examination of cardiomyocytes from patients with congenital abnormalities of the ventricular myocardium and healthy CON biopsy samples were obtained with patient consent and approval from the Maine Medical Center Tissue Biobank. Of note, Given the invasive nature of procurement for an endomyocardial biopsies, and the sensitivity of cardiac muscle to any fluctuation in oxidative/metabolic stress (i.e. medical trauma), it was not possible to obtain “true” controls, especially from pediatric patients. Instead, we opted to compare the CM of individual CHD pediatric patients with and without a ventricular myocardial phenotype, as documented by corresponding pathology reports. In the cases included for the following analyses, the “experimental” patients (i.e. pediatric CHD patients with a ventricular myocardial phenotype), were pathologically classified as having “Myocardial Disarray”(Ariga et al., 2019). From a histological perspective, our results remained consistent with this original diagnosis, where the size, orientation and general cytology of the CM from CHD patients with myocardial disarray were profoundly distorted in size and general organization (Figure 5.5).

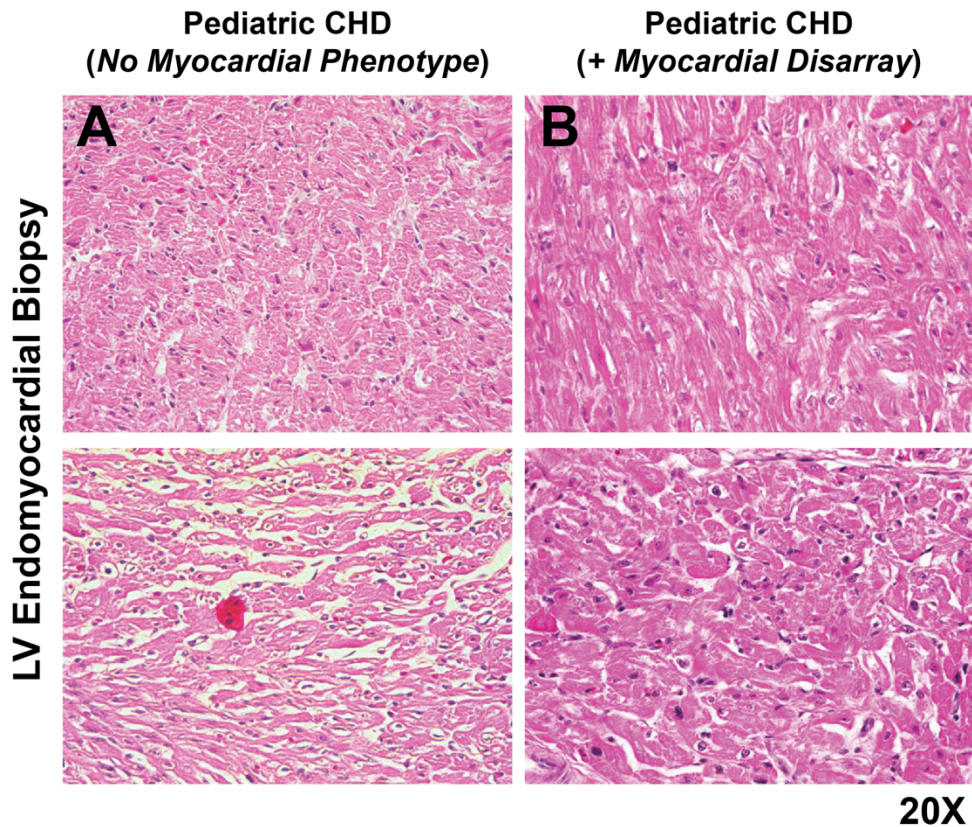


Figure 5.5 Analysis of primary cilia prevalence of human tissue(s) using endomyocardial biopsies from pediatric CHD patients with and without myocardial disarray. Histologic characterization of human, pediatric endomyocardial biopsies collected from CHD patients with and without ventricular, myocardial phenotypes. (Left) Images of pediatric patients with CHD without a myocardial phenotype photographed at 20X magnification. (Right) Images of pediatric patients with CHD with myocardial disarray pathology, photographed at 20X magnification. FFPE samples were obtained from MMC Biobank and were sectioned and stained with standard H&E.

However, the general histology of our initial comparison were entirely consistent with the results described in the pathology reports corresponding to individual patient samples. The focus of the subsequent experiments were therefore, to probe further into how the histology corresponded to the presence/absence and general morphology of primary cilia of individual patient samples.

5.3.3 Alterations in Primary Cilia Abundance and Morphology in Human CHD with and without Myocardial Disarray.

Immunofluorescence analysis of primary cilia in human samples revealed differences in distribution and length of primary cilia of CM and non-CM cells from patients with CHD when compared to non-diseased controls (Figure 5.6).

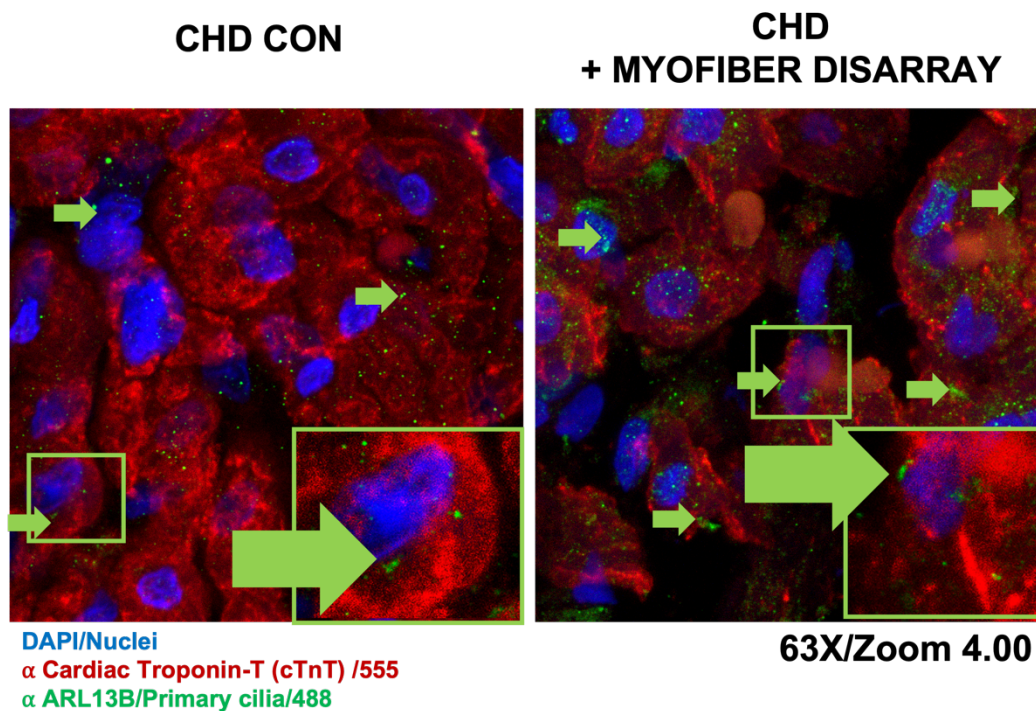


Figure 5.6 Characterization of primary cilia in human, pediatric CHD obtained through endomyocardial biopsy. Immunofluorescence analysis of primary cilia from human, pediatric CHD samples (FFPE) with no known myocardial phenotype (CHD CON; left) alongside samples from pediatric CHD patients with myocardial disarray (CHD + Myofiber Disarray; right) stained with primary antibodies against cTnT (CM/red) and Arl13B (primary cilia/green), and counterstained with DAPI (blue) nuclear stain. Images were collected at 63X magnification with a Zoom factor of 4.00 using confocal microscopy (Leica Microsystems). Green arrows indicate the presence of an intact primary ciliary axoneme which is associated with a fully intact nucleus (DAPI+) of a cTnT+ ventricular cardiomyocyte. Green boxes indicate the reference location for the magnified inset images of select/intact representative primary cilia from CHD+CON (left) and CHD + Myofiber Disarray (right).

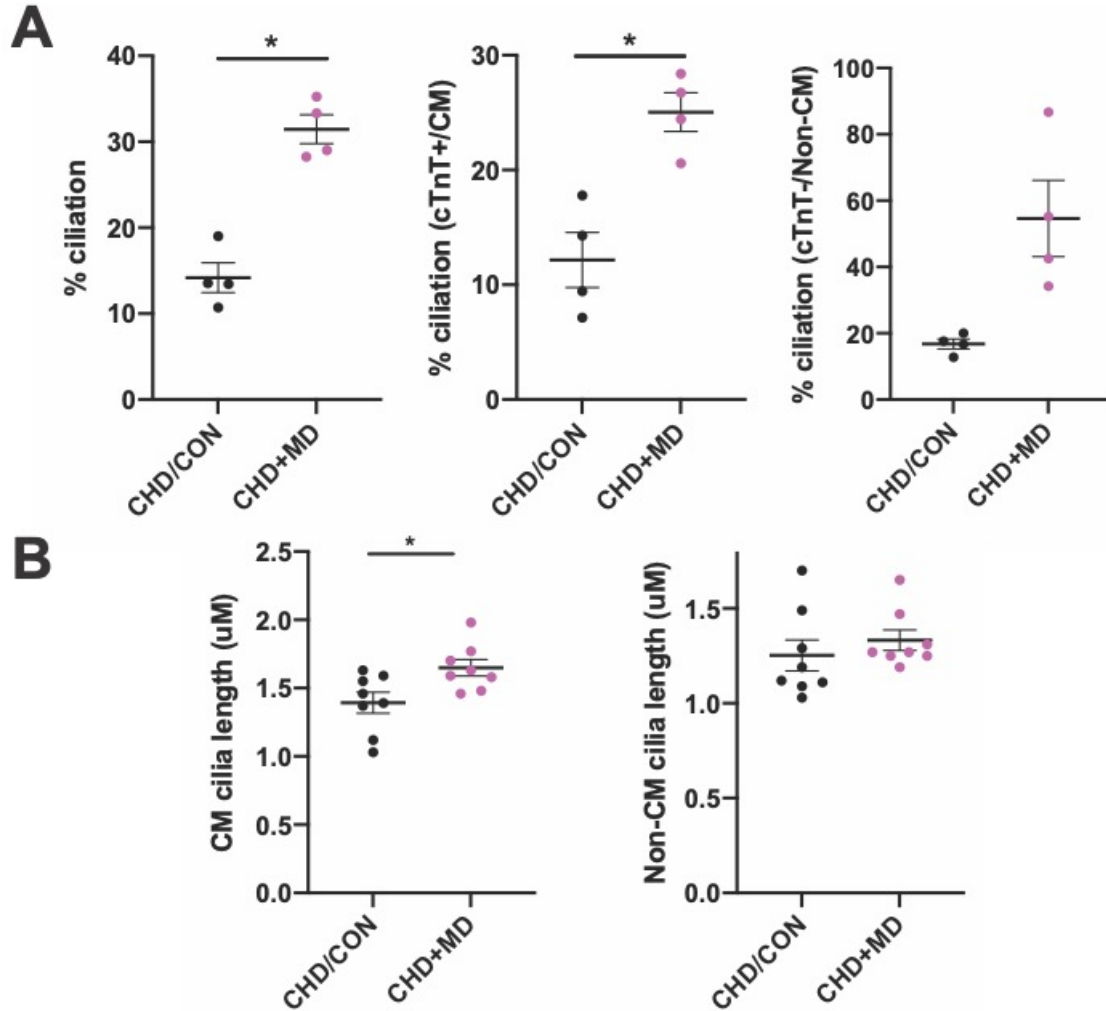


Figure 5.7 Quantitative characterization of cardiomyocyte primary cilia from endomyocardial biopsies taken from human, pediatric CHD patients with and without myocardial disarray. (A) Percentage of total cells with an intact primary cilium, percent ciliation in cTnT+ CM and percent ciliation in cTnT-/DAPI+ biopsies from CHD/CON (n=4; black) and CHD+MD (n=4; magenta). Each data point represents individual case mean values, calculated from 6 representative image fields per case. (B, left) Mean values for individual primary cilia lengths in cTnT+ (CM) cells of CHD/CON (n=4) and CHD+MD (n=4) cases. (B, right) Mean values for individual primary cilia lengths in cTnT- (Non-CM) cells of CHD/CON (n=4) and CHD+MD (n=4) cases. (B) Each datapoint represents an average of primary cilia length values measured in at least 6 primary cilia per imaging field (63X), where an average of 2 images were collected per individual patient case. *p<0.05

While it would have been ideal to have “true” control pediatric myocardial tissue obtained from human patients, the focus of this pilot investigation with human samples was primarily to determine if primary cilia are even present within the cells of the ventricular myocardium of patients with CHD. Additionally, among CHD patients with an OFT defect only-phenotype, we felt it was important to determine whether the cilia of the ventricular myocardium were morphologically and/or quantitatively significantly different in the presence or absence of CHD/OFT defects with a myocardial phenotype. Loss of primary cilia from CM in the developing heart alters cellular organization and thickness of the ventricular myocardium. Primary cilia of CM may therefore be mediators of congenital abnormalities of the ventricular myocardium, with a potential implication for primary cilia as mechanosensors of cardiac muscle cells in the developing heart.

CHAPTER 6

DISCUSSION & CONCLUSIONS

6.1 Manipulation of CNCC Resulting in a Novel Ventricular Phenotype

Cardiac neural crest cells are known contributors to the developing outflow tract, endocardial cushions, and atrial and ventricular septa, with some evidence of contribution to the coronary vasculature, and the ventricular myocardium (Abdul-Wajid et al., 2018; Jain et al., 2011; Keyte & Hutson, 2012; Kirby & Waldo, 1995; Saint-Jeannet, 2006). Primary cilia of CNCC are required to carry out many critical developmental mechanisms in these regions of the heart through sensory propagation of signal transduction pathways involving close physical interaction with or proximity to the physical scaffold of the cilium itself, depicted in Figure 1.1. Most well-known, is Hedgehog signaling in the developing heart, which is known to be essential for complete septation of the cardiac OFT (Smoak et al., 2005), as well as interatrial and interventricular septation (Goddeeris et al., 2008).

We utilized an *in vivo* model of CHD in the embryonic mouse, resulting from the genetic elimination of primary cilia of CNCC in the developing heart (Figure 6.1).

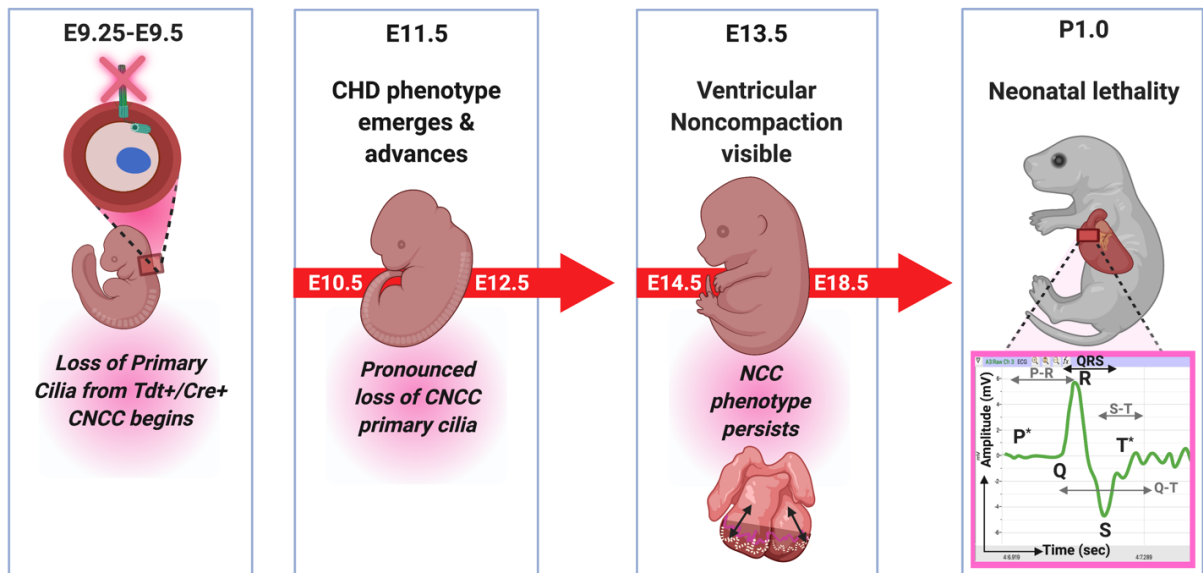


Figure 6.1 Summary of CNCC primary cilia mediated conditional knockout and resulting phenotype. (From Left to Right) Disappearance of primary cilia was observed beginning at E9.25, and the first aspects of the MUT cardiac phenotype resulting from CNCC loss of primary cilia were visible beginning at E10.5. By E11.5, a near-global loss of CNCC primary cilia was observed in *Tdt+* cells of MUT embryos along with the emergence of a full array of CHDs, including OFT defects and noncompaction of the ventricular myocardium. CHDs manifesting in MUT embryos persists through the first postnatal day, where perinatal lethality occurs prior to P2.0.

Use of the *Tdt* reporter revealed that *Cre* activation began at E7.5, where recombination at *Ift88 loxP* sites resulted in the failure of CNCC to elaborate primary cilia in the anterograde direction (Figure 6.1). The CHD phenotype resulting from CNCC loss of primary cilia included OFT defects and a novel ventricular myocardial phenotype, which we have classified as noncompaction of the ventricular myocardium, visible by ~E11.5 but most pronounced and diagnostically significant by E14.5 in MUT embryos. The array of CHDs in MUT embryos results in severe, cardiac ventricular arrhythmia apparent in the brief postnatal period occurring prior to perinatal lethality prior to the second postnatal day.

To our knowledge, we are the first not only to characterize elaboration of primary cilia of CNCC, but also assess the array of expected and unexpected CHD resulting from the genetically-induced elimination of primary cilia specifically in CNCC. The fact that loss of primary cilia in CNCC leads to the formation of OFT defects is not surprising, given that congenital, laterality/septation defects have long been independently and causally linked to BOTH primary cilia of cardiac progenitor cell populations as well as to the (cardiac) neural crest cells, themselves (Kirby & Waldo, 1995; Smoak et al., 2005; Waldo et al., 1999). The emergence (and thorough characterization) of the co-occurring ventricular phenotype also manifesting as a result of CNCC loss of primary cilia, on the other hand, represents an entirely novel and mechanistically relevant outcome.

6.1.1 CNCC (Tdt/Cre+) Presence in the Ventricular Myocardium

We present a diverse body of evidence to support a novel role for primary cilia of CNCC in promoting and supporting proper ventricular maturation in the developing mammalian heart. However, it remains unclear whether the ventricular phenotype is manifesting as a direct result of CNCC presence in the ventricular myocardium, where the loss of CNCC primary cilia is a causal factor in preventing proper cardiac chamber maturation. One central dogma ingrained in basic developmental biology curricula, is that neural crest cells (and CNCC) contribute exclusively to the developing pharyngeal arches, cardiac OFT/ECC and IVS of the developing mammalian heart (Bookman et al., 1987; Kirby, Gale, & Stewart, 1983). For the most part, phenotypic findings in both chick and mouse models resulting from manipulation of CNCC therein, has remained

consistent with this (Keyte & Hutson, 2012; Scholl & Kirby, 2009; Smoak et al., 2005). In other words, defective capacity for CNCC to properly migrate, proliferation, and position themselves appropriately within the developing mammalian heart, has consistently produced CHD phenotypes involving OFT and ECC septation, laterality and proliferative defects. From this perspective, at least in the context of the OFT/ECC phenotypes resulting from CNCC loss of primary cilia, our findings are consistent with previous research looking at CNCC-mediated CHD phenotypes. However, the ventricular phenotype we describe is a finding that is entirely novel, but also unexpected when working with a CNCC population of interest. Probing further, we entertained the possibility that the loss of primary cilia *could* promote an aberrant CNCC contribution to the developing ventricular myocardium.

Neural crest contributions to the ventricular myocardium have been well-characterized in the amniote heart (Tang et al., 2019). Aside from being required for normal cardiac morphogenesis in zebrafish, there is evidence to support that CNCC remaining in the postnatal ventricular myocardium could be one explanation for the extensive resiliency to disease and regenerative capacity of the zebrafish ventricle not seen in the mammalian ventricular myocardium (Abdul-Wajid et al., 2018; Stottmann, Choi, Mishina, Meyers, & Klingensmith, 2004). Scientific evidence in support of CNCC contributions to the mammalian ventricular myocardium have been posed (Hatzistergos et al., 2015; Waldo et al., 1999), including a more recent, and thorough characterizations of the inter-species variability between zebrafish, mice and humans (George, Maldonado-Velez, & Firulli, 2021). In particular, George *et al.*, provided a comprehensive review of the scientific literature supporting the feasibility of CNCC

contributions as the sole mediator for the capacity of the adult ventricular myocardial to regenerate, although the molecular dynamics remain a mystery (George et al., 2021).

One possible explanation for a CNCC-primary cilia-mediated mechanism of ventricular impairment could be explained by the extent of Tdt+ signal observed throughout the both left and right ventricles, beginning as early as E9.5 in both CON and MUT embryonic hearts (Figure 4.1). If, in fact, the Tdt+ signal is reflective of true, Cre+/CNCC lineage/status, then the loss of CNCC primary cilia within the developing ventricular myocardium could easily explain the hypertrabeculation and noncompaction aspects of the phenotype. However, Tdt+ (presumably Cre+) contributions were consistently observed in the ventricular myocardium of *Wnt1:Cre* (1-2)+/*Ift88*+/+ (WT/CON), *Cre*+/*Ift88**flox*/+ (HET/CON) and *Cre*+/*Ift88**flox*/*flox* (MUT) embryos. From these observations it would be reasonable to conclude while CNCC may contribute to the developing ventricular myocardium, introduction of either the *Ift88* heterozygous or the homozygous *Ift88* mutations (i.e. the elimination of some, or all CNCC primary cilia) in the presence of the CNCC Cre recombination was likely not a causal variable to explain the presence of Tdt+/Cre+ signal in the developing ventricular myocardium. That said, quantification of %ciliation in Tdt+/Cre+ cells of CON and MUT at E9.5 and E11.5 revealed a consistent and statistically significant decrease in percent of Tdt+ cells elaborating intact primary cilia in the MUT vMyoC when compared to Tdt+ ciliation quantified in the CON at identical embryonic timepoints (Figure 4.1). If loss of primary cilia in Tdt+ cells of the ventricular myocardium is truly reflective of CNCC presence in this region, this findings would support a mechanistic explanation for the hypertrabeculation and noncompaction aspects of the observed phenotype.

CNCC contributions to the ventricular myocardium are highly controversial. Thus, while our findings provide evidence in support of this phenomenon, the authors wish to convey these results with caution. Of critical relevance to this paper, is the fact that our models of CNCC loss of primary cilia using multiple Wnt1:Cre and primary cilia-specific conditional knock-out mouse models (Table 1.1), consistently produce a noncompaction phenotype that is statistically, biologically and clinically significant. This finding remains independent of the presence or absence of Tdt+/Cre+ cells observed within the developing ventricular myocardium.

6.2 CNCC Primary cilia are Associated with ErbB-Mediated Mechanisms of CM Proliferation, Cardiac Chamber Morphogenesis and Ventricular Compaction.

Proper organization, maturation, and compaction of the ventricular myocardium depends on/requires intimate communication between many of the distinct layers contained within this muscle, including the developing endocardium, the cardiac jelly, myocardium, epicardium and even pericardial layers. CHD of the vMyoC that have been causally linked with ErbB signaling are typically attributed to downregulation of either or both the Erk1/2/MAPK and PI3K/Akt pathways (described in Figure 1.5). Both pathways attenuate CM/sarcomeric protein synthesis and discourage CM survival and proliferation via a negative feedback loop (Baliga et al., 1999; Y.-Y. Zhao et al., 1998).

We observed a downregulation of ErbB2 and ErbB4 in CM of the E12.5 MUT ventricular myocardium. One explanation for this finding could be that the decreased ErbB2/4 observed, may fail to activate the Erk1/2 mechanism of cardioprotective effects promoting adequate CM/sarcomeric protein synthesis and protecting against ischemia.

However, the downregulation of CM ErbB2/ErbB4 in MUT observed in E12.5 came from ventricular tissue displaying hypertrabeculation not yet significantly (or diagnostically) different from that of the CON. Given that hypertrabeculation (and even normal expansion of trabecular myocardium) at E12.5 requires proliferation of ventricular CM, the biological responses typical of ErbB2/4 downregulation are not consistent with either phenotype or the increased proliferation of ventricular CM we observed at this timepoint (Figure 4.7).

While the downregulation of CM ErbB2/4 protein expression may not be consistent with the E12.5 ventricular phenotype, decreased CM ErbB (via Erk1/2) could be promoting the upregulation of Hh observed in the ventricular tissue at this timepoint. (Figure 4.11). Downregulation of ErbB/Erk resulting in upregulation of Hh via Gli has been documented in human keratinocytes (Kasper et al., 2006). Of note, this is a cell population which is known to be neural crest-derived (Jiang, Rowitch, Soriano, McMahon, & Sucov, 2000), but these findings may not be directly applicable to embryonic cardiac tissue. Activation of ErbB2/4-Erk1/2 mechanisms of Hh upregulation have been observed in numerous models of ischemia reperfusion injury in normal and diabetic hearts (Paulis et al., 2015; Xiao et al., 2012). In this context, ErbB/Erk1/2 activation of Hh is associated with better clinical outcomes and tissue integrity but is reflective of ischemia-induced upregulation of ErbB/Erk1/2, and is observed in diseased myocardial tissue coming from postnatal hearts.

Taken together, our findings indicate that CNCC loss of primary cilia leads to a reduction in CM population as well as downregulation of CM ErbB2 and ErbB4. We speculate that CM downregulation of ErbB2/4 could upregulate CM proliferation via a

noncanonical or negative feedback mechanism. Alternatively, or concurrently, decreased CM Erb2/4 may be directly or indirectly promoting the upregulation of Hh signaling observed in the MUT ventricular myocardium. However, it remains unclear how or if decreased ErbB2/4 in MUT CM is directly and/or causally responsible for the hypertrabeculation and noncompaction phenotypes observed in the MUT.

6.3 Loss of CNCC Primary Cilia Upregulates Hh Signaling and CM Proliferation Resulting in Noncompaction of the Ventricular Myocardium.

Shh is mostly dependent upon the primary cilium for propagation Hh signal transduction, but this codependency can also be temporary, and/or entirely a product of any given cellular/environmental circumstances. CNCC elimination of primary cilia leads to upregulation of Hh signaling via increased expression (and protein production) of Gli1. One explanation for this finding could be attributed to the changes in length of primary cilia observed in both Tdt+/CNCC and Tdt-/Non-CNCC cells of the developing cardiac OFT. We report that the loss of CNCC primary cilia leads to the lengthening of Tdt-/Non-CNCC primary cilia and shortening of any primary cilia remaining on Tdt+/CNCC of the MUT the developing cardiac outflow tract (Figure 4.1). Although a large body of evidence in chondrocytes concluding that ciliary length is associated with decreased sensitivity (or complete resistance) to HH signaling (Jenks et al., 2018; Z. Wang et al., 2016), there is also evidence to support the feasibility that lengthening of the cilium may also reflect upregulation of Hh signaling (Canterini et al., 2017; E. K. Ho & Stearns, 2021). If the lengthening of primary cilia is the source or instigator of the

upregulation of cardiac Hh observed, this would suggest that CNCC loss of primary cilia leads to increased Hh signaling carried out (in a paracrine fashion) by Tdt-/non-CNCC.

An alternate or additional explanation for the increased Hh seen in both the OFT and the ventricular myocardium of the MUT could reflect a transient and compensatory increase in Shh ligand production which is accumulating within the heart. Presumably, this would include unbound/lingering Shh ligand that was originally intended, but is no longer able to bind directly to CNCC in the absence of primary cilia. Regardless of whether a positive Tdt signal present in the MUT ventricular myocardium is reflective of the “true” presence of CNCC in this region, the indisputable presence of CNCC in the MUT cardiac OFT lacking primary cilia clearly initiate the upregulation of Hh signaling via increased Gli1 in a manner that may directly and/or indirectly affect the more inferior, ventricular myocardial regions not historically considered as CNCC contribution sites.

Unlike its transcriptional siblings, *Gli1* does not proteolyze, and therefore, only functions as a transcriptional activator (Yao & Chuang, 2015) and subsequently, a transcriptional readout reflective of the activation of Hh signaling. If upregulated Hh is resulting directly from CNCC loss of primary cilia, it is possible that upregulation of Hh could be originating from the small number of primary cilia remaining in Tdt+/CNCC. It is also possible that increased Hh signaling could be originating from the MUT Tdt+/CNCC themselves, but this would require a Gli1-mediated upregulation of Hh that is not dependent upon the presence of an intact ciliary axoneme.

According to Ruel and Therond (2009), primary cilia of mammalian cells (and specifically, in the mouse) can utilize Suppressor of Fused (Sufu) to suppress Hh signaling, as originally reported by Chen *et al.*, 2009 (M.-H. H. Chen et al., 2009; Dong

et al., 2019; Ruel & Thérond, 2009). Sufu expression localizes to the base of the primary cilium within the basal body region, a region that appears to remain intact following the elimination of CNCC primary cilia. Sufu's primary function is to promote full-length transcription of Gli proteins (also known as Gli/Hh activators), which has been shown to function independently from the primary cilium (Dong et al., 2019). Another study by Tukachinsky *et al.*, found that activation or upregulation of Hh signaling via Smo, activates Gli1 and Sufu inhibition of other Gli activator proteins (Tukachinsky, Lopez, & Salic, 2010). As a result, full-length Gli factors are able to translocate to the nucleus to carry out transcriptional activation (Nozawa, Lin, & Chuang, 2013; Tukachinsky et al., 2010). Interestingly, a recent study by Zhao *et al.*, found that cancerous tumor cells can become resistant to pharmacologically-induced Smo inhibition (and subsequent Hh inhibition), (X. Zhao et al., 2017). This effect is brought about via the loss of primary cilia, which results in a compensatory upregulation of Hh-mediated/oncogenic proliferation of resistant tumor cells, even in the presence of synthetic Hh inhibition (X. Zhao et al., 2017).

Introduction of Hh *GoF* via the SMOM2 model supports the possibility of a Gli1-mediated upregulation of Hh (independent from primary cilia) with two important findings. Firstly, introduction of SMOM2 in CNCC in the presence of some intact cilia exacerbated both OFT and ventricular aspects of the original cardiac phenotype resulting from CNCC loss of primary cilia only, potentially functioning as a *loss of function (LoF)* series of experiments (Figure 4.10). Secondly, introduction of the SMOM2 in MUT (CNCC lacking primary cilia) appears to positively affect, minimize, and potentially even reverse many of the molecular changes seen in the MUT and

SMOM2+cilia mutants (Figure 4.11). More specifically, Hh signaling in the ventricular myocardium of SMOM2+cilia mutants, resulted in a sustained, or increased upregulation Hh signaling, as evidenced by increased RNA and protein expression of ventricular Gli1 and Ptch1 (Figure 4.11). However, Hh *GoF* in SMOM2-cilia revealed expression of ventricular Gli1 and Ptch1 values that were no longer statistically significant from CON (Figure 4.11). This outcome stands alone in contradicting the majority of our interpretations of Hh upregulation seen in MUT and SMOM2+cilia as being carried out by increased Gli1 mechanisms functioning in the absence of primary cilia. With regard to the phenotypic aspects corresponding to constitutively active Hh (via SMO M2) in the MUT (SMOM2-cilia), there appears to be some recovery of/adequate formation of the compact ventricular myocardium and potentially, a ventricle that may be more capable of adequate force production (contractility and ejection fraction). Taken together, these data support a phenomenon we have termed “The Goldilocks phenomenon,” whereby too little Hh (MUT) as well as too much Hh (Hh *GoF*) both disrupt embryonic heart development and lead to CHD. In other words, proper OFT and ventricular maturation occur only in the presence of just the right amount of Hh, a Hh “sweet spot.”

Hh upregulation resulting from CNCC loss of primary cilia may also affect the production, secretion and general integrity of Hh ligand originating from the post-migratory CNCC remaining in the ventral aspects of pharyngeal region. Given that cells of the pharyngeal endoderm are the primary producers of Hh ligand, and are essential for the maintenance of the Hh signaling gradient orchestrating many of the cell signaling processes within the developing heart (Gritli-Linde, Lewis, McMahon, & Linde, 2001), it

is reasonable to suspect that alterations in Hh ligand production could occur as a result of CNCC loss of primary cilia in this region.

The ability of Hh ligand to be secreted in its “active” form, requires a complex series of rate-limiting structural modifications which are mediated by an even greater number of intra- and extracellular conditions (Gallet, 2010). Firstly, secretion of Hh ligand requires cleavage of its precursor ligand to yield an N-terminal secreted peptide containing covalent modifications of BOTH the C-terminus as well as palmitic acid located at the N-terminus (Gallet, 2010). Thus, the secreted form of Hh ligand is referred to as HH-NP, where “P” is indicative of its “processed” status. In order for a Hh-producing cell to carry out long-range, paracrine Hh signaling, the ligand must be released from the plasma membrane in its HH-NP form (Gallet, 2010; Ryan & Chiang, 2012). Autocrine and juxtacrine mechanisms of Hh signaling require the HH-NP structure, but can be carried out in even when HH-NP remains linked to the outer leaflet of the plasma membrane.

Thus, the preparation (cleavage) and protein structure required for Hh ligand secretion alone, raise several relevant questions to be considered in probing further into the mechanistic aspects of CHD resulting from CNCC loss of primary cilia, many of which can only be speculated upon at this time. Furthermore, we must ask the question if CNCC are even capable of (simultaneously) producing *and* secreting Hh ligand under any circumstances, let alone in the context of modeling disease (CHD). To the best of our knowledge at this time, Hh ligand production inherent to CNCC has not definitively been characterized. In the present study, we provide preliminary evidence in support of CNCC’s capacity to produce Hh ligand, specifically as evidenced by overlapping protein

expression patterns observed using immunofluorescence analysis of Shh, Smo and Gli in Tdt+ CNCC of CON embryos (Figures 4.13, 4.14). However, whether the loss of CNCC primary cilia affects the ability of the cell to produce and/or secrete Hh ligand remains unclear.

If CNCC do provide a source of cardiac Hh, and *if* the loss of primary cilia from CNCC disrupts this process, this could negatively impact the necessary mechanisms of CNCC-mediated Hh paracrine signaling. As described by Galley *et al.*, the absence or impairment of plasma membrane (and cholesterol) modifications to Hh ligand can lead to unrestrained upregulation of Hh, accompanied by ectopic expression of Hh target genes (primarily Gli proteins), (Gallet, 2010). In the context of the current project, CNCC loss of primary cilia could initiate the pathogenesis of CHD via plasma membrane accumulation of Hh, which could explain the upregulation and expression of Gli1, Ptch1, and Smo Hh targets. Of critical importance, Galley *et al.*, also emphasizes that HH-NP oligomers involved in solubilization of HH-NP are required in order carry out a maximal activation of Hh (when compared to the structural capacity of Hh ligand in its monomeric form), (Gallet, 2010). Thus, it comes as no surprise that errors in Hh-oligomerization have been shown promote premature and or inappropriate HH-NP release from a cell, resulting in the inadvertent long-range spread of Hh signal. Moreover, premature and or inappropriate HH-NP release from a cell can also decrease the binding affinity of secreted Hh ligand (Gallet, 2010). In our model of CHD resulting from CNCC loss of primary cilia, increased Hh observed in the OFT and ventricular myocardium could reflect an accumulation of Hh ligand with a reduced binding affinity. In other words, CNCC elimination of primary cilia in the ventral aspects of the pharyngeal region may

disrupt oligomerization and subsequent binding affinity of Hh ligand, rendering Hh less effective/biologically potent upon arrival within the developing heart and OFT.

6.4 Conclusions

Results from our investigations allow us to conclude that conditional elimination of CNCC primary cilia disrupts normal mammalian heart development and leads to a variety of CHD. As such, we present a novel disease model for the study of CHD in mammals. CNCC loss of primary cilia resulted in an unexpected upregulation of Hh signaling in the PA, OFT and vMyoC at the level of both RNA and protein expressions. Introduction of a Hh *GoF* component to this model in the presence of intact primary cilia, further upregulated Hh signaling, thus recapitulating our results from the initial series of experiments. Of particular importance, is the fact that our additional series of experiments looking at the conditional elimination of primary cilia in embryonic CM, did not produce a phenotype identical to the noncompaction observed in the CNCC primary cilia conditional knockout. We report that the use of both *Wnt1:Cre* mouse models suggests the possibility of CNCC contributions to the developing ventricular myocardium. However, CNCC loss of primary cilia consistently produces a novel and unexpected ventricular phenotype, which we have further characterized as non-compaction of the ventricular myocardium, and which persistent in the absence of the Tdt reporter. Finally, we provide evidence that OFT and vMyoC upregulation of Hh signaling resulting from CNCC loss of primary cilia is either originating from non-CNCC with intact primary cilia and/or may also be carried out in a primary-cilia-independent mechanism of Hh upregulation via *Gli1*. Taken together, the authors conclude that

although there may be multiple scenarios where Hh signaling is not dependent upon primary cilia to regulate cellular proliferation and laterality during development, it is clear that there CNCC primary cilia regulate Hh signaling in a way that is not only unique but also critical for healthy heart development.

REFERENCES

- Abdul-Wajid, S., Demarest, B. L., & Yost, H. J. (2018). Loss of embryonic neural crest derived cardiomyocytes causes adult onset hypertrophic cardiomyopathy in zebrafish. *Nature Communications*, 9(1). <https://doi.org/10.1038/S41467-018-07054-8>
- Adams, M., Smith, U. M., Logan, C. V., & Johnson, C. A. (2008). Recent advances in the molecular pathology, cell biology and genetics of ciliopathies. *Journal of Medical Genetics*, 45(5), 257–267. <https://doi.org/10.1136/JMG.2007.054999>
- Adams, Matthew, Simms, R. J., Abdelhamed, Z., Dawe, H. R., Szymanska, K., Logan, C. V., ... Johnson, C. A. (2012). A meckelin-filamin A interaction mediates ciliogenesis. *Human Molecular Genetics*, 21(6), 1272–1286. <https://doi.org/10.1093/HMG/DDR557>
- Alexander, S. P. H., Kelly, E., Mathie, A., Peters, J. A., Veale, E. L., Armstrong, J. F., ... Wong, S. S. (2019). THE CONCISE GUIDE TO PHARMACOLOGY 2019/20: Introduction and Other Protein Targets. *British Journal of Pharmacology*, 176(S1), S1–S20. <https://doi.org/10.1111/BPH.14747>
- Allen, B. L., Tenzen, T., & McMahon, A. P. (2007). The Hedgehog-binding proteins Gas1 and Cdo cooperate to positively regulate Shh signaling during mouse development. *Genes & Development*, 21(10), 1244–1257. <https://doi.org/10.1101/GAD.1543607>
- Almeida, A. G., & Pinto, F. J. (2013). Myocardial disease: Non-compaction cardiomyopathy. *Heart*, 99(20), 1535–1542. <https://doi.org/10.1136/heartjnl-2012-302048>
- Ariga, R., Tunnicliffe, E. M., Manohar, S. G., Mahmood, M., Raman, B., Piechnik, S. K., ... Watkins, H. (2019). Identification of Myocardial Disarray in Patients With Hypertrophic Cardiomyopathy and Ventricular Arrhythmias. *Journal of the American College of Cardiology*, 73(20), 2493–2502. <https://doi.org/10.1016/J.JACC.2019.02.065>
- Artap, S., Manderfield, L. J., Smith, C. L., Poleshko, A., Aghajanian, H., See, K., ... Epstein, J. A. (2018). Endocardial Hippo signaling regulates myocardial growth and cardiogenesis. *Developmental Biology*, 440(1), 22–30. <https://doi.org/10.1016/J.YDBIO.2018.04.026>
- Badano, J. L., Mitsuma, N., Beales, P. L., & Katsanis, N. (2006). The Ciliopathies: An Emerging Class of Human Genetic Disorders. *Annual Review of Genomics and Human Genetics*, 7(1), 125–148. <https://doi.org/10.1146/annurev.genom.7.080505.115610>

- Balaskas, N., Ribeiro, A., Panovska, J., Dessaud, E., Sasai, N., Page, K. M., ... Ribes, V. (2012). Gene Regulatory Logic for Reading the Sonic Hedgehog Signaling Gradient in the Vertebrate Neural Tube. *Cell*, *148*(1–2), 273–284. <https://doi.org/10.1016/J.CELL.2011.10.047>
- Baliga, R. R., Pimental, D. R., Zhao, Y.-Y., Simmons, W. W., Marchionni, M. A., Sawyer, D. B., & Kelly, R. A. (1999). NRG-1-induced cardiomyocyte hypertrophy. Role of PI-3-kinase, p70^{S6K}, and MEK-MAPK-RSK. *American Journal of Physiology-Heart and Circulatory Physiology*, *277*(5), H2026–H2037. <https://doi.org/10.1152/ajpheart.1999.277.5.H2026>
- Bonnafe, E., Touka, M., AitLounis, A., Baas, D., Barras, E., Ucla, C., ... Reith, W. (2004). The transcription factor RFX3 directs nodal cilium development and left-right asymmetry specification. *Molecular and Cellular Biology*, *24*(10), 4417–4427. <https://doi.org/10.1128/MCB.24.10.4417-4427.2004>
- Bookman, D. E., Redmond, M. E., Waldo, K., Davis, H., & Kirby, M. L. (1987). Effect of neural crest ablation on development of the heart and arch arteries in the chick. *American Journal of Anatomy*, *180*(4), 332–341.
- Boulter, C., Mulroy, S., Webb, S., Fleming, S., Brindle, K., & Sandford, R. (2001). Cardiovascular, skeletal, and renal defects in mice with a targeted disruption of the Pkd1 gene. *Proceedings of the National Academy of Sciences of the United States of America*, *98*(21), 12174–12179. <https://doi.org/10.1073/PNAS.211191098>
- Bowles, E. J. A., Wellman, R., Feigelson, H. S., Onitilo, A. A., Freedman, A. N., Delate, T., ... Wagner, E. H. (2012). Risk of heart failure in breast cancer patients after anthracycline and trastuzumab treatment: A retrospective cohort study. *Journal of the National Cancer Institute*, *104*(17), 1293–1305. <https://doi.org/10.1093/jnci/djs317>
- Brennan, D., Chen, X., Cheng, L., Mahoney, M., & Riobo, N. A. (2012). Noncanonical Hedgehog signaling. *Vitamins and Hormones*, *88*, 55–72. <https://doi.org/10.1016/B978-0-12-394622-5.00003-1>
- Briggs, L. E., Burns, T. A., Lockhart, M. M., Phelps, A. L., Van den Hoff, M. J. B., & Wessels, A. (2016). Wnt/ β -catenin and sonic hedgehog pathways interact in the regulation of the development of the dorsal mesenchymal protrusion. *Developmental Dynamics: An Official Publication of the American Association of Anatomists*, *245*(2), 103–113. <https://doi.org/10.1002/DVDY.24339>
- Burnicka-Turek, O., Steimle, J. D., Huang, W., Felker, L., Kamp, A., Kweon, J., ... Moskowitz, I. P. (2016). Cilia gene mutations cause atrioventricular septal defects by multiple mechanisms. *Human Molecular Genetics*, *0*(0), ddw155. <https://doi.org/10.1093/hmg/ddw155>

- Burns, T. A., Deepe, R. N., Bullard, J., Phelps, A. L., Toomer, K. A., Hiriart, E., ... Wessels, A. (2019). A Novel Mouse Model for Cilia-Associated Cardiovascular Anomalies with a High Penetrance of Total Anomalous Pulmonary Venous Return. *Anatomical Record (Hoboken, N.J. : 2007)*, 302(1), 136–145. <https://doi.org/10.1002/AR.23909>
- Canterini, S., Dragotto, J., Dardis, A., Zampieri, S., De Stefano, M. E., Mangia, F., ... Fiorenza, M. T. (2017). Shortened primary cilium length and dysregulated Sonic hedgehog signaling in Niemann-Pick C1 disease. *Human Molecular Genetics*, 26(12), 2277–2289. <https://doi.org/10.1093/HMG/DDX118>
- Cao, H., Yu, F., Zhao, Y., Zhang, X., Tai, J., Lee, J., ... Hsiai, T. K. (2014). Wearable multi-channel microelectrode membranes for elucidating electrophysiological phenotypes of injured myocardium. *Integrative Biology : Quantitative Biosciences from Nano to Macro*, 6(8), 789–795. <https://doi.org/10.1039/C4IB00052H>
- Caspary, T., Larkins, C. E., & Anderson, K. V. (2007). The Graded Response to Sonic Hedgehog Depends on Cilia Architecture. *Developmental Cell*, 12(5), 767–778. Retrieved from <http://www.cell.com/article/S1534580707001049/fulltext>
- Castellan, R. F. P., Thomson, A., Moran, C. M., & Gray, G. A. (2020). Electrocardiogram-gated Kilohertz Visualisation (EKV) Ultrasound Allows Assessment of Neonatal Cardiac Structural and Functional Maturation and Longitudinal Evaluation of Regeneration After Injury. *Ultrasound in Medicine & Biology*, 46(1), 167. <https://doi.org/10.1016/J.ULTRASMEDBIO.2019.09.012>
- Chen, J., Long, J. B., Hurria, A., Owusu, C., Steingart, R. M., & Gross, C. P. (2012). Incidence of heart failure or cardiomyopathy after adjuvant trastuzumab therapy for breast cancer. *Journal of the American College of Cardiology*, 60(24), 2504–2512. <https://doi.org/10.1016/j.jacc.2012.07.068>
- Chen, M.-H. H., Wilson, C. W., Li, Y.-J. J., Law, K. K. Lo, Lu, C.-S. S., Gacayan, R., ... Chuang, P.-T. T. (2009). Cilium-independent regulation of Gli protein function by Sufu in Hedgehog signaling is evolutionarily conserved. *Genes and Development*, 23(16), 1910–1928. Retrieved from <http://www.genesdev.org>.
- Cheng, L., Al-Owais, M., Covarrubias, M. L., Koch, W. J., Manning, D. R., Peers, C., & Riobo-Del Galdo, N. A. (2018). Coupling of Smoothed to inhibitory G proteins reduces voltage-gated K⁺ currents in cardiomyocytes and prolongs cardiac action potential duration. *Journal of Biological Chemistry*, 293(28), 11022–11032. <https://doi.org/10.1074/JBC.RA118.001989>

- Christ, A., Marczenke, M., & Willnow, T. E. (2020). LRP2 controls sonic hedgehog-dependent differentiation of cardiac progenitor cells during outflow tract formation. *Human Molecular Genetics*, 29(19), 3183–3196. <https://doi.org/10.1093/HMG/DDAA200>
- Chu, V., Otero, J. M., Lopez, O., Morgan, J. P., Amende, I., & Hampton, T. G. (2001). Method for non-invasively recording electrocardiograms in conscious mice. *BMC Physiology* 2001 1:1, 1(1), 1–6. <https://doi.org/10.1186/1472-6793-1-6>
- Cleary, J. O., Price, A. N., Thomas, D. L., Scambler, P. J., Kyriakopoulou, V., McCue, K., ... Lythgoe, M. F. (2009). Cardiac phenotyping in ex vivo murine embryos using μ MRI. *NMR in Biomedicine*, 22(January), 857–866. <https://doi.org/10.1002/nbm.1400>
- Clement, C. A., Kristensen, S. G., Møllgård, K., Pazour, G. J., Yoder, B. K., Larsen, L. A., ... Christensen, S. T. (2009). The primary cilium coordinates early cardiogenesis and hedgehog signaling in cardiomyocyte differentiation. *Journal of Cell Science*, 122(Pt 17), 3070–3082. <https://doi.org/10.1242/jcs.049676>
- Corbit, K. C., Aanstad, P., Singla, V., Norman, A. R., Stainier, D. Y. R., & Reiter, J. F. (2005). Vertebrate Smoothed functions at the primary cilium. *Nature*, 437(7061), 1018–1021.
- Crone, S. a, Zhao, Y.-Y., Fan, L., Gu, Y., Minamisawa, S., Liu, Y., ... Lee, K.-F. (2002). ErbB2 is essential in the prevention of dilated cardiomyopathy. *Nature Medicine*, 8(5), 459–465. <https://doi.org/10.1038/nm0502-459>
- Danielian, P. S., Muccino, D., Rowitch, D. H., Michael, S. K., & McMahon, A. P. (1998). *Modification of gene activity in mouse embryos in utero by a tamoxifen-inducible form of Cre recombinase.*
- Delling, M., Indzhykulyan, A. A., Liu, X., Li, Y., Xie, T., Corey, D. P., & Clapham, D. E. (2016). Primary cilia are not calcium-responsive mechanosensors. *Nature* 2016 531:7596, 531(7596), 656–660. <https://doi.org/10.1038/NATURE17426>
- Diguet, N., Le Garrec, J.-F. F., Lucchesi, T., & Meilhac, S. M. (2015). *Imaging and analyzing primary cilia in cardiac cells.* 127, 55–73. <https://doi.org/10.1016/BS.MCB.2015.01.008>
- Dong, H., Liu, H., Zhou, W., Zhang, F., Li, C., Chen, J., ... Yu, P. (2019). GLI1 activation by non-classical pathway integrin $\alpha\beta 3$ /ERK1/2 maintains stem cell-like phenotype of multicellular aggregates in gastric cancer peritoneal metastasis. *Cell Death and Disease*, 10(8). <https://doi.org/10.1038/s41419-019-1776-x>
- Dummer, A., Poelma, C., DeRuiter, M. C., Goumans, M. J. T. H., & Hierck, B. P. (2016). Measuring the primary cilium length: Improved method for unbiased high-throughput analysis. *Cilia*, 5(1), 7. <https://doi.org/10.1186/s13630-016-0028-2>

- Dunwoodie, S. L. (2007). Combinatorial signaling in the heart orchestrates cardiac induction, lineage specification and chamber formation. *Seminars in Cell & Developmental Biology*, 18(1), 54–66.
<https://doi.org/10.1016/j.semcdb.2006.12.003>
- Durst, R., Sauls, K., Peal, D. S., DeVlaming, A., Toomer, K., Leyne, M., ... Slaughter, S. A. (2015). *Mutations in DCHS1 cause mitral valve prolapse*. 525(7567), 109–113. Retrieved from <https://pubmed.ncbi.nlm.nih.gov/26258302/>
- Dyer, L. A., & Kirby, M. L. (2009). Sonic hedgehog maintains proliferation in secondary heart field progenitors and is required for normal arterial pole formation. *Developmental Biology*, 330(2), 305–317.
<https://doi.org/10.1016/j.ydbio.2009.03.028>
- Echelard, Y., Epstein, D. J., St-Jacques, B., Shen, L., Mohler, J., McMahon, J. A., & McMahon, A. P. (1993). Sonic hedgehog, a member of a family of putative signaling molecules, is implicated in the regulation of CNS polarity. *Cell*, 75(7), 1417–1430. [https://doi.org/10.1016/0092-8674\(93\)90627-3](https://doi.org/10.1016/0092-8674(93)90627-3)
- Egorova, A. D., Khedoe, P. P. S. J., Goumans, M. J. T. H., Yoder, B. K., Nauli, S. M., Ten Dijke, P., ... Hierck, B. P. (2011). Lack of primary cilia primes shear-induced endothelial-to-mesenchymal transition. *Circulation Research*, 108(9), 1093–1101.
<https://doi.org/10.1161/CIRCRESAHA.110.231860>
- Epstein, J. a, Li, J., Lang, D., Chen, F., Brown, C. B., Jin, F., ... Lo, C. W. (2000). Migration of cardiac neural crest cells in Splotch embryos. *Development (Cambridge, England)*, 127(9), 1869–1878. Retrieved from <http://www.ncbi.nlm.nih.gov/pubmed/10751175>
- Fitzsimons, L. A., Brewer, V. L., Forrester, J., Moran, A. M., & Tucker, K. L. (2020). Noninvasive electrocardiography in the perinatal mouse. *Journal of Visualized Experiments*, 2020(160), 1–12. <https://doi.org/10.3791/61074>
- Francis, R. J. B., Christopher, A., Devine, W. A., Ostrowski, L., & Lo, C. (2012). Congenital heart disease and the specification of left-right asymmetry. *American Journal of Physiology. Heart and Circulatory Physiology*, 302(10).
<https://doi.org/10.1152/AJPHEART.01118.2011>
- Fulmer, D., Toomer, K. A., Glover, J., Guo, L., Moore, K., Moore, R., ... Norris, R. A. (2020). *Desert hedgehog-primary cilia cross talk shapes mitral valve tissue by organizing smooth muscle actin*. 463(1), 26–38.
<https://doi.org/10.1016/J.YDBIO.2020.03.003>

- Fulmer, D., Toomer, K., Guo, L., Moore, K., Glover, J., Moore, R., ... Lipschutz, J. H. (2019). Defects in the exocyst-cilia machinery cause bicuspid aortic valve disease and aortic stenosis. *Circulation*, *140*(16), 1331–1341. <https://doi.org/10.1161/CIRCULATIONAHA.119.038376>
- Gallet, A. (2010). Hedgehog morphogen: from secretion to reception. *Trends in Cell Biology*, *21*, 238–246. <https://doi.org/10.1016/j.tcb.2010.12.005>
- Garratt, A. N., Özcelik, C., & Birchmeier, C. (2003). ErbB2 pathways in heart and neural diseases. *Trends in Cardiovascular Medicine*, *13*(2), 80–86. [https://doi.org/10.1016/S1050-1738\(02\)00231-1](https://doi.org/10.1016/S1050-1738(02)00231-1)
- Garrod, A. S., Zahid, M., Tian, X., Francis, R. J., Khalifa, O., Devine, W., ... Lo, C. W. (2014). Airway ciliary dysfunction and sinopulmonary symptoms in patients with congenital heart disease. *Annals of the American Thoracic Society*, *11*(9), 1426–1432. <https://doi.org/10.1513/ANNALSATS.201405-222OC>
- George, R. M., Maldonado-Velez, G., & Firulli, A. B. (2021). The heart of the neural crest: Cardiac neural crest cells in development and regeneration. *Development (Cambridge)*, *147*(20). <https://doi.org/10.1242/DEV.188706/225875>
- Gerhardt, C., Lier, J. M., Kuschel, S., Rü, U., & Rütger, U. (2013). The Ciliary Protein Ftm Is Required for Ventricular Wall and Septal Development. *PLoS ONE*, *8*(2), e57545: 1-15. <https://doi.org/10.1371/journal.pone.0057545>
- Gittenberger-De Groot, A. C., Bartelings, M. M., Deruiter, M. C., & Poelmann, R. E. (2005). Basics of cardiac development for the understanding of congenital heart malformations. *Pediatric Research*, *57*(2), 169–176. <https://doi.org/10.1203/01.PDR.0000148710.69159.61>
- Goddeeris, M. M., Rho, S., Petiet, A., Davenport, C. L., Johnson, G. A., Meyers, E. N., ... Goddeeris, M. M. (2008). Intracardiac septation requires hedgehog-dependent cellular contributions from outside the heart. *Development*, *135*(10), 1887–1895. Retrieved from <https://journals.biologists.com/dev/article/135/10/1887/64686/Intracardiac-septation-requires-hedgehog-dependent>
- Goddeeris, M. M., Schwartz, R., Klingensmith, J., & Meyers, E. N. (2007). Independent requirements for Hedgehog signaling by both the anterior heart field and neural crest cells for outflow tract development. *Development (Cambridge, England)*, *134*(8), 1593–1604. <https://doi.org/10.1242/dev.02824>
- Goenezen, S., Rennie, M. Y., & Rugonyi, S. (2013). Biomechanics of Early Cardiac Development. *Biomechanics and Modeling in Mechanobiology*, *11*(8), 1187–1204. <https://doi.org/10.1007/s10237-012-0414-7.Biomechanics>

- Goetz, S. C., & Anderson, K. V. (2010). The primary cilium: A signalling centre during vertebrate development. *Nature Reviews Genetics*, 11(5), 331–344. <https://doi.org/10.1038/NRG2774>
- Grego-bessa, J., Luna-zurita, L., Monte, G., Bolós, V., Arandilla, A., Garratt, A. N., ... Pompa, D. (2007). Notch Signalling is essential for ventricular development. *Developmental Cell*, 12(3), 415–429. <https://doi.org/10.1016/j.devcel.2006.12.011>.Notch
- Gritli-Linde, A., Lewis, P., McMahon, A. P., & Linde, A. (2001). The Whereabouts of a Morphogen: Direct Evidence for Short- and Graded Long-Range Activity of Hedgehog Signaling Peptides. *Developmental Biology*, 236(2), 364–386. <https://doi.org/10.1006/DBIO.2001.0336>
- Günthel, M., Barnett, P., & Christoffels, V. M. (2018). Development, Proliferation, and Growth of the Mammalian Heart. *Molecular Therapy*, 26(7), 1599–1609. <https://doi.org/10.1016/J.YMTHE.2018.05.022>
- Gustafsson, M. V., Zheng, X., Pereira, T., Gradin, K., Jin, S., Lundkvist, J., ... Bondesson, M. (2005). Hypoxia requires Notch signaling to maintain the undifferentiated cell state. *Developmental Cell*, 9(5), 617–628. <https://doi.org/10.1016/j.devcel.2005.09.010>
- Han, Y. G., Kim, H. J., Dlugosz, A. A., Ellison, D. W., Gilbertson, R. J., & Alvarez-Buylla, A. (2009). Dual and opposing roles of primary cilia in medulloblastoma development. *Nature Medicine* 2009 15:9, 15(9), 1062–1065. <https://doi.org/10.1038/NM.2020>
- Hatzistergos, K. E., Takeuchi, L. M., Saur, D., Seidler, B., Dymecki, S. M., Mai, J. J., ... Hare, J. M. (2015). *cKit*⁺ cardiac progenitors of neural crest origin. *Proceedings of the National Academy of Sciences*, 112(42), 201517201. <https://doi.org/10.1073/pnas.1517201112>
- Haycraft, C. J., Zhang, Q., Song, B., Jackson, W. S., Detloff, P. J., Serra, R., & Yoder, B. K. (2007). Intraflagellar transport is essential for endochondral bone formation. *Development (Cambridge, England)*, 134(2), 307–316. <https://doi.org/10.1242/dev.02732>
- Heier, C. R., & DiDonato, C. J. (2015). ECG in neonate mice with spinal muscular atrophy allows assessment of drug efficacy. *Frontiers in Bioscience (Elite Edition)*, 7(1), 122–133. <https://doi.org/10.2741/E721>
- Heier, C. R., Hampton, T. G., Wang, D., & DiDonato, C. J. (2010). Development of electrocardiogram intervals during growth of FVB/N neonate mice. *BMC Physiology*, 10(1), 1–9. <https://doi.org/10.1186/1472-6793-10-16/FIGURES/3>

- Ho, D., Zhao, X., Gao, S., Hong, C., Vatner, D. E., & Vatner, S. F. (2011). Heart Rate and Electrocardiography Monitoring in Mice. *Current Protocols in Mouse Biology*, 1(1), 123. <https://doi.org/10.1002/9780470942390.MO100159>
- Ho, E. K., & Stearns, T. (2021). *Hedgehog signaling and the primary cilium: implications for spatial and temporal constraints on signaling*. <https://doi.org/10.1242/dev.195552>
- Hoffman, J. I. E., Kaplan, S., & Liberthson, R. R. (2004). Prevalence of congenital heart disease. *American Heart Journal*, 147(3), 425–439. <https://doi.org/10.1016/j.ahj.2003.05.003>
- Hoffmann, A. D., Peterson, M. A., Friedland-Little, J. M., Anderson, S. A., & Moskowitz, I. P. (2009). Sonic hedgehog is required in pulmonary endoderm for atrial septation. *Development*, 136(10), 1761–1770. <https://doi.org/10.1242/dev.034157>
- Hofherr, A., & Köttgen, M. (2016). Polycystic kidney disease: Cilia and mechanosensation revisited. *Nature Reviews. Nephrology*, 12(6), 318–319. <https://doi.org/10.1038/NRNEPH.2016.61>
- Hoyer-Fender, S. (2013). Primary and motile cilia: their ultrastructure and ciliogenesis. In K. L. Tucker & T. Caspary (Eds.), *Cilia and Nervous System Development and Function*. (Springer S, pp. 1–53).
- Ichida, F., Hamamichi, Y., Miyawaki, T., Ono, Y., Kamiya, T., Akagi, T., ... Tomimatsu, H. (1999). Clinical features of isolated noncompaction of the ventricular myocardium: Long-term clinical course, hemodynamic properties, and genetic background. *Journal of the American College of Cardiology*, 34(1), 233–240. [https://doi.org/10.1016/S0735-1097\(99\)00170-9](https://doi.org/10.1016/S0735-1097(99)00170-9)
- Jain, R., Engleka, K. A., Rentschler, S. L., Manderfield, L. J., Li, L., Yuan, L., & Epstein, J. A. (2011). Cardiac neural crest orchestrates remodeling and functional maturation of mouse semilunar valves. *The Journal of Clinical Investigation*, 121(1). Retrieved from <http://www.jci.org>
- Jenks, A. D., Vyse, S., Wong, J. P., Kostaras, E., Keller, D., Burgoyne, T., ... Tanos, B. E. (2018). Primary Cilia Mediate Diverse Kinase Inhibitor Resistance Mechanisms in Cancer. *Cell Reports*, 23(10), 3042–3055. <https://doi.org/10.1016/J.CELREP.2018.05.016>
- Jeong, J., Mao, J., Tenzen, T., Kottmann, A. H., & McMahon, A. P. (2004). *Hedgehog signaling in the neural crest cells regulates the patterning and growth of facial primordia*. 18(8). <https://doi.org/10.1101/GAD.1190304>
- Jeong, M. H., Leem, Y. E., Kim, H. J., Kang, K., Cho, H., & Kang, J. S. (2016). A Shh coreceptor Cdo is required for efficient cardiomyogenesis of pluripotent stem cells.

Journal of Molecular and Cellular Cardiology, 93, 57–66.
<https://doi.org/10.1016/j.yjmcc.2016.01.013>

Jiang, X., Rowitch, D. H., Soriano, P., McMahon, A. P., & Sucov, H. M. (2000). Fate of the mammalian cardiac neural crest. *Development (Cambridge, England)*, 127(8), 1607–1616. <https://doi.org/10.1242/DEV.127.8.1607>

Jiao, K., Kulesa, H., Tompkins, K., Zhou, Y., Batts, L., Baldwin, H. S., & Hogan, B. L. M. (2003). An essential role of Bmp4 in the atrioventricular septation of the mouse heart. *Genes & Development*, 17(19), 2362–2367.
<https://doi.org/10.1101/gad.1124803>

Kaese, S., & Verheule, S. (2012). Cardiac electrophysiology in mice: A matter of size. *Frontiers in Physiology*, 3 SEP, 345.
<https://doi.org/10.3389/FPHYS.2012.00345/BIBTEX>

Karp, N., Grosse-Wortmann, L., & Bowdin, S. (2012). Severe aortic stenosis, bicuspid aortic valve and atrial septal defect in a child with Joubert Syndrome and Related Disorders (JSRD) - a case report and review of congenital heart defects reported in the human ciliopathies. *European Journal of Medical Genetics*, 55(11), 605–610.
<https://doi.org/10.1016/J.EJMG.2012.07.010>

Kasper, M., Schnidar, H., Neill, G. W., Hanneder, M., Klingler, S., Blaas, L., ... Aberger, F. (2006). Selective Modulation of Hedgehog/GLI Target Gene Expression by Epidermal Growth Factor Signaling in Human Keratinocytes. *Molecular and Cellular Biology*, 26(16), 6283–6298. https://doi.org/10.1128/MCB.02317-05/SUPPL_FILE/KASPER_ET_AL_REVISIED_TABLES2.ZIP

Kaur, S., McGlashan, S. R., & Ward, M.-L. (2018). Evidence of primary cilia in the developing rat heart. *Cilia*, 7(1), 4. <https://doi.org/10.1186/s13630-018-0058-z>

Kawagishi, H., Xiong, J., Rovira, I. I., Pan, H., Yan, Y., Fleischmann, B. K., ... Finkel, T. (2018). Sonic hedgehog signaling regulates the mammalian cardiac regenerative response. *Journal of Molecular and Cellular Cardiology*, 123, 180–184.
<https://doi.org/10.1016/J.YJMCC.2018.09.005>

Kelly, R. G., Buckingham, M. E., & Moorman, A. F. (2016). *Heart Fields and Cardiac Morphogenesis*. 1–11. <https://doi.org/10.1101/cshperspect.a015750>

Keyte, A., & Hutson, M. R. (2012). The Neural Crest in Cardiac Congenital Anomalies. *Differentiation; Research in Biological Diversity*, 84(1), 25.
<https://doi.org/10.1016/J.DIFF.2012.04.005>

- Kirby, M. L., Gale, T. F., & Stewart, D. E. (1983). Neural crest cells contribute to normal aorticopulmonary septation. *Science*, 220(4601), 1059–1061. <https://doi.org/10.1126/science.6844926>
- Kirby, M. L., & Waldo, K. L. (1995). Neural crest and cardiovascular patterning. *Circulation Research*, 77(2), 211–215. <https://doi.org/10.1161/01.RES.77.2.211>
- Kirchhoff, S., Kim, J. S., Hagendorff, A., Thönnissen, E., Krüger, O., Lamers, W. H., & Willecke, K. (2000). Abnormal cardiac conduction and morphogenesis in connexin40 and connexin43 double-deficient mice. *Circulation Research*, 87(5), 399–405. <https://doi.org/10.1161/01.RES.87.5.399>
- Klena, N. T., Gibbs, B. C., & Lo, C. W. (2017). Cilia and Ciliopathies in Congenital Heart Disease. *Cold Spring Harbor Perspect Biol*, 9(8), a028266. Retrieved from <http://www.ncbi.nlm.nih.gov/pubmed/28159874>
- Koefoed, K., Veland, I. R., Bang, L., Lars, P., Larsen, A., Christensen, S. T., ... Christensen, S. T. (2014). Cilia and coordination of signaling networks during heart development. *Organogenesis*, 10(1), 108–125. <https://doi.org/10.4161/org.27483>
- Koizumi, A., Sasano, T., Kimura, W., Miyamoto, Y., Aiba, T., Ishikawa, T., ... Furukawa, T. (2015). Genetic defects in a His-Purkinje system transcription factor, IRX3, cause lethal cardiac arrhythmias. *European Heart Journal*, ehv449. <https://doi.org/10.1093/eurheartj/ehv449>
- Kojima, Y., Tam, O. H., & Tam, P. P. L. (2014). Timing of developmental events in the early mouse embryo. *Seminars in Cell & Developmental Biology*, 34, 65–75. <https://doi.org/10.1016/j.semcdb.2014.06.010>
- Krishnan, A., Samtani, R., Dhanantwari, P., Lee, E., Yamada, S., Shiota, K., ... Lo, C. W. (2014). A detailed comparison of mouse and human cardiac development. <https://doi.org/10.1038/pr.2014.128>
- Kyndt, F., Gueffet, J. P., Probst, V., Jaafar, P., Legendre, A., Le Bouffant, F., ... Schott, J. J. (2007). Mutations in the gene encoding filamin A as a cause for familial cardiac valvular dystrophy. *Circulation*, 115(1), 40–49. <https://doi.org/10.1161/CIRCULATIONAHA.106.622621>
- Lewis, A. E., Vasudevan, H. N., O'Neill, A. K., Soriano, P., & Bush, J. O. (2013). The widely used Wnt1-Cre transgene causes developmental phenotypes by ectopic activation of Wnt signaling. *Developmental Biology*, 379(2), 229. <https://doi.org/10.1016/J.YDBIO.2013.04.026>
- Lewis, E. B. (1978). A gene complex controlling segmentation in *Drosophila*. *Nature*, 276(5688), 565–570. <https://doi.org/10.1038/276565A0>

- Li, L. X., & Li, X. (2021). Epigenetically Mediated Ciliogenesis and Cell Cycle Regulation, and Their Translational Potential. *Cells* 2021, Vol. 10, Page 1662, 10(7), 1662. <https://doi.org/10.3390/CELLS10071662>
- Li, Y., Klena, N. T., Gabriel, G. C., Liu, X., Kim, A. J., Lemke, K., ... Lo, C. W. (2015). Global genetic analysis in mice unveils central role for cilia in congenital heart disease. *Nature*, 521(7553), 520–524. <https://doi.org/10.1038/nature14269>
- Liang, X., Wang, G., Lin, L., Lowe, J., Zhang, Q., Bu, L., ... Evans, S. M. (2013). HCN4 dynamically marks the first heart field and conduction system precursors. *Circulation Research*, 113(4), 399–407. <https://doi.org/10.1161/CIRCRESAHA.113.301588>
- Lindsey, S. E., Butcher, J. T., & Yalcin, H. C. (2014). Mechanical regulation of cardiac development. *Frontiers in Physiology*, 5. <https://doi.org/10.3389/FPHYS.2014.00318>
- Liu, J., Bressan, M., Hassel, D., Huisken, J., Staudt, D., Kikuchi, K., ... Stainier, D. Y. (2010). A dual role for ErbB2 signaling in cardiac trabeculation. *Development*, 137(22), 3867–3875. <https://doi.org/10.1242/dev.053736>
- Livak, K. J., & Schmittgen, T. D. (2001). Analysis of Relative Gene Expression Data Using Real-Time Quantitative PCR and the 2- $\Delta\Delta$ CT Method. *Methods*, 25(4), 402–408. <https://doi.org/10.1006/METH.2001.1262>
- Luck, D. J. L. (1984). Genetic and biochemical dissection of the eucaryotic flagellum. *The Journal of Cell Biology*, 98(3), 789. <https://doi.org/10.1083/JCB.98.3.789>
- Lumiaho, A., Miettinen, R., Niemitukia, L., Laitinen, T., Rantala, A., Lampainen, E., ... Hartikainen, J. (2001). *Mitral Valve Prolapse and Mitral Regurgitation Are Common in Patients With Polycystic Kidney Disease Type 1*. <https://doi.org/10.1053/ajkd.2001.29216>
- Ma, P., Gu, S., Karunamuni, G. H., Jenkins, M. W., Watanabe, M., & Rollins, A. M. (2016). Cardiac neural crest ablation results in early endocardial cushion and hemodynamic flow abnormalities. *American Journal of Physiology - Heart and Circulatory Physiology*, ajpheart.00188.2016. <https://doi.org/10.1152/ajpheart.00188.2016>
- Madisen, L., Zwingman, T. A., Sunkin, S. M., Oh, S. W., Zariwala, H. A., Gu, H., ... Zeng, H. (2010). A robust and high-throughput Cre reporting and characterization system for the whole mouse brain. *Nature Neuroscience*, 13(1), 133–140. <https://doi.org/10.1038/nn.2467>

- Manasek, F. J. (1968). Embryonic development of the heart. I . A light and electron microscopic study of myocardial development in the early chick embryo. *Journal of Morphology*, 125(3), 329–365. <https://doi.org/10.1002/JMOR.1051250306>
- Marszalek, J. R., Liu, X., Roberts, E. A., Chui, D., Marth, J. D., Williams, D. S., & Goldstein, L. S. B. (2000). Genetic evidence for selective transport of opsin and arrestin by kinesin-II in mammalian photoreceptors. *Cell*, 102(2), 175–187. [https://doi.org/10.1016/S0092-8674\(00\)00023-4](https://doi.org/10.1016/S0092-8674(00)00023-4)
- Martí, E., Takada, R., Bumcrot, D. A., Sasaki, H., & McMahon, A. P. (1995). Distribution of Sonic hedgehog peptides in the developing chick and mouse embryo. *Development*, 121(8), 2537–2547. <https://doi.org/10.1242/dev.121.8.2537>
- Martinelli, D. C., & Fan, C. M. (2007). Gas1 extends the range of Hedgehog action by facilitating its signaling. *Genes & Development*, 21(10), 1231–1243. <https://doi.org/10.1101/GAD.1546307>
- Meilhac, S. M., & Buckingham, M. E. (2018). The deployment of cell lineages that form the mammalian heart. *Nature Reviews Cardiology* 2018 15:11, 15(11), 705–724. <https://doi.org/10.1038/S41569-018-0086-9>
- Meilhac, S. M., Lescroart, F., Blanpain, C. D., & Buckingham, M. E. (2014). Cardiac Cell Lineages that Form the Heart. *Cold Spring Harbor Perspectives in Medicine*, 4(9). <https://doi.org/10.1101/CSHPERSPECT.A013888>
- Menzl, I., Lebeau, L., Pandey, R., Hassounah, N. B. N. N. B., Li, F. W., Nagle, R., ... Tlsty, T. (2014). Loss of primary cilia occurs early in breast cancer development. *Cilia*, 3(1), 7. <https://doi.org/10.1186/2046-2530-3-7>
- Miquerol, L., Beyer, S., & Kelly, R. G. (2011). Establishment of the mouse ventricular conduction system. *Cardiovascular Research*, 91(2), 232–242. <https://doi.org/10.1093/CVR/CVR069>
- Miquerol, L., Moreno-Rascon, N., Beyer, S., Dupays, L., Meilhac, S. M., Buckingham, M. E., ... Kelly, R. G. (2010). Biphasic development of the mammalian ventricular conduction system. *Circulation Research*, 107(1), 153–161. <https://doi.org/10.1161/CIRCRESAHA.110.218156/FORMAT/EPUB>
- Mirvis, M., Siemers, K. A., Nelson, W. J., & Stearns, T. P. (2019). *Primary cilium loss in mammalian cells occurs predominantly by whole-cilium shedding*. 17(7). <https://doi.org/10.1371/JOURNAL.PBIO.3000381>
- Moorman, A. F. M., & Christoffels, V. M. (2003). Cardiac chamber formation: development, genes, and evolution. *Physiological Reviews*, 83(4), 1223–1267. <https://doi.org/10.1152/PHYSREV.00006.2003>

- Muthukrishnan, S. D., Ryzhov, S., Karolak, M., & Oxburgh, L. (2018). Nephron progenitor cell death elicits a limited compensatory response associated with interstitial expansion in the neonatal kidney. *Disease Models & Mechanisms*, *11*(1), dmm030544. <https://doi.org/10.1242/dmm.030544>
- Nakhleh, N., Francis, R., Giese, R. A., Tian, X., Li, Y., Zariwala, M. A., ... Lo, C. W. (2012). High Prevalence of Respiratory Ciliary Dysfunction in Congenital Heart Disease Patients With Heterotaxy. *Circulation*, *125*(18), 2232. <https://doi.org/10.1161/CIRCULATIONAHA.111.079780>
- Nauli, S. M., Jin, X., AbouAlaiwi, W. A., El-Jouni, W., Su, X., & Zhou, J. (2013). Non-motile primary cilia as fluid shear stress mechanosensors. *Methods in Enzymology*, *525*, 1–20. <https://doi.org/10.1016/B978-0-12-397944-5.00001-8>
- Nozawa, Y. I., Lin, C., & Chuang, P. T. (2013). Hedgehog signaling from the primary cilium to the nucleus: an emerging picture of ciliary localization, trafficking and transduction. *Current Opinion in Genetics & Development*, *23*(4), 429–437. <https://doi.org/10.1016/J.GDE.2013.04.008>
- Odiete, O., Hill, M. F., & Sawyer, D. B. (2012). Neuregulin in cardiovascular development and disease. *Circulation Research*, *111*(10), 1376–1385. <https://doi.org/10.1161/CIRCRESAHA.112.267286>
- Padula, S. L., Velayutham, N., Yutzey, K. E., Yutzey, N. ;, Transcriptional, K. E., & Org, K. Y. (2021). Transcriptional Regulation of Postnatal Cardiomyocyte Maturation and Regeneration. *International Journal of Molecular Sciences 2021, Vol. 22, Page 3288*, *22*(6), 3288. <https://doi.org/10.3390/IJMS22063288>
- Paige SL, Plonowska K, Zu A, W. S., Paige, S. L., Plonowska, K., Xu, A., & Wu, S. M. (2015). Molecular regulation of cardiomyocyte differentiation. *Circulation Research*, *116*(2), 341–353. <https://doi.org/10.1161/CIRCRESAHA.116.302752>
- Pala, R., Jamal, M., Alshammari, Q., & Nauli, S. M. (2018). The Roles of Primary Cilia in Cardiovascular Diseases. *Cells*, *7*(233), 1–18. <https://doi.org/10.3390/cells7120233>
- Pan, J., Wang, Q., & Snell, W. J. (2005). Cilium-generated signaling and cilia-related disorders. *Laboratory Investigation*, *85*(4), 452–463. <https://doi.org/10.1038/labinvest.3700253>
- Pappano, Achilles J., W. G. W. (2019). *Cardiovascular Physiology - 9780323594844* (11th ed.). Retrieved from <https://www.us.elsevierhealth.com/cardiovascular-physiology-9780323594844.html>

- Parmantier, E., Lynn, B., Lawson, D., Turmaine, M., Namini, S. S., Chakrabarti, L., ... Mirsky, R. (1999). Schwann cell-derived Desert hedgehog controls the development of peripheral nerve sheaths. *Neuron*, *23*(4), 713–724. [https://doi.org/10.1016/S0896-6273\(01\)80030-1](https://doi.org/10.1016/S0896-6273(01)80030-1)
- Patel, S. I., & Souter, M. J. (2008). Equipment-related electrocardiographic artifacts: causes, characteristics, consequences, and correction. *Anesthesiology*, *108*(1), 138–148. <https://doi.org/10.1097/01.ANES.0000296537.62905.25>
- Pathi, S., Pagan-Westphal, S., Baker, D. P., Garber, E. A., Rayhorn, P., Bumcrot, D., ... Williams, K. P. (2001). *Comparative biological responses to human Sonic, Indian, and Desert hedgehog*. *106*(1–2), 107–117. [https://doi.org/10.1016/S0925-4773\(01\)00427-0](https://doi.org/10.1016/S0925-4773(01)00427-0)
- Paulis, L., Fauconnier, J., Cazorla, O., Thireau, J., Soleti, R., Vidal, B., ... Lacampagne, A. (2015). Activation of Sonic hedgehog signaling in ventricular cardiomyocytes exerts cardioprotection against ischemia reperfusion injuries. *Scientific Reports*, *5*. <https://doi.org/10.1038/SREP07983>
- Pazour, G. J., Dickert, B. L., Vucica, Y., Seeley, E. S., Rosenbaum, J. L., Witman, G. B., & Cole, D. G. (2000). Chlamydomonas IFT 88 and Its Mouse Homologue, Polycystic Kidney Disease Gene Tg 737, Are Required for Assembly of Cilia and Flagella. *The Journal of Cell Biology*, *151*(3), 709–718. Retrieved from <http://www.jcb.org/cgi/content/full/151/3/709>
- Pieperhoff, S., Bennett, W., & Farrell, A. P. (2009). The intercellular organization of the two muscular systems in the adult salmonid heart, the compact and the spongy myocardium. *Journal of Anatomy*, *215*(5), 536–547. <https://doi.org/10.1111/J.1469-7580.2009.01129.X>
- Pietrobono, S., Gagliardi, S., & Stecca, B. (2019). Non-canonical hedgehog signaling pathway in cancer: Activation of GLI transcription factors beyond smoothed. *Frontiers in Genetics*, *10*(JUN), 556. <https://doi.org/10.3389/FGENE.2019.00556/BIBTEX>
- Polizio, A. H., Chinchilla, P., Chen, X., Manning, D. R., & Riobo, N. A. (2011). Sonic Hedgehog activates the GTPases Rac1 and RhoA in a Gli-independent manner via coupling of Smoothed to G i proteins. *Sci Signal.*, *4*(200), pt7. <https://doi.org/10.1126/scisignal.2002396>
- Praetorius, H. A., & Spring, K. R. (2001). Bending the MDCK cell primary cilium increases intracellular calcium. *The Journal of Membrane Biology*, *184*(1), 71–79. <https://doi.org/10.1007/S00232-001-0075-4>

- Rash, J. E., Shay, J. W., & Biesele, J. J. (1969). Cilia in Cardiac Differentiation. *J. ULTRASTRUCTURE RESEARCH*, 29, 470–484.
- Reiter, J. F., & Leroux, M. R. (2017). Genes and molecular pathways underpinning ciliopathies. *Nature Reviews Molecular Cell Biology* 2017 18:9, 18(9), 533–547. <https://doi.org/10.1038/NRM.2017.60>
- Robbins, D. J., Fei, D. L., & Riobo, N. A. (2012, October 16). The hedgehog signal transduction network. *Science Signaling*, Vol. 5. <https://doi.org/10.1126/scisignal.2002906>
- Rochais, F., Mesbah, K., & Kelly, R. G. (2009). Signaling pathways controlling second heart field development. *Circulation Research*, 104(8), 933–942. <https://doi.org/10.1161/CIRCRESAHA.109.194464>
- Rohatgi, R., Milenkovic, L., & Scott, M. P. (2007). Patched1 regulates hedgehog signaling at the primary cilium. *Science*, 317(5836), 372–376.
- Rudy, Y., & London, B. (2001). Cardiac Arrhythmias: From (Transgenic) Mice to Men. *Journal of Cardiovascular Electrophysiology*, 12(9), 1089–1091. <https://doi.org/10.1046/J.1540-8167.2001.01089.X>
- Ruel, L., & Thérond, P. P. (2009). Variations in Hedgehog signaling: divergence and perpetuation in Sufu regulation of Gli. *Genes & Development*, 23(16). <https://doi.org/10.1101/GAD.1838109>
- Ryan, K. E., & Chiang, C. (2012). Hedgehog Secretion and Signal Transduction in Vertebrates. *The Journal of Biological Chemistry*, 287(22), 17905. <https://doi.org/10.1074/JBC.R112.356006>
- Saint-jean, L., Barkas, N., Harmelink, C., Tompkins, K. L., Oakey, R. J., & Baldwin, H. S. (2019). Myocardial differentiation is dependent upon endocardial signaling during early cardiogenesis in vitro. *The Company of Biologists*. <https://doi.org/10.1242/dev.172619>
- Saint-Jeannet, J.-P. (2006). Neural crest induction and differentiation. In *Advances in experimental medicine and biology*. <https://doi.org/10.1007/978-0-387-46954-6>
- Samsa, L. A., Givens, C., Tzima, E., Stainier, D. Y. R. R., Qian, L., & Liu, J. (2015). Cardiac contraction activates endocardial Notch signaling to modulate chamber maturation in zebrafish. *Development*, 142(23), 4080–4091. <https://doi.org/10.1242/dev.125724>

- Samsa, L. A., Yang, B., & Liu, J. (2013). Embryonic cardiac chamber maturation: Trabeculation, conduction, and cardiomyocyte proliferation. *American Journal of Medical Genetics, Part C: Seminars in Medical Genetics*, 163(3), 157–168. <https://doi.org/10.1002/ajmg.c.31366>
- Satir, P., Pedersen, L. B., & Christensen, S. T. (2010). The primary cilium at a glance. *Journal of Cell Science*, 123(Pt 4), 499–503. <https://doi.org/10.1242/jcs.050377>
- Schindelin, J., Arganda-Carreras, I., Frise, E., Kaynig, V., Longair, M., Pietzsch, T., ... Cardona, A. (2012). Fiji: an open-source platform for biological-image analysis. *Nature Methods*, 9(7), 676–682. <https://doi.org/10.1038/nmeth.2019>
- Scholey, J. M. (2003). Intraflagellar Transport. *Http://Dx.Doi.Org.Wv-o-Ursus-Proxy02.Ursus.Maine.Edu/10.1146/Annurev.Cellbio.19.111401.091318*, 19, 423–443. <https://doi.org/10.1146/ANNUREV.CELLBIO.19.111401.091318>
- Scholl, A. M., & Kirby, M. L. (2009). Signals controlling neural crest contributions to the heart. *Wiley Interdisciplinary Reviews: Systems Biology and Medicine*, 1(2), 220–227. <https://doi.org/10.1002/wsbm.8>
- Sedmera, D., Hu, N., Weiss, K. M., Keller, B. B., Denslow, S., & Thompson, R. P. (2002). Cellular changes in experimental left heart hypoplasia. *Anatomical Record*, 267(2), 137–145. <https://doi.org/10.1002/ar.10098>
- Sedmera, D., Pexieder, T., Hu, N., & Clark, E. B. (1998). A quantitative study of the ventricular myoarchitecture in the stage 21–29 chick embryo following decreased loading. *European Journal of Morphology*, 36(2), 105–119. <https://doi.org/10.1076/ejom.36.2.105.4775>
- Sedmera, D., Pexieder, T., Rychterova, V., Hu, N., & Clark, E. B. (1998). *Remodeling of Chick Embryonic Ventricular Myoarchitecture Under Experimentally Changed Loading Conditions*.
- Sedmera, D., Pexieder, T., Vuillemin, M., Thompson, R. P., & Anderson, R. H. (2000). Developmental Patterning of the Myocardium. *THE ANATOMICAL RECORD*, 258, 319–337. [https://doi.org/10.1002/\(SICI\)1097-0185\(20000401\)258:4](https://doi.org/10.1002/(SICI)1097-0185(20000401)258:4)
- Sedmera, D., & Thompson, R. P. (2011). Myocyte proliferation in the developing heart. *Developmental Dynamics: An Official Publication of the American Association of Anatomists*, 240(6), 1322–1334. <https://doi.org/10.1002/DVDY.22650>
- Sigafoos, A. N., Paradise, B. D., Fernandez-Zapico, M. E., & Stecca, B. (2021). *cancers Hedgehog/GLI Signaling Pathway: Transduction, Regulation, and Implications for Disease*. <https://doi.org/10.3390/cancers13143410>

- Sisakian, H. (2014). Cardiomyopathies: Evolution of pathogenesis concepts and potential for new therapies. *World Journal of Cardiology*, 6(6), 478. <https://doi.org/10.4330/WJC.V6.I6.478>
- Slough, J., Cooney, L., & Brueckner, M. (2008). Monocilia in the embryonic mouse heart suggest a direct role for cilia in cardiac morphogenesis. *Developmental Dynamics*, 237(9), 2304–2314. <https://doi.org/10.1002/dvdy.21669>
- Smook, I. W., Byrd, N. A., Abu-issa, R., Goddeeris, M. M., Anderson, R., Morris, J., ... Meyers, E. N. (2005). Sonic hedgehog is required for cardiac outflow tract and neural crest cell development. *Developmental Biology*, 283(2), 357–372. <https://doi.org/10.1016/j.ydbio.2005.04.029>
- Snell, W. J., Pan, J., & Wang, Q. (2004). Cilia and flagella revealed: from flagellar assembly in *Chlamydomonas* to human obesity disorders. *Cell*, 117(6), 693–697. <https://doi.org/10.1016/J.CELL.2004.05.019>
- SPARANO, J. (2001). Cardiac toxicity of trastuzumab (Herceptin): Implications for the design of adjuvant trials. *Seminars in Oncology*, 28, 20–27. [https://doi.org/10.1016/S0093-7754\(01\)90189-7](https://doi.org/10.1016/S0093-7754(01)90189-7)
- Staudt, D. W., Liu, J., Thorn, K. S., Stuurman, N., Liebling, M., & Stainier, D. Y. R. (2014). High-resolution imaging of cardiomyocyte behavior reveals two distinct steps in ventricular trabeculation. *Development (Cambridge, England)*, 141(3), 585–593. <https://doi.org/10.1242/dev.098632>
- Stottmann, R. W., Choi, M., Mishina, Y., Meyers, E. N., & Klingensmith, J. (2004). BMP receptor IA is required in mammalian neural crest cells for development of the cardiac outflow tract and ventricular myocardium. *Development*, 131(9), 2205–2218. <https://doi.org/10.1242/dev.01086>
- Sun, S., Fisher, R. L., Bowser, S. S., Pentecost, B. T., & Sui, H. (2019). Three-dimensional architecture of epithelial primary cilia. *Proceedings of the National Academy of Sciences of the United States of America*, 116(19), 9370–9379. <https://doi.org/10.1073/PNAS.1821064116/-/DCSUPPLEMENTAL>
- Tang, W., Martik, M. L., Li, Y., & Bronner, M. E. (2019). Cardiac neural crest contributes to cardiomyocytes in amniotes and heart regeneration in zebrafish. *ELife*, 8. <https://doi.org/10.7554/ELIFE.47929>
- Tasouri, E., & Tucker, K. L. (2011). Primary cilia and organogenesis: Is Hedgehog the only sculptor? *Cell and Tissue Research*, 345(1), 21–40. <https://doi.org/10.1007/s00441-011-1192-8>

- Tenbaum, S., Arqués, O., Chicote, I., Tenbaum, S., Puig, I., & G. Palmer, H. (2012). Standardized Relative Quantification of Immunofluorescence Tissue Staining. *Protocol Exchange*. <https://doi.org/10.1038/PROTEX.2012.008>
- Tenzen, T., Allen, B. L., Cole, F., Kang, J. S., Krauss, R. S., & McMahon, A. P. (2006). The cell surface membrane proteins Cdo and Boc are components and targets of the Hedgehog signaling pathway and feedback network in mice. *Developmental Cell*, 10(5), 647–656. <https://doi.org/10.1016/J.DEVCEL.2006.04.004>
- Toomer, K. A., Fulmer, D., Guo, L., Drohan, A., Peterson, N., Swanson, P., ... Norris, R. A. (2017). A role for primary cilia in aortic valve development and disease. 246(8), 625–634. Retrieved from <http://doi.wiley.com/10.1002/dvdy.24524>
- Toomer, K. A., Yu, M., Fulmer, D., Guo, L., Moore, K. S., Moore, R., ... Norris, R. A. (2019). Primary cilia defects causing mitral valve prolapse. *Science Translational Medicine*, 11(493). <https://doi.org/10.1126/scitranslmed.aax0290>
- Torrisi, F., Alberghina, C., Lo Furno, D., Zappalà, A., Valable, S., Li Volti, G., ... Parenti, R. (2021). Connexin 43 and Sonic Hedgehog Pathway Interplay in Glioblastoma Cell Proliferation and Migration. *Biology 2021, Vol. 10, Page 767*, 10(8), 767. <https://doi.org/10.3390/BIOLOGY10080767>
- Towbin, J. A., & Jefferies, J. L. (2017). Cardiomyopathies due to left ventricular noncompaction, mitochondrial and storage diseases, and inborn errors of metabolism. *Circulation Research*, 121(7), 838–854. <https://doi.org/10.1161/CIRCRESAHA.117.310987>
- Tsukui, T., Capdevila, J., Tamura, K., Ruiz-Lozano, P., Rodriguez-Esteban, C., Yonei-Tamura, S., ... Belmonte, J. C. I. (1999). Multiple left-right asymmetry defects in Shh-/- mutant mice unveil a convergence of the Shh and retinoic acid pathways in the control of Lefty-1. *Proceedings of the National Academy of Sciences of the United States of America*, 96(20), 11376–11381. <https://doi.org/10.1073/pnas.96.20.11376>
- Tukachinsky, H., Lopez, L. V., & Salic, A. (2010). A mechanism for vertebrate Hedgehog signaling: recruitment to cilia and dissociation of SuFu–Gli protein complexes. *Journal of Cell Biology*, 191(2), 415–428. <https://doi.org/10.1083/JCB.201004108>
- Unverferth, B. J., Magorien, R. D., Balcerzak, S. P., Leier, C. V, & Unverferth, D. V. (1983). Early changes in human myocardial nuclei after doxorubicin. *Cancer*, 52(2), 215–221.
- Van Der Heiden, K., Groenendijk, B. C. W., Hierck, B. P., Hogers, B., Koerten, H. K., Mommaas, A. M., ... Poelmann, R. E. (2006). Monocilia on chicken embryonic endocardium in low shear stress areas. *Developmental Dynamics : An Official*

Publication of the American Association of Anatomists, 235(1), 19–28.
<https://doi.org/10.1002/DVDY.20557>

Vestergaard, M. L., Grubb, S., Koefoed, K., Anderson-Jenkins, Z., Grunnet-Lauridsen, K., Calloe, K., ... Andersen, C. Y. (2017). Human Embryonic Stem Cell-Derived Cardiomyocytes Self-Arrange with Areas of Different Subtypes during Differentiation. *Stem Cells and Development*, 26(21), 1566–1577.
<https://doi.org/10.1089/SCD.2017.0054/ASSET/IMAGES/LARGE/FIGURE5.JPEG>

Villalobos, E., Criollo, A., Schiattarella, G. G., Altamirano, F., French, K. M., May, H. I., ... Hill, J. A. (2019). Fibroblast Primary Cilia Are Required for Cardiac Fibrosis. *Circulation*, 139(20), 2342–2357.
<https://doi.org/10.1161/CIRCULATIONAHA.117.028752>

Von Gise, A., & Pu, W. T. (2012). Endocardial and epicardial epithelial to mesenchymal transitions in heart development and disease. *Circulation Research*, 110(12), 1628–1645. <https://doi.org/10.1161/CIRCRESAHA.111.259960>

Waldo, K., Zdanowicz, M., Burch, J., Kumiski, D. H., Stadt, H. A., Godt, R. E., ... Kirby, M. L. (1999). A novel role for cardiac neural crest in heart development. *The Journal of Clinical Investigation*, 103(11), 1499–1507.
<https://doi.org/10.1172/JCI6501>

Wang, Y., Lu, P., Zhao, D., & Sheng, J. (2017). Targeting the hedgehog signaling pathway for cardiac repair and regeneration. *Herz*, 42(7), 662–668.
<https://doi.org/10.1007/S00059-016-4500-Y/TABLES/3>

Wang, Z., Wann, A. K. T., Thompson, C. L., Hassen, A., Wang, W., & Knight, M. M. (2016). IFT88 influences chondrocyte actin organization and biomechanics. *Osteoarthritis and Cartilage*, 24(3), 544–554.
<https://doi.org/10.1016/j.joca.2015.10.003>

Wann, A. K. T., Zuo, N., Haycraft, C. J., Jensen, C. G., Poole, C. A., McGlashan, S. R., & Knight, M. M. (2012). Primary cilia mediate mechanotransduction through control of ATP-induced Ca²⁺ signaling in compressed chondrocytes. *FASEB Journal : Official Publication of the Federation of American Societies for Experimental Biology*, 26(4), 1663–1671. <https://doi.org/10.1096/FJ.11-193649>

Wessels, A., & Sedmera, D. (2004). Developmental anatomy of the heart: A tale of mice and man. *Physiological Genomics*, 15, 165–176.
<https://doi.org/10.1152/PHYSIOLGENOMICS.00033.2003/ASSET/IMAGES/LARGE/H70840442007.JPEG>

Wheatley, D. N., Wang, A. M., & Strugnell, G. E. (1996). Expression of primary cilia in mammalian cells. *Cell Biology International*, 20(1), 73–81.
<https://doi.org/10.1006/CBIR.1996.0011>

- Whewey, G., Nazlamova, L., & Hancock, J. T. (2018). Signaling through the Primary Cilium. *Frontiers in Cell and Developmental Biology*, 6, 8. <https://doi.org/10.3389/fcell.2018.00008>
- Whitfield, J. F. (2008). The solitary (primary) cilium – A mechanosensory toggle switch in bone and cartilage cells. *Cellular Signaling*, 20, 1019–1024. <https://doi.org/10.1016/j.cellsig.2007.12.001>
- Willaredt, Marc A., Hasenpusch-Theil, K., Gardner, H. A. R., Kitanovic, I., Hirschfeld-Warneken, V. C., Gojak, C. P., ... Tucker, K. L. (2008). A crucial role for primary cilia in cortical morphogenesis. *The Journal of Neuroscience : The Official Journal of the Society for Neuroscience*, 28(48), 12887–12900. <https://doi.org/10.1523/JNEUROSCI.2084-08.2008>
- Willaredt, Marc August, Gorgas, K., Gardner, H. A. R. R., & Tucker, K. L. (2012). Multiple essential roles for primary cilia in heart development. *Cilia*, 1(1), 23. <https://doi.org/10.1186/2046-2530-1-23>
- Williams, K., Carson, J., & Lo, C. (2019). Genetics of congenital heart disease. *Biomolecules*, 9(12). <https://doi.org/10.3390/biom9120879>
- Wong, S. Y., Seol, A. D., So, P.-L. L., Ermilov, A. N., Bichakjian, C. K., Epstein, E. H., ... Reiter, J. F. (2009). Primary cilia can both mediate and suppress Hedgehog pathway–dependent tumorigenesis. *Nature Medicine* 2009 15:9, 15(9), 1055–1061. <https://doi.org/10.1038/nm.2011>
- Wood, J. A., Dodd, R. T., Van Schmus, R. J., Wasson, J. T. ; W. R., Afiattalab, F., Wasson, J. T. ; W. R., ... Hutchison, R. (1980). Mutations affecting segment number and polarity in *Drosophila*. *Nature* 1980 287:5785, 287(5785), 795–801. <https://doi.org/10.1038/287795A0>
- Wu, G., Markowitz, G. S., Li, L., D'Agati, V. D., Factor, S. M., Geng, L., ... Somlo, S. (2000). *Cardiac defects and renal failure in mice with targeted mutations in Pkd2*. 24(1), 75–78. <https://doi.org/10.1038/71724>
- Xiao, Q., Hou, N., Wang, Y. P., He, L. S., He, Y. H., Zhang, G. P., ... Luo, J. D. (2012). Impaired sonic hedgehog pathway contributes to cardiac dysfunction in type 1 diabetic mice with myocardial infarction. *Cardiovascular Research*, 95(4), 507–516. <https://doi.org/10.1093/CVR/CVS216>
- Yamashita, J. K. (2016). Expanding Reprogramming to Cardiovascular Progenitors. *Cell Stem Cell*, 18(3), 299–301. <https://doi.org/10.1016/j.stem.2016.02.010>

- Yang, X., Kilgallen, S., Andreeva, V., Spicer, D. B., Pinz, I., & Friesel, R. (2010). Conditional expression of *Spry1* in neural crest causes craniofacial and cardiac defects. *BMC Developmental Biology*, *10*. <https://doi.org/10.1186/1471-213X-10-48>
- Yao, E., & Chuang, P.-T. (2015). *Hedgehog signaling: From basic research to clinical applications*. <https://doi.org/10.1016/j.jfma.2015.01.005>
- Zehendner, C. M., Luhmann, H. J., & Yang, J. W. (2013). A Simple and Novel Method to Monitor Breathing and Heart Rate in Awake and Urethane-Anesthetized Newborn Rodents. *PLOS ONE*, *8*(5), e62628. <https://doi.org/10.1371/JOURNAL.PONE.0062628>
- Zhang, W., Chen, H., Qu, X., Chang, C. P., & Shou, W. (2013). Molecular mechanism of ventricular trabeculation/compaction and the pathogenesis of the left ventricular noncompaction cardiomyopathy (LVNC). *American Journal of Medical Genetics, Part C: Seminars in Medical Genetics*, *163*(3), 144–156. <https://doi.org/10.1002/ajmg.c.31369>
- Zhang, X. M., Ramalho-Santos, M., & McMahon, A. P. (2001). Smoothed mutants reveal redundant roles for Shh and Ihh signaling including regulation of L/R asymmetry by the mouse node. *Cell*, *105*(6), 781–792. [https://doi.org/10.1016/S0092-8674\(01\)00385-3](https://doi.org/10.1016/S0092-8674(01)00385-3)
- Zhang, Y., Li, T. S., Lee, S. T., Wawrowsky, K. A., Cheng, K., Galang, G., ... Marbán, E. (2010). Dedifferentiation and Proliferation of Mammalian Cardiomyocytes. *PLOS ONE*, *5*(9), e12559. <https://doi.org/10.1371/JOURNAL.PONE.0012559>
- Zhao, X., Pak, E., Ornell, K. J., Pazyra-Murphy, M. F., Mackenzie, E. L., Chadwick, E. J., ... Segal, R. A. (2017). A Transposon Screen Identifies Loss of Primary Cilia as a Mechanism of Resistance to SMO Inhibitors. *CANCER DISCOVERY*, 1437. <https://doi.org/10.1158/2159-8290.CD-17-0281>
- Zhao, Y.-Y., Sawyer, D. R., Baliga, R. R., Opel, D. J., Han, X., Marchionni, M. A., & Kelly, R. A. (1998). *Neuregulins Promote Survival and Growth of Cardiac Myocytes PERSISTENCE OF ErbB2 AND ErbB4 EXPRESSION IN NEONATAL AND ADULT VENTRICULAR MYOCYTES**. Retrieved from <http://www.jbc.org/>
- Zhao, Y., Cao, H., Beebe, T., Zhang, H., Zhang, X., Chang, H., ... Hsiai, T. K. (2015). Dry-contact microelectrode membranes for wireless detection of electrical phenotypes in neonatal mouse hearts. *Biomedical Microdevices*, *17*(2). <https://doi.org/10.1007/S10544-014-9912-Y>
- Zimmermann, K. W. (1898). Beiträge zur Kenntniss einiger Drüsen und Epithelien. *Archiv Für Mikroskopische Anatomie 1898* 52:3, 52(3), 552–706. <https://doi.org/10.1007/BF02975837>

APPENDIX A:
SUPPLEMENTARY PROTOCOLS:
CARDIAC CELL STAINING FOR FLOW CYTOMETRY
(Ryzhov Laboratory, MMCRI)

ACK lysis solution – BioWhittaker, cat# 10-548

FACS buffer - PBS/05% BSA/ 2 mM EDTA

DPBS(-/-) – DPBS no Ca²⁺, no Mg²⁺ (Corning, cat# 21-031-CV)

VioDye – ThermoFisher LIVE/DEAD Fixable Violet Dead Cell stain (cat # L34955).

Prepare stock solution by diluting vial content in 50 µl of DMSO. Working solution – 1.9 µl of stock solution per 2 ml of DPBS(-/-)

Cell surface antibody mix – per 1 ml of FACS buffer:

- 6 µl of CD45-FITC (clone:30-F11)
- 6 µl of PeCy7-VCAM-1 (clone:429)
- 6 µl of APC-CD31 (clone:390)
- 6 µl of CD29-APC/Cy7 (clone:HMB1-1)

BD cytofix/cytoperm kit – BD Fixation/ Permeabilization solution contains two parts – (1) fixation/permeabilization solution and (2) Perm/Wash buffer, cat # 554714

Cardiac Troponin Ab – Start with 10 µl of Ab per 1 ml of 1X BD Perm/Wash buffer

Staining on embryonic cardiac cells for flow cytometry.

1. Transfer equal number of cells into 2 x FACS tubes (12 x 75 mm),

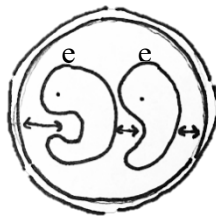
2. Centrifuge tubes at 500 x g for 3 min,
3. Aspirate supernatant, add 100 µl of ACK Lysis solution, resuspend cell pellet and incubate for 3-5 min,
4. Add 1 ml of FACS buffer and centrifuge at 500 x g for 3 min. aspirate supernatant,
5. Add 100 µl of DPBS(-/-) to each tube. Resuspend cells.
6. Add 100 µl of Amino-reactive fluorescent dye (VioDye) to cells. Incubate cells at room temperature for 30 min. NB! VioDye is a light-sensitive compound. Cover tubes with aluminum foil to prevent the decrease in the fluorescence intensity.
7. Add 2 ml of DPBS(-/-). Centrifuge tubes at 500 x g for 3 min. Aspirate supernatant.
8. Resuspend cell pellet in 100 µl of FACS buffer,
9. Add 100 µl of cell-surface antibody mix to each tube, vortex and incubate at 4⁰C for 30 min,
10. Add 2 ml of FACS buffer to each tube, centrifuge at 500 x g for 3 min. Aspirate supernatant.
11. Vortex cell pellet. Add 200 µl of 1X fixation/permeabilization solution (BD cytofix/cytoperm kit). Incubate for 20 min at room temperature in a dark place.
12. Add 2 ml of 1X BD Perm/Wash buffer (BD cytofix/cytoperm kit). Centrifuge tubes at 500 x g for 3 min. Aspirate supernatant.
13. Resuspend in 100 µl of 1X BD Perm/Wash buffer.
14. Add 100 µl of cardiac Troponin Antibody (in BD Perm/Wash buffer) into one tube and 100 µl of BD Perm/Wash buffer (fluorescence minus one (FMO) control) to another tube. Incubate at 4⁰C for 30 min.
15. Add 2 ml of 1X BD Perm/Wash buffer (BD cytofix/cytoperm kit). Centrifuge tubes at 500 x g for 3 min. Aspirate supernatant.
16. Resuspend cells in FACS buffer.
17. Proceed with flow cytometry.

APPENDIX B:
SUPPLEMENTARY PROTOCOLS:
EMBEDDING WHOLE EMBRYOS IN AGAROSE FOR MICRO-MRI
(Pinz Laboratory, MMCRI)

1. Put 50 ml of double-distilled/DI H₂O into a 125-ml Erlenmeyer flask
2. Add 1 g Agarose
3. Weigh the flask with the H₂O-Agarose mixture and record the weight.
4. Microwave very gently, first 30 seconds, then for 20 seconds. Remove flask from the microwave and swirl gently for approx. 2 minutes to lower temp slightly. Then microwave in additional, 10 second bursts as needed until the agarose has dissolved completely into solution. **DO NOT LET THE SOLUTION BOIL TO AVOID ACCUMULATION OF EXCESS AIR BUBBLES!!!**
5. Place on a stir-plate and a small stir bar and stir VERY slowly to allow the air bubbles to dissipate. You can use a warming plate to keep the agarose in a liquid state (set temperature to ~80°C and check/stir regularly to avoid skin formation).
6. **Add 400 microliters (0.4 ml) of 125x Gadolinium Solution using a p1000 pipette.**
7. Mix well using stir bar for additional 5-10 minutes.
8. Pipette the agarose into a 50-ml Conical Tube, **about 20 ml**. Use a blue tip for a P1000 pipette (or a Pasteur pipette) The conical tube can be placed into an

ice/slush bucket to speed up the process. Use a metal spatula to scrape away any air bubbles that form during the pouring process.

9. Take two (or three) embryos in Gadolinium solution at 4 mM and place in a Petri dish.
10. Pat them dry with a Kimwipe, this is important. Don't squash them!! You can use the tiny ladle/strainer spoon to gently turn the embryo over and over on top of the Kim wipe. This worked very well to remove excess liquid to avoid touching/pressing on the embryo.
11. Put embryos into the 50-m tube on top of the solidified agarose. They should be lying on their side, **each facing the same direction** (see below). The embryos should have some distance from the edge of the conical tube and between each other.



12. Dribble a small amount of molten agarose over the embryos to secure them in place. Let harden. Be patient please.
13. Pour additional 20 ml agarose over the fixed embryos until they are covered. Use the metal spatula to scrape away and visible air bubbles. Let harden (~10 minutes in slush)
14. Store at 4 degrees.

APPENDIX C:
SUPPLEMENTARY PROTOCOLS:
IMMUNOFLUORESCENCE PROTOCOL FOR FIXED, FROZEN,
OCT-EMBEDDED TISSUE(S)
(Tucker Laboratory, UNE)

Tissue type: Frozen tissue sections (embryonic/postnatal mouse);

Fixation: 4% Paraformaldehyde;

Storage: Embedded in OCT/VWR frozen tissue medium; CAT# X; stored @-80C

I. PREPARE BUFFERS (fresh or thaw):

A. BLOCKING BUFFER (Table C.1)*: **Modified from CST Protocol (pre-made stock available for purchase - Cat#124115; Ortiz de Montellano, P.R. et al. (1988) Biochemistry 27, 5470-6); Can be pre-made in batches, aliquoted and stored @ -20C (Do not store @-80C); prepare a 1X PBS / 5% normal serum / 0.3% TritonX-100 buffer by adding 0.5 mL normal serum from the same species as the secondary antibody (e.g., Normal Goat Serum) and 30 μ L TritonX-100 to 9.5 mL 1X PBS.*

Table C.1. Blocking Buffer Recipe for Immunofluorescence with Fixed, Frozen Tissue.

Reagent/Cat#	[stock]	[working]	10mL	100mL	200mL	500mL
TritonX-100	100%	*0.25-0.3%	30uL (0.3%)	300uL	600uL	1500uL (1.5mL)
Normal (Goat*) Serum	100%	5%	0.5mL	5mL	10mL	25mL
1X PBS			9.5mL	94.7mL	189.4mL	473.5mL

NOTES:

- a. Use fresh and store at 4°C for up to one month; freeze immediately and store at -20C for one year; avoid freeze/thaw; once thawed (warm water bath), store at 4C for up to two weeks.
- b. We have a [working] 10% NGS solution (Cat# /Invitrogen; stored @4C) if needed; this is primarily used as a “No primary” control medium (if AB diluent alone is not available)
- c. Primary cilia and basal body stains are sustainable using a 0.3% TritonX-100 blocking buffer; you can lower this as desired for more sensitive/less nuclear primary antibody/stains (e.g. Neuregulin-1/#MA12896-Invitrogen)
- d. *Substitute Donkey serum as needed; Cat# ; stored @-20C/1.5mL aliquots, labeled “NDS” [100%]

B. ANTIBODY DILUTION BUFFER (Table C.2)*: (*aka “AB diluent”*); *Modified from CST Protocol (pre-made stock available for purchase - Cat#12378; Ortiz de Montellano, P.R. et al. (1988) *Biochemistry* 27, 5470-6); Can be pre-made in batches of desired volume (examples below), aliquoted and stored @ -20C (Do not store @-80C); prepare a 1X PBS / 1% BSA / 0.3% TritonX-100 buffer by adding 0.1 g BSA and 30 μ L TritonX-100 to 10 mL 1X PBS.

Table C.2. Antibody Dilution Buffer Recipe for Immunofluorescence with fixed, frozen tissue.

Reagent/Cat#	[stock]	[working]	10mL	100mL	200mL	500mL
TritonX-100 (Cat# 327371000/Acros)	100%	*0.25-0.3%	30uL (0.3%)	300uL	600uL	1500uL (1.5mL)
BSA (Cat #0332/Amaresco)	100% (powder)	1%	0.1g	1g	2g	5g
1X PBS			9.5mL	94.7mL	189.4mL	473.5mL

NOTES:

- a. Use fresh and store at 4°C for up to two weeks; freeze immediately and store at -20C for one year; avoid freeze/thaw; once thawed (warm water bath), store at 4C for up to one week.

- b. IMPORTANT: If incubating with primary antibody at 4C/overnight, take Ab diluent out to room temp with slides and allow to warm to RT to avoid shocking tissue with cold buffer!

II. PERMEABILIZATION (BLOCKING)

1. Prepare/thaw blocking buffer as indicated in AG Tucker Lab protocol (Table C.1; 0.3% TritonX-100; 5% NGS/NDS in 1X PBS; frozen aliquots stored at -20C)
2. Remove pre-selected slides from -80C and rehydrate with droplet of 1XPBS; let sit 1-2 min at room temp.
3. Aspirate PBS or tap off slide; use a lint-free wipe to clear the edges/back of slides of excess moisture; apply PAP pen (shake well!) to draw a liberal border around each individual tissue section on the slide; let sit to dry ~2 minutes prior to applying blocking buffer; if tissue looks dry, use a micropipette to apply a SMALL droplet of 1X PBS to keep the tissue from drying out; DO NOT use excess liquid here! If you apply too much, it will spread to the lipid border you have just drawn and drag the lipid into/over the tissue itself...THIS IS BAD!
4. Repeat one slide at a time until each slide has a lipid border and has been allotted an appropriate amount of time to set; you can set slides on staining tray but do not fill with liquid until after the pap borders have set!

5. Fill the base of the staining tray with de-I H₂O; you can also add in some paper towel strips to help retain moisture within the chamber
6. Apply (**THAWED!**) blocking buffer liberally to each tissue section of each slide; blocking buffer should ideally be at/slightly below room temp to avoid shocking the tissue too much! Cover chamber and incubate at room temperature for **30**-45 minutes (*Absolutely* NO MORE THAN 1HR for cilia stains!)
7. Prepare primary antibody solutions

CHECK POINT: Primary Ab HOST

If you plan to use a primary (or secondary) antibody of a host species other than rodent (mouse, rat, rabbit) or goat, you may need to block using additional serum specific for your target; the most common substitution in AG Tucker Lab is the secondary antibody/fluorophore Alexa647 donkey α (anti-) rabbit (stored at 1:2 @-20C); donkey serum is stored in 1.5mL (1:1/100%) aliquots at -20C; add directly to blocking buffer containing goat serum or make separate solution if designating for a single tissue section on a slide)

III. PRIMARY ANTIBODY APPLICATION & INCUBATION

1. Prepare/thaw antibody dilution buffer (aka "Ab diluent"; Table C.2) fresh or from frozen aliquot (use warm water bath to thaw and then let sit benchtop at RT for ~5-10 minutes)

2. Write out your experiment (including individual slides selected) in your lab notebook; calculate all dilution factors ahead-of-time, using Ab spec sheets for reference and/or previous experiment records (if troubleshooting a new Ab).
3. Collect each of your primary antibody stocks (or aliquots) from either 4C or -20C and place in a benchtop cooler.

CHECK POINT: [stock]!

Most of the Tucker Lab antibodies are stored at -20 at 1:1 stock (in 50% glycerol), but some stocks/aliquots may be at 1:2 in 50% glycerol (e.g. acetylated alpha-tub, gamma-tubulin---both SIGMA/aliquoted) ...READ LABELS CAREFULLY! If you are unsure of the stock concentration, ASK Lindsey or Dr. Tucker, DO NOT GUESS (antibodies = \$\$\$\$\$\$)!!!

CHECK POINT: [Ab storage location]:

Storage location/temp and [stock] will vary by antibody—check with LAF and or refer to individual Ab spec sheet; if Ab stock contains 40-50% glycerol, it will be stored at -20C; if stock only contains sodium azide and no glycerol, it will be stored at 4C; if 50% glycerol has been ADDED to stock, it will be indicated on stock/aliquot vile AND lab spec sheet and will then be stored at -20C.

4. Always pipette Ab diluent FIRST----in designated volume into microcentrifuge tube; this way, if you make a mistake, you are not wasting precious antibody!

5. Add primary antibody(ies) one at a time into your working primary antibody master mix solution. USE FILTERED PIPETTE TIPS and DO NOT DOUBLE DIP (use a new tip every time you draw from the stock bottle to avoid contamination!)

CHECKPOINT: Primary Ab HOST SPECIES

When using more than a single primary antibody for a given experiment, you may “co-stain” only with target antigens raised in different species and/or IgG isoforms. AG Tucker Lab has primary polyclonal (rabbit IgG) and primary monoclonal (rabbit IgG, rat IgG, mouse IgG1, mouse IgG2a, mouse IgG2b) antibody stocks. Depending on the experimental design, you may need an isotype-specific secondary antibody(fluorophore) of a specific color---this needs to be planned out ahead of time in your lab notebook!!!

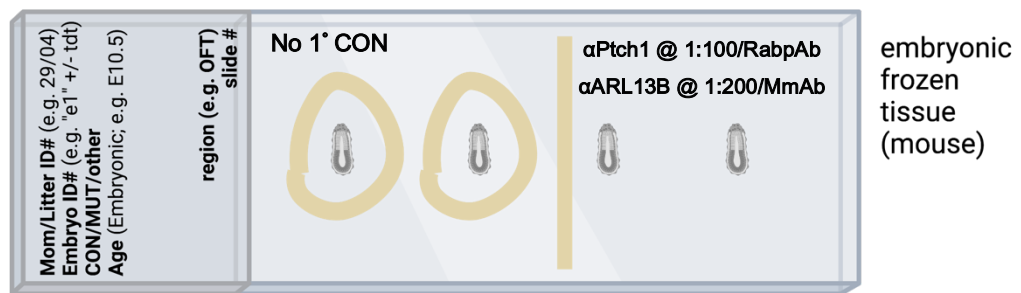
6. Immediately return primary antibody stocks to original storage location (4C or -20C)—DO NOT LET SIT BENCHTOP for a period of time longer than is necessary for pipetting! Label EACH primary antibody master mix with contents, date and dilution; leftover primary antibody master mix solutions may be stored at 4C and used within 1 week of original date made.

7. Remove cover from slide staining chamber; aspirate or gently tap off blocking buffer solution from each slide and place back onto staining rack

- USE A NEW, FILTERED, PIPETTE TIP to pipette primary antibody solution to each of your designated tissue sections.

CHECK POINT: Mapping your assigned targets

For co-stains, (new) Ab troubleshooting and more complicated/higher volume experiments, it can be helpful to draw out your experiment in your lab notebook with detailed labels/locations of tissue and corresponding antibody targets



- Cover staining chamber and incubate overnight at 4C in the dark; make sure that slide chamber LIES FLAT in the refrigerator—clear a spot for the chamber before you carry it over to the fridge

CHECKPOINT: Timeline

(OPTIONAL MODIFICATION) – Incubate in primary antibody solution at room temperature for one hour in humid chamber; NOTE- stains for primary cilia look best if done overnight @4C, but can be done at RT if need be.

10. This would be a good time to write out the remainder of your experiment(s) and calculate your dilutions for secondary antibodies so that you are prepared to start immediately the following day. OPTIONAL STEP- *you can prepare your secondary antibody master mix solutions ahead of time and store at 4C overnight; make sure to take them out along with your slides to allow them to warm slightly; leftovers may be stored @4C and used within a week.*

(Day 2 of 2)

IV. SECONDARY ANTIBODY APPLICATION & INCUBATION

1. Remove slide chamber from 4C/fridge and set benchtop for ~15-20 minutes to allow to reach room temperature; keep cover on chamber to maintain humidity; ALSO remove leftover Ab diluent (or thaw fresh) from 4C and allow to come to RT; SET a timer as a reminder!
2. Proceed with preparing secondary antibody master mix solutions while slides equilibrate; make sure to do this before you start the wash series to avoid disruptions
3. If you haven't already, write out the remainder of your experiment (for secondary antibodies, including individual slides selected) in your lab notebook; calculate all dilution factors ahead-of-time, using Ab spec sheets for reference and/or previous experiment records (if troubleshooting a new Ab). Most secondary antibodies in AG Tucker Lab are stored at 1:1 (100%) at 4C in a black storage box labelled "Secondary Ab Stocks." Select the

stock secondary antibodies you need for your experiment(s) and place in a portable benchtop cooler to keep cool while you are pipetting.

CHECK POINT: Mapping your assigned targets

Document your secondary antibody master mix recipes and/or add a record of your “slide map” which can be used when you go (back) to image your slides.



- Once you have made up your secondary antibody master mix solutions, return stocks to 4C/box (or -20 if applicable) and keep master mixes in the benchtop cooler while you proceed with washes.
- Once the timer goes off (indicating the slides have equilibrated), remove the cover to the slide chamber and gently tap off (or aspirate) the primary antibody solution from each slide and place back into slide chamber (one at a time).

CHECK POINT: Avoid contamination with multiple primaries!

If you have multiple experiments/targets on a single slide, aspiration of the solution is preferred to avoid possible contamination of alternate tissue

sections that can occur when you tap off liquid; **MAKE SURE TO CHANGE YOUR PIPETTE/TIP** for each tissue section for a given target/set of targets.

6. **WASH (3 X 5min) with 1X PBS:** Use disposable transfer pipette or regular pipette to apply 1X PBS (or other wash buffer) to each tissue section; set timer for 3 min let sit at room temp for the remainder of the washes. Aspirate or tap off 1X PBS and repeat with fresh 1X PBS (each time!) for a total of 3 washes.
7. After you aspirate/tap off the final 1X PBS wash, place all slides back in chamber. Apply secondary antibody master mix solutions to corresponding tissue sections; follow and/or update your slide map if changes are needed. If possible, perform this step with the lights off/dimmed to minimize any photobleaching.
8. Place cover on humid chamber and let incubate at room temperature for 45 minutes IN THE DARK (up to 1 hour). Use a timer!

CHECK POINT: Minimize photobleaching!

If you are using a dark staining chamber already, disregard and proceed with incubation. If you are NOT already using a dark slide chamber (i.e. **BLACKED OUT!**), make sure the chamber (or cover) is covered with a dark/opaque cloth or aluminum foil to minimize light exposure during incubation with secondary fluorophores!

9. Aspirate or tap off the secondary antibody solution and place slides back in chamber.

10. **WASH (5 X 5min) with 1X PBS:** Use disposable transfer pipette or regular pipette to apply 1X PBS (or other wash buffer) to each tissue section; set timer for **5 min** let sit at room temp for the remainder of the washes. Aspirate or tap off 1X PBS and repeat with fresh 1X PBS (each time!) for a **total of 5 washes**. **NOTE-** *this step is particularly important to minimize any residues or lingering fluorophore proteins that may remain on/within the tissue. If absolutely necessary, you can minimize to 3x5min washes, but it is BEST to complete all 5 washes!!!*

11. For the final wash, leave slides sitting in the chamber with the final wash solution. Remove one slide at a time to aspire/tap off PBS followed by (BRIEFLY) dipping the slide into de-I H₂O in a coplin jar (or equivalent immersion chamber). Tap off excess moisture and wipe back/edges of slide with lint-free wipe. Avoid touching/smudging/spreading the lipid borders when you are wiping away excess water!

NOTE: *if excess fluid accumulates within the lipid border/around the tissue, angle the slide downwards and use a dry corner of the lint-free wipe to carefully draw up the excess liquid away from the tissue section.*

V. SLIDE MOUNTING/COVER SLIPPING

1. Place slide flat on benchtop and apply mounting medium (with DAPI); coverslip and place slide in a cardboard slide folder to let set. Close the folder to keep the slide in dark while you continue mounting/cover-slipping

the remainder of your slides. If imaging immediately, allow to slides to sit and set at room temperature for about 30 minutes

CHECK POINT: Cover-slipping/minimizing bubbles

Mounting medium should be applied in a single, smooth motion, spreading the medium using the tip of the bottle; avoid touching the tissue itself. If a pap pen has been used, apply individual droplets of mounting medium just inside/within the pap pen border of each tissue section before cover-slipping. If bubbles form immediately following cover-slipping, let sit for a few minutes to see if bubbles will dissipate; if not, use the back side of a clean pipette tip (the larger, circular opening that faces you when you open the box) and press down evenly (perpendicular to the coverslip) and gently guide the bubbles away from the tissue in a single, even motion. While ideally you will not have any bubbles, some bubble formation may be unavoidable. The goal here is to try to guide the bubbles far enough outside/away from the tissue so that you can image the slides properly.

***NOTE:** If using mounting medium with DAPI, let sit at room for additional 5-10 minutes before attempting to move any bubbles—this is important to ensure that the nuclear stain is able to adequately penetrate the tissue before you press down on it.*

Additionally, this mounting medium is particularly sensitive to temperature---remove from storage at 4C and allow to come to RT prior to cover-slipping slides, and allow slides to sit/set at room temperature for at least 15-20 minutes before you return/store

them at 4C. DO NOT RUSH this, as the DAPI mounting medium may form excess bubbles if moved too quickly into 4C storage!

2. LABEL slide folder with Name, Date of stains, Tissue type/specs and list

primary/secondary antibodies used; proceed with imaging or store labelled slide folder at 4C indefinitely.

NOTE: *Slides must be transferred from slide folders into labelled slide boxes to save storage space/folders following imaging. This transfer should be done only after the mounting medium has set to avoid any slipping of the coverslip/leakage of the mounting medium and adherence of the slide to the corkboard in base in the slide box—give the slides at least one day at 4C before transferring.*

BSA (Albumin-Bovine- Biotech grade)

Amaresco Cat# 0332-25G; LOT# 3284C392 ; CAS# 9048-46-8

COVERSLIPS

- 1) VWR Cat# 16004-098; 1oz (24 X 50mm; #1)
- 2) VWR Cat# 16004-094; 1oz (22 X 22mm; #1)
- 3) (Older) ThermoScientific “Slip-Rite” Cat#152450; LOT# 022714-9)

DAPI MOUNTING MEDIUM (“Fluoroshield Mounting Medium w/ DAPI” - 20mL)

Abcam Cat# ab104139; LOT#GR3182624-4; Rec'd Nov '20

NORMAL GOAT SERUM

Abcam Cat #7481

TritonX-100

Acros- 100mL (98% for Mol bio)

Cat#327371000; LOT# A0333719

APPENDIX D:
SUPPLEMENTARY PROTOCOLS:
IMMUNOFLUORESCENCE PROTOCOL FOR FORMALIN-FIXED,
PARAFFIN-EMBEDDED TISSUE(S)
(Tucker Laboratory, UNE)

Tissue type: Formalin-Fixed, Paraffin-Embedded (FFPE; Human, embryonic/postnatal mouse)

Fixation: Formalin (Biobank tissue) or 4% Paraformaldehyde in 1X PBS (AG Tucker Lab)

Storage: Paraffin sections on glass slides (unbaked); stored in slide boxes at room temp

(Day 1 of 2)

I. PARAFFIN REMOVAL

1. Bake slides at 65C for 1 hour; turn on oven in HISTO CORE and put slides (in rack) in oven right away; with “heat up” time, 1 HR baking is actually more like 35-40 minutes at 65C (FYI)
2. Remove from oven (shut off oven!) and set benchtop for ~ 15-20 minutes to allow to cool/come to room temp
3. Proceed with de-paraffinization with Xylenes...
 - Xylene slide bins (100% ea/x3 bins---3X3minutes—USE TIMER!); pick up slides and tap off in between EACH Xylene immersion; gently lift EACH slide up to ensure that molten paraffin does not adhere it to the rack
 - Absolute Ethanol (100% EtOH; 2X2min)
 - 95% EtOH (1X1min)
 - 70% EtOH (1X1min)

4. Remove slides from 70% EtOH and immediately immerse (BACKWARDS FACING) in running de-I H₂O (or 1X PBS); DO NOT LET SLIDES DRY OUT HERE!!!

II. ANTIGEN RETRIEVAL

5. Use COBRE Histology & Imaging Core “Decloaking Chamber” (BioCare Medical); plug in the chamber and power on using the green () button on the front screen; press this button a couple times to initiate heating; screen is broken so you will not be able to adjust any of the settings; remove cover and place silver basket inside the pot. Use a graduated cylinder to measure out 500mL of de-I H₂O and pour into the pot.
6. Collect the 3 slide bins (charcoal with white interior); fill the outer two with 250mL of de-I H₂O; fill the center bin with Tris EDTA Buffer (pH9.0; stock 10mM; working 1mM); Listen for the first alarm (beep) from the machine, indicating the chamber is ready for you to insert slides
7. Submerge your slide rack (containing your paraffin-free slides) into the center bin containing Tris EDTA Buffer.
8. Secure the cover and make sure the lock is in place before walking away. it is automatically set to heat to 95C for 15 minutes once started, and will sound a beeping alarm once the temperature has been reached. Set a timer for 15 minutes (the machine will also automatically begin to cool down after 15 minutes but will continue to beep. Once the timer finishes, remove the cover lid and allow the steam to clear from the pot. Use caution lifting out the center tub containing your slides in buffer, IT WILL BE HOT!

9. Place entire center bin (containing your slides in Tris EDTA Buff) into a tub/bath/bin with running de-I H₂O for 15 minutes (**OPTIONAL STEP**- you can also take out this bin and let sit benchtop at RT for 10-15 minutes to allow for cool-down prior to submerging in de-I H₂O)
10. Remove slide rack from bin/Buffer solution and submerge slides directly in de-I H₂O running water bath; make sure that the slides are facing AWAY from turbulent water flow to minimize any possible disruption to the tissue; let sit in running water bath for 15 minutes.
11. Remove slides from water bath and immerse in new slide container with de-I H₂O or 1X PBS (at room temp—NOT cold!!!) and proceed with tissue permeabilization for IF.

III. PERMEABILIZATION (BLOCKING)

12. Prepare/thaw blocking buffer as indicated in AG Tucker Lab protocol (0.3% TritonX-100; 5% NGS/NDS in 1X PBS; frozen aliquots stored at -20C)
13. Remove slides from de-I H₂O/1XPBS one at a time and use a lint-free wipe to clear the edges/back of slides of excess moisture; apply PAP pen (shake well!) to draw a liberal border around each individual tissue section on the slide; let sit to dry ~2 minutes prior to applying blocking buffer; if tissue looks dry, use a micropipette to apply a SMALL droplet of 1X PBS to keep the tissue from drying out; DO NOT use excess liquid here! If you apply too much, it will spread to the lipid border you have just drawn and drag the lipid into/over the tissue itself...THIS IS BAD!)

14. Repeat one slide at a time until each slide has a lipid border and has been allotted an appropriate amount of time to set; you can set slides on staining tray but do not fill with liquid until after the pap borders have set!
15. Fill the base of the staining tray with de-I H₂O; you can also add in some paper towel strips to help retain moisture within the chamber
16. Apply (**THAWED!**) blocking buffer liberally to each tissue section of each slide; blocking buffer should ideally be at/slightly below room temp to avoid shocking the tissue too much! Cover chamber and incubate at room temperature for **30-45** minutes (*Absolutely* NO MORE THAN 1HR for cilia stains!)

CHECK POINT: Primary Ab HOST

If you plan to use a primary (or secondary) antibody of a host species other than rodent (mouse, rat, rabbit) or goat, you may need to block using additional serum specific for your target; the most common substitution in AG Tucker Lab is the secondary antibody/fluorophore Alexa647 donkey α (anti-) rabbit (stored at 1:2 @-20C); donkey serum is stored in 1.5mL (1:1/100%) aliquots at -20C; add directly to blocking buffer containing goat serum or make separate solution if designating for a single tissue section on a slide)

17. Prepare primary antibody solutions

IV. PRIMARY ANTIBODY APPLICATION & INCUBATION

18. Prepare/thaw antibody dilution buffer (aka “Ab diluent”) fresh or from frozen aliquot (use warm water bath to thaw and then let sit benchtop at RT for ~5-10 minutes)
19. Write out your experiment (including individual slides selected) in your lab notebook; calculate all dilution factors ahead-of-time, using Ab spec sheets for reference and/or previous experiment records (if troubleshooting a new Ab).

CHECK POINT: [stock]!

Most of the Tucker Lab antibodies are stored at -20 at 1:1 stock (in 50% glycerol), but some stocks/aliquots may be at 1:2 in 50% glycerol (e.g. acetylated alpha-tub, gamma-tubulin---both SIGMA/aliquoted) ...READ LABELS CAREFULLY! If you are unsure of the stock concentration, ASK Lindsey or Dr. Tucker, DO NOT GUESS (antibodies = \$\$\$\$\$\$!)!!!

20. Collect each of your primary antibody stocks (or aliquots) from either 4C or -20C and place in a benchtop cooler.

CHECK POINT: [Ab storage location]:

Storage location/temp and [stock] will vary by antibody—check with LAF and or refer to individual Ab spec sheet; if Ab stock contains 40-50% glycerol, it will be stored at -20C; if stock only contains sodium azide and no glycerol, it will be stored at 4C; if 50% glycerol has been ADDED to stock, it will be indicated on stock/aliquot vile AND lab spec sheet and will then be stored at -20C.

21. Always pipette Ab diluent FIRST---in designated volume into microcentrifuge tube; this way, if you make a mistake, you are not wasting precious antibody!

22. Add primary antibody(ies) one at a time into your working primary antibody master mix solution. USE FILTERED PIPETTE TIPS and DO NOT DOUBLE DIP (use a new tip every time you draw from the stock bottle to avoid contamination!)

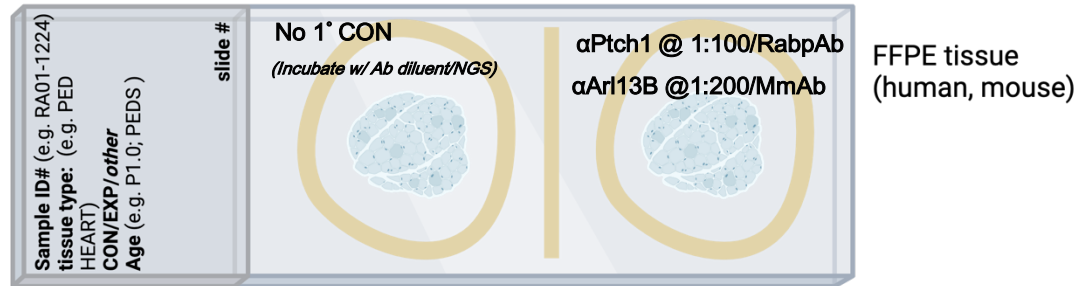
CHECKPOINT: Primary Ab HOST SPECIES

When using more than a single primary antibody for a given experiment, you may “co-stain” only with target antigens raised in different species and/or IgG isoforms. AG Tucker Lab has primary polyclonal (rabbit IgG) and primary monoclonal (rabbit IgG, rat IgG, mouse IgG1, mouse IgG2a, mouse IgG2b) antibody stocks. Depending on the experimental design, you may need an isotype-specific secondary antibody(fluorophore) of a specific color---this needs to be planned out ahead of time in your lab notebook!!!

23. Immediately return primary antibody stocks to original storage location (4C or -20C)—DO NOT LET SIT BENCHTOP for a period of time longer than is necessary for pipetting! Label EACH primary antibody master mix with contents, date and dilution; leftover primary antibody master mix solutions may be stored at 4C and used within 1 week of original date made.
24. Remove cover from slide staining chamber; aspirate or gently tap off blocking buffer solution from each slide and place back onto staining rack
25. USE A NEW, FILTERED, PIPETTE TIP to pipette primary antibody solution to each of your designated tissue sections.

CHECK POINT: Mapping your assigned targets

For co-stains, (new) Ab troubleshooting and more complicated/higher volume experiments, it can be helpful to draw out your experiment in your lab notebook with detailed labels/locations of tissue and corresponding antibody targets



26. Cover staining chamber and incubate overnight at 4C in the dark; make sure that slide chamber LIES FLAT in the refrigerator—clear a spot for the chamber before you carry it over to the fridge

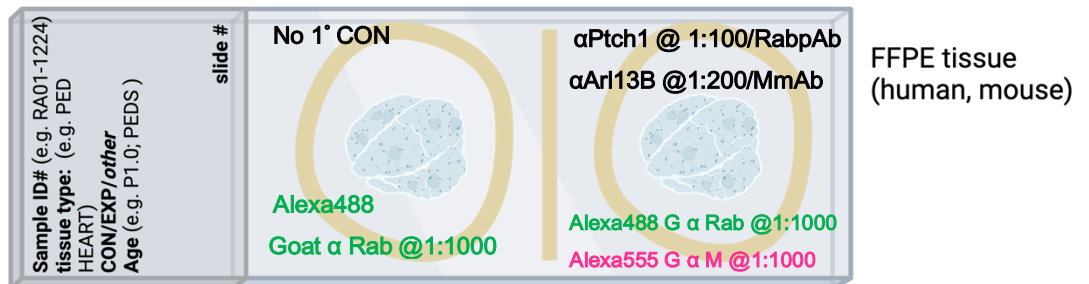
CHECKPOINT: Timeline

(OPTIONAL MODIFICATION) – Incubate in primary antibody solution at room temperature for one hour in humid chamber; NOTE- stains for primary cilia look best if done overnight @4C, but can be done at RT if need be.

27. This would be a good time to write out the remainder of your experiment(s) and calculate your dilutions for secondary antibodies so that you are prepared to start immediately the following day. OPTIONAL STEP- *you can prepare your secondary antibody master mix solutions ahead of time and store at 4C overnight; make sure to take them out along with your slides to allow them to warm slightly; leftovers may be stored @4C and used within a week.*

V. SECONDARY ANTIBODY APPLICATION & INCUBATION

28. Remove slide chamber from 4C/fridge and set benchtop for ~15-20 minutes to allow to reach room temperature; keep cover on chamber to maintain humidity; ALSO remove leftover Ab diluent (or thaw fresh) from 4C and allow to come to RT; SET a timer as a reminder!
29. Proceed with preparing secondary antibody master mix solutions while slides equilibrate; make sure to do this before you start the wash series to avoid disruptions
30. If you haven't already, write out the remainder of your experiment (for secondary antibodies, including individual slides selected) in your lab notebook; calculate all dilution factors ahead-of-time, using Ab spec sheets for reference and/or previous experiment records (if troubleshooting a new Ab). Most secondary antibodies in AG Tucker Lab are stored at 1:1 (100%) at 4C in a black storage box labelled "Secondary Ab Stocks." Select the stock secondary antibodies you need for your experiment(s) and place in a portable benchtop cooler to keep cool while you are pipetting.



CHECK POINT: Mapping your assigned targets

Document your secondary antibody master mix recipes and/or add a record of your “slide map” which can be used when you go (back) to image your slides.

31. Once you have made up your secondary antibody master mix solutions, return stocks to 4C/box (or -20 if applicable) and keep master mixes in the benchtop cooler while you proceed with washes.

32. Once the timer goes off (indicating the slides have equilibrated), remove the cover to the slide chamber and gently tap off (or aspirate) the primary antibody solution from each slide and place back into slide chamber (one at a time).

CHECK POINT: Avoid contamination with multiple primaries!

If you have multiple experiments/targets on a single slide, aspiration of the solution is preferred to avoid possible contamination of alternate tissue sections that can occur when you tap off liquid; **MAKE SURE TO CHANGE YOUR PIPETTE/TIP** for each tissue section for a given target/set of targets.

33. **WASH (3 X 5min) with 1X PBS:** Use disposable transfer pipette or regular pipette to apply 1X PBS (or other wash buffer) to each tissue section; set timer for 3 min let sit at room temp for the remainder of the washes. Aspirate or tap off 1X PBS and repeat with fresh 1X PBS (each time!) for a total of 3 washes.

34. After you aspirate/tap off the final 1X PBS wash, place all slides back in chamber. Apply secondary antibody master mix solutions to corresponding tissue sections; follow and/or update your slide map if changes are needed. If possible, perform this step with the lights off/dimmed to minimize any photobleaching.

35. Place cover on humid chamber and let incubate at room temperature for 45 minutes IN THE DARK (up to 1 hour). Use a timer!

CHECK POINT: Minimize photobleaching!

If you are using a dark staining chamber already, disregard and proceed with incubation. If you are NOT already using a dark slide chamber (i.e. BLACKED OUT!), make sure the chamber (or cover) is covered with a dark/opaque cloth or aluminum foil to minimize light exposure during incubation with secondary fluorophores!

36. Aspirate or tap off the secondary antibody solution and place slides back in chamber.

37. **WASH (5 X 5min) with 1X PBS:** Use disposable transfer pipette or regular pipette to apply 1X PBS (or other wash buffer) to each tissue section; set timer for **5 min** let sit at room temp for the remainder of the washes. Aspirate or tap off 1X PBS and repeat with fresh 1X PBS (each time!) for a **total of 5 washes**.

NOTE- *this step is particularly important to minimize any residues or lingering fluorophore proteins that may remain on/within the tissue. If absolutely necessary, you can minimize to 3x5min washes, but it is BEST to complete all 5 washes!!!*

38. For the final wash, leave slides sitting in the chamber with the final wash solution. Remove one slide at a time to aspire/tap off PBS followed by (BRIEFLY) dipping the slide into de-I H₂O in a coplin jar (or equivalent immersion chamber). Tap off excess moisture and wipe back/edges of slide with lint-free wipe. Avoid touching/smudging/spreading the lipid borders when you are wiping away excess water!

NOTE: *if excess fluid accumulates within the lipid border/around the tissue, angle the slide downwards and use a dry corner of the lint-free wipe to carefully draw up the excess liquid away from the tissue section*

V-part II (OPTIONAL AUTOFLUORESCENCE BLOCKING)

39. For tissue that is particularly (and inherently) auto-fluorescent (like human/mouse lung, heart, muscle...) you can perform an optional autofluorescence blocking step prior to cover-slipping.
40. Use clean transfer pipette to apply 1-2 droplets of 0.1% Typogen Black solution in 70% EtOH (filter before each use!); let sit at room temp for 5 minutes, then aspirate
41. Perform additional washing step: WASH 2X2min with 1X PBS and proceed with de-I H₂O dip/cover-slipping

VI. SLIDE MOUNTING/COVER SLIPPING

42. Place slide flat on benchtop and apply mounting medium (with DAPI); coverslip and place slide in a cardboard slide folder to let set. Close the folder to keep the slide in dark while you continue mounting/cover-slipping the remainder of your slides. If imaging immediately, allow to slides to sit and set at room temperature for about 30 minutes

CHECK POINT: Cover-slipping/minimizing bubbles

Mounting medium should be applied in a single, smooth motion, spreading the medium using the tip of the bottle; avoid touching the tissue itself. If a pap pen has been used, apply individual droplets of mounting medium just inside/within the pap pen border of each tissue section before cover-slipping. If bubbles form

immediately following cover-slipping, let sit for a few minutes to see if bubbles will dissipate; if not, use the back side of a clean pipette tip (the larger, circular opening that faces you when you open the box) and press down evenly (perpendicular to the coverslip) and gently guide the bubbles away from the tissue in a single, even motion. While ideally you will not have any bubbles, some bubble formation may be unavoidable. The goal here is to try to guide the bubbles far enough outside/away from the tissue so that you can image the slides properly.

NOTE: *If using mounting medium with DAPI, let sit at room for additional 5-10 minutes before attempting to move any bubbles—this is important to ensure that the nuclear stain is able to adequately penetrate the tissue before you press down on it. Additionally, this mounting medium is particularly sensitive to temperature---remove from storage at 4C and allow to come to RT prior to cover-slipping slides and make sure that slides are allowed to sit/set at room temperature for at least 15-20 minutes before you return/store them at 4C. DO NOT RUSH this, as the DAPI mounting medium may form excess bubbles if moved too quickly into 4C storage!*

43. LABEL slide folder with Name, Date of stains, Tissue type/specs and list primary/secondary antibodies used; proceed with imaging or store labelled slide folder at 4C indefinitely.

NOTE: *Slides can (...and eventually SHOULD) be transferred from slide folders into labelled slide boxes to save storage space/folders following imaging. This transfer should be done only after the mounting medium has set to avoid any slipping of the coverslip/leakage of the mounting medium and adherence of the*

slide to the corkboard in base in the slide box—give the slides at least one day at 4C before transferring.

ANTIBODY DILUENT (****see IF/frozen tissue protocol for recipe breakdowns****)

1% BSA

0.3% TritonX-100

1X PBS

ANTIGEN RETRIEVAL BUFFER: Tris EDTA, pH 9.0 (DEFAULT)

Sakara/Genemed Ref#10-0037 (purchased through ThermoFisher Scientific)

20X stock (100mL concentrate; stored at 4C); LOT#00190131

BLOCKING BUFFER (****see IF/frozen tissue protocol for recipe breakdowns****)

5% Normal Goat Serum (and/or Normal Donkey Serum, as needed)

0.3% TritonX-100

1X PBS

BSA (Albumin-Bovine- Biotech grade)

Amaresco Cat# 0332-25G; LOT# 3284C392 ; CAS# 9048-46-8

COVERSLIPS

4) VWR Cat# 16004-098; 1oz (24 X 50mm; #1)

5) VWR Cat# 16004-094; 1oz (22 X 22mm; #1)

6) (Older) ThermoScientific “Slip-Rite” Cat#152450; LOT# 022714-9)

DAPI MOUNTING MEDIUM (*“Fluoroshield Mounting Medium w/ DAPI” - 20mL*)

Abcam Cat# ab104139; LOT#GR3182624-4; Rec'd Nov '20

NORMAL GOAT SERUM

Abcam Cat #7481

TritonX-100

Acros- 100mL (98% for Mol bio)

Cat#327371000; LOT# A0333719

TYPOGEN BLACK STOCK

Aldrich Cat#4197-25-5; LOT#TR07014HN; exp Sept '98; #19.966-4 (25g)

(formerly known as "Sudan Black")

0.1% in 70% Ethanol solution (deH₂O); store at RT and filter for EACH use to avoid chunks!

APPENDIX E:
SUPPLEMENTARY PROTOCOLS:
Trans-Cardiac Perfusion Protocol
Mouse
Materials & Set-up

Protocol Overview:

1. Apparatus Setup
2. Preparation
3. Perfusion Protocol
4. Tissue Collection
5. Dissection Tools
6. Tissue Fixation & Storage

Materials:

- **BAXTER ClearLink Solution Set**

BHL2C8401H; MedVet

76" (1.9 m); \$7.50/ea

- **BAXTER Interlink T-Connector Extension Set**

2N3326;

Male luer slip adaptor

15.3cm (6") in length

T Housing volume (0.11 ml)

Total volume (0.30 ml); \$1.50/ea

- **BSTEAN Dispensing Needle**

25 gauge; 1/2 " **blunt** tip

Outer diameter (0.51 mm)

Inner diam. (0.26 mm)

Amazon.com; \$12.89/box 50

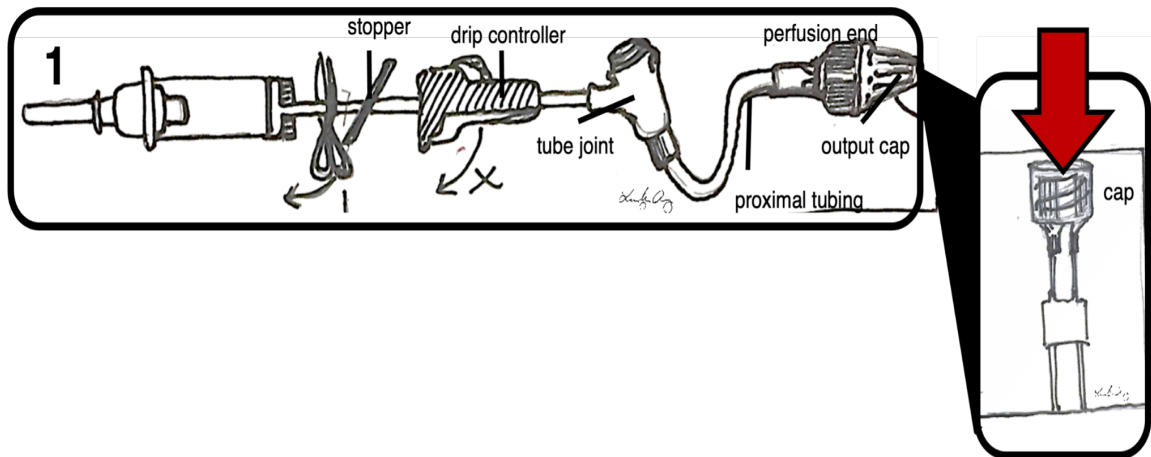


Figure E1. Perfusion Apparatus Setup

BAXTER ClearLink Solution Set:

1. Remove the stopper and drip controller from the tubing
2. Cut diagonally across the far end of the tubing (opposite from the perfusion end) to match desired length of perfusion tubing
3. Remove/unscrew the output cap to reveal the female input location

BAXTER Interlink T-Connector Extension Set

1. Remove the stopper from tubing; remove/unscrew the cap (male) from the syringe end (female)

2. Make a diagonal cut through the central tubing, approximately 2 inches from the syringe end.

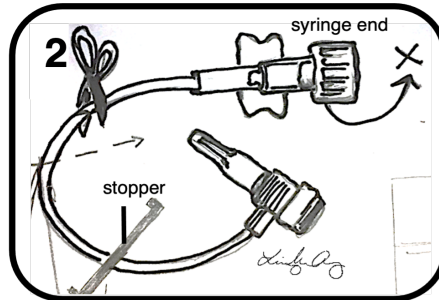


Figure E2. Baxter Interlink T-Connector Extension Set

Connecting *BAXTER ClearLink* Solution Set (perfusion end) to *BAXTER Interlink T-Connector* Extension Set (syringe end)

1. Insert the tubing from the *BAXTER ClearLink* into the larger tubing end of the *BAXTER Interlink T-Connector*; you will need to REALLY wiggle the larger tubing so that it surrounds the lip of the plastic tip of the syringe end (NOT JUST AROUND THE TUBING!)
2. Make a diagonal cut through the central tubing, approximately 2 inches from the syringe end.

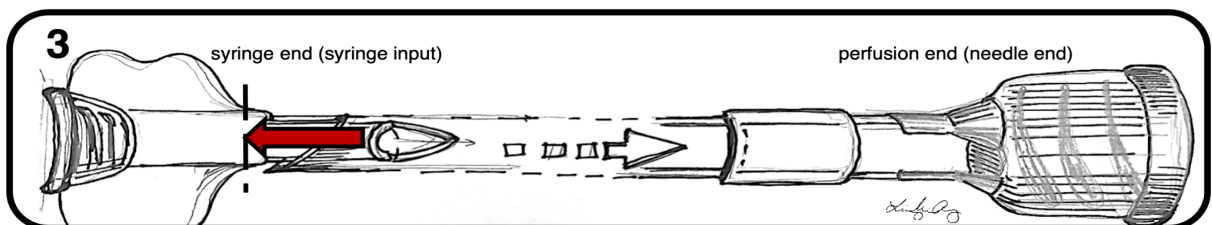


Figure E3. Connecting T-Connector to Perfusion Apparatus

Preparation:

Overview of System Set-Up

Connect the Perfusion tubing to desired needle (Figure E4) and prepare perfusion station setup as depicted in Figure E5.

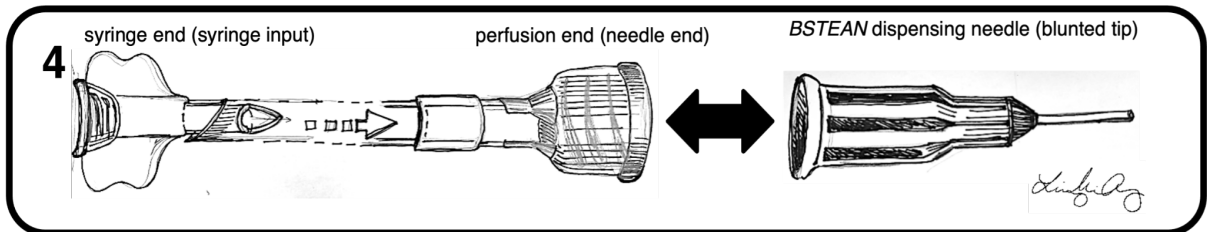


Figure E4. Overview of System Set-Up

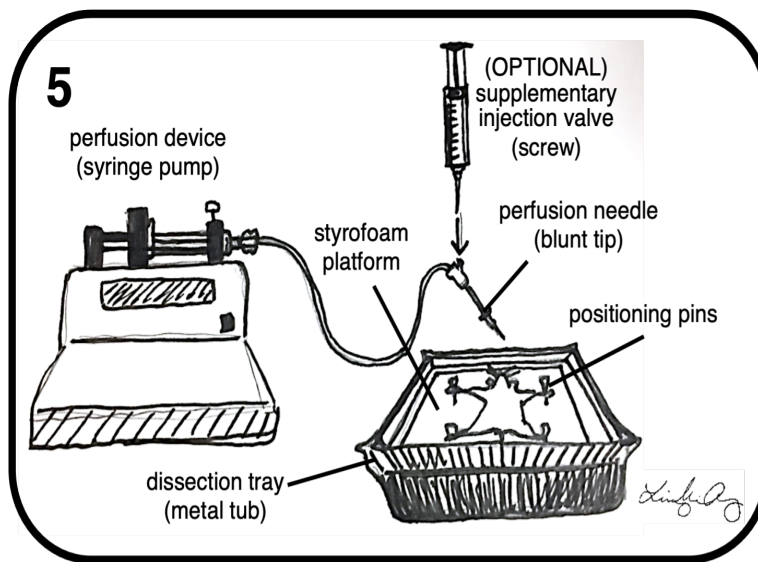


Figure E5. Complete set-up for trans-cardial perfusion (in mice).

1. Locate and fill the x3 60-cc syringes, according to their corresponding label: 1) *Amaresco*; 2) *sterile water*; 3) PBS.
2. After affixing the 1) *sterile water*; 2) PBS syringe to the perfusion device and securing perfusion tubing, flush hose with 1) *sterile water*; followed by

2) (1X) PBS, ensuring bubbles have been eliminated prior to perfusing the animal.

NOTE: *Amaresco is most commonly used as a fixative for perfusion & fixation of brain tissue and is desirable because it does not contain formalin or glutaraldehyde ingredients, known to exacerbate brain auto-fluorescence. Other fixative solutions used in the Townsend Lab include: 2%, 4% Paraformaldehyde (PFA), 10% Formalin-Buffered Solution (for adipose tissue), 2% and 4% glutaraldehyde solution (for SEM/TEM electron microscopy).*

Euthanasia:

1. (See *Ketamine solution protocol for appropriate dosing/drug preparation*)
2. Confirm the mouse is unresponsive by using the toe pinch test on hind limb feet.
3. Spray/wet fur with 70% ethanol solution. Pin the mouse to the styrofoam dissection tray by inserting a green-top positioning pin in the center of each hand/foot.

Perfusion Protocol:

Expose Pericardial Cavity:

1. Using forceps and sharp dissection scissors, make a central incision just superior to the umbilicus; the incision should span across the thorax of the mouse just below the ribcage. (Figure E6, a-b)

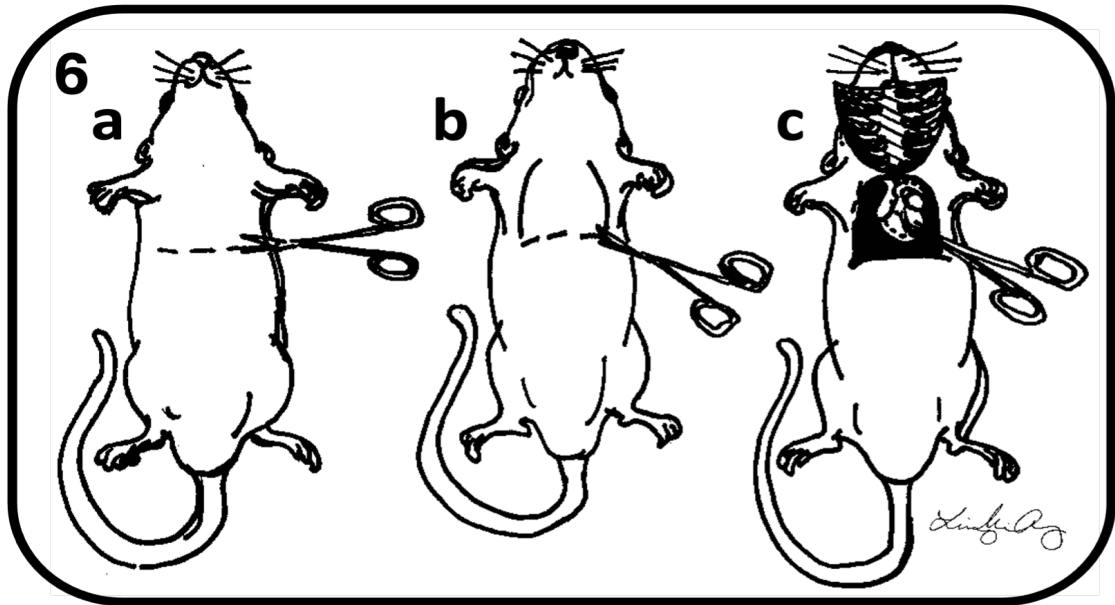


Figure E6. Illustrative schema depicting desired mouse body positioning (supine) and approximate anatomical location for surgical incisions.

2. After penetrating the subcutaneous layer of (epi-)dermis, use dissections tools to cut through and into the peritoneum/peritoneal cavity, resecting back the liver to identify the inferior to the diaphragm (membrane-like tissue that will be pink with mucosal lining); Enter into the pericardial cavity

an expand incision bilaterally (on both sides) to reveal the heart. (Figure E6, b-c) **Jugular Vein Incision (blood outlet):**

1. Cut the mouse's R (**YOUR L-side; Figure E7**) jugular vein and trim the skin in the surrounding throat/neck area. (Figure E7)

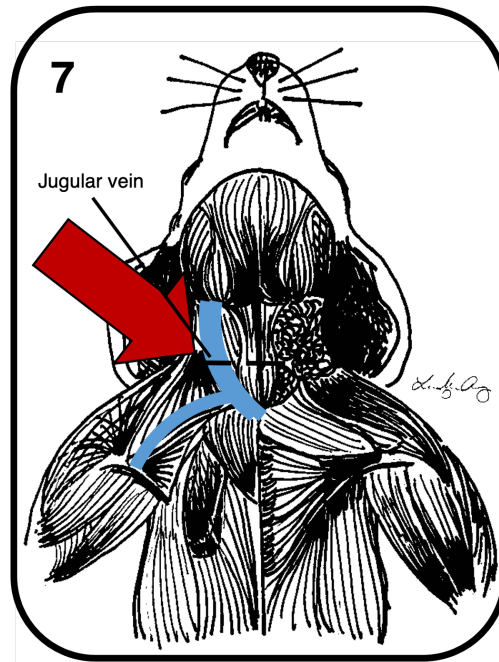


Figure E7. Approximate location of jugular vein (right) in adult mouse.

2. Once perfusion begins, this outlet will allow the blood to freely exit the circulation and drain into the dissection tray (and NOT into the open thoracic cavity).

Right Atrial Incision (alternate Blood Outlet):

1. Using the iris scissors, carefully clip a small opening on the lateral (outside edge) of the right atrium. This will cause blood flow to directly drain into the pericardial cavity

Cardiac Puncture (fixative point of entry)

1. Use forceps OR fingertips to insert the blunted perfusion needle tip into the left ventricle of the heart. Some force may be required to puncture through the thick, muscular myocardial wall (Figure E8).

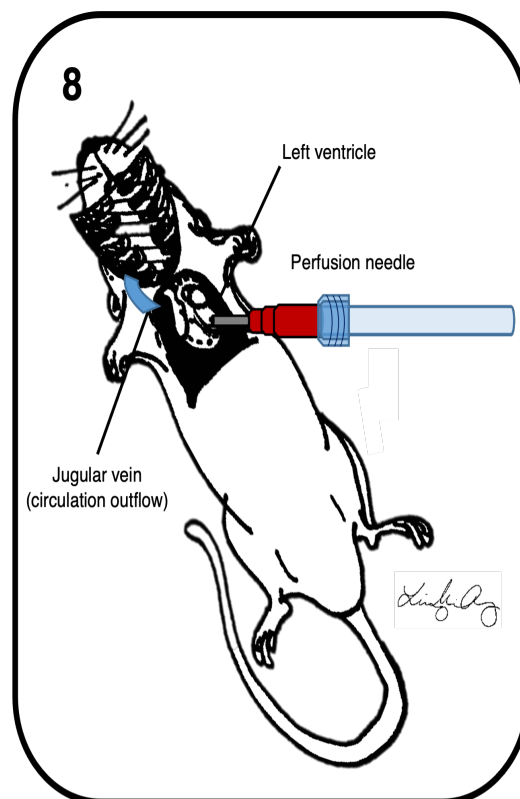


Figure E8. Cardiac Puncture for Fixative Point of Entry.

2. Once the needle tip is properly positioned, the needle can be held by hand
OR secured to the ventricle using an alligator clamp.

NOTES:

Once the tip is in place and fluid perfusion has begun, the perfusion needle MAY NOT be removed and re-inserted into the heart ventricle! A hemostat (plastic is preferable) may be used in the event that an alligator clamp is not available but MUST BE USED WITH CAUTION TO AVOID DAMAGING OR TEARING THE HEART VENTRICLE.

FLUID PERFUSION

1. Once the needle is securely in place, turn on the syringe pump to push the PBS fluid through the heart and out of the right, jugular opening. Allow to run for approx. 5 min or until ~15 mL of fluid has circulated through. Turn OFF the syringe pump BUT DO NOT REMOVE THE PERFUSION NEEDLE!
2. Remove PBS syringe and attach Amaresco (or alt. fixative) syringe to perfusion tubing. Repeat step (1) for fixative solution, allowing to run for ~5 min or until approx. 15 mL of fluid has passed through.

NOTES:

As the blood continues to exit systemic circulation, tissues that begin to receive increasing amounts PBS/fixative and decreasing quantities of blood (O₂) will begin to “blanch,” or change palor.

Additionally, some tissues may also distend (expand) with increasing fluid volume; if this happens, you may see bubbling and excess fluid accumulation in the oral (mouth) and nasal cavities of the mouse. IF this happens, you can try to decrease the resistance to flow pressure to minimize fluid accumulation in the trachea, indicating poor perfusion to the brain/other tissues of interest.

You may notice muscle twitching and increasing muscle stiffness, most evident in auxillary limbs. This is a side effect of the fixative and will correspond to the increasing concentration of fixative used

Tissue Collection:

ADIPOSE TISSUE DEPOTS

Collect all depots following PBS infusion (FIGURE 9). Selected tissues should be collected bilaterally (*on both sides*) unless otherwise specified; bilateral samples should be labeled to indicate laterality of origin (i.e. right/left) and stored (fixed or flash frozen) according to their respective destinations.

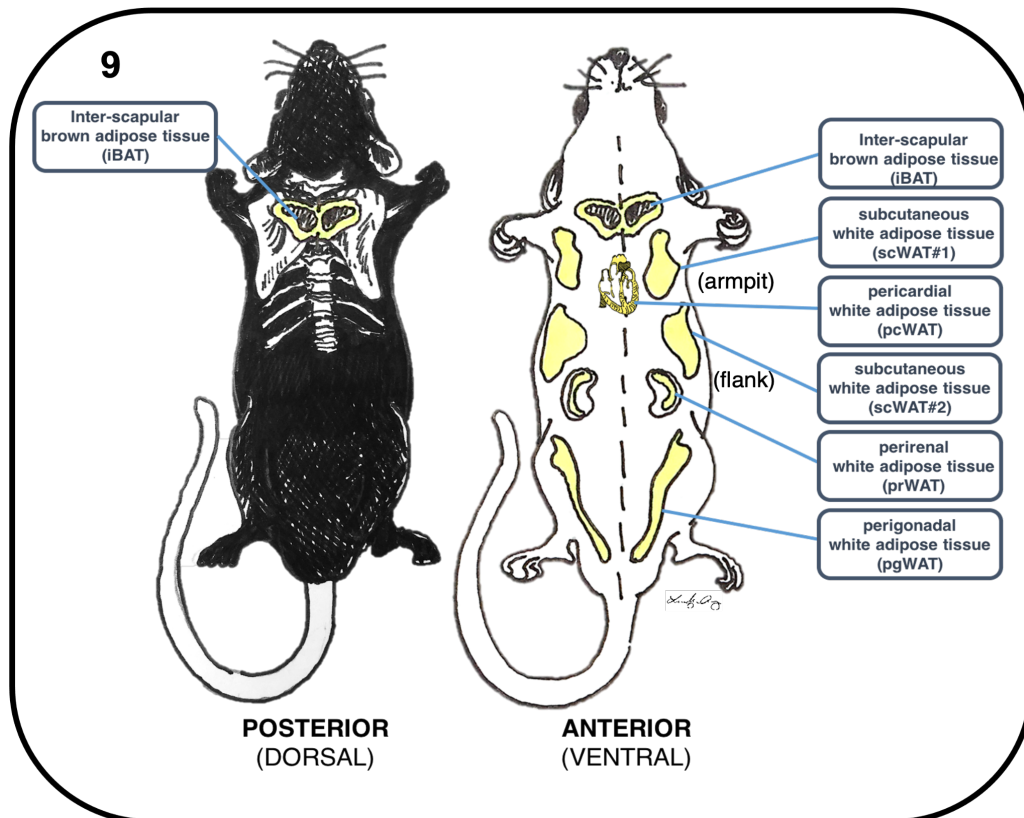


Figure E9. Overview and Approximate Locations of Adipose Collection Sites in the Adult Mouse.

NOTE: ALL ADIPOSE DEPOTS MUST BE COLLECTED PRIOR TO PERFUSION WITH FIXATIVE (Amaresco, PFA, Formalin, etc)!

Tissue Collection: BRAIN*

*See 'Tissue Fixation & Storage' for detailed procedures...

1. Use surgical scissors to decapitate the euthanized mouse, using one smooth cut from BEHIND both mouse ears (Figure E10).

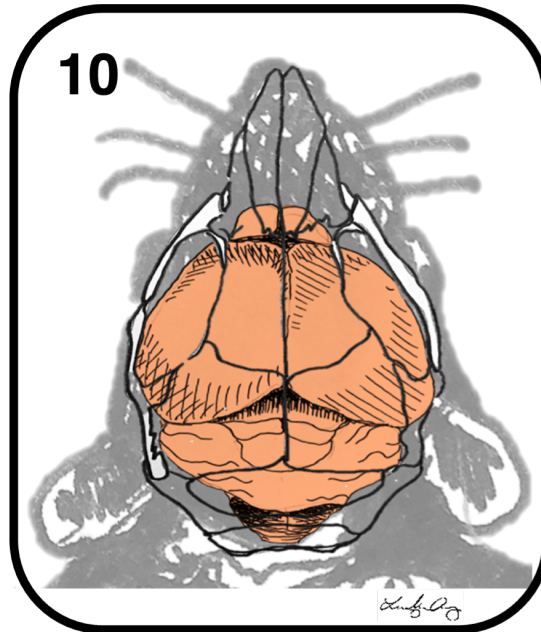


Figure E10. Illustrative Approximation of mouse brain (including olfactory bulb) with the skull when the mouse is positioned in the prone position. NOTE* Brain tissue must be collected *FOLLOWING* perfusion. Mouse body may be repositioned in the prone position for brain tissue collection following completion of perfusion excretion.

2. Use scissors to make an additional incision between the ears of the decapitated head and pull the skin up, over and behind the eyes to expose the skull. Some additional small incisions may be required

through soft and connective tissues in order to free the skin from the skull.

3. The first incision to excise the top of the skull cap should start at the posterior midline of the skull—or the most caudal part of the parietal bone and extending towards the area just above the ears in the temporal (side) region of the skull (Figure E11).

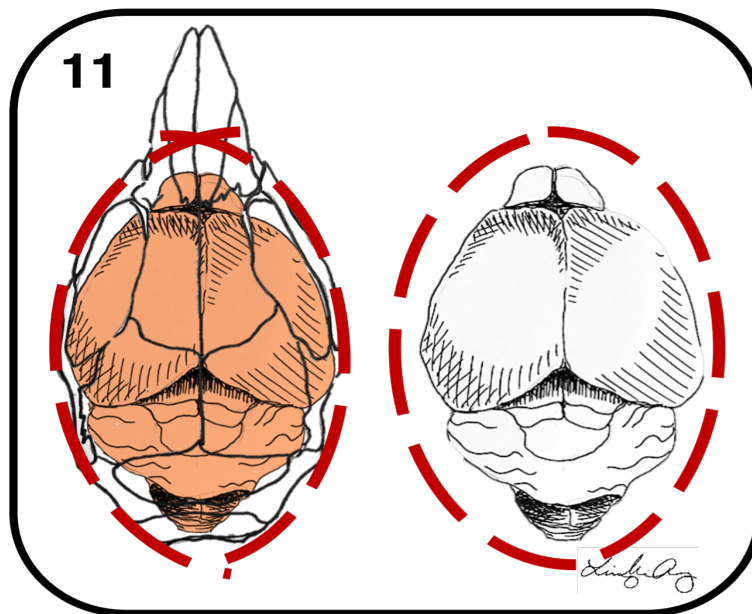


Figure E11. Indication and approximate location of incision points for the excision and dissection of mouse brain tissue (olfactory intact).

CAUTION: BE SURE NOT TO CUT THROUGH THE BRAIN TISSUE!!

If using curved scissors, aim the upwards part of the curve AWAY from the brain and towards the internal edge of the skull.

4. Repeat this cut on both the (R) and (L) sides of the skull, aiming for a cut in one smooth motion towards the direction of the olfactory bulb
5. (Foremost part of the brain located within the deep nasal region of the snout. One final cut may be necessary to join your lateral cuts completely (Figure E11).
6. Once you have determined that the circumference of the skull has been cut, begin at the occipital region (The end towards the snout) and CAREFULLY begin lifting away the skull cap by gradually guiding the brain tissue away from the skull bone. If your bone cuts are performed correctly, the skull cap should EASILY be flipped up and off, exposing the brain tissue (Figure E11).
7. Once the skull cap has been removed, repeat the tissue guiding motion to lift the brain up, back and off of the base of the skull and directly into the paraffin cassette. If all goes smoothly, the olfactory bulb will remain intact in addition to the hindbrain and brain stem.

BLOOD (serum & plasma)

1. Extract blood via cardiac puncture; this may be performed directly by opening up and exposing the pericardial cavity behind the rib cage OR indirectly by inserting the needle tip of a syringe through the upper abdomen, aiming for the apex of the heart and slightly towards the left side of the heart (left ventricle; Figure E12).

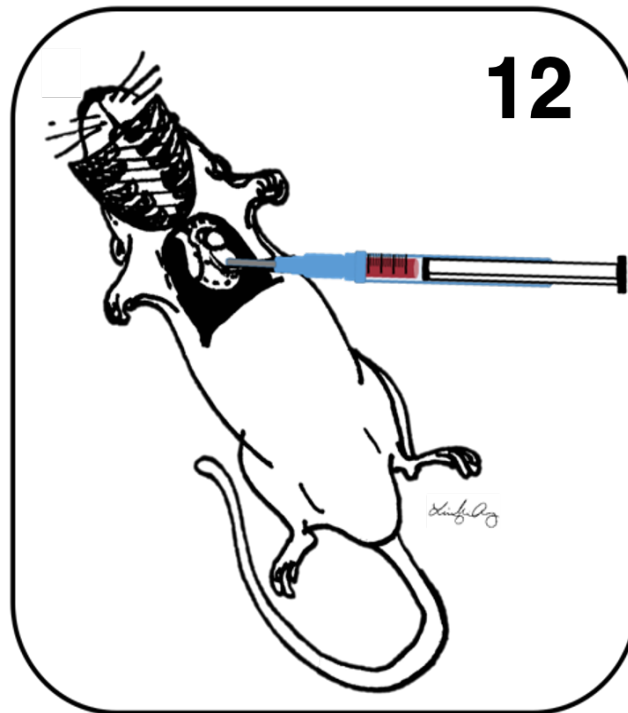


Figure E12. Approximate location for cardiac puncture to extract blood tissue collection. NOTE:* Blood collection must take place *PRIOR TO* injection of fixative into the perfusion/circulation unit.

2. Pull back on the syringe to extract the blood. If your needle is placed correctly inside the left ventricle, blood should FREELY pump into your syringe with very little effort. If pulling back on the syringe yields resistance and/or very little blood, you can slightly shift the angle of the needle, push forward or pull backward to find 'the sweet spot.' Assuming no punctures are made to the ventricle and your needle is correctly positioned, cardiac puncture can yield between 5 and 9ML of arterial blood, which will appear dark red in color (reflective of a highly oxygenated status).
3. Following blood extraction, carefully screw off the needle tip to the syringe and place in the appropriate sharps disposal container.
4. Immediately expel the blood from the syringe into a 1.7mL Eppendorf tube to prevent excess clotting of the blood inside the syringe.
5. Once all blood samples have been acquired, centrifuge as soon as possible, according to the time and speed specifications labeled/located immediately above the mini-centrifuge.

SKELETAL MUSCLE (HINDLIMB) for INTRA-MUSCULAR ADIPOSE

1. Carefully amputate the hind limb opposite to the limb that has received the anesthetic injection. This is usually the Mouse's LEFT hind-limb if the mouse is lying prone (on their stomach). Identify concrete anatomical landmarks prior to dissecting limb from body. This is best achieved by extending the limb away from the body and cutting perpendicular to the femur as close to the pelvis as possible, WITHOUT cutting through the groin/genitalia.
2. Once the limb has been separated from the body, carefully remove the excess skin and adipose surrounding the muscular structure of the limb. Keep the foot/ankle attached until after the femur/tibia have been removed (Figure E13).

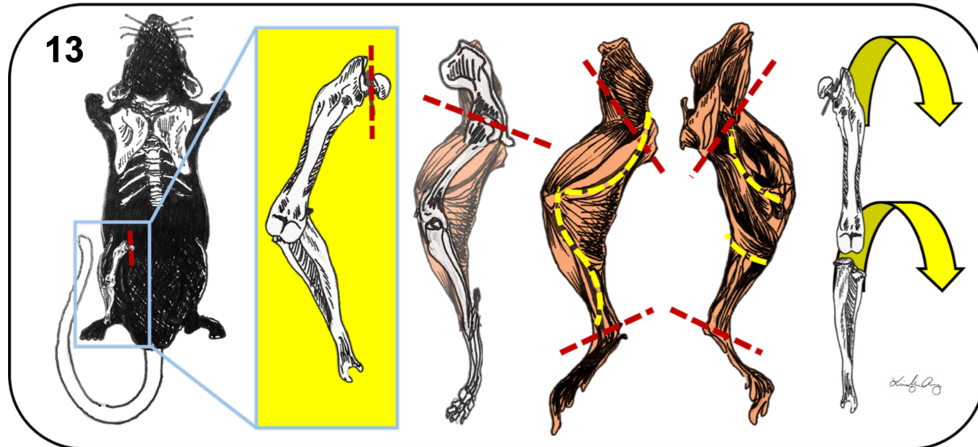


Figure E13. Anatomical approximation of location and incision orientation for the collection of perfused, skeletal muscle tissue extraction from the hindlimb of the adult mouse.

3. To 'de-bone' the leg, identify the edge of the lateral leg muscles and gently pull these back to cut carefully through the fascia (thin layer of connective tissue) until you reach/see the femur. NEVER cut THROUGH the muscle. Rather, pull away muscle bellies to expose the bone and cut only when necessary.

4. During the SAC and while you are tending to individual legs, remaining amputated hind limbs can be placed in 1X PBS in a container over ice. *MAKE SURE that each limb is correctly labeled with appropriate mouse ID; limbs can be stored in a 50mL Falcon tube which can be re-used for storage in fixation medium.*

5. Fixe for 24-48 hours in fixative of choice. Remove from fixative and section transversely into x3 sections: 1) FEMORAL; 2) POPLITEAL (knee); and 3) TIBIAL. Be sure to note on histology transfer sheet how to orient these samples! (Figure E14).

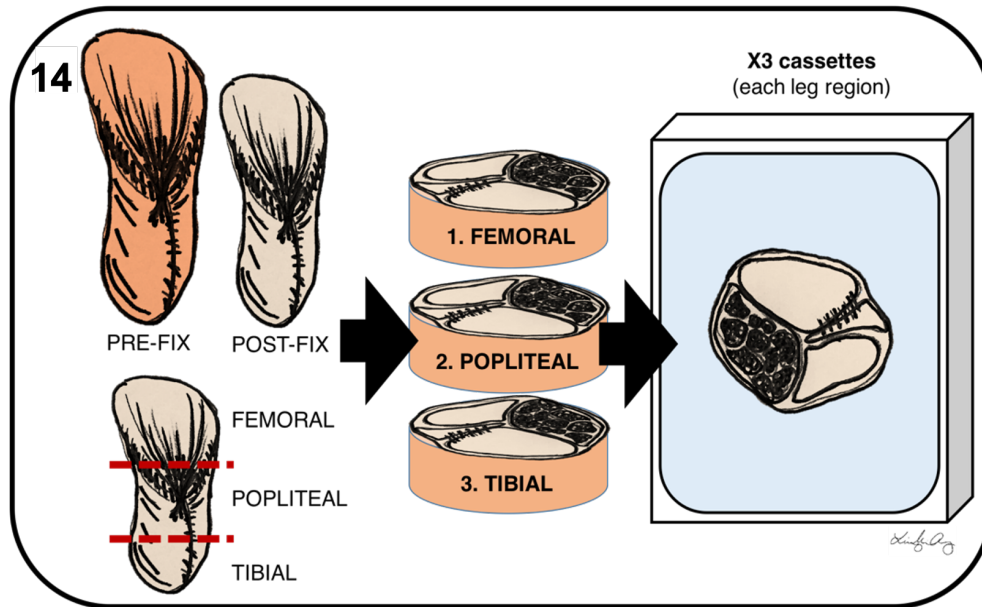


Figure E14. Overview of post-excision mouse hindlimb skeletal muscle preparation and orientation for embedding in paraffin.

Liver (Lobe or whole organ)

1. Liver tissue(s) can be extracted as either whole organ or as individual lobe(s). (Figure E15)

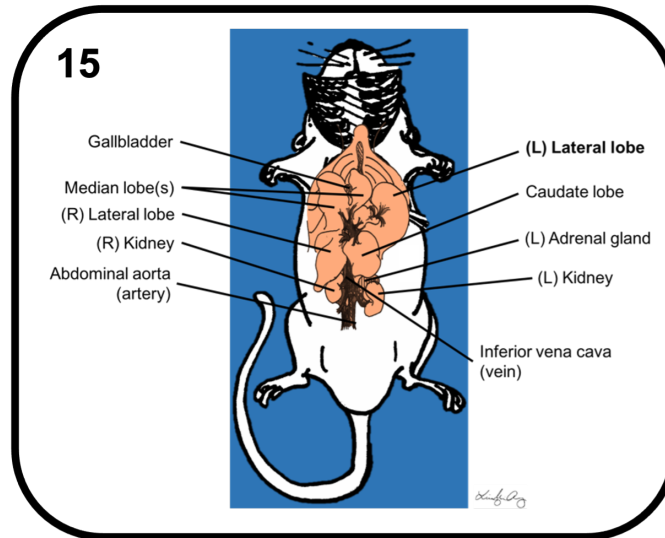


Figure E15. Anatomy and approximate location of tissues of interest located within the peritoneal cavity of the adult mouse.

OTHER TISSUES RELEVANT FOR TISSUE COLLECTION/TISSUE BANKING:

Pancreas

Heart

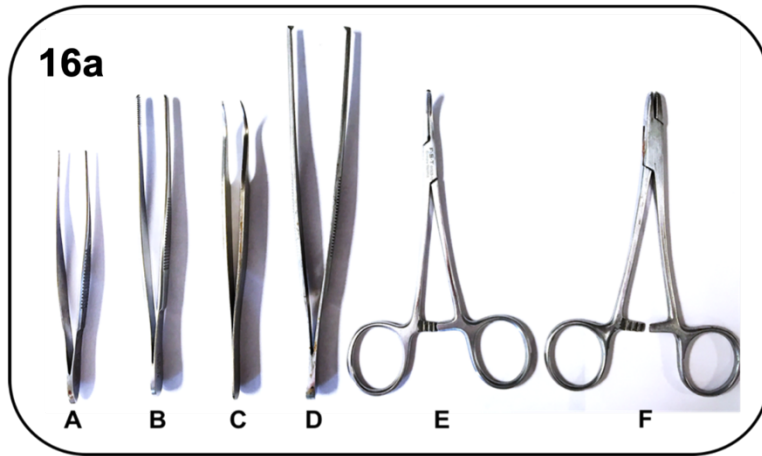
Thymus

Gastrointestinal (GI) tract

Lung (whole organ or lobe(s); x4 lobes in mouse)

Other.... (project dependent)

Dissection Tools



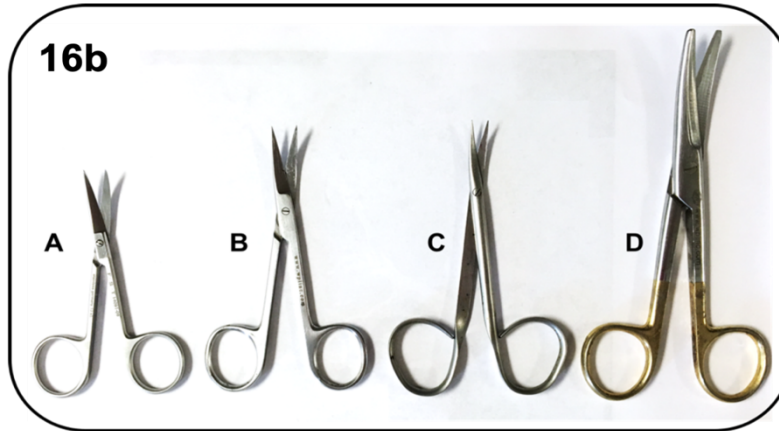
Fine forceps

Forceps

Micro-forceps (curved)

Tissue/toothed (pick-up) forceps

Hemostat forceps
(curved or straight)

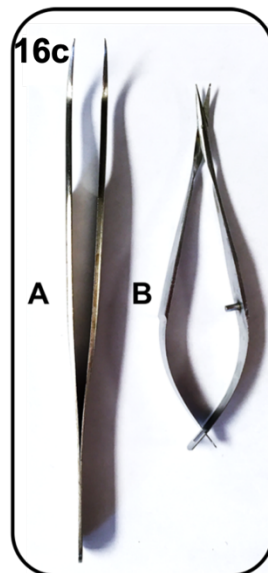


A. Iris scissors (straight)

A. Iris scissors (curved)

A. Iris scissors (curved)
a. BRAIN ONLY!!!

A. Surgical ('Mayo's') scissors:
a. Decapitation
b. Hind limb amputation



Micro-forceps (curved)

Iris scissors (micro)

Table E1. Tissue Fixation and Storage:

Tissue	Fixative	Fixation Duration	Additional Post-Fix (If applicable...)	Storage and transfer Medium
Brains (Perfused, for histology)	Amaresco (RESUSE)	24-48 hours	N/A	1X PBS
Brains (Perfused with 4% glutaraldehyde; <i>for EM ONLY!!!</i>)	2-4% Glutaraldehyde <u>MAKE FRESH</u>	48 hours	Cacodylic Buffer (48 hours)	1X PBS <i>(or can remain in <u>labeled</u> Cacodylic Buffer)</i>
Adipose depots (All)	10% Buffered Formalin Solution (RE-USE)	24-48 hours	N/A	1X PBS
Organs (All*) <i>*Unless otherwise specified</i>	10% Buffered Formalin Solution (RE-USE)	24-48 hours	N/A	1X PBS
Skeletal Muscle (Perfused; for histology)	4% PFA Amaresco <u>OR</u> 10% Formalin (RE-USE all but PFA)	24-48 hours	N/A	1X PBS* <i>(*If doing immunostaining, add 0.1% NaN₃/sodium azide to PBS)</i>

APPENDIX F:

SUPPLEMENTARY METHODS:

Primary Antibody Validation for Immunofluorescence Analysis

All primary antibodies not previously used in the Tucker laboratory underwent a series of vigorous troubleshooting and validation experiments prior to being used for data collection in control and mutant/experimental tissues:

1. WORKING CONCENTRATION/ ANTIBODY SPECIFICITY

Preliminary immunofluorescence was performed with each antibody using a series of dilution factors representative of high, middle and lower concentrations based within the range suggested by the antibody manufacturer. For example, if the manufacturer suggested a working dilution range of 1:100 up to 1:500, the antibody was trialed at working dilutions of 1:100, 1:200, and 1:500. One glass slide containing ~3 frozen tissue sections/slide was selected for each experimental primary antibody concentration. The tissue section closest to the left side (and label) of the slide was consistently labeled and used as a “No primary control (No 1° CON),” reflective of the fact that that individual tissue sample was not incubated with any primary antibody, only with the primary antibody diluent, containing 0.3% Triton X-100 and 1% BSA in 1X PBS (pH 7.4). Every step of IF staining protocol was observed as detailed in Appendix B, including identical overnight incubations at 4°C in a dark. Secondary fluorophores were selected according to the antigen species of the primary antibody

undergoing validation and were used at working concentration (1:1000) identical for the No 1° CON, 1:100, 1:200 and 1:500 dilution conditions. All tissues were mounted with mount medium containing DAPI (Abcam Fluormount), a nuclear stain. Each section was imaged using epifluorescence microscopy (Keyence Inc.), where all imaging/collection parameters were kept consistent across tissue sections and between individual slides. Raw data imaging files were reviewed by Dr. Tucker, Lindsey Fitzsimons and Peter Caradonna, the Lab Manager and expert microscopist and lab manager of the COBRE Histology & Imaging Core at the University of New England, Biddeford Campus (Maine, USA) to evaluate antibody specificity, relative signal to noise ratios, and if further troubleshooting would be required to determine a more optimal working concentration.

2. ANTIBODY SPECIFICITY & TISSUE SPECIFICITY

Given that the biological and mechanistic focus of the K.L. Tucker Laboratory at UNE is the primary cilium and its role in murine embryonic (heart) development, validation of primary antibodies designed for specificity against the cilium itself of direct, molecular targets of the cilium (i.e Hh signaling components Shh, Ptch1, Gli1...etc.), we require that part of the validation for these primary antibodies includes testing using embryonic mouse tissue and relevant positive and negative control tissue contained therein. Additionally, and if possible, we prefer to test cilia and Hh target primary antibodies in *cbbs* mutant embryos (*Ift88 hypomorph*) along with their respective littermate controls that are wildtype for *cbbs* allele. The Tucker laboratory has published using this exact mouse model

to demonstrate that near-global loss of primary cilia in the developing mouse embryos results in a widespread reduction and/or loss of Hh signaling throughout the embryo (Marc A. Willaredt et al., 2008; Marc August Willaredt et al., 2012) [Willaredt 2012, Willaredt 2008]. Of relevance for troubleshooting/validating primary cilia and Hh target antibodies, this embryonic tissue allows for an effective and accurate manipulation of phenotype/tissue environment to critically evaluate the specificity of the primary antibodies undergoing validation. In other words, tissue sections from the *cbbs* MUT should not reveal the presence of primary cilia in any abundance, and should indicate signal specificity reflective of increased Hh signaling when compared to the *cbbs* CON (Figure F1).

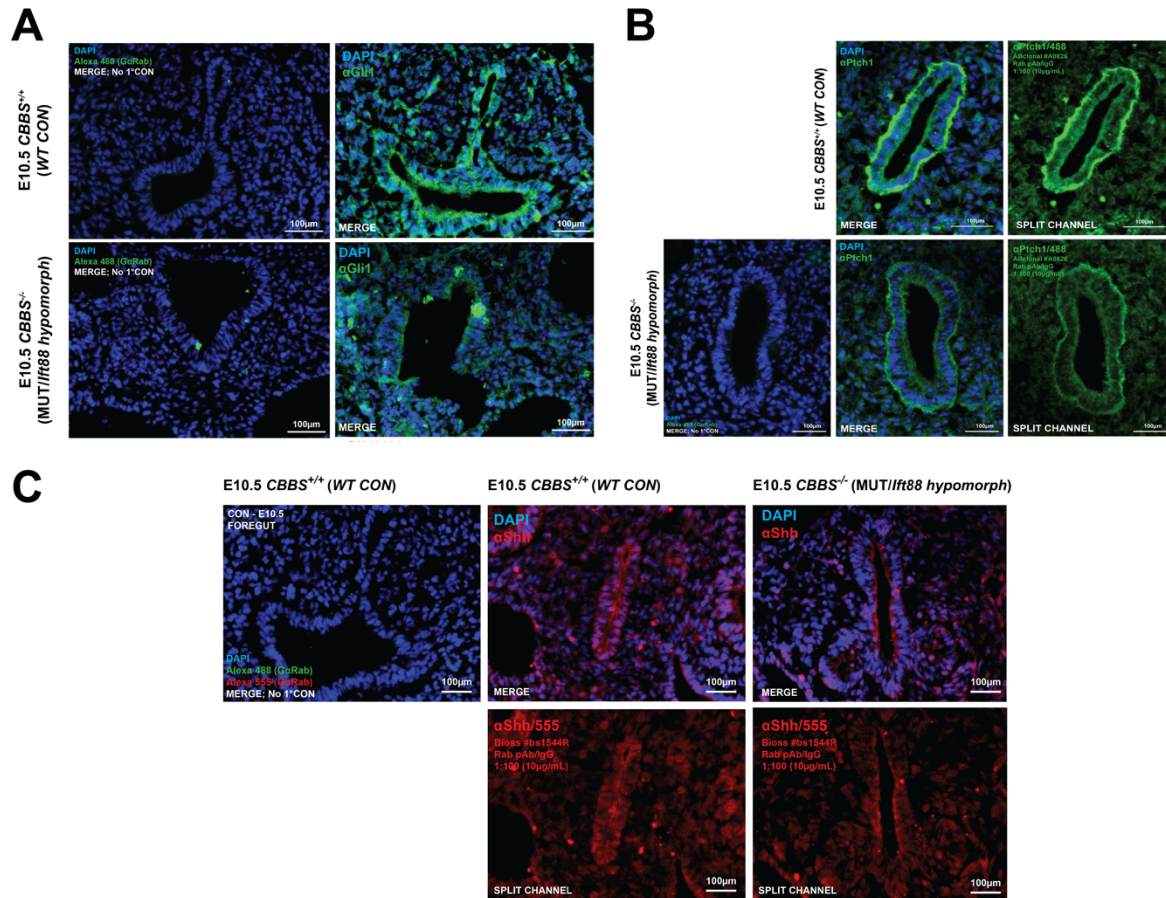


Figure F1. Validation of primary cilia and Hh signaling primary antibodies for immunofluorescence analysis. Representative images of E10.5 *cbbs* WT/CON and MUT embryos immersion fixed with 4% PFA in 1X PBS (pH7.4), embedded in OCT frozen tissue medium, cryo-sectioning at 10μm thickness and stained with primary and/or secondary antibodies indicated above. Tissue sections were intentionally selected from the developing foregut region of E10.5 *cbbs* CON and MUT embryos, and specifically at the ventral bifurcation of the foregut. **(A)** Representative images from *cbbs* CON foregut sections stained with DAPI (blue) and secondary antibody only (Green/Alexa 488, GαRab; LEFT) as compared to *cbbs* CON foregut sections stained with both DAPI and the αGli1 primary antibody (@1:100) as well as Alexa 488, GαRab secondary antibody. This experiment was repeated in the *cbbs* MUT foregut sections (A, bottom). **(B)** Same as (A) but using the αPtch1 primary antibody at a dilution of 1:100. **(C)** Representative images from the validation series for the αShh primary antibody (red) and Alexa 555 GαRab secondary fluorophore in *cbbs* CON (top) and *cbbs* MUT (bottom) E10.5 ventral bifurcation of the foregut.

BIOGRAPHY OF THE AUTHOR

Lindsey Avery Fitzsimons was born in Portland, Maine and was raised in Cumberland, Maine and later attended boarding school in Southborough Massachusetts, where she graduated from St. Mark's School in 2006. Lindsey then moved to Saratoga Springs, New York, where she attended Skidmore College and graduated in 2010 with a Bachelor of Science degree in Health & Exercise Sciences. Having transitioned quickly from a Studio Art/Art History majors to the Biological Sciences at Skidmore, Lindsey decided to devote more time further her interests and education in the human performance sciences. After finishing her Master of Science degree in Clinical Exercise Physiology from East Stroudsburg University (East, Stroudsburg, PA), she continued on to start her PhD in Biokinesiology at the University of Southern California in Los Angeles, California. After 3 years of intensive coursework, designing/overseeing clinical research and teaching graduate courses, Lindsey decided to leave USC and return to Maine, where she restarted her PhD work in 2015 at the University of Maine, Graduate School of Biomedical Science & Engineering. After completing her first-year rotations in the Reagan Lab (MMCRI), the Tucker Lab (UNE/UNE COM) and the Townsend Lab (University of Maine, Orono), Lindsey accepted a position to finish her PhD research at UNE, in the laboratory of Dr. Kerry Tucker. During her time at UNE, Lindsey was awarded a teaching instructorship through the Department of Biomedical Sciences at the University of New England, College of Osteopathic Medicine, where she taught Gross Anatomy, Histology, Embryology and Radiology to first-year medical students

fellowship at The Jackson Laboratories (Bar Harbor, ME) in the laboratory of Dr. Ron Korstanje, where she will continue her work studying primary cilia, but with a new focus in the genetics of kidney disease(s), including Alports Disease.

Lindsey currently resides with her husband, John, her 4.5 year-old son, James, and her black lab, Gertie (aka "Dodo") in Falmouth, Maine. Lindsey is a candidate for the Doctor of Philosophy degree in Biomedical Science from the University of Maine in May 2022.